Targeted BRAF inhibitors: Immunological effects and combination with immunotherapy

Alanna May Cameron

A thesis submitted to the Victoria University of Wellington in fulfilment of the requirements for the degree of Doctor of Philosophy

Victoria University of Wellington

2015

Abstract

Metastatic melanoma is the most aggressive form of skin cancer, associated with a poor prognosis, and the incidence worldwide is increasing. Recently, selective mutant BRAF inhibitors and checkpoint blockade immunotherapy have advanced clinical treatment of metastatic melanoma. However, efficacy of these therapies individually is limited. Combining treatments may allow BRAF inhibition to augment immunotherapy by increasing tumour antigen availability and improving immune system targeting of tumours. The success of this approach depends upon fully elucidating immunological interactions of BRAF inhibitors, and optimizing combination strategies.

To study the immunological effects of BRAF inhibitors and their combination with immunotherapy, novel murine *Braf*^{V600E} *Pten*$^{-/-}$ *Cdkn2a* cell lines were characterized. These were found to be moderately sensitive to BRAF inhibition compared with the widely used human BRAF^{V600E} cell lines A375 and SK-mel-5. *In vitro* targeted BRAF inhibition was shown to induce cell death through apoptosis, and partially reverse melanoma-mediated immunosuppression by human melanoma cell lines.

Utilising subcutaneously injected syngeneic, murine BRAF^{V600E} cell lines, the BRAF inhibitor PLX4720 was shown to decrease tumour growth *in vivo.* Host immune involvement in BRAF inhibitor efficacy was determined by comparing PLX4720 treatment in NOD/Scid and C57BL/6 mice. PLX4720 control of tumour growth was significantly less effective in immunocompromised mice, resulting in reduced survival advantage. These findings demonstrate that the anti-tumour effects of mutant BRAF inhibitors are partially immune dependent, although the nature of this immune involvement remains to be defined. It was further shown that BRAF^{V600E} inhibition directly affected immune responses. *In vitro,* both human and murine T cell activation were boosted by low concentrations of mutant BRAF inhibitors. This was confirmed *in vivo,* with antigen-specific T cell proliferation significantly increased by PLX4720 treatment.

The final chapters of this thesis explored the combination of active immunotherapy with targeted BRAF inhibition. A vaccine was devised that consisted of irradiated, autologous tumour cells loaded with the adjuvant α-galactosylceramide. This vaccine was shown to be effective in both prophylactic and therapeutic settings in a $BRAF^{V600E}$ melanoma model. Mechanistically, vaccine increased effector T cell responses and decreased frequencies of Tregs. Vaccine efficacy was $CD4^+$ T cell-dependent, and did not require $CD8^+$ T cells. Combination of vaccine with targeted BRAF inhibition was investigated in different settings. A combination therapy strategy was developed that achieved additive, but not synergistic benefit. Additionally, targeting specific aspects of the tumour microenvironment that may confer tumour resistance to BRAF inhibitor-mediated cell death was investigated. Both depletion of Tregs and inhibition of TNFα were explored, but did not result in a significant improvement in therapy.

In summary, the studies undertaken in this thesis demonstrate that BRAF inhibitors can augment vaccine-induced T cell responses. Moreover, this research revealed the anti-tumour efficacy of $BRAF^{V600E}$ inhibition is partially immune dependent and can be improved by combination with active immunotherapy. These discoveries generated a combination therapy strategy with improved efficacy over single agent treatment. Further studies are needed to realise the full potential of this combination therapy approach, and achieve a synergistic benefit.

Acknowledgements

The completion of my thesis would not have been possible without the help, guidance and support of many people. Below I acknowledge those who have had the greatest involvement, but there are countless more who have contributed to my PhD experience, and I thank you all.

Thank you to my supervisor and mentor, Mike Berridge, for giving me this amazing opportunity and supporting me throughout. Your endless patience and the generosity you have shown with your time and knowledge is much appreciated. I have learnt so much about the scientific research process through your guidance, and I aspire to one day have a depth of knowledge even close to yours. It has been a privilege working for you. Thank you to my co-supervisor, Patries Herst, your encouragement, advice and quick proofreading has been very appreciated.

The Malaghan Institute has been an incredible place to do my PhD. I would like to thank everyone who has provided encouragement, practical help and thought-provoking discussion. Thank you to the members of the 'MB' research group past and present, in particular James Baty, Carole Grasso and An Tan, for training me in cell culture and cancer biology. I am also grateful to Ian Hermans and his research group for their generosity with immunology protocols and reagents. Olivier Gasser and Astrid Authier-Hall thank you for sharing your human immunology expertise and antibodies, and to Taryn Osmond and Chingwen Tang for your knowledge of (and reagents for) all things αGalCer-related.

I have been privileged to share this experience with a fantastic group of PhD students, and their support has been invaluable. I am especially grateful to Cameron Field, Catherine Plunkett, Naomi Daniels, Ryan Kyle and Sotaro Ochiai. Thank you for your help with the long lab days, for teaching me new techniques, gavaging my mice on weekends and for providing moral support.

Thank you to Gideon Bollag at Plexxikon for generously providing me with PLX4720 and Vemurafenib, and for hosting my visit in San Francisco. Thank

you to Marcus Bosenberg at Yale University for the $BRAF^{V600E}$ models that have been essential to this thesis, and to Katie Meeth who generated the cell lines and organised the shipping.

I would also like to acknowledge Kylie Price and Alfonso Schmidt for all the flow cytometry support, especially the help with late night and weekend problems. Thank you to the BRU staff breeding and taking care of my mice with such good humour, you have helped my experiments run smoothly.

I gratefully acknowledge and thank the funding bodies that have supported me to undertake my PhD research. The Genesis Oncology Trust for the initial support that established this project; as well as the Wellington Division of the Cancer Society and the Wellington Medical Research Foundation for vital research funding in the later stages of the project. I would also like to thank the National Division of the Cancer Society and Victoria University for jointly funding my PhD Scholarship. I have had the amazing experience of attending and presenting my work at several national and international conferences, thanks to travel grants provided by the aforementioned funding bodies.

My heartfelt thanks to my family and friends, you have been incredibly supportive throughout my PhD. Thank you for celebrating the successes with me and picking up the pieces on bad days. Irene, thank you for always being there and keeping me sane. Your practical help (including cleaning my house) has helped me survive. To my siblings, Duane, Justine, Todd, Fenella and Sara, and my nephews Leo and Nate, thank you for being so proud of my achievements, always believing in me and looking after your "Princess" so well. Mum and Dad, I could not have done this without you. Thank you for your encouragement and your endless generosity. Your absolute confidence in me, and the work ethic you have given me carried me through my PhD. Finally, to my amazing PIC, Cam, sharing this journey with you has made it so much more enjoyable. You've inspired me to read more, harvest faster and work harder. Thank you for always being there to help me, for encouraging me and for making me laugh. Most of all, thank you for your love and support, which got me through the hardest of days.

Disclosures

I received non-financial support from Roche/Plexxikon in the form of several deliveries of the inhibitors PLX4720 and Vemufarenib. Data generated using these inhibitors was presented to the research staff of Plexxikon during a visit to their laboratories in February 2014. Roche/Plexxikon did not provide any financial backing for this research, nor were any of their staff involved in the planning, execution or analysis of the data presented in this thesis.

With these disclosures, I declare that the content of this document is my own work.

Table of Contents

Abstract iii
Acknowledgements v
Disclosures vii
Table of Contents viii
List of Figures xiii
List of Tables xvi
Abbreviations xvii

CHAPTER 1: General Introduction 1
1.1 Metastatic melanoma: the clinical problem 3
1.2 Melanoma development and the mitogen activated protein kinase (MAPK) pathway 4
1.2.1 RAF protein kinases 6
1.2.2 Mutant BRAF 7
1.2.3 Mouse models of BRAF mutant melanoma 8
1.3 BRAF Inhibitors 10
1.3.1 The clinical development of Vemurafenib 12
1.3.2 BRAF inhibitor effects on wild-type BRAF cells 15
1.3.3 BRAF inhibitor resistance 16
1.4 The role of the immune system in tumour biology 18
1.4.1 Tumour antigens 19
1.4.2 Dendritic cells 21
1.4.3 T cells 23
1.4.3.1 T cell development 23
1.4.3.2 T cell activation 24
1.4.3.3 Subsets of effector T cells 26
1.4.3.4 Resolution of T cell responses and generation of memory T cells 29
1.4.4 Natural killer cells 30
1.4.5 Invariant natural killer T cells 31
1.4.6 Immunoediting and tumour-mediated immune suppression 33
1.5 Melanoma immunotherapy 36
1.5.1 Adoptive cell transfer 37
1.5.2 Checkpoint blockade 38
1.5.3 Vaccines 40
1.5.3.1 Peptide vaccines 40
1.5.3.2 Dendritic cell vaccines 41
1.5.3.3 Whole tumour cell vaccines 42
1.6 Rationale for combination of BRAF inhibitor treatment with immunotherapy 43
1.7 Impact of BRAF inhibitor treatment on immune cells 44
1.7.1 BRAF inhibitor effects on tumour antigenicity 44
1.7.2 BRAF inhibitor effects on DCs 45
1.7.3 BRAF inhibitor effects on T cells 47

1.7.4 BRAF inhibitor effects on melanoma-mediated immune suppression....51
1.8 Combining Vemurafenib with immunotherapy....52
1.9 Aims....55
1.9.1 Specific Aims....55

CHAPTER 2: Materials and Methods....57
2.1 Materials....58
2.1.1 Labware....58
2.1.2 Reagents and Buffers....59
2.1.2.1 Cell culture reagents and buffers....59
2.1.2.2 Enzymes....61
2.1.2.3 Peptides/Antigens....61
2.1.2.4 Cytokines....62
2.1.2.5 Purified Antibodies....62
2.1.2.6 Inhibitors....63
2.1.2.7 Flow cytometry reagents....64
2.1.2.8 Human flow cytometry antibodies....65
2.1.2.9 Murine flow cytometry antibodies....65
2.1.2.10 Flow viability dyes....66
2.1.3 Cell lines....66
2.1.3.1 Human cell lines....66
2.1.3.2 Murine cell lines....67
2.1.4 Mice....67
2.1.4.1 Maintenance and ethical approvals....67
2.1.4.2 Mouse Strains....67
2.2 Methods....69
2.2.1 Cell culture techniques....69
2.2.1.1 General cell culture....69
2.2.1.2 Harvesting adherent tumour cells....69
2.2.1.3 Mycoplasma testing....69
2.2.1.4 Mycoplasma treatment....70
2.2.2 Cell isolation/purification....70
2.2.2.1 Isolation of human peripheral blood mononuclear cells (PBMCs) from whole blood....70
2.2.2.2 Preparation of murine lymphocyte single cell suspensions....71
2.2.2.3 Magnetic Cell Separation (MACs)....71
2.2.3 Viability assays....72
2.2.3.1 Trypan blue exclusion....72
2.2.3.2 Annexin V apoptosis assays....72
2.2.4 MTT dye reduction assay....73
2.2.5 Characterization of tumour cell surface markers....73
2.2.5.1 CD1d expression....73
2.2.5.2 IFNγ and TNFα exposure and cell-surface marker expression....74
2.2.6 Proliferation assays....74
2.2.6.1 One-way Mixed Lymphocyte Reaction....74
2.2.6.2 α-CD3/28 assays....75
2.2.7 Fluorescent labelling of cells and analysis by flow cytometry....77
2.2.7.1 Staining for extracellular marker expression....77
2.2.7.2 Detection of apoptosis markers....78
2.2.7.3 Labelling of cells with CFSE....78

2.2.7.4 Intracellular transcription factor staining 79
2.2.7.5 Ex vivo restimulation 79
2.2.7.6 Detection of intracellular effector molecules 80
2.2.7.7 Acquisition 80
2.2.7.8 Compensation 81
2.2.7.9 Flow cytometric data analysis 81
2.2.8 In vivo T cell assays 81
2.2.8.1 Adoptive T cell transfer 82
2.2.8.2 PLX4720 preparation and dosing 82
2.2.8.3 Vaccination 83
2.2.8.4 Analysis 83
2.2.9 Tumour challenge experiments 83
2.2.9.1 Tumour challenge 83
2.2.9.2 Vaccine generation and delivery 84
2.2.9.3 PLX4720 preparation and dosing 84
2.2.9.4 Analysis of tumour infiltrating lymphocytes (TIL) 84
2.2.9.5 Analysis of immune cell populations in peripheral lymphoid tissues 85
2.2.10 Statistical analyses 85

CHAPTER 3: Characterizing BRAF^{V600E} melanoma models 87
3.1 Introduction 89
3.1.1 Aims 91
3.2 Results 91
3.2.1 *In vitro* sensitivity of a range of human and murine cancer cell lines to BRAF inhibition 91
3.2.1.1 Human cell lines 92
3.2.1.2 Murine cell lines 94
3.2.2 BRAF inhibitors induce cell death in sensitive BRAF^{V600E} cell lines in a time and concentration dependent manner 98
3.2.3 BRAF^{V600E} melanoma cells die by apoptosis following BRAF inhibitor treatment 101
3.2.4 Melanoma production of soluble immunosuppressive factors can be partially reversed by BRAF inhibition 107
3.2.5 PX4720 treatment slows YUMM1.1 and YUMM1.7 growth *in vivo* and increases survival 113
3.3 Discussion 117
3.3.1 Conclusions 120

CHAPTER 4: Direct effects of BRAF inhibitors on immune cells 123
4.1 Introduction 125
4.1.1 Aims 126
4.2 Results 127
4.2.1 Human and murine T cells are susceptible to inhibition by targeted BRAF inhibitors *in vitro* 127
4.2.2 Serum protects T cells against detrimental effects of BRAF inhibitors *in vitro* 132
4.2.3 BRAF inhibitor treatment has paradoxical effects on sub-optimally stimulated human and murine T cells 136

4.2.4 Anti-tumour vaccination is unaffected by BRAF inhibition, while tumour growth is enhanced in a BRAF wild-type mouse model 144
4.3 Discussion 148
4.3.1 Conclusions 150

CHAPTER 5: Developing an autologous vaccine for BRAF^{V600E} tumours 151
5.1 Introduction 153
5.1.1 Aims 155
5.2 Results 155
5.2.1 Vaccination with irradiated, αGalCer-loaded YUMM1.1 and YUMM1.7 cells induces T cell-mediated immune responses 155
5.2.2 Autologous vaccination is partially protective against YUMM1.1 tumours but has minimal anti-tumour activity in YUMM1.7 tumours 164
5.2.3 YUMM1.1 vaccination of tumour-bearing mice alters the frequencies of T cell sub-populations but does not significantly change NK, NKT or myeloid populations 169
5.2.3.1 Tumour infiltrating lymphocytes 170
5.2.3.2 Tumour infiltrating myeloid cells 174
5.2.3.3 Immune cell subsets within the spleen and tumour draining iLN 176
5.2.4 Vaccination does not significantly alter lymphocyte production of IFNγ and TNFα 182
5.2.4.1 IFNγ and TNFα production by TILs 183
5.2.4.2 IFNγ and TNFα production by immune cells within the spleen and tumour draining iLN 186
5.2.4.3 IFNγ exposure causes YUMM1.1 and YUMM1.7 upregulation of PD-L1 expression, but not of MHC Class II expression. 190
5.2.5 Anti-tumour efficacy of YUMM1.1 vaccination is CD4$^+$ but not CD8$^+$ T cell dependent. 191
5.3 Discussion 196
5.3.1 Conclusions 201

CHAPTER 6: Combining autologous whole tumour cell vaccination and BRAF inhibitor therapy 202
6.1 Introduction 204
6.1.1 Aims 206
6.2 Results 207
6.2.1 The anti-tumour effects of PLX4720 in a BRAF^{V600E} tumour model are partially dependent on host-mediated immunity 207
6.2.2 PLX4720 does not alter the frequency of immune cell subsets present within the tumour milieu 210
6.2.3 TNFα inhibition does not augment the anti-tumour effects of PLX4720 treatment 217
6.2.4 PLX4720 and autologous vaccination can be combined to achieve an additive, but not synergistic, anti-tumour effect 220
6.2.5 Treg depletion does not improve vaccine, PLX4720 or combination therapy efficacy 227

6.3 Discussion **232**
6.3.1 Conclusions 236

CHAPTER 7: General Discussion **238**
7.1.1 Modelling $BRAF^{V600E}$ melanoma and BRAF inhibitor responses in mice 239
7.1.2 Immune interactions of targeted BRAF inhibitors 241
7.1.3 Active immunotherapy for $BRAF^{V600E}$ melanoma 243
7.1.4 Combining targeted BRAF inhibition with immunotherapy 246
7.2 Conclusions **248**
7.3 Future Directions **249**

References **252**
Appendix A: Representative flow cytometry plots **294**
Appendix B: Experimental validation **306**
Appendix C: Immunophenotyping of spleens and mdLN following PLX4720 treatment **309**

List of Figures

Figure 1.1: MAPK Pathway with mutant BRAF and BRAF inhibition.....12

Figure 1.2: Differentiation phenotypes of activated $CD4^+$ T cells.. 28

Figure 1.3: iNKT cells interact with and modulate DC, NK and T cell functions. 32

Figure 3.1: BRAF mutation status determines human melanoma cell line sensitivity to highly targeted BRAF inhibitors *in vitro*.. 93

Figure 3.2: Human melanoma cell line sensitivity to broad spectrum RAF inhibition *in vitro* is not determined by BRAF mutation status. 94

Figure 3.4: Murine melanoma cell line sensitivity to broad spectrum RAF inhibition *in vitro* is not determined by BRAF mutation status. 96

Figure 3.5: A375 sensitivity to PLX4720 and Vemurafenib is time and concentration dependent.. 98

Figure 3.6: YUMM1.1 sensitivity to PLX4720 and Vemurafenib is time and concentration dependent**.** 100

Figure 3.7: YUMM1.7 sensitivity to PLX4720 and Vemurafenib is time and concentration dependent.. 101

Figure 3.9: PLX4720 and Vemurafenib induce YUMM1.1 cell death by apoptosis.....105

Figure 3.10: PLX4720 and Vemurafenib induce YUMM1.7 cell death by apoptosis.....106

Figure 3.11: A375 supernatant suppression of T cell proliferation is partially reversed by PLX4720 treatment**.**. 108

Figure 3.12: SK-mel-5 production of soluble immunosuppressive factors is abrogated by PLX4720 treatment.....110

Figure 3.13: YUMM1.1 and YUMM1.7 cells do not produce soluble factors that suppress T cell proliferation. 112

Figure 3.14: PLX4720 treatment slows YUMM1.1 growth *in vivo* and increases survival, but does not induce tumour regression**.** 114

Figure 3.15: PLX4720 treatment slows YUMM1.7 growth *in vivo* and increases survival, but does not induce tumour regression. 116

Figure 4.1: PLX4720 and Vemurafenib inhibit human T cell proliferation and viability *in vitro* in mixed lymphocyte cultures. 128

Figure 4.2: High concentrations of PLX4720 and Vemurafenib inhibit human T cell proliferation and viability *in vitro* with strong anti-CD3 and anti-CD28 stimulus. 130

Figure 4.3: PLX4720 and Vemurafenib inhibit human CD4 and CD8 T cell proliferation following strong anti-CD3 and anti-CD28 stimulation. 130

Figure 4.4: High concentrations of PLX4720 and Vemurafenib inhibit murine T cell proliferation and viability *in vitro* following strong anti-CD3 and anti-CD28 stimulation.....132

Figure 4.7: Low concentrations of Vemurafenib boost human T cell proliferation *in vitro* with sub-optimal anti-CD3 and anti-CD28 stimulation. 139

Figure 4.8: Low concentrations of PLX4720 and Vemurafenib boost murine T cell proliferation *in vitro* with sub-optimal anti-CD3 and anti-CD28 stimulation. 141

Figure 4.9: PLX4720 boosts sub-optimal, but not optimal, antigen specific stimulation of OTI T cells *in vivo.* 143

Figure 4.10: PLX4720 has no effect on anti-tumour vaccination in a $BRAF^{WT}$ B16.Ova tumour model, but directly stimulated $BRAF^{WT}$ tumour growth.....147

Figure 4.11: PLX4720 stimulates $BRAF^{WT}$ B16.Ova melanoma growth *in vitro*.....147

Figure 5.1: Whole tumour cell vaccination induces an immune response. 158

Figure 5.2: Vaccination decreases frequencies of Tregs and increases frequencies of effector T cells within the spleen.....160

Figure 5.3: Vaccination decreases frequencies of both non-regulatory $CD4^+$ T cells and Tregs and increases frequencies of CD8 T cells and effector T cells within the mdLN. 161

Figure 5.4: Vaccination favourably increases ratios of splenic non-regulatory and effector T cells to Tregs. 162

Figure 5.5: Vaccination favourably increases ratios of mdLN non-regulatory and effector T cells to Tregs. 163

Figure 5.6: Prophylactic and therapeutic autologous whole tumour cell vaccination slows YUMM1.1 growth and increases survival.....166

Figure 5.7: Prophylactic but not therapeutic autologous whole tumour cell vaccination slows YUMM1.7 growth but does not increase survival. 168

Figure 5.8: YUMM1.1 and YUMM1.7 cells do not express CD1d.. 168

Figure 5.9: Flow cytometric gating strategy used to define lymphoid and myeloid populations within the tumour, spleen and draining iLN. 171

Figure 5.10: Vaccination increases frequencies of intratumoural non-regulatory $CD4^+$ T cells and decreases frequencies of Tregs. 173

Figure 5.12: Vaccination does not alter intratumoural frequencies of myeloid, macrophage or moMDSCs, but may increase grMDSCs. 175

Figure 5.13: Vaccination decreases frequencies of Tregs and of non-regulatory cells expressing PD-1 within the spleen. 178

Figure 5.14: Vaccination does not alter frequencies of lymphocyte populations within the draining iLN. 180

Figure 5.15: Vaccination increases splenic ratio of non-regulatory CD4 T cells and effector CD4 and CD8 T cells to Tregs.. 180

Figure 5.16: Vaccination does not alter splenic frequencies of myeloid cells or macrophages but may alter frequencies of MDSCs.. 181

Figure 5.17: Vaccination does not alter frequencies of myeloid cells or MDSCs but can increases the frequency of macrophages within the draining iLN. 182

Figure 5.18: Flow cytometric gating strategy used to define IFNγ and TNFα producing lymphocytes within the tumour, spleen and draining iLN.. 184

Figure 5.19: Vaccination does not significantly alter tumour frequencies of T cells, NK cells or NKT cells producing IFNγ and/or TNFα..... 186

Figure 5.20: Vaccination does not significantly alter splenic frequencies of T or NK cells producing IFNγ and/or TNFα, but increases the percentage of NKT cells producing both IFNγ and TNFα.. 188

Figure 5.21: Vaccination does not significantly alter draining iLN frequencies of T cells or NK cells producing IFNγ and/or TNFα, but increases frequencies of NKT cells producing IFNγ alone or with TNFα..... 190

Figure 5.22: YUMM1.1 and YUMM1.7 cells upregulate expression of PD-L1, but not MHC Class II, following IFNγ exposure.. 191

Figure 5.23: Autologous, whole tumour cell vaccination against YUMM1.1 tumours is not $CD8^+$ T cell-dependent. 194

Figure 5.24: Autologous, whole tumour cell vaccination against YUMM1.1 tumours is $CD4^+$ T cell-dependent. 195

Figure 6.1: PLX4720 treatment of YUMM1.1 tumours is partially dependent on host-mediated immunity.. 210

Figure 6.2: PLX4720 treatment does not alter intratumoural frequencies of lymphocytes. 213

Figure 6.3: PLX4720 treatment does not alter the intratumoural ratio of Tregs to non-regulatory CD4 T cells or CD8 T cells, or effector T cells.. 214

Figure 6.4: PLX4720 treatment does not significantly alter intratumoural frequencies of myeloid, macrophage or MDSCs. 215

Figure 6.5: PLX4720 treatment does not significantly alter intra-tumoural frequencies of lymphocytes producing IFNγ and/or TNFα. 217

Figure 6.6: TNFα inhibition does not augment anti-tumour effects of PLX4720 treatment of YUMM1.1 tumours. 220

Figure 6.7: Combination therapy with 20 mg/kg PLX4720 followed by vaccination does not significantly improve anti-tumour efficacy.. 223

Figure 6.8: Combination therapy with vaccination followed by 20 mg/kg PLX4720 does not significantly improve anti-tumour efficacy. 225

Figure 6.9: Combination therapy with vaccination followed by 50 mg/kg PLX4720 significantly improves anti-tumour efficacy. 227

Figure 6.10: Depletion of Tregs does not augment anti-tumour effects of therapeutic vaccination against YUMM1.1 tumours.. 229

Figure 6.11: Depletion of Tregs does not augment anti-tumour effects of combination PLX4720 and vaccine therapy. 231

List of Tables

Table 3-1: BRAF mutation status determines human and murine melanoma cell line sensitivity to targeted mutant BRAF inhibitors 97

Table 3-2: Tumour cell line sensitivity to broad spectrum RAF inhibition *in vitro* is not determined by BRAF mutation status. 97

Abbreviations

AML	Acute myeloid leukemia
ANOVA	Analysis of variance
APC	Antigen presenting cell
α (prefix)	Anti-
αGalCer	Alpha-galactosylceramide
BSA	Bovine serum albumin
CD	Cluster of differentiation molecule
CFSE	Carboxyfluorescein succinimidyl ester
CMC	Carboxymethyl cellulose
CTL	Cytotoxic T lymphocyte (or cytotoxic $CD8^+$ T cell)
CTLA-4	Cytotoxic T-lymphocyte antigen-4
DAPI	4′,6-diamidino-2-phenylindole
DC	Dendritic cell
DMF	Dimethylformamide
DMSO	Dimethyl sulfoxide
dPBS	Dulbecco's phosphate buffered saline
EDTA	Ethylenediaminetetraacetic acid
EGFR	Endothelial growth factor
ERK	Extracellular signal-related kinase
FACS	Fluorescence-activated cell sorting

FAK	Focal adhesion kinase
FasL	Fas ligand
FCS	Foetal calf serum
FDA	Food and drug administration
FLT-3	Fms-related tyrosine kinase-3
FoxP3	Forkhead box P3
FSC	Forward scatter
GFP	Green fluorescent protein
GM-CSF	Granulocyte macrophage colony-stimulating factor
grMDSC	Granulocytic myeloid derived suppressor cell
GTPase	Guanosine-5'-triphosphatase
Gy	Gray
HER2	Human epidermal growth factor receptor 2
HGF	Hepatocyte growth factor
HLA	Human leukocyte antigen
HPV	Human papilloma virus
IC50	Half maximal inhibitory concentration
IDO	Indoleamine 2,3-dioxygenase
IFNγ	Interferon-gamma
IG	Intragastric
IGFR	Insulin-like growth factor 1 receptor
IL-	Interleukin-

ILC	Innate lymphoid cell
iLN	Inguinal lymph node
IMDM	Iscove's modified Dulbecco's medium
iNKT	Invariant Natural Killer T [cell]
IP	Intraperiotneal
IRC	Independent review committee
IV	Intravascular
LAG-3	Lymphocyte activation gene-3
LDFB	Live dead fixable blue
LN	Lymph node
MAGE-1	Melanoma antigen-1
MART-1	Melanoma antigen recognized by T cells
MAPK	Mitogen-activated protein kinase
MDSC	Myeloid derived suppressor cell
MEK	MAP/ERK kinase
MFI	Median fluorescence intensity
MHC	Major histocompatibility complex
moDC	Monocyte derived dendritic cell
moMDSC	Monocytic myeloid derived suppressor cell
MTD	Maximum tolerated dose
MTT	3-(4,5-dimethylthiazol-2-yl)-2,5-diphenyltetrazolium bromide
mdLN	Mediastinal lymph node

NaN_3	Sodium azide
NFκB	Nuclear factor-κB
NK	Natural killer [cell]
NKT	Natural killer T [cell]
NRAS	Neuroblastoma RAS viral oncogene
OVA	Ovalbumin
PBMC	Peripheral blood mononuclear cell
PBS	Phosphate buffered saline
PCR	Polymerase chain reaction
PDGFR	Platelet-derived growth factor receptor
PD-1	Programmed cell death protein-1
PD-L1	Programmed death ligand-1
PGE_2	Prostaglandin E2
PI3K	Phosphoinositide 3-kinase
PMA	Phorbol 12-myristate 13-acetate
PTEN	Phophatase and tensin homolog
RAF	Rapidly accelerated fibrosarcoma
Rb	Retinoblastoma
RBC	Red blood cell
RNAi	Ribonucleic acid interference
RTK	Receptor tyrosine kinase
SC	Subcutaneous

S.D.	Standard deviation
SDS	Sodium dodecyl sulphate
SEM	Standard error of the mean
SSC	Side scatter
TAA	Tumour associated antigens
TAM	Tumour associated macrophage
T_{CM}	Central memory T cell
TCR	T cell receptor
T_{EM}	Effector memory T cell
Tfh	T follicular helper [cell]
TGFβ	Transforming growth factor beta
Th	T helper
TIL	Tumour infiltrating lymphocyte
TIM-3	T cell immunoglobulin and mucin-3
TNFα	Tumour necrosis factor alpha
Treg	Regulatory T cell
T_{RM}	Tissue-resident memory T cell
TSA	Tumour specific antigens
VEGF	Vascular endothelial growth factor
WT	Wild-type
4-HT	4-hydroxytamoxifen

CHAPTER 1:
General Introduction

1.1 Metastatic melanoma: the clinical problem

Melanoma is caused by the malignant transformation of pigment producing melanocytes within the epidermis and is the deadliest form of skin cancer (Schadendorf et al., 2015a). Global incidence of melanoma is 15-25 cases per 100,000 individuals, making it the fifth most common cancer in males and sixth most common in females (Schadendorf and Hauschild, 2014; Siegel et al., 2012). However, incidence varies significantly between populations and the highest rates worldwide are in Australia and New Zealand where 60 cases are recorded per 100,000 people annually (Nikolaou and Stratigos, 2014). Over the past thirty years worldwide incidence of melanoma has risen dramatically, and this concerning trend is continuing (Giblin and Thomas, 2007; Siegel et al., 2014).

The stage of melanoma at clinical presentation has significant impact on prognosis and the course of treatment (Trotter et al., 2013). The broad classification of melanoma is determined by the tumour, node and metastasis system (TNM) (Balch et al., 2009). Stage I and II melanomas are localized tumours, which are further classified into sub-stages based on tumour thickness, ulceration and mitotic rate. The prevailing gold standard treatment for localized disease is surgical resection, and the 10-year survival for this group of patients ranges from 93% for stage IA, to 39% for stage IIC (Balch et al., 2009; Schadendorf et al., 2015a). Following disease progression, patients with metastases to local lymph nodes are classed as having stage III 'regional metastatic melanoma'. Sub-classification of stage III patients is based on local tumour size, the number of metastatic lymph nodes and the burden within nodes and has 10-year survival of 25-70% (Balch et al., 2009). Finally, metastatic melanoma with distant and visceral organ metastases is classified as stage IV melanoma. In 2010 this aggressive disease had an average survival of 8-9 months with a 3-year survival rate of only 10-15%, making it almost invariably incurable (Balch et al., 2009; Eggermont, 2010).

In the decades leading up to 2010, improvements in radiation therapy delivery, cytotoxic chemotherapies and targeted therapies yielded significant advances in other forms of cancer. However, the application of these

therapies to metastatic melanoma achieved little benefit due to its near universal resistance to standard therapies (Mehnert and Kluger, 2012). Chemotherapy provided minimal improvement in patient survival outcomes, and adjuvant chemotherapy was found to be ineffective (Jilaveanu et al., 2009). Cytokine therapy could achieve some anti-tumour responses, however only a small proportion of patients were responsive and within this cohort there was a trade-off between the modest benefit and the severe toxicities of treatment (Flaherty and McArthur, 2010). Thus, the only treatments that were US Food and Drug Association (FDA) approved in 2010 for metastatic melanoma were the cytokine therapy high-dose interleukin 2 (IL-2) and the alkylating chemotherapy Dacarbazine (Flaherty et al., 2010). In Europe in 2010 only Dacarbazine was approved (Eggermont, 2010). These treatments achieved response rates of just 10-20%, with a small proportion of complete responses and no benefit in overall survival (Atkins et al., 1999; Comis, 1976). As a result, metastatic melanoma presented a dire situation that had progressed little over the previous 50 years and was in desperate need of new therapies.

1.2 Melanoma development and the mitogen activated protein kinase (MAPK) pathway

The development of melanoma occurs as a result of a complex process, involving both changes in genetic and environmental factors. This process is in part driven by an accumulation of genetic mutations that allow unregulated proliferation and survival of cells. Mutations are commonly somatic events, acquired over a lifetime, but in some cases mutations can be of germline origin, which generally promote cancer susceptibility but alone do not result in malignant transformation (Croce, 2008). A familial background of germline mutations is present in around 8% of melanoma patients, with the remaining melanomas being of sporadic origin (Schadendorf et al., 2015a). Mutations occurring in critical genes that regulate cell proliferation, differentiation and death are termed "driver mutations" (Stratton, 2011). These usually result in constitutive activation of the gene product, or activation under conditions in which the wild-type gene product

is inactive. The remaining mutations are recessively acting and occur in "tumour suppressor" genes, which encode proteins that switch off cell cycle progression. Mutations in tumour suppressor genes often result in inactivation or reduced activity of the gene product, allowing unregulated cell cycle progression (Stratton et al., 2009).

Of all cancers, melanoma is one of the richest in genetic mutations per megabase of DNA. There are diverse genetic profiles across patients and tumours, although certain gene families are commonly mutated (Curtin et al., 2005; Ilieva et al., 2014). Approximately 90% of all melanomas have alterations in the genes of the retinoblastoma pathway, which controls the progression of the cell cycle from G0 or G1 to the DNA replication phase (Schadendorf et al., 2015a). These events are primarily inactivating mutations occurring in the tumour suppressor encoding *Cdkn2a* or *Cdk4* genes. Phosphatase and tensin homolog (PTEN) is another tumour suppressor commonly mutated in melanoma, which results in phosphoinositide 3-kinase (PI3K) pathway activation and promotes cell survival. Loss of PTEN function, through mutation or epigenetic silencing, occurs in 40-50% of melanomas (Mehnert and Kluger, 2012). In addition to mutations in tumour suppressors there are several activating mutations that commonly occur in melanoma. The most notable of which are mutations in the MAPK pathway.

The MAPK pathway is a membrane-to-nucleus signal transduction cascade that mediates cellular responses to growth signals (mitogens). In response to mitogen binding to extracellular receptors, MAPK signalling regulates transcription factor activity to control a variety of essential cellular functions, including cell proliferation, differentiation, survival and apoptosis (Peyssonnaux and Eychene, 2001).

Extracellular binding of a mitogen to a receptor tyrosine kinase (RTK) initiates MAPK signalling through activation of the membrane-bound guanosine-5'-triphosphatase (GTPase), RAS. There are a diverse range of RTKs which can interact with RAS, including receptors for epidermal growth factor (EGF), vascular endothelial growth factor (VEGF), platelet-derived growth factor, c-KIT and fms-related tyrosine kinase-3 (FLT-3) (Fecher et al., 2008). Binding of

these receptors activates RAS to recruit one of the three rapidly accelerated fibrosarcoma (RAF) kinases, ARAF, BRAF or CRAF (RAF-1), to the membrane. The RAF kinases then undergo RAS-dependent phosphorylation, and conformational changes (Beeram et al., 2005). Activated RAF kinases then trigger MAP/ERK kinase activation, which, subsequently phosphorylates and activates extracellular signal-related kinase (ERK) (Kolch, 2000). Once activated, the primary function of ERK is to translocate to the nucleus and regulate transcription factor activity (Peyssonnaux and Eychene, 2001), as shown in Figure 1.1. ERK has two isoforms, ERK-1 and ERK-2, which are generally co-expressed, and are thought to be functionally equivalent with a few exceptions (Kolch, 2000). ERK functions through targeting of a large number of downstream substrates, including approximately 50 transcription factor targets, as well as kinase, cytoskeletal, signalling and apoptotic protein targets (Yoon and Seger, 2006). The large number of substrates targeted by ERK explains the vast number of integrated cellular functions regulated by the MAPK pathway. However, it also raises the question of how MAPK pathway activation results in targeting of the appropriate substrate for a specific response. Several mechanisms seem to control this, including substrate availability as determined by subcellular localization, and docking domains which guide phosphorylation (Kolch, 2000). The complexity of the MAPK pathway and its pleotropic effects are also thought to be due to the diversity within the kinases (RAF/MEK/ERK), with several genes encoding each kinase (Peyssonnaux and Eychene, 2001).

1.2.1 RAF protein kinases

The greatest diversity in the MAPK pathway is due to the presence of three isoforms of RAF kinase, encoded by distinct genes A-raf, B-raf and C-raf (Daum et al., 1994). Studies using knockout mice have shown the three RAF isoforms have both common and unique functions, as well distinct expression profiles (Chong et al., 2003; Mercer et al., 2002; Mikula et al., 2001; Wojnowski et al., 1997). CRAF is ubiquitously expressed in most tissues, whilst ARAF and BRAF have more limited expression. ARAF is primarily expressed in urogenital tissues and BRAF in neural, testicular, splenic and haematopoietic tissues (Beeram et al., 2005; Jaiswal et al., 1996). However, the most striking

difference between the three isoforms is not location, but function. Although the three proteins share MEK as their only downstream target, they differ significantly in their abilities to activate MEK. ARAF, the least well-characterized isoform, appears to be a poor MEK activator and can only phosphorylate MEK1 (Pritchard et al., 1995). CRAF and BRAF are able to activate both MEK1 and MEK2, but BRAF has been identified as the most effective MEK activator, despite the much higher abundance of CRAF (Jaiswal et al., 1996; Mikula et al., 2001). Even in cells where BRAF expression is barely detectable by western blotting it remains the primary MEK activator, with a 50-fold higher affinity for MEK than CRAF (Papin et al., 1998; Pritchard et al., 1995). The RAF isoforms also differ in their regulatory mechanisms. BRAF has the highest basal kinase activity, whilst ARAF and CRAF require additional phosphorylation events to become active (Beeram et al., 2005).

1.2.2 Mutant BRAF

Constitutively active mutant RAF proteins have been identified in a number of cancers, including malignant melanoma, colorectal cancer, thyroid cancer and haematopoietic cancers. Initial investigations aimed at identifying RAF mutations were focussed on CRAF, however, in 2002 high-throughput sequencing revealed BRAF mutations as the most common aberration, present in 8% of all cancers (Davies et al., 2002). Activating BRAF mutations are present in approximately 40-70% of metastatic melanomas, and at lower frequencies in other forms of cancer (Davies et al., 2002; Lee et al., 2011; Long et al., 2011). 70-90 % of BRAF mutations occur at a single codon, with a valine to glutamic acid substitution (V600E). Valine to lysine substitution (V600K) accounts for 10-20 % of genotypes with other mutations occurring at a lower frequency(Long et al., 2011). These mutations disrupt the interaction between the glycine-rich loop and the activation segment, mimicking phosphorylation, which normally occurs at residues adjacent to V600. This allows the kinase to fold into the active conformation, and as such these mutations result in constitutively active BRAF proteins.

This RAS-independent BRAF activation results in the constitutive activation of MEK and downstream ERK, causing cell proliferation, clonal expansion and survival. Whilst, mutant BRAF contributes to the development of malignant melanoma, $BRAF^{V600E}$ mutations are also commonly found in benign nevi indicating this mutation alone is not sufficient for melanoma transformation *in vivo* (Pollock et al., 2003). This was confirmed in a mouse model where induction of conditional melanocyte-specific $BRAF^{V600E}$ expression resulted in benign melanocytic hyperplasia, but not melanoma. When expression of $BRAF^{V600E}$ was combined with silencing of the PTEN tumour suppressor, as is observed in 40-50% of human melanoma tumours (Hodis et al., 2012), transformation to malignant melanoma occurred (Dankort et al., 2009). Despite the requirement for cooperating oncogenic mutations to achieve transformation, BRAF mutations are an important therapeutic target. BRAF mutations are the earliest and most common mutation found in malignant melanoma, and melanomas possessing mutant BRAF are dependent on MAPK pathway activation not only for melanoma initiation but to provide essential tumour maintenance (Hoeflich et al., 2006; Sharma et al., 2005). This pathway addiction renders mutant BRAF an ideal therapeutic target.

1.2.3 Mouse models of BRAF mutant melanoma

Murine models are important pre-clinical tools for understanding disease characteristics and for studying therapeutic responses and interactions. Two main mouse models of $BRAF^{V600E}$ melanoma have been developed. The first is a transgenic mouse model that has melanocytic expression of $BRAF^{V600E}$ and was developed by Goel and colleagues (Goel et al., 2009). To develop this model the $BRAF^{V600E}$ gene was cloned from the human melanoma cell line A375, and inserted into the vector downstream of the murine tyrosinase locus control region (promoter enhanced). This construct was injected into single cell embryos, and founder lines were generated. Transgene expression was identified in the skin (including melanocytes), brain and weakly in the lung. Mice expressing the transgene develop widespread benign melanocytic hyperplasia, similar to human melanocytic nevi. In some animals, melanocytic hyperplasia progresses to melanoma, with incidence dependent

on the levels of BRAF expression. Where melanoma development was observed disruption of the *Cdkn2a* locus and concurrent loss of CDKN2A was detected. These mice were backcrossed for more than 20 generations with C57BL/6 mice (Goel et al., 2009), resulting in stable $BRAF^{V600E}$ transgenic mice. Subsequently, the SM1 cell line was derived by Koya and colleagues from a spontaneous melanoma harvested from the $BRaf^{V600E}$ transgenic mice. The tumour was excised, minced and first implanted in the highly immune-deficient NOD/Scid gamma (NSG) mice, which lack T, B and NK cells and cytokine signalling, and thus also have many defects in the innate immune system (Schultz et al., 1995). The cell line was then passaged through NSG mice, and implanted in C57BL/6 mice to develop progressively growing tumours. After establishing a stable cell line, and confirming $BRAF^{V600E}$ expression, an OVA expressing SM1 line was also developed through lentiviral transduction. The SM1 cell line is a $BRAF^{V600E}$ driven murine melanoma cell line, which is syngeneic to immunocompetent mice (Koya et al., 2012).

The second mouse model of $BRAF^{V600E}$ melanoma is a conditionally expressed, melanocyte-specific model developed by Dankort and colleagues. Initially, they developed a mouse model designated $BRaf^{CA}$. These mice harbour a germline conditional $BRaf^{V600E}$ allele expressed at physiological levels following Cre-mediated recombination (Dankort et al., 2007). This conditionally-active BRaf allele was generated by modifying exons 14-16 of BRaf. Exon 16 was replaced with an HSV-thymidine kinase cassette, whilst a LoxP-flanked cassette containing the human BRAF exons 15-18 and mouse BRaf polyadenylation sequences and a PGK-neo cassette was inserted into intron 14. Finally, a modified exon 15 encoding $BRaf^{V600E}$ and a silent Xba1 restriction site polymorphism was inserted. $BRaf^{CA}$ mice were generated using homologous recombination in embryonic stem cells. As a result, when these mice were infected with an adenovirus containing Cre recombinase, $BRAF^{V600E}$ expression was induced in one allele of BRaf (Dankort et al., 2007). The $BRaf^{CA}$ mice were combined with a Tyr::CreER transgene, which encodes the 4-hydroxytamoxifen (4-HT)-inducible Cre recombinase estrogen receptor fusion transgene, under the control of the melanocyte-specific tyrosinase promoter (Bosenberg et al., 2006). In the absence of 4-HT application the

Tyr::CreER ; $BRAF^{CA}$ mice develop no distinguishable phenotype over ~18 months. However, topical application of 4-HT to fur-bearing or smooth skin, or systemic administration of 4-HT leads to the appearance of highly pigmented lesions within 21-28 days. These highly pigmented lesions fail to progress to malignant melanoma over 15-20 months. Therefore, to create a model of inducible, malignant melanoma Tyr::CreER; $BRAF^{CA}$ mice homozygous for the $Pten^{lox5/lox5}$ conditional allele were generated. The $Pten^{lox5}$ allele permits Cre recombinase-mediated deletion of exon 5 of *Pten*, resulting in a loss of PTEN in the presence of Cre recombinase. The *Tyr::CreER;* $BRAF^{CA}$*;* $Pten^{lox5/lox5}$ mice when treated with topical 4-HT display dramatic expansion of highly pigmented lesions, which progress rapidly to advanced malignancy and require animal euthanasia within 25-50 days following 4-HT administration. The melanomas developed by these mice consist of $Braf^{V600E}$; $Pten^{-/-}$ cells which are highly invasive and metastatic (Dankort et al., 2007). Cell lines were derived by resecting tumours from the *Tyr::CreER;* $BRAF^{CA}$*;* $Pten^{lox5/lox5}$ mice and manually processing these into single cell suspensions. However, it was found that these cell lines could not be immortalized *in vitro* (Assoc Prof Marcus Bosenberg, personal communication, 2011). *Tyr::CreER;* $BRAF^{CA}$; $Pten^{lox5/lox5}$ mice were then crossed to $Cdkn2a^{-/-}$ mice. Tumours were induced, again resected and manually processed into single cell suspensions. These $Braf^{V600E}$; $Pten^{-/-}$; $Cdkn2a^{-/-}$ cell lines were spontaneously immortalized creating malignant melanoma cell lines, syngeneic to C57BL/6 mice, which possess a genetic profile similar to human melanoma (Assoc Prof Marcus Bosenberg, personal communication, 2011).

1.3 BRAF Inhibitors

Early attempts to target RAF kinases were primarily aimed at CRAF, which was presumed to be the key player in oncogenic MAPK signalling prior to the discovery of the BRAF oncogene. The first RAF inhibitor to be progressed to the clinic was Sorafenib (BAY 43-9006), which was initially identified by high-throughput screening as having potent inhibitory activity against CRAF. Further characterization showed that Sorafenib also inhibited both wild-type and mutant BRAF and a range of RTKs involved in tumour angiogenesis

(Wilhelm et al., 2004). Despite, or perhaps due to, its broad-spectrum inhibitory profile Sorafenib achieved underwhelming responses for metastatic melanoma patients clinically. Single-agent Sorafenib was shown to be ineffective in the treatment of metastatic melanoma (Eisen et al., 2006). Progression-free survival was improved when Sorafenib was combined with Temozolomide or Dacarbazine, but no substantial clinical benefit was achieved, as overall survival remained the same (Amaravadi et al., 2009; McDermott et al., 2008). The clinical failure of Sorafenib is thought to be due to inadequate inhibition of the MAPK pathway even when delivered at maximum tolerated dose (MTD) (Sullivan and Flaherty, 2013).

Following the disappointing clinical performance of Sorafenib, the focus of RAF inhibitor research moved to targeting the mutant BRAF protein. $BRAF^{V600E/K}$ encoded kinases possess a deep ATP-binding pocket which provides an ideal site for inhibitor binding. However, identification of selective inhibitors had been impeded by the difficulty in crystallizing the RAF kinase structure. In 2004 the crystal structure of both wild-type and mutant BRAF was finally described (Wan et al., 2004), paving the way for the development of highly selective and potent inhibitors of mutant BRAF. A scaffold- and structure-based technique using the crystal structure of $BRAF^{V600E}$ was implemented to discover a potent and selective inhibitor of this kinase. A library of 20,000 "scaffold-like" compounds was initially screened for biochemical activity. From this 238 candidates were analysed by co-crystallography to determine three-dimensional binding interactions with protein targets. This structural information allowed rational design of the next generation of compounds, and within a year the potent and selective sister compounds PLX4720 and Vemurafenib (PLX4032, Zelboraf) were developed. These two compounds demonstrated similar inhibition of the mutant BRAF protein in biochemical assays. PLX4720 inhibited $BRAF^{V600E}$ with an IC_{50} of 13 nM and Vemurafenib with an IC_{50} of 31 nM, 10-fold and 3-fold lower respectively, than the concentration at which they inhibit wild-type BRAF (Bollag et al., 2010; Tsai et al., 2008). Despite demonstrating modest selectivity in enzymatic assays, the selectivity for $BRAF^{V600E}$ over wild-type BRAF in cellular assays was extraordinary. PLX4720 had greater than 100-fold cellular selectivity for $BRAF^{V600E}$ in multiple cell lines, with similar

results obtained for Vemurafenib (Lee et al., 2010, Tsai, 2008 #40; Tsai et al., 2008; Yang et al., 2010). Vemurafenib was selected for further clinical development over PLX4720, due to a more favourable pharmacokinetic profile, with greater bioavailability in beagle dogs and cynomolgus monkeys (Bollag et al., 2010). However, PLX4720 is the preferred compound for use in pre-clinical mouse models, due to better pharmacokinetics in rodents (Bollag et al., 2012).

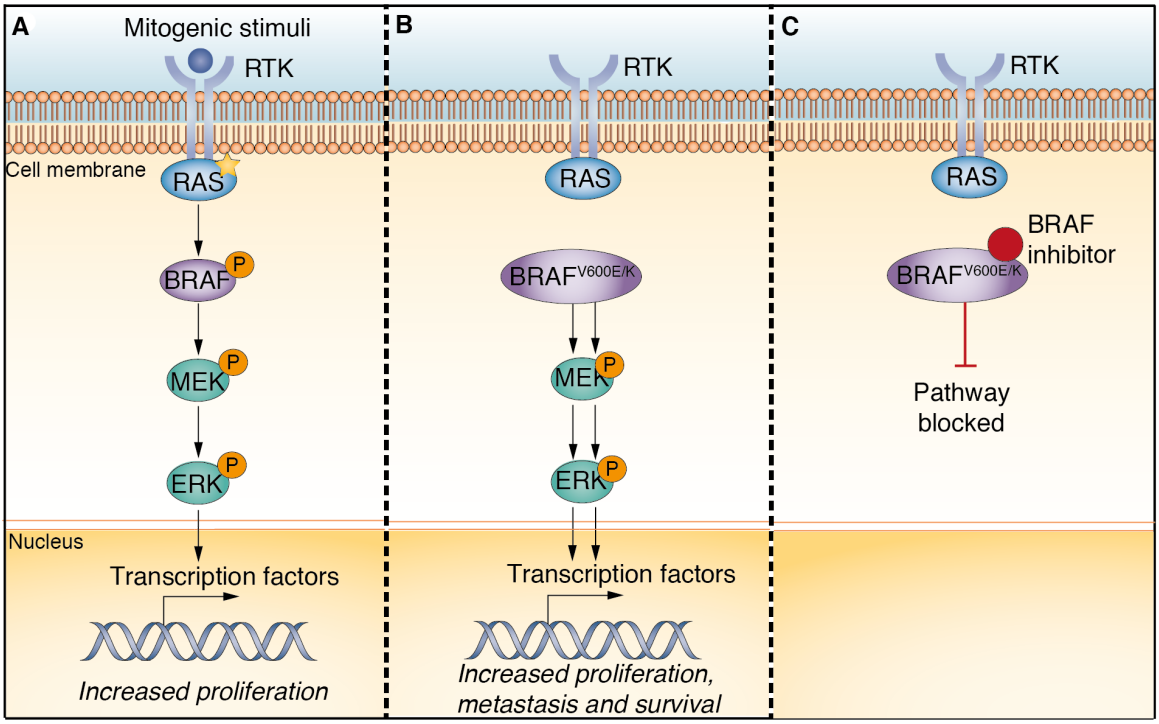

Figure 1.1: MAPK Pathway with mutant BRAF and BRAF inhibition. A. The MAPK pathway under normal physiological conditions following mitogen binding to RTK. **B.** RAS-independent activation of the MAPK pathway as a result of an activating V600E or V600K mutation in BRAF. **C.** Targeted inhibitor of mutant BRAF inhibiting constitutive MAPK pathway activation. Adapted from (Gibney et al., 2013; Xing, 2013)

1.3.1 The clinical development of Vemurafenib

The first phase I clinical trial of Vemurafenib was a multicentre trial conducted by K.T. Flaherty and colleagues in 2009 (Flaherty et al., 2010). The initial dose-escalation phase of the study included 21 patients with metastatic melanoma, 16 of whom carried the $BRAF^{V600E}$ mutation. These patients were enrolled in cohorts and received escalating doses from 200 mg to 1600 mg

twice daily. The initial crystalline formulation was found to have poor bioavailability and no anti-tumour activity. Trial enrolment was halted while reformulation was undertaken, and a microprecipitated bulk powder was developed with significantly increased bioavailability. The reformulated Vemurafenib was used for the remainder of the trial at doses of 160, 240, 360, 720 and 1120 mg, twice daily. Dose limiting side effects were observed at the 720 mg regime, and in a significant proportion of patients receiving 1120 mg twice daily. A dose of 960 mg twice daily was evaluated, and recommended for phase II trials. Following this recommendation, a phase I extension cohort enrolled 32 patients with $BRAF^{V600E}$ mutations which were treated at the recommend Phase II dose. Of the patients with $BRAF^{V600E}$ melanoma partial responses were demonstrated in 62% of patients in the dose-escalation phase and 75% of patients in the extension phase. Three complete responses were obtained, one in the dose-escalation cohort and two in the extension cohort. Overall, Vemurafenib caused partial or complete regression in 81% of patients with $BRAF^{V600E}$ mutations. The primary side effect was development of keratocanthomas or cutaneous squamous-cell carcinomas, which were evident in 31% of patients. Keratocanthomas were effectively managed with simple resection, however they were an indication of differential effects of Vemurafenib on BRAF wild-type cells. Nonetheless, the phase I clinical trial demonstrated a reliable, early response to Vemurafenib in patients with the $BRAF^{V600E}$ mutation. However, the duration of tumour regression was limited, with responses ranging from 2 to 18 months and requiring continuous treatment (Flaherty et al., 2010).

Following on from the successful phase I trial, 132 patients were enrolled in a multicentre phase II study (Sosman et al., 2012). All patients had previously treated metastatic melanoma, with a BRAF V600 mutation as detected by a polymerase chain reaction (PCR) based assay. At the efficacy data cut-off date the median follow-up was 12.9 months. An independent review committee (IRC) determined that a complete response was achieved in 6% of patients, and a partial response in 47% of patients, resulting in an overall response rate of 53%. The IRC response rates were similar to the investigator assessed overall response rate of 57%, with partial responses in 52% of patients and complete responses in 5% of patients. The majority of patients experienced at

least one adverse event, of which the most common were joint inflammation (arthralgia), rash, photosensitivity reactions, fatigue and hair loss (alopecia). Dose reduction was required in 59% of patients and dose interruption in 64%. Despite the common occurrence of toxic side effects, the majority of these were not severe and were able to be clinically managed to allow administration of the full dose to continue. Similar to the stage I trial, keratocanthomas developed in 26% of patients. Overall, the phase II clinical trial yielded positive results, with a final overall response rate of 56% and a median survival of 16 months, impressive achievements in a group of patients with less than favourable baseline characteristics (Sosman et al., 2012).

Building on the results of the phase I and II trials, 675 patients with previously untreated, $BRAF^{V600E}$ metastatic melanoma were enrolled in a multicentre phase III clinical trial (Chapman et al., 2011). Patients were randomized to receive either Vemurafenib (960 mg orally twice-daily) or Dacarbazine (1000 mg per square meter of body-surface area intravenously every 3 weeks). Vemurafenib achieved an overall response rate of 48% compared with 5% for Dacarbazine, and at 6 months the overall survival was 84% in the Vemurafenib group and 64% in the Dacarbazine group. At the interim analysis point, a year after the trial began, the data and safety monitoring board recommended that patients being treated with Dacarbazine be allowed to cross over to Vemurafenib treatment, due to its greater clinical benefit. Overall, the median progression free survival with Vemurafenib was 5.3 months compared with 1.6 months for Dacarbazine. Toxic side effects similar to those in the phase I and II clinical trials were recorded, however, few grade 3 or above adverse events were reported. Fewer patients (38%) required dose modification than in earlier clinical trials. Keratocanthomas were again reported, but at a lower frequency of 18% than in the phase I and II trials. At the conclusion of the study Vemurafenib was associated with a relative reduction of 63% in the risk of death, and 74% in the risk of tumour progression, as compared with Dacarbazine treatment. (Chapman et al., 2011).

The pivotal phase III clinical trial confirmed that, as was seen in phase I and II studies, Vemurafenib reliably achieves rapid responses in approximately 50%

of patients with advanced, $BRAF^{V600E}$ metastatic melanoma, and across all three trials provided a median progression-free survival of ~7 months (Chapman et al., 2011; Flaherty et al., 2010; Sosman et al., 2012). As a result of these trials Vemurafenib received Food and Drug Administration (FDA) approval for use in the USA in August 2011, and subsequently European Medicines Agency approval for use in Europe in February 2012. While Vemurafenib was the first oncogenic-targeted BRAF inhibitor to be approved, other inhibitors have been developed such as Dabrafenib, which received FDA approval in 2013 and is currently the only other clinically approved mutant-BRAF inhibitor. However, due to the two-year lead Vemurafenib had on the market the majority of research surrounding targeted BRAF inhibition to date has focussed on Vemurafenib. The success of Vemurafenib is compelling, especially when compared with the 10% response rates and ~2-month progression free survival historically achieved with Dacarbazine treatment (Bollag et al., 2012). However, the duration of tumour regression with Vemurafenib therapy is limited and continuous treatment is required. As a result, nearly all patients relapse eventually due to the development of resistance.

1.3.2 BRAF inhibitor effects on wild-type BRAF cells

The presentation of squamous cell carcinomas, or keratocanthomas in 18-31% of patients involved in the Phase I-III Vemurafenib clinical trials was noteworthy, although easily manageable (Chapman et al., 2011; Flaherty et al., 2010). These growths indicate that whilst Vemurafenib is highly targeted to mutant BRAF, it also has clinically relevant effects on wild-type (WT) BRAF cells. These observations led to the discovery that Vemurafenib paradoxically activates the MAPK pathway in BRAF wild-type cells, promoting cellular growth. In both RAS mutant, and RAS/RAF wild-type cells, Vemurafenib induces the formation of BRAF-CRAF heterodimers and CRAF-CRAF homodimers. Dimerization results in RAF activation, localization to the membrane and interaction with RAS-GTP, triggering downstream activation of the pathway, and subsequent MEK/ERK activation (Halaban et al., 2010; Hatzivassiliou et al., 2010; Heidorn et al., 2010; Poulikakos et al., 2010). Vemurafenib activation of ERK has been shown to

occur in a concentration-dependent manner, in a range of BRAF wild-type tumour cells (Joseph et al., 2010; Yang et al., 2010). Furthermore, both PLX4720 and Vemurafenib can stimulate the growth of some $BRAF^{WT}$ tumour cells *in vitro* and *in vivo* (Halaban et al., 2010; Hatzivassiliou et al., 2010). This paradoxical activation of the MAPK pathway in BRAF wild-type cells accounts for the undesirable effects of Vemurafenib treatment on normal skin cells. Additionally, this highlights the need for rigorous testing and selection of patients with mutant BRAF for Vemurafenib treatment.

1.3.3 BRAF inhibitor resistance

In addition to the unexpected development of keratocanthomas in patients involved in the Phase I-III clinical trials of Vemurafenib, a second issue arose that is clinically much more significant. The development of acquired therapy resistance in the majority of patients who were initially responsive compromised successful Vemurafenib treatment.

There are two types of therapy resistance, inherent or *de novo* resistance, and secondary or acquired resistance, both of which commonly occur with targeted therapies. Although the majority of BRAF mutant melanoma patients treated with Vemurafenib show some clinical response, approximately 10-20% of mutant BRAF patients are refractory to initial BRAF inhibitor treatment, which is indicative of inherent resistance (Chapman, 2013; Chapman et al., 2011). This variation in sensitivity to BRAF inhibition is also present in melanoma cell lines, and has been the subject of several investigations. The main mechanism of *de novo* resistance appears to be activation of the PI3K pathway, through the loss of PTEN. PTEN loss has been shown to confer resistance to both PLX4720- and Vemurafenib-induced apoptosis (Deng et al., 2012; Paraiso et al., 2011; Xing et al., 2012; Ye et al., 2013). However, loss of PTEN has inconsistent effects on growth inhibition by BRAF inhibitors. Some BRAF-mutant PTEN-null cell lines are resistant to both apoptosis and growth inhibition, while others retain varying degrees of sensitivity to growth inhibition (Deng et al., 2012; Xing et al., 2012; Ye et al., 2013). Although PTEN loss plays a significant role in resistance to BRAF inhibitor-induced cell death, there is heterogeneity in BRAF-mutant PTEN-

null melanomas and PTEN loss is not always predictive of BRAF inhibitor resistance. This heterogeneity may be a result of the involvement of additional factors, which are yet to be fully elucidated. It has been shown that concurrent loss of the tumour suppressor RB1 and PTEN abrogates melanoma dependence on the MAPK pathway, rendering cells resistant to MAPK targeting (Xing et al., 2012). Whilst PI3K activation has been the main focus in studies of *de novo* resistance, other mechanisms have also been implicated. There is evidence that inherent resistance to BRAF inhibitors can be a result of ERK activation through RAF signalling-independent mechanisms. Expression of COT (a *MAP3K8* encoded protein) can reactivate the MAPK pathway in the presence of BRAF inhibition and has been shown to drive *de novo* BRAF inhibitor resistance in melanoma cell lines (Johannessen et al., 2010). These pathways are potential therapeutic targets in patients with inherent BRAF inhibitor resistance, and pre-clinical data indicates PI3K and mTOR inhibitors can sensitise inherently resistant melanoma to BRAF inhibition (Deng et al., 2012; Paraiso et al., 2011).

In addition to the issues associated with *de novo* resistance, acquired resistance presents a major hurdle to long-term tumour remission with Vemurafenib treatment. Patients who initially benefit from Vemurafenib have a limited duration of response, with the majority relapsing within a year (Bollag et al., 2012; Chapman et al., 2011). This relapse is indicative of acquired resistance, which develops as a result of continuous Vemurafenib dosing and despite the persistence of the original $BRAF^{V600}$ mutation (Nazarian et al., 2010; Villanueva et al., 2010). Many investigators are exploring the problem of BRAF inhibitor resistance, and numerous mechanisms have been proposed and investigated. The most commonly described mechanisms to date involve reactivation of the MAPK pathway, through a variety of intermediary alterations. The intrinsic negative feedback mechanism of the MAPK pathway, active in all tumours, is the first mechanism that can result in pathway reactivation. The high levels of ERK-mediated negative feedback that result from constitutive MAPK signalling suppress RAS. When mutant BRAF is inhibited, negative feedback is abrogated and RAS activation increases resulting in the formation of BRAF dimers (Lito et al., 2012). BRAF dimerization allows Vemurafenib to

transactivate RAF and subsequently reactivate MEK and ERK (Poulikakos et al., 2010). Inhibition of MEK has been shown to circumvent this pathway reactivation in *in vitro* models (Lito et al., 2012). This resistance arising from inherent pathway regulation may be the reason for the majority of clinical responses only being partial responses that are not sustained over time (Chapman, 2013). Secondary activating mutations in neuroblastoma RAS viral oncogene (*NRAS*), aberrantly spliced hyperactive $BRAF^{V600E}$ and the previously described COT1/2 upregulation can also result in reactivation of the MAPK pathway through enhanced BRAF dimerization and Vemurafenib transactivation of RAF (Johannessen et al., 2010, Nazarian, 2010 #56; Nazarian et al., 2010; Poulikakos et al., 2011). Additionally, increased RTK expression can lead to BRAF inhibitor resistance, either through reactivation of the MAPK pathway or through activation of alternative survival pathways. The parallel PI3K pathway is the most commonly implicated alternative survival pathway. PI3K/AKT can be activated through PTEN loss as previously discussed, as well as by increased expression of the RTKs including insulin-like growth factor 1 receptor (IGFR) and platelet-derived growth factor receptor (PDGFR) (Nazarian et al., 2010; Villanueva et al., 2010), thus rescuing melanoma cells from BRAF inhibition.

The mechanisms of resistance described above only cover those that have been shown in melanoma models, and confirmed in clinical specimens. This list is far from exhaustive with additional mechanisms of resistance constantly emerging. Regardless of the mechanism of secondary resistance, it is evident that melanoma cells are highly plastic and capable of adapting to extreme selection pressures. Multi-pronged targeted treatments or alternative combination therapy approaches will be required to thwart the development of resistance.

1.4 The role of the immune system in tumour biology

The tumour microenvironment is a fundamental aspect of cancer biology, which contributes to tumour development and progression, as well as therapy response and resistance. One important component of the

microenvironment is the cells of the immune system. The immune system has evolved to protect an individual from infection and disease, and as such can recognize "danger" from "non-danger" signals. In the same way that the immune system can identify viral or bacterial pathogens, and mount a response that targets only that pathogen, the immune system is capable of specifically recognizing and eliminating tumour cells. Some immune cells are particularly important for driving potent anti-tumour immune responses, including natural killer (NK) cells, dendritic cells (DCs) and T cells.

1.4.1 Tumour antigens

The accumulation of genetic alterations that is characteristic of cancer results in tumour expression of proteins not usually present on normal tissues, which allow the immune system to distinguish tumour cells from "normal" cells. The first evidence of this was reported by Gross in 1943; mice were inoculated intradermally with low doses of a syngeneic sarcoma, and in approximately 18% of animals spontaneous tumour regression was observed. Mice that were able to clear the initial tumours were resistant to re-challenge, indicating they had developed anti-tumour immunity (Gross, 1943). The ability of the immune system to recognize and target tumours in animal models was subsequently confirmed by other groups (Boon and Van Pel, 1978; Prehn and Main, 1957; Van Pel and Boon, 1982). Following on from the discovery that tumours express specific rejection antigens, further work was undertaken investigating types of antigens, their corresponding expression profiles and immunogenicity. We now know tumour antigens can be split into two main classes; neoantigens, also termed tumour-specific antigens (TSAs) and self-antigens, otherwise designated tumour-associated antigens (TAAs) (Heemskerk et al., 2013).

Neoantigen expression is strictly limited to tumour cells, and these tumour-specific antigens are most commonly derived from genetic mutations and rearrangements, but can also arise from oncogenic viruses. The presence of genetic mutations leads to new peptide sequences through amino acid changes, alterations in reading frame or altering stop codons. These novel peptides are then expressed on the tumour cell surface, and can be recognized

by T cells with the appropriate antigen specificities. Neoantigens may also be peptides that are displayed at the surface of tumour cells due to mutations increasing major histocompatibility complex (MHC) molecule binding affinity, allowing for antigen presentation (Heemskerk et al., 2013). As a result, neoantigen expression is linked to the mutational profile of the tumour. Thus, cancers with a high mutation rate such as lung carcinomas resulting from tobacco smoking and ultraviolet radiation-induced melanomas are likely to have greater neoantigen expression (Coulie et al., 2014). Additionally, in the small subset of virus-associated cancers, such as the human papilloma virus (HPV)-triggered cervical cancer, antigens derived from viral open reading frames can contribute to the neo-epitope profile. However, as the vast majority of tumours lack viral etiology, oncogenic virus encoded peptides contribute little to the overall burden of neoantigens (Schumacher and Schreiber, 2015). As neoantigens result from somatic mutations or viral gene expression they are primarily unique antigens, which are patient specific.

In addition to neoantigens, tumours can also overexpress self-antigens or express them in abnormal locations. Self-antigens can be categorized as cancer-germline antigens (e.g. cancer-testis antigens), tissue differentiation antigens or overexpressed antigens. Cancer-testis antigens are, as their name implies, proteins normally found in the male germ cells in the testis but can also be expressed on tumour cells. Germ cells represent an immune privileged site, and as such do not express MHC molecules, meaning testis-associated antigens are not normally presented to T cells. On tumours these antigens are frequently overexpressed due to epigenetic changes, which facilitate gene expression (Chomez et al., 2001). The first cancer germline antigen identified was melanoma antigen-1 (MAGE-1) (van der Bruggen et al., 1991) which is expressed on spermatogenic cells of the testis as well as on 44% of tumours including malignant melanomas, breast carcinomas, lung adenocarcinomas, glioma and acute myeloid leukaemia (Amaravadi et al.) (Li et al., 2015).

The second class of self-antigens, tissue differentiation antigens, are expressed by both tumour cells and their tissue of origin. A well-known example is

MART-1 (melanoma antigen recognized by T cells-1), which is expressed both on malignant melanoma cells and non-malignant melanocytes (Kawakami et al., 1994). Finally, tumours can also overexpress proteins that are found in lower levels on non-related, normal tissues. One example of this is human epidermal growth factor receptor 2 (HER2), which is essential for embryonic development and is normally expressed on multiple tissues including epithelium, endometrium, pancreas, liver and lung tissues. HER2 is also commonly over-expressed on ovarian and breast cancers, where tumour expression is 100-200-fold higher than expression on normal tissues (Fisk et al., 1995).

Although both neoantigens and self-antigens can be recognized by the immune system, neoantigens are considered to be more immunogenic. Targeting of self-antigens is likely to be fraught with issues surround tolerance, which does not apply to neoantigens due to their tumour specificity. T cells specific for self-antigens have a high chance of being tolerogenic, due to the development of central T cell tolerance, and T cell reactivity against self-antigens can only occur when self-tolerance is incomplete. In contrast, the tumour specificity of neoantigens means central tolerance does not present an issue. Furthermore, successful targeting of self-antigens is likely to be associated with autoimmune toxicities, which do not occur with immune responses targeting tumour-specific antigens. Despite this, at present our knowledge of self-antigens is much more comprehensive. Their commonality across multiple tumour types and shared expression between patients makes them easier to study, and to generate therapies against. Irrespective of the type of antigen expressed, the presence of tumour antigens is not sufficient to generate immunogenicity. The context in which the antigen is presented to the immune system is of utmost importance for generating an active immune response versus immune tolerance.

1.4.2 Dendritic cells

DCs are critical players in inducing and coordinating adaptive immune responses, and are known as professional antigen presenting cells (APCs) due to their efficiency at acquiring and presenting antigen, and at stimulating T

cell responses. DCs are widely distributed throughout tissues and are regarded as "sentinels" of the immune system, optimally poised to constantly sample antigens from their environment and transmit this information back to T and B cells of the adaptive immune system. It has been demonstrated in mouse models that DCs are essential for the generation of anti-tumour immune responses *in vivo* (Diamond et al., 2011; Fuertes et al., 2011).

In an immature state DCs are characterized by low surface expression of MHC II and T cell-stimulating accessory molecules and are specialized for antigen sampling of their environment. Immature DCs can capture antigen through a variety of endocytosis mechanisms including phagocytosis, macropinocytosis, and receptor-mediated endocytosis (Trombetta and Mellman, 2005). Antigens are then processed intracellularly, and peptides are presented on MHC I or MHC II molecules. Classically, endogenous cellular antigens such as viral proteins are presented on MHC class I, whilst exogenous antigens including microbial proteins or proteins from apoptotic cells are presented on MHC class II. However, as professional APCs, DCs are also capable of "cross-presenting" endogenous antigens on MHC II and exogenous antigens on MHC I (Mellman and Steinman, 2001). Additionally, lipid antigens undergo alternative processing, and as a result are loaded onto the CD1d non-classical MHC molecules (Porcelli and Modlin, 1999). Following antigen capture DCs migrate to draining lymph nodes (LN). In the absence of 'danger signals' DCs remain in an immature state with antigens presented to T cells in the absence of co-stimulation. Presentation of antigen by immature DCs induces tolerance, through clonal deletion of antigen-specific T cells or the generation of inducible T regulatory cells (Steinman et al., 2003). When DCs acquire antigen in the presence of danger signals, such as microbial or viral products, they undergo maturation. Mature DCs have decreased antigen uptake and high surface expression of MHC-peptide complexes and co-stimulatory molecules (Mellman and Steinman, 2001). Additionally, once matured, DCs express elevated levels of the chemokine receptors CCR7 and CXCR4, allowing them to home to T cell zones of the LN and spleen (Sallusto et al., 1998). This allows the DCs to present antigen to a large number of naïve T cells in search of their cognate antigen, and upon recognition induce T cell activation to effector phenotype. Therefore, whilst

antigen-loaded immature DCs can induce tolerance, mature DCs induce immunity through the priming of antigen-specific T cells.

Although mature DCs are associated with the generation of immunity, not all mature DCs are created equal with regard to immunogenicity. The cytokine milieu present at the time of DC activation can alter the phenotype of mature DCs, resulting in immunogenic, tolerogenic or inflammatory DC populations (Palucka and Banchereau, 2012). Furthermore, within the tumour microenvironment the continuum of DC activation states is even more complex. Tumour cells directly interfere with DC function through immunosuppressive signals, as discussed in more detail later. In well-established tumours cancer cells actively maintain DCs in the favourable immature state to promote tolerogenicity (Dudek et al., 2013). A murine model of ovarian cancer demonstrated that DCs could undergo phenotypic switching from immunogenic to immunosuppressive, which was associated with cancer progression (Scarlett et al., 2012). Within early stage tumours DCs were shown to be immunocompetent, inducing expansion of tumour-specific T cells. However, within advanced tumours T cells were no longer responsive, despite tumours remaining antigenic. This was shown to be a result of DCs acquiring an immunosuppressive phenotype through expression of increased levels of programmed death ligand-1 (PD-L1) and strong arginase production, both of which suppress T cell effector functions. A similar phenotype was also observed in DCs isolated from advanced human ovarian tumours (Scarlett et al., 2012).

1.4.3 T cells

1.4.3.1 T cell development

T cells are derived from common lymphoid progenitors, which originate from the bone marrow and migrate to the thymus. Once in the thymus, 'double negative' T cell precursors undergo germline recombination of the γ and δ or β T cell receptor (TCR) genes; the vast majority (> 95%) of cells will develop TCR-β expression and go on to express an αβ TCR with a unique specificity

(Murphy, 2011). Subsequently, T cells develop expression of both the CD4 and CD8 co-receptors, rendering them double positive ($CD4^+$ $CD8^+$), followed by rearrangement and expression of the TCR-α chain (Lind et al., 2001). Double positive T cells with complete TCRs then begin a two round selection process (Starr et al., 2003). During the first stage, termed 'positive selection', T cells are tested for appropriate interactions with MHC molecules, to ensure they can recognize peptide in an MHC-restricted manner. T cells which recognize MHC with neither too strong nor too weak an affinity receive survival signals. The process of positive selection also determines CD4 and CD8 expression; cells with affinity for MHC II molecules retain $CD4^+$ expression, whilst cells with affinity for MHC I remain $CD8^+$. T cells that successfully survive positive selection subsequently migrate to the thymic medulla and undergo negative selection, to eliminate T cells with self-reactivity. T cells specific for self-proteins are induced to apoptose or in some cases of intermediate to high affinity for self-antigen, become the immune modulating $CD4^+$ natural T regulatory cells (nTregs) (Starr et al., 2003). As a result of positive and negative selection a mature T cell repertoire is generated, which is MHC-restricted and self-tolerant.

1.4.3.2 T cell activation

The relatively few T cells which successfully complete thymic development then enter the blood stream and migrate to secondary lymphoid organs. These mature, antigen-inexperienced "naïve" T cells recirculate through the lymphatics and peripheral lymphoid tissues in search of their cognate antigen (Murphy, 2011). Naïve T cell recirculation is facilitated by the expression of CCR7 and CD62L, and during migration, naïve T cells bind transiently to APCs they encounter, sampling antigen (Sallusto et al., 1999). When the TCR binds to antigen with sufficient affinity, TCR signalling induces a conformational change that stabilizes the APC-T cell interaction. TCR signalling induced by antigen recognition is the first of 3 signals required for T cell activation: TCR engagement (or 'signal 1') alone is insufficient to generate effector T cells. The additional signals required are usually supplied by the same APC, and it is for this reason that the conformational change which stabilizes the APC-T cell interaction is important. The additional

signals required for T cell priming consist of the pro-survival and expansion co-stimulatory signal ('signal 2'), which is delivered through binding of T cell-expressed CD28 to APC CD80 and CD86 (also known as B7.1/7.2 respectively) (Boomer and Green, 2010). Finally, the cytokine mediated 'signal 3' is required to direct $CD4^+$ T cell differentiation into one of a number of effector subsets or to achieve optimal $CD8^+$ T cell activation (Curtsinger et al., 1999).

Following T cell activation a number of proteins are upregulated to sustain or modulate ongoing co-stimulation. The first of these is upregulation of IL-2 production and expression of the α chain of the IL-2 receptor (also known as CD25) (Malek, 2008). The IL-2 receptor is composed of three chains: α, β and γ; resting T cells express the moderate affinity receptor composed of β and γ chains. Addition of the α chain stabilizes the receptor and endows it with much higher IL-2 affinity. Costimulation through CD28 also contributes to increasing T cell IL-2 production. The production of IL-2 by activated T cells, and the expression of the high affinity IL-2 receptor is of utmost importance as IL-2 is a survival and growth factor required for the generation of effector T cells. In addition to upregulating IL-2 and CD25 expression, activated T cells begin to express a number of proteins with co-stimulatory functions, one of the earliest expressed activation markers is CD69 (Biselli et al., 1992; Risso et al., 1991).

In addition to the expression of co-stimulatory markers following activation, T cells also begin to express surface molecules with negative regulatory functions, to control peripheral T cell activation. Cytotoxic T lymphocyte antigen-4 (CTLA-4) is a CD28-like molecule, which also binds CD80/86. However, CTLA-4 has a much stronger affinity for CD80/86 than CD28 does, and its effect is to inhibit rather than activate the T cell (Alegre et al., 2001). Upregulation of CTLA-4 on the surface of T cells following activation makes them less sensitive to APC stimulation than naïve cells, thereby limiting IL-2 production and the proliferative responses of activated T cells. Following antigen recognition and upregulation of co-stimulatory receptors, activated T cells then undergo 4-5 days of rapid proliferation (termed clonal expansion) induced by IL-2. Clonal expansion produces large numbers of progeny with

the same antigen specificity that will differentiate into effector T cells. The key distinction of effector T cells is their ability to perform their effector function upon recognition of their target antigen without the requirement for co-stimulation (Lanzavecchia and Sallusto, 2000). The effector functions of different T cell subsets are described in detail below. After acquiring effector status T cells alter expression of a number of cell-surface molecules to aid in trafficking to sites of infection. One example of this is upregulation of expression of the adhesion molecule CD44, which mediates T cell extravasation (DeGrendele et al., 1997).

1.4.3.3 Subsets of effector T cells

Naïve T cells can be primarily classified into two types: $CD4^+$ and $CD8^+$ T cells. Once activated, T cells differentiate into specific subsets related to their effector function. $CD8^+$ T cells become cytotoxic $CD8^+$ T cells, also called cytotoxic T lymphocytes (CTLs), which acquire the ability to directly kill target cells following recognition of antigen expressed on MHC class I. As a result, CTLs are particularly important for the control of intracellular pathogens such as viruses and in surveillance against tumours. CTLs can induce target cells to undergo apoptosis through a number of mechanisms, the most common of which is the release of preformed, specialized cytotoxic granules (Kagi et al., 1996). Cytotoxic granules are modified lysosomes that contain the proteins perforin and granzymes. Perforin is involved in the delivery of the contents of cytotoxic granules through target-cell membranes. Granzymes are serine proteases, of which there are five subclasses in humans and ten in mice. They induce apoptosis in target cells by activating caspases, which trigger an intrinsic apoptotic signalling cascade resulting in DNA fragmentation. Whilst granzymes are the central apoptotic mediators, perforin is required for their delivery into the cell. This was demonstrated by the inability of perforin knockout mice to generate a CTL response to many viruses (Kagi and Hengartner, 1996; Kagi et al., 1994). A second mechanism of inducing apoptosis involves the extrinsic apoptotic pathway. This pathway is facilitated by death receptors of the tumour necrosis factor (TNF) family, the best characterized of which is Fas. Activated $CD8^+$ T cells upregulate Fas ligand (FasL) following TCR engagement, allowing CTLs to induce apoptosis

of cells expressing Fas through caspase activation. This mechanism is primarily used to regulate lymphocyte numbers; activated lymphocytes express Fas allowing CTLs to reduce lymphocyte numbers following clearance of infection. Induction of apoptosis is the primary effector function of CTLs, although they can also release a number of cytokines including interferon-γ (IFNγ), TNFα and lymphotoxin-α (Fong and Mosmann, 1990). IFNγ has roles in controlling viral replication and increasing expression of MHC I, which increases the likelihood of target cells being recognized. IFNγ and TNFα can also synergize to activate and recruit macrophages.

$CD4^+$ T cells, also known as T helper (Th) cells, can differentiate into one of a number of diverse subsets with distinct functions (Figure 1.2). The activation phenotype of a $CD4^+$ T cell is partially determined by the cytokine environment in which the cell was activated (Zhu and Paul, 2010). $CD4^+$ T cell effector activity primarily involves cytokine secretion, with cytokines acting on target cells to direct their function. The first two subsets of T helper cells were identified by Mosmann and Coffman in 1986, and were defined by their cytokine secretion profiles as being the IFNγ-producing Th1 cells and the IL-4-producing Th2 cells (Mosmann et al., 1986). As the original T helper subsets, a large body of work has been generated describing the roles of Th1 and Th2 cells in disease and homeostasis. Th1 cells are characterized by production of high levels of IFNγ but can also produce TNFα, IL-2 and granulocyte macrophage colony-stimulating factor (GM-CSF). Th1 cells are primarily associated with inflammatory conditions and play a critical role in the control of intracellular bacterial infections by activating macrophages. The cytokine signature of Th2 cells is IL-4, IL-5 and IL-13, and these effector cells are associated with response to parasite infection, but also promote allergic disease. The third subset of T helper cells to be identified was the Treg subset, defined by their immunosuppressive function and production of the cytokines IL-10 and TGFβ (Gershon and Kondo, 1970; Sakaguchi et al., 1995). Additional subsets are now recognized including: IL-17-producing Th17 cells, critical in antifungal responses and the autoimmune responses in multiple sclerosis (Veldhoen et al., 2006); Th22 cells, which produce IL-22 and play a role in the maintenance of mucosal microbial populations and wound repair (Trifari et al., 2009); IL-9-producing Th9 cells involved in airway

inflammation and anti-helminth responses (Dardalhon et al., 2008); and finally T follicular helper cells (Tfh) which reside within the germinal centres and promote B cell antibody class switching (Schaerli et al., 2000).

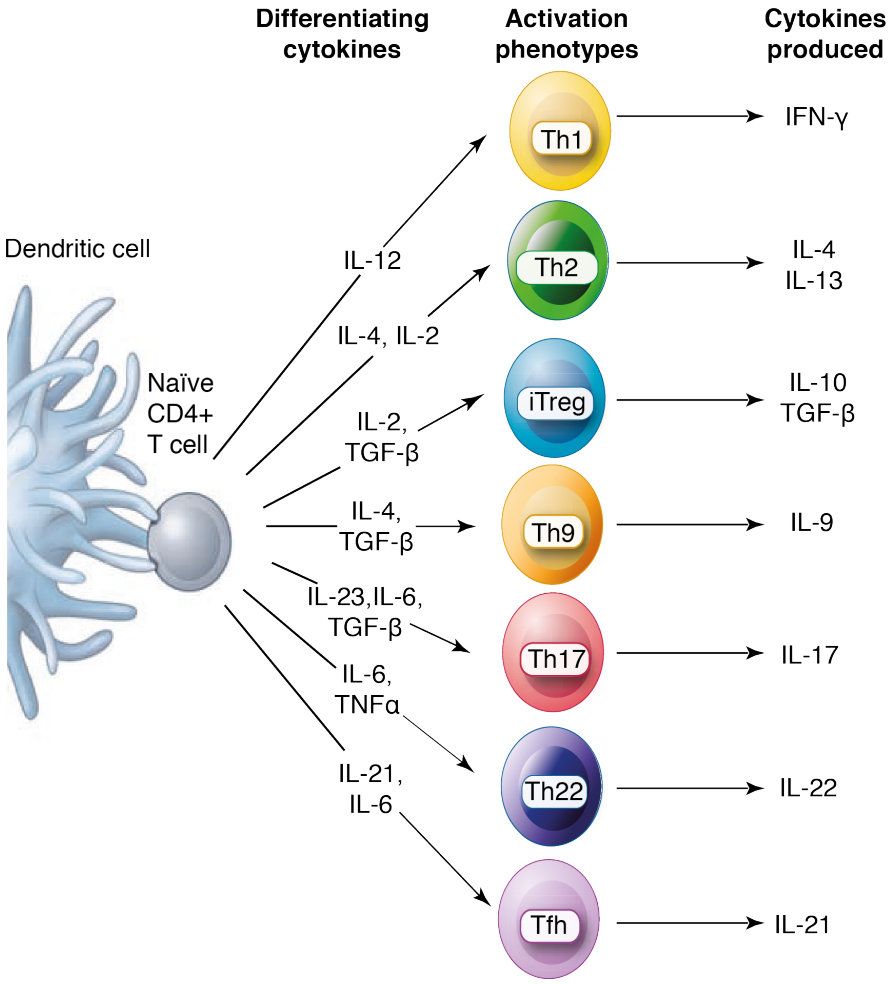

Figure 1.2: Differentiation phenotypes of activated CD4⁺ T cells. Upon activation CD4⁺ T cells differentiate into one of seven distinct subsets. The cytokine environment at differentiation contributes to the activation phenotype developed. Once differentiated the subsets of CD4⁺ T cells can be in part be defined by their cytokine secretion profiles. Adapted from (O'Shea and Paul, 2010).

T cells can mediate anti-tumour responses through a number of the effector functions described. The most obvious of these is the cytotoxic effects of CTLs, which upon recognition of tumour-associated antigens induce direct tumour cell killing through the release of cytotoxic granules or through the expression of apoptosis-inducing ligands. However, perhaps due to the highly destructive capability of CTL responses, CD8⁺ T cell activation

generally requires 'help' from $CD4^+$ effector T cells (Zhang et al., 2009). One of the major forms of $CD4^+$ T cell help comes in the form of T helper membrane expression of CD40L, which interacts with DC expressed CD40. This interaction provides an additional signal to further activate DCs and enhance MHC and co-stimulatory molecule expression, providing additional co-stimulation to naïve cells. T helper cells also produce IL-2, which is indispensable for the production of CTL responses (Zhang et al., 2009). Therefore, the first role of $CD4^+$ T cells in anti-tumour settings (amongst other inflammatory settings) is to augment CTL responses, and it is well established that a Th1 response is essential for successful anti-tumour immunity (Nishimura et al., 2000). CTLs and Th1-differentiated $CD4^+$ T cells can also mediate anti-tumour immunity through the production of IFNγ and TNFα. These cytokines enhance immune responses by causing the upregulation of MHC I expression on tumour cells and increasing MHC II expression by tumour-resident APCs and in some cases, on tumour cells (Wang and Lin, 2008; Zaidi and Merlino, 2011). Additionally, Th1 and Th2 cells can activate innate immune mechanisms with anti-tumour activity, including the recruitment of macrophages, eosinophils and NK cells (Hung et al., 1998). Finally, T helper cells can have direct anti-tumour functions through the production of TNFα or by inducing death via the extrinsic receptor-mediated apoptotic pathway (Fas-FasL interactions amongst others) (Haabeth et al., 2014). However, in most models the major contribution of $CD4^+$ T cells appears to be in the recruitment of accessory cells (APCs, NK cells) and supporting CTL anti-tumour responses.

1.4.3.4 Resolution of T cell responses and generation of memory T cells

In a primary immune response, which occurs when a pathogen is encountered for the first time, the clonal expansion and differentiation of effector cells will take several days from pathogen recognition. In the majority of cases the cells of the adaptive immune system will effectively target the pathogen, leading to clearance of infection, and downregulation of the immune response. To prevent an overly active immune response from developing after the peak of effector T cell expansion, there is contraction of the immune response, which results in the elimination of 90-95% of T cells

(Kaech et al., 2002). During this phase, 5-10% of effector cells are retained and differentiate into long-lasting memory T cells (Kaech and Wherry, 2007). The mechanisms that determine which effector T cells undergo apoptosis and which become memory cells are still unclear, as are the mechanisms by which memory cells maintain long-term survival. Regardless of the mechanisms, maintenance of memory T cell populations enables the immune system to respond more rapidly and effectively to reinfection. Memory T cells possess high proliferative potential and have a lower requirement for antigenic stimulation and co-stimulation than naïve T cells (Kaech et al., 2002). Following reinfection memory T cells rapidly begin to undergo clonal expansion, produce effector molecules and differentiate into secondary effector T cells generating a fast and robust antigen-specific immune response. Memory T cells are a heterogeneous population consisting of effector memory (T_{EM}), central memory (T_{CM}) and tissue-resident memory (T_{RM}) cells (Sallusto et al., 1999; Schenkel and Masopust, 2014). These subsets can be distinguished by their localization with T_{EM} cells circulating through non-lymphoid tissues, T_{CM} homing to secondary lymphoid tissues and T_{RM} being found in peripheral tissues with requirements for specific chemoattractant and homing receptor expression for T cell recruitment (Shin and Iwasaki, 2013).

1.4.4 Natural killer cells

In addition to the anti-tumour responses of adaptive immune cells, innate lymphoid cells (ILCs), which arise from the same lymphoid progenitors as T cells and develop in the bone marrow, can also contribute to anti-tumour immunity. NK cells are a subset of cytotoxic ILCs which were initially identified through their ability to directly kill tumour cells (Herberman et al., 1975a; Herberman et al., 1975b) An important feature of NK cells is their capacity to identify stressed cells (such as tumour cells) from healthy ones, and directly kill either through cytotoxic granule release similar to that used by $CD8^+$ T cells, or through death receptor pathways which induce apoptosis (e.g. Fas-FasL). Whilst NK cells share a number of similarities with T cells, there are also key differences. NK cells recognize conserved motifs of "missing-self" and of stress, as opposed to specific antigens. Tumours and

virally infected cells commonly downregulate MHC I, and NK cells can recognize this "missing self" and become activated. Additionally, NK cells express receptors including the NKG2D receptor, which recognizes stress-induced proteins such as MICA and MICB. Receptor binding to stress ligands also results in NK cell activation. Upon activation, NK cells eliminate the target cell directly, through the release of cytotoxic granules or surface ligand binding, or indirectly through the release of IFNγ and recruitment of other immune cells. NK cells were first shown to effectively eliminate tumour cells in mouse models (Gorelik et al., 1984; Riccardi et al., 1980), and have since been shown to kill MHC I-deficient tumours both *in vitro* and *in vivo* (Karre et al., 1986; Ljunggren and Karre, 1985). Following these initial investigations the anti-tumour effects of NK cells have been demonstrated in a number of mouse models and human tumours. NK cells play an important role in anti-tumour immunity not only through their direct cytolytic killing, but also through the release of IFNγ, and shaping of downstream adaptive immune responses.

1.4.5 Invariant natural killer T cells

A second group of non-T lymphocytes that can play important roles in anti-tumour immunity are natural killer T cells (NKTs), which bridge the innate and adaptive immune systems. NKT cells arise from the same common lymphoid progenitors as conventional T cells, and also develop in the thymus. There are four different groups of NKT cells, the best studied of which is the invariant NKT (iNKT) cell subset, also known as Type I NKT cells. Following αβ gene rearrangement and the generation of double positive ($CD4^+$ $CD8^+$) T cells, the iNKT cells diverge from T cell development and develop a semi-invariant TCR (Vα14-Jα18 in mice and Vα24-Jα18 in humans). This receptor recognizes a variety of glycolipids presented on the MHC-like molecule CD1d, thus iNKT activation is CD1d-restricted. CD1d is expressed on APCs including DCs and B cells, and can also be expressed on tumour cells, with CD1d expression documented in renal cell carcinoma, breast carcinoma and lymphoma amongst other tumours. When DCs present lipid antigens, such as the potent iNKT ligand α-galactosylceramide (αGalCer), on

CD1d to iNKTs, they induce cellular activation (Figure 1.3) (Kawano et al., 1997). Subsequent to activation, iNKTs upregulate expression of CD40, which in turn provides a maturation signal to the DC known as "licensing"; stimulating DC production of IL-12. IL-12 is a potent Th1 polarizing cytokine, and it has been established that Th1 responses are critical for successful anti-tumour immunity. Additionally, activated iNKT cells can rapidly release large amounts of cytokines including IFNγ, which recruits T cells and NK cells to directly kill the target cells (Motohashi and Nakayama, 2008). In anti-tumour immunity, iNKT cells have been shown to exert direct anti-tumour killing capacity, including cytotoxic granule release and FasL expression. However, when stimulated by αGalCer, anti-tumour effects are the result of IFNγ-mediated recruitment of $CD8^+$ T cells and NK cells which mediate tumour killing, not a result of direct iNKT killing (Vivier et al., 2012).

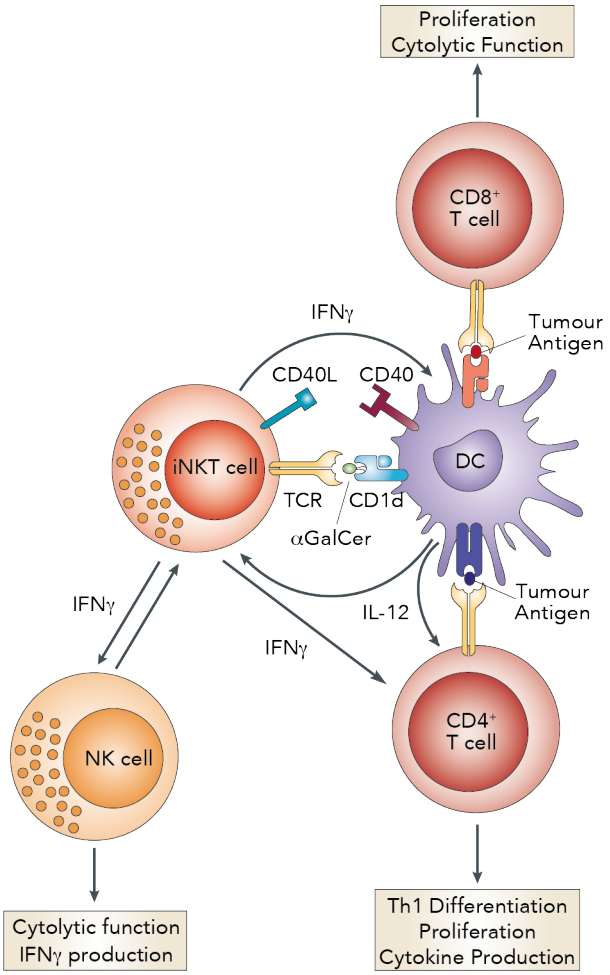

Figure 1.3: iNKT cells interact with and modulate DC, NK and T cell functions. iNKT cells have bi-directional interaction with DCs; DCs present

lipid antigens on CD1d to activate iNKT cells and iNKTs license DCs through CD40-CD40L. iNKTs also directly and indirectly modulate the cytokine environment recruiting NK and T cells. Adapted from (Cerundolo et al., 2009).

1.4.6 Immunoediting and tumour-mediated immune suppression

While the immune system is capable of generating powerful anti-tumour responses, the progression of tumours to advanced stages is evidence that such responses are not always effective. A large body of work now demonstrates that the immune system can have paradoxical, and dynamic effects on tumour development, both preventing or facilitating tumour growth and impacting tumour immunogenicity.

Over 50 years ago Burnet originally proposed the 'immune surveillance theory' hypothesizing that the immune system could recognize and eliminate nascent transformed cells, and that adaptive immunity was responsible for preventing cancer development in immunocompetent hosts (Burnet, 1970). However, Burnet's immune surveillance theory did not take into consideration the immune escape that underpins tumour progression in immunocompetent hosts. It is now proposed that there is a cancer immunoediting process composed of three distinct phases; elimination, equilibrium and escape (Dunn et al., 2002). In the elimination phase the cells of the innate and adaptive immune systems effectively target and kill developing tumours before they become clinically apparent. A number of the mechanisms and molecules employed in this process have been described above, and more remain to be elucidated. If the elimination phase is successful the host remains tumour free and the immunoediting process is circumvented. However, if some tumour cells survive elimination the process advances to the equilibrium phase, where tumour growth is prevented but tumour cells persist. This phase is mediated by adaptive immune mechanisms including T cell responses, and IL-12 and IFNγ involvement (Koebel et al., 2007). Equilibrium can be the endpoint of immunoediting, with the immune system able to restrain outgrowth of tumour cells for the lifetime of the host. However, as a consequence of the selective immune pressures placed on

genetically unstable tumour cells, the equilibrium phase can result in editing of tumour immunogenicity. Over time, this process can generate tumour cell variants that either lose antigen expression, are resistant to the immune effector mechanisms at play, or are able to create an immunosuppressive microenvironment. Due to the emergence of tumour cell variants, or as a result of immune exhaustion or inhibition, tumour cells may proceed from the equilibrium phase to enter the escape phase. In the escape phase the balance between anti-tumour immune responses and the tumour is lost, in favour of tumour outgrowth. This results in cancer progression. It is worth noting that the three phases of cancer immunoediting are not necessarily linear, but rather this is a dynamic process with some tumours skipping phases. Overall, the immunoediting hypothesis incorporates dual host-protective and tumour-promoting roles, and explains the role the immune system plays in shaping tumour immunogenicity (Dunn et al., 2002; Dunn et al., 2006; Schreiber et al., 2011). Although studies of tumour development in mice formed the basis of the cancer immunoediting hypothesis, there is increasingly substantive evidence of this process occurring in human tumours (Dunn et al., 2004)

One central mechanism of immune escape is the creation of an immunosuppressive tumour microenvironment. Progressive tumour growth has been shown to occur despite the retention of tumour antigen expression and the presence of effector tumour infiltrating lymphocytes (TILs) with tumour antigen specificity (Prevost-Blondel et al., 1998; Rosenberg et al., 2005; van der Bruggen et al., 1991). In this setting, progression is likely a result of tumour immunosuppressive mechanisms abrogating effector T cell function. Tumour cells employ a number of mechanisms to generate a highly immune suppressive microenvironment, including expression of suppressive cytokines and molecules and the recruitment or induction of regulatory immune cells with suppressor functions. Immune suppression can be mediated through intrinsic tumour mechanisms or via extrinsic suppression facilitated by regulatory cell populations or non-cancerous cells within the tumour microenvironment, such as stromal cells and mesenchymal stem cells (Le Blanc et al., 2004; Nauta and Fibbe, 2007; Spaggiari et al., 2008). The first mechanism of suppression is the production of suppressive factors by tumour

or associated cells. Some tumours, and tumour-associated myeloid cells, have increased arginase-1 activity and overproduce nitric oxide, both of which inhibit T cell function. Additionally, numerous human tumours have been shown to produce indoleamine 2,3-dioxygenase (IDO) which catalyzes the degradation of tryptophan, an amino acid essential for T cell function. IDO catabolism of tryptophan can block $CD8^+$ T cell proliferation (Uyttenhove et al., 2003) and promote $CD4^+$ T cell apoptosis (Terness et al., 2002). The tumour microenvironment also contains a number of factors, produced by tumour cells or stromal cells, which can inhibit the differentiation, maturation and function of DCs, including VEGF, IL-6, IL-10, transforming growth factor-β (TGFβ), and prostaglandin E2 (PGE_2) amongst others (Dudek et al., 2013; Zitvogel et al., 2006). Thus, the tumour maintains infiltrating DCs in the favourable immature state, with some immature DCs competent to express IDO (Munn et al., 2004). As a result, DCs within the tumour microenvironment mediate immunosuppressive, not immunostimulatory, effects and promote the differentiation of T helper cells into Tregs.

Tregs are a major extrinsic mediator of immunosuppression within the tumour microenvironment. T helper cell differentiation into Tregs is supported within the tumour by a number of mechanisms including previously described antigen presentation by immature tumour infiltrating DCs. Numerous molecules expressed at high levels in the tumour microenvironment also support Treg development such as TGFβ and IL-10, IDO and CTLA-4. These factors and ligands are commonly expressed by tumour cells or associated cells, with several redundant sources ensuring they are present in the majority of established tumours. Thus, Tregs are present in elevated numbers in many tumours, and inhibit the effector functions of tumour-specific T cells through contact-dependent mechanisms involving the expression of inhibitory ligands, and through the production of IL-10 and TGFβ. Additionally, Tregs with their high expression of CD25 act as sinkholes for IL-2 sequestering it away from the IL-2 dependent CTLs, and similarly sequestering the amino acids arginine, tryptophan or cysteine which are all required for T cell effector function. The tumour microenvironment also induces myeloid precursor cells to develop the immunosuppressive phenotype of 'myeloid derived suppressor cells' (MDSCs). MDSCs promote

tumour growth by enhancing angiogenesis and metastasis and inhibit anti-tumour T cell responses in a similar manner to Tregs by TGFβ production or sequestering of amino acids. Additionally, MDSCs reduce effector T cells and boost immunosuppression by inducing T cell differentiation into Tregs. MDSCs, amongst other cells in the tumour microenvironment, can also polarize macrophages towards tumour-promoting 'tumour associated macrophages' (TAMs). These TAMs can produce high levels of IL-10 and little IL-12, promoting immune suppression and can support tumour progression by facilitating angiogenesis, invasion and metastasis (Ostrand-Rosenberg et al., 2012). However, there is no singular phenotype associated with TAMs, and macrophages in the tumour microenvironment can also have anti-tumour functions.

In tumours, the accumulation and suppressive activity of Tregs, MDSCs and TAMs is initiated by factors produced by the tumour and surrounding stromal cells. However, interactions between the suppressive cell populations exacerbate the development of the immunosuppressive environment. Regulatory cells within the tumour microenvironment function not only to tolerize the immune system to the tumour and subdue anti-tumour immunity but also have supportive functions for tumour development. Many of the immunosuppressive factors within the microenvironment are produced by multiple cell types in the tumour bed, and have numerous subsequent suppressive activities. IL-10 and TGFβ are a prime example – produced by tumour cells, stromal cells, Tregs, MDSCs and TAMS, they act on multiple immune cell types and promote the development of the same suppressive cells which produce them. This regulatory loop, with both redundant production of inhibitory factors and redundant downstream actions results in the orchestration of a self-promoting immunosuppressive environment, which is highly effective at shutting down attempts by the immune system to target tumour cells. In order to mount a successful anti-tumour immune response the effector cells must be able to overcome this immunosuppression.

1.5 Melanoma immunotherapy

The ability of the immune system to mount anti-tumour responses has been outlined. In reality, however, the immune system regularly fails to mount a sufficient response and overcome tumour-mediated immunosuppression. The underlying basis of immunotherapy, when applied to the treatment of cancer, is to potentiate the inherent anti-tumour responses and overcome immune suppression. New York surgeon William B. Coley pioneered the first attempt at cancer immunotherapy in 1891. After observing complete remission in a patient following acute infection with *Streptococcus pyogenes* Coley began treating patients with inoperable soft-tissue sarcomas with a streptococcal and bacillus bacterial preparation, which became known as "Coley's toxin". His results were first published in 1893 (Coley, 1893), and over 40 years he treated almost 900 patients with a cure rate of over 10% (Coley, 1910; Parish, 2003). Despite successes, Coley's toxin was not widely accepted scientifically or in the clinic, likely in part due to the dramatic fevers associated with treatment, perceived low cure rates and the lack of immunological understanding. Over 100 years have passed since Coley first attempted to treat cancer with immunotherapy and a greater understanding of the immune system has facilitated changing attitudes in favour of immunotherapy and yielded significant immunotherapeutic advancements. Recent clinical successes have demonstrated the potential of immunotherapy to change the treatment paradigm in many forms of cancer, but particularly in metastatic melanoma. The three main approaches to immunotherapy are adoptive cell transfer (ACT), immunomodulation through checkpoint blockade and active immunization using cancer vaccines.

1.5.1 Adoptive cell transfer

ACT involves the treatment of patients with autologous T cell populations that have been expanded *ex vivo*, and are then reinfused to traffic to and mediate destruction of the tumour. Traditionally, ACT involves the isolation of TILs from tumours, followed by expansion of tumour-specific T cell populations *ex vivo* with IL-2. Prior to the transfer of the expanded tumour-specific T cells, patients undergo lymphocyte depletion, which enhances persistence of the reinfused TILs by reducing systemic immunosuppression associated with advanced cancer. Reinfusion of T cells is often accompanied

by the administration of exogenous IL-2, to support T cell effector function and expansion. This approach has yielded some positive results. In a clinical trial of advanced metastatic melanoma patients TIL therapy achieved objective response rates of 49-72% and complete tumour regression in 22% of patients, which was shown to be durable (Rosenberg and Dudley, 2009; Rosenberg et al., 2011). Despite this success, the reasons for variation in patient responsiveness remain elusive, and naturally occurring TIL populations can currently only be isolated and expanded from melanoma. This has motivated the development of ACT approaches employing genetically engineered T cells to expand the reach of ACT therapy. Genetically engineering T cells has the ability to generate tumour reactive T cells with higher affinity and specificity for tumour antigens. A number of gene engineering techniques have been employed, with varying success. One approach centres on the cloning of TCRs with tumour specificity, and insertion of their genes into lentiviral or retroviral vectors, which are used to transfer the antigen specificity and avidity to autologous T cells from patients (Restifo et al., 2012). A second technique involves chimeric antigen receptors (CARs), which incorporate a single chain variable region of an antibody fused to intracellular TCR domains, resulting in antibody-like non-MHC-restricted specificity with the capability of T cell activation without co-stimulation (Rosenberg and Restifo, 2015). Genetic engineering of T cells for ACT therapy still faces a number of questions surrounding optimal T cell specificity, and which population of T cells to transduce. However, this represents a promising, albeit commercially challenging, immunotherapeutic approach.

1.5.2 Checkpoint blockade

Checkpoint blockade therapy targets regulatory pathways, known as immune "checkpoints", to unleash T cell responses, and has emerged as one of the most promising immunotherapeutic strategies. Immune checkpoint pathways maintain self-tolerance in normal tissues, but are hijacked by tumour cells to suppress anti-tumour immunity. Inhibitory immune signalling molecules that represent checkpoint blockade targets include the previously described CTLA-4, as well as programmed death 1 (PD-1) and PD-L1, T cell immunoglobulin and mucin-3 (TIM-3) and lymphocyte activation gene 3

(LAG-3) amongst others. Agents that block these targets are in various stages of preclinical or clinical development, with checkpoint blockade therapies targeting CTLA-4 and PD-1 currently approved for use in metastatic melanoma.

The anti-CTLA-4 antibody Ipilimumab was the first checkpoint blockade therapy to approved, with approval for use in the treatment of metastatic melanoma passed in the United States and Europe in 2011 following phase III clinical trials which achieved an overall survival benefit (Hodi et al., 2010; Robert et al., 2011). Ipilimumab is a human, monoclonal antibody that blocks the engagement of the inhibitory molecule CTLA-4. Clinically this can potentiate robust anti-tumour responses, which are durable with some responses lasting a decade or more. However, only a small proportion of patients respond to anti-CTLA-4 therapy, with tumour regressions (complete or partial) observed in 11% of patients (Schadendorf et al., 2015a). Interestingly, meta-analysis of Ipilimumab trials revealed durable increases in overall survival were achieved in approximately 20% of patients, double the number of patients with measurable tumour regression (Schadendorf et al., 2015b; Topalian et al., 2015).

Since the approval of Ipilimumab, the PD-1 blocking antibodies Nivolumab and Pembrolizumab have both received FDA-approval. Nivolumab is a fully human, anti-PD-1 monoclonal antibody, which achieved response rates of 24-40% and a 1-year survival rate of 62-73% (Robert et al., 2015a; Topalian et al., 2014). Pembrolizumab is a humanized monoclonal anti-PD-1 antibody and has demonstrated response rates of 26-38% in patients with metastatic melanoma (Hamid et al., 2013; Robert et al., 2014). The activity of these agents in patients pre-treated with Ipilimumab lead to both receiving accelerated FDA-approval, with Pembrolizumb approved in September 2014 and Nivolumab in December 2014 (Schadendorf et al., 2015a). PD-1/PD-L1 blockade has enhanced tumour specificity and reduced toxicity when compared to anti-CTLA-4 therapy. This translates into significantly increased response rates and overall survival, in addition to decreased adverse events when Pembrolizumab was compared head-to-head with Ipilimumab (Robert et al., 2015b). However, the majority of patients treated with anti-PD-1/PD-L1

only experienced partial tumour regressions and did not achieve objective responses (Topalian et al., 2015). The discovery of predictive biomarkers to identify cohorts of patients that will respond to checkpoint blockade therapy will be critical to treatment optimization and elucidating mechanisms that determine responsiveness. There is already some evidence that anti-PD-1 therapies achieve better responses in patients with tumours expressing PD-L1 (Topalian et al., 2015). The combination of anti-PD-1 and anti-CTLA-4 also appears to achieve increased response rates, although this was accompanied by elevated severity of adverse events (Postow et al., 2015). Combination of checkpoint blockade is likely to be increasingly favoured going forward, with new combinations being generated as new checkpoints are successfully targeted.

1.5.3 Vaccines

Therapeutic cancer vaccines are active drivers of anti-tumour immune responses, which aim to enhance anti-tumour immunity within the patient. There are a number of strategies for cancer vaccination including vaccination based on specific tumour-expressed antigens, dendritic cells or inactivated whole tumour cells.

1.5.3.1 Peptide vaccines

Peptide vaccines incorporate one or multiple short or long amino acid sequences from defined tumour antigens. One of the most common approaches involves the delivery of MHC class I restricted peptides to activate $CD8^+$ T cell responses. Peptides can be delivered alone or with adjuvants to increase immune responses to the associated antigens (Butterfield, 2015). Due to the difficulty in identifying neoantigens, which are patient-specific, peptide vaccines usually target more frequently expressed self-antigens, such as MAGE-1 and MART-1. Targeting self-antigens requires overcoming T cell tolerance and as such has had difficulty in achieving tumour responses. Meta-analysis of 323 patients treated with peptide vaccines derived from melanoma differentiation antigens or cancer-testis antigens

showed nine patients achieved a partial response and two patients a complete response, with an overall objective response rate of 2.9% (Rosenberg et al., 2004). These disappointingly low objective response rates indicate major limitations of peptide vaccines as single agent therapies. However, optimal adjuvants and peptide combinations are still being identified and such optimisation may enhance outcomes in the future. Peptide based approaches still hold strong appeal due to the simplicity and low manufacturing costs associated with peptide production, as well as the ability for large-scale manufacture and ease of transport and storage.

1.5.3.2 Dendritic cell vaccines

Vaccination strategies involving dendritic cells cultured and primed *ex vivo* have been developed due to the crucial role DCs play in initiating immune responses and their outstanding capacity to induce effective T cells responses. DC based cancer vaccines have particular merit when tumour antigens are poorly immunogenic and have the advantage of bypassing the induction of immune tolerance associated with tumour-mediated immunosuppression. Generally, autologous DCs are harvested and cultured *ex vivo* with adjuvant and peptides for known tumour antigens or patient-derived antigens/tumour lysate. Matured, immunogenic DCs loaded with tumour antigens are then reinfused back in to the patient. The first major success for DC-based vaccines was achieved with the 2010 FDA-approval of 'Sipuleucel-T' for the treatment of metastatic prostate cancer (Palucka and Banchereau, 2012). Dendritic cell vaccines have also been trialled rigorously for metastatic melanoma. Analysis of several DC vaccine trials in metastatic melanoma, which had a combined total of 1250 patients, revealed an 8.5% objective response rate (Anguille et al., 2014). This objective response rate is comparable to that achieved with Ipilimumab treatment for metastatic melanoma. DC vaccines also proffer additional advantages such as increasing the diversity of neoantigen-specific T cells in melanoma (Carreno et al., 2015). The implementation of next-generation dendritic cell vaccines with improved immunostimulatory activity has improved immunogenicity. The potential to augment efficacy through combination of DC vaccines with other cancer therapies is likely to be a focus of future DC vaccine development (Anguille et al., 2014).

1.5.3.3 Whole tumour cell vaccines

One of the major challenges associated with anti-tumour vaccines is the selection of the appropriate antigen or antigens, to evoke a strong and tumour-specific immune response. It has been previously shown that neoantigens are more immunogenic than self-antigens, however immunotherapeutic targeting of these unique peptides has been difficult as they are highly variable between patients (Schumacher and Schreiber, 2015). The majority of immunotherapies favour use of conserved tumour associated antigens, such as MAGE, which are often poorly immunogenic due to peripheral tolerance. Sequencing a tumour sample to identify patient specific neo-antigens, performing algorithm based analysis of peptide:MHC binding and identifying immunogenic targets is a lengthy and expensive process, taking more time than is feasible in the treatment of cancer patients. Using whole tumour cells, irradiated or otherwise inactivated, as the basis for anti-tumour vaccines makes it possible to target neoantigens, circumventing the need for identification of antigenic expression and selection of target antigens. Instead, whole tumour cell vaccines stimulate the immune system against a complement of tumour-expressed antigens, likely including both neoepitopes and tumour-associated antigens, with both $CD4^+$ and $CD8^+$ T cell reactivity.

Autologous whole tumour cell vaccines, including irradiated IFNγ and IFNβ-treated B16.F10 and irradiated GM-CSF-transfected B16 have demonstrated strong anti-tumour efficacy with the induction of CTL responses in mouse models of melanoma (Dezfouli et al., 2003; Dranoff et al., 1993; Scheffer et al., 2003). These are just a few examples of the success of a variety of autologous tumour cell vaccine preparations in pre-clinical models of melanoma. To elicit strong immune responses, whole-tumour cell vaccines require an adjuvant to induce appropriate activation of DCs (Finn, 2003). In clinical trials, several whole tumour cell vaccines with different adjuvants have been shown to elicit strong anti-tumour immune responses in melanoma patients (Baars et al., 2000; Berd et al., 2004; Janetzki et al., 2000; Soiffer et al., 1998). Numerous patients demonstrated expansion of tumour-specific CTLs as well as tumour infiltration with NK cells, DCs and macrophages. However, as a result of the single arm trial designs it is difficult to form conclusions about the effects of

vaccination on overall survival, due to lack of a control arm. When compared to historical controls, whole tumour cell vaccination in the studies by Baars and by Berd improved patient 5-year survival rates (de Gruijl et al., 2008). Additionally, the use of allogeneic tumour cells as the basis for whole tumour cell vaccines has also shown benefit in pre-clinical mouse models (Ward et al., 2002) and bypasses the difficulty associated with producing personalised whole tumour cell vaccines on a patient-by-patient basis. These whole tumour cell vaccine approaches represent a promising avenue of immunotherapy with strong pre-clinical and early clinical work supporting their efficacy. As with other immunotherapies, future use of whole tumour cell vaccines is likely to focus on combination therapy approaches. The ability of whole tumour cell vaccines to provide positive stimulation of the immune system against a complement of tumour antigens is likely to be highly beneficial in combination therapy approaches.

1.6 Rationale for combination of BRAF inhibitor treatment with immunotherapy

The last five years have seen significant advances in treatment of metastatic melanoma. The approval of new mechanism-based therapies has shifted the treatment paradigm away from non-specific cytotoxics to more targeted, and effective treatments. Despite this substantial improvement limitations of the new therapeutics have been revealed and the long-term prognosis remains poor for many patients. BRAF inhibitor treatment achieves high initial response rates with rapid, dramatic responses, but effects are short-lived. In contrast, immunotherapies deliver durable responses but only in a small subset of patients. To achieve improved clinical outcomes in metastatic melanoma it is now widely accepted that it is going to be essential to combine therapies. One promising approach is the combination of Vemurafenib and immunotherapy.

Chemotherapy-induced tumour cell death generally occurs via apoptosis, and numerous studies have shown that apoptotic tumour cell death can be highly immunogenic as determined by calreticulin exposure (Obeid et al., 2007;

Zitvogel et al., 2010). Chemotherapy has also been shown to enhance tumour immunogenicity and increase the susceptibility of tumour cells to CTL-mediated killing with immunotherapy (Giampietri et al., 1981; Ramakrishnan et al., 2010). This suggests that Vemurafenib-induced apoptosis may play an immunostimulatory role. Furthermore, the potential of Vemurafenib to cause rapid tumour regression is associated with a window of decreased tumour-mediated immune suppression, and release of large amounts of tumour antigens (Vanneman and Dranoff, 2012). This would generate a favourable environment for anti-tumour immunity, providing the opportunity for immunotherapy to achieve potent effects. Thus, Vemurafenib is expected to be immune-stimulating and, unlike traditional chemotherapies, does not induce lymphopaenia, due to its targeted nature. Additionally, the combination of Vemurafenib and immunotherapy has the potential to prevent the development of acquired BRAF inhibitor resistance by targeting tumour cells more broadly and increasing the likelihood of tumour cytotoxicity. The complementary strengths and weaknesses in response rates and response durability, in addition to the potential for synergy provide a strong rationale for combining Vemurafenib and immunotherapy.

1.7 Impact of BRAF inhibitor treatment on immune cells

To inform optimal combination of BRAF inhibition and immunotherapy, the direct effects of BRAF inhibitors on immune cells must first be elucidated. It was initially assumed that mutant BRAF-targeted inhibitors would have no impact on the function of cells of the immune system. However, the discovery that PLX4720 and Vemurafenib interact with wild-type BRAF and CRAF to alter the growth characteristics of $BRAF^{WT}$ melanocytes or melanoma cells suggests these inhibitors may also modulate immune cell function.

1.7.1 BRAF inhibitor effects on tumour antigenicity

BRAF inhibition has been shown to increase the expression of tumour differentiation antigens in some pre-clinical models and in patient-derived

cell lines and tumour samples. PLX4720 treatment of several $BRAF^{V600E}$ human melanoma cell lines, including SK-mel-28, resulted in upregulation of MART-1 expression and of MHC Class I expression (Boni et al., 2010). Vemurafenib treatment of human $BRAF^{V600E}$ melanoma cell lines enhanced MHC I and MHC II expression induced by IFNγ. However, MHC upregulation with BRAF inhibitor treatment was specific to $BRAF^{V600E}$ homozygous cell lines such as SK-mel-28 and A375 but did not occur in $BRAF^{V600E}$ heterozygous cell lines including SK-mel-5 (Sapkota et al., 2013). Similar findings were observed in *ex vivo* patient samples with Vemurafenib treatment *in vitro* of short-term cultured mutant-$BRAF^{V600}$ cell lines increasing tumour-associated antigen expression. Increased antigenicity was correlated with upregulation of genes in the MHC I presentation pathway (Donia et al., 2012b). These effects were confirmed *in vivo* with patient biopsies showing increased MART-1, gp100, Tryp-1 and Tryp-2 expression after 10-14 days of Vemurafenib treatment, when compared to baseline biopsies (Frederick et al., 2013). In contrast, Koya and colleagues demonstrated that Vemurafenib treatment had no effect on gp100 antigen expression or MHC I expression in the SM1 murine melanoma cell line (Koya et al., 2012). Although it is possible SM1 may be heterozygous for the $BRAF^{V600E}$ mutation, no information is available detailing this. However, heterozygosity would be consistent with SM1 having a relatively high IC50 of 14 μM for Vemurafenib. Thus, these data may confirm that $BRAF^{V600E}$ homozygous cell lines are susceptible to BRAF inhibitor-induced antigen expression whilst heterozygous cell lines are not. The underlying mechanisms of BRAF inhibitor-stimulated upregulation of melanoma differentiation antigens remain to be fully elucidated. Overexpression of oncogenic BRAF has been demonstrated to suppress MHC I expression (Sapkota et al., 2013), accordingly BRAF inhibition directly reverses this suppression. It has been postulated that a similar mechanism is at play with oncogenic BRAF suppressing antigen expression (Ott and Bhardwaj, 2013), however this remains to be confirmed.

1.7.2 BRAF inhibitor effects on DCs

The direct effects of mutant BRAF inhibition on human monocyte derived DC (moDC) viability and function were investigated in two studies with different

inhibitors, Ott and colleagues used Vemurafenib (Ott and Bhardwaj, 2013), while Vella *et al*. used Dabrafenib (Vella et al., 2014). Both inhibitors were found to have no DC toxicity, with moDC viability unaffected when treated for 24-48 hours at concentrations of up to 2 μM Dabrafenib and 50 μM Vemurafenib. Dabrafenib, again at concentrations of up to 2 μM, was shown to have no effect on moDC cross-presentation of NY-ESO-1 complexes to antigen specific $CD8^+$ T cells, and no significant impact on lipopolysaccharide (Fong and Mosmann) activation of moDCs as measured by expression of the activation markers CD83, CD86 and human leukocyte antigen (Avruch et al.)-DR (Vella et al., 2014). Likewise, concentrations of up to 10 μM Vemurafenib had no effect on DC expression of CD40, CD83, CD86 or MHC, production of IL-12 or TNFα or on DC stimulation of T cell proliferation. However, treatment of moDCs with 50 μM Vemurafenib significantly inhibited IL-12 and TNFα production. The effect of this relatively high concentration of Vemurafenib on other read-outs of DC effector function was not assessed, with activation marker expression and T cell stimulation assays performed at lower Vemurafenib concentrations. Overall, these studies indicate that BRAF inhibitors have no impact on human moDC viability or effector function at concentrations of up to 10 μM, however at 50 μM there is evidence that Vemurafenib can negatively impact DC function.

In addition to the direct effects of BRAF inhibition on DC viability and function, DC function in relation to melanoma-mediated immune suppression has been investigated with BRAF inhibitors. The tumour microenvironment contains immunosuppressive factors, produced by tumour cells or stromal cells, which maintain DCs in the immunosuppressive, immature state favourable to tumour progression as shown by Sumimoto and colleagues in an *in vitro* human $BRAF^{V600E}$ melanoma model. Culture of immature moDCs with A375 supernatant resulted in reduced IL-12 and TNFα production by DCs following LPS maturation. Thus, exposure of immature DCs to melanoma-produced factors led to compromised DC maturation. This inhibitory effect was attributed to A375 cells producing immunosuppressive cytokines VEGF, IL-6 and IL-10. Pre-treatment of the A375 cells with RNA interference (RNAi) specific for $BRAF^{V600E}$ reversed the suppressive activity on DCs and reduced production of immunosuppressive cytokines (Sumimoto et

al., 2006). These results were supported by a separate study conducted by Ott and colleagues, using human melanoma-DC co-cultures (Ott et al., 2013). Both $BRAF^{V600E}$ and WT cells were co-cultured with immature moDCs following which moDCs were matured with polyI:C. Co-culture with melanoma cells inhibited DC production of IL-12 and TNFα, and resulted in reduced expression of the activation markers CD80, CD83 and CD86. Similar to the Sumimoto study, melanoma inhibition of DC effector function was not cell-contact dependent. However, the soluble suppressive factor could not be identified. Pre-treatment of the melanoma cell lines with Vemurafenib for 24 hours prior to co-culture partially reversed the inhibitory effects of $BRAF^{V600E}$ but not $BRAF^{WT}$ cells, restoring DC cytokine secretion and partially restoring activation marker expression (Ott et al., 2013). BRAF inhibition by both RNAi and Vemurafenib treatment did not result in melanoma cell death. Therefore, abrogation of DC suppression was a direct effect of reduced production of suppressive factors by melanoma cells. Together, these data indicate that constitutive activation of the MAPK pathway in $BRAF^{V600E}$ melanoma cells can suppress DC function through immunosuppressive soluble mediators, which can be overcome by inhibition of mutant BRAF.

1.7.3 BRAF inhibitor effects on T cells

Increased antigen expression and promotion of immunogenic DC function associated with BRAF inhibition will indirectly enhance T cell response to tumours. Boni and colleagues investigated the direct and indirect effects of BRAF inhibition *in vitro* using PBMCs isolated from melanoma patients (Boni et al., 2010). At concentrations of up to 10 μM, PLX4720 had no effect on T cell viability or proliferation, and did not directly impact T cell secretion of IFNγ in response to target antigens. However, treatment of a co-culture of target melanoma cells and T cells with PLX4720 resulted in increased T cell IFNγ production. This was attributed to a response to the increased expression of MART-1 on melanoma cells and not a direct effect on T cells. Similarly, Vemurafenib increased tumour recognition by T cells in an *in vitro* system using patient short-term cell lines and autologous TILs. However, this was directly attributed to increased MDA expression since melanoma cells were

pre-treated with minimal exposure of T cells to BRAF inhibitors (Donia et al., 2012b). Thus, in an indirect manner, BRAF inhibitors can augment T cell recognition of tumour cells.

BRAF inhibition has also been shown to induce increased tumour infiltration by T cells. In xenograft models of human melanoma, PLX4720 has been shown to promote tumour infiltration of adoptively transferred antigen-specific T cells. Enhanced T cell infiltration was specific for $BRAF^{V600E}$ tumours, with no increase of TILs in $BRAF^{WT}$ tumours, and was attributed to decreased melanoma production of VEGF (Liu et al., 2013). Improved T cell infiltration of tumours has also been demonstrated in patients, with tumour biopsies showing increased numbers of $CD8^+$ T cells after 10-14 days of Vemurafenib treatment when compared to baseline. Increased $CD8^+$ T cell infiltration of tumours was accompanied by significantly higher expression of markers of cytotoxicity, with T cells demonstrating greater production of granzyme B and perforin (Frederick et al., 2013), although as has already been described, patient tumour samples exhibited increased melanoma antigen expression. Therefore, increased T cell infiltration and augmented effector function is potentially a result of both higher melanoma antigen expression and improved T cell recognition of tumours. Nonetheless, increases in TILs are not consistently observed with BRAF inhibitor treatment. In an inducible murine model of $BRAF^{V600E}$ melanoma, a decreased frequency of tumour resident T cells, NK cells, macrophages and MDSCs was observed following PLX4720 administration (Hooijkaas et al., 2012a). Ho and colleagues confirmed this finding in an independent study, which used a similar but independently developed mouse model of inducible $BRAF^{V600E}$ melanoma. Their results demonstrated no change in the frequency of effector TILs following PLX4720 treatment, but revealed increased $CD4^+$ T cell expression of the effector molecules CD40L and IFNγ. Although effector T cell infiltration remained unaltered with PLX4720, reduced accumulation of Tregs and MDSCs was detected making it difficult to delineate if the increased CD4 effector functionality was a direct result of BRAF inhibition or a product of a less suppressive microenvironment (Ho et al., 2014).

In addition to these ancillary effects of BRAF inhibitors on T cells, the direct impact of BRAF inhibition on T cell function has also been investigated. Dabrafenib treatment of human peripheral blood monocytes (PBMCs) in *in vitro* cultures demonstrated no direct cytotoxicity (Vella et al., 2014). There was also no effect on $CD4^+$ or $CD8^+$ T cell proliferation or effector functions as measured by IFNγ and IL-17 or IFNγ and TNFα production respectively (Vella et al., 2014). The effects of Vemurafenib in similar conditions were investigated by Comin-Anduix and colleagues, who showed Vemurafenib decreased viability of resting PBMCs with an IC_{50} of between 50 and 150 μM (variation in individuals was observed). Activated lymphocytes showed increased resistance to cytotoxic effects with no inhibition of viability, no effect on cell cycle progression and no induction of apoptosis at concentrations of up to 250 μM. At 50 μM increased pERK1/2 was detected in both $CD4^+$ and $CD8^+$ T cells but not in $CD20^+$ B cells. IFNγ, IL-5 and IL-10 release by $CD4^+$ T cells in response to specific antigen recognition were unaffected at 1 and 10 μM Vemurafenib but were significantly decreased with 50 μM treatment, although CTL-mediated killing was unaltered (Comin-Anduix et al., 2010). Although the variation in drug concentrations makes it difficult to directly compare these results, the data indicate there may be a differential impact of Dabrafenib and Vemurafenib treatment when directly assessing T cell effects.

The disparity in the effects of Dabrafenib and Vemurafenib on T cells has also been observed *in vivo.* A study by Schilling and colleagues evaluated the peripheral lymphocyte populations of 65 Dabrafenib-treated and 277 Vemurafenib treated patients. Dabrafenib was found to have no effect on peripheral lymphocyte numbers, whilst Vemurafenib treatment was associated with a significant decrease of 24.3% in the total numbers of peripheral lymphocytes. This reduction was related to a selective decrease in $CD4^+$ T cells, with $CD8^+$ T cell and B cell numbers remaining unaffected, while NK cell numbers increased (Schilling et al., 2014). In contrast, in clinical trials of Vemurafenib, no lymphopaenia was observed. It is possible that the decrease in lymphocyte numbers measured in the study by Schilling *et al*. may have been subclinical. Alternatively, there may be variation between patients, or patient groups. Further confirmation of this study-to-study

variation is evident in the effects observed by Gargett and colleagues. In contrast to the work by Comin-Anduix and Vella, these authors did not report differential effects of Dabrafenib and Vemurafenib treatment. This study directly compared the effects of Dabrafenib and Vemurafenib on T cell viability, activation and proliferation *in vitro* using healthy human PBMCs and T cells transduced with a tumour-specific CAR (Gargett et al., 2015). Cell growth, as measured in an ATP assay of unstimulated PBMCs and CAR T cells, was found to be unaffected by both inhibitors, with an IC50 ≥ 150 μM. In contrast to the results of Comin-Anduix *et al*., stimulated PBMCs showed increased sensitivity with IC50s ranging from 11-53 μM with Dabrafenib or 6-42 μM with Vemurafenib, the variation depending on the method of stimulation. Both drugs at 50 μM significantly inhibited activation, as determined by CD25 expression, and proliferation, and Vemurafenib demonstrated some inhibition at 5 μM. Overall, both Vemurafenib and Dabrafenib had similar ability to adversely affect T cell viability and activation, although T cells may be more sensitive to Vemurafenib (Gargett et al., 2015). Collectively, these studies indicate variability in the effects of BRAF inhibition on T cells. It appears Vemurafenib is more likely than Dabrafenib to have T cell selective inhibitory effects, which may be specific to $CD4^+$ T cells and are highly concentration dependent.

Despite the detrimental effects to T cells observed at relatively high inhibitor concentrations, it appears Vemurafenib and PLX4720 can have paradoxical effects with augmentation of T cell responses reported at lower concentrations. Callahan and colleagues demonstrated that PLX4720 could significantly increase *in vitro* T cell activation as determined by CD69 expression. The augmented T cell activation was shown to be a direct result of BRAF inhibitor potentiation of MAPK signalling, as indicated by increased pERK expression. This PLX4720 enhanced T cell activation was concentration-dependent, with beneficial effects evident in a dose range of 500 nM to 20 μM, with greatest CD69 and pERK expression detected at 5 μM and 2 μM respectively (Callahan et al., 2014). These findings were confirmed by Irving and colleagues who also demonstrated that PLX4720 enhanced TCR-driven proliferation *in vitro*. The same stimulatory effect was evident *in vivo* when BRAF inhibition was combined with vaccination for the treatment of BRAF

wild-type tumours (Irving et al., 2013). Collectively the current literature demonstrates that Vemurafenib and PLX4720 treatment can have indirect effects, which support anti-tumour T cell immunity, with enhanced tumour antigen expression and DC activation stimulating greater T cell recognition of tumours. The direct effects of both PLX4720 and Vemurafenib on T cell responses appear to be paradoxical, with variation observed between models and patients, and concentration dependent effects.

1.7.4 BRAF inhibitor effects on melanoma-mediated immune suppression

In addition to stimulating anti-tumour immunity, BRAF inhibitors can diminish the immune suppression associated with the tumour microenvironment. IL-6, IL-10 and VEGF play and immunosuppressive role in the tumour microenvironment, and BRAF inhibition has been shown to decrease $BRAF^{V600E}$ melanoma production of these factors *in vitro* (Sumimoto et al., 2006). Similar findings have been demonstrated in patients, with biopsies following Vemurafenib treatment exhibiting decreased levels of the immunosuppressive cytokines IL-6 and IL-8 when compared to pre-treatment biopsies, although no change was observed in IL-10 and TGFβ production (Frederick et al., 2013). BRAF inhibition not only reduces immune suppression by abrogating production of suppressive factors but also decreases the frequency of regulatory cell types. This has been demonstrated pre-clinically in an inducible model of $BRAF^{V600E}$ melanoma in two independent studies. Steinberg and colleagues demonstrated that PLX4720 selectively decreased numbers and proportions of Tregs within the tumour after 10 days of treatment. This reduction in Tregs was not a result of reduced recruitment or increased conversion of Tregs to an alternate T helper subset. Rather, PLX4720 promoted loss of pre-existing Tregs through the induction of apoptosis. The numbers and frequencies of intratumoural MDSCs were also depleted with PLX4720 treatment, however this was not attributed to apoptosis and the underlying mechanism was not identified. In addition to a decreased MDSC population, the myeloid cells isolated from PLX4720-treated tumours have diminished suppressive function *in vitro* when compared to those from untreated tumours (Steinberg et al., 2014). Ho *et al*. demonstrated

similar findings with reduced accumulation of Tregs and MDSCs within tumours following PLX4720 treatment. However, their data showed the decreased frequency of Tregs was a result of reduced recruitment or formation of inducible Tregs within the tumour. Likewise, the reduced proportions of MDSCs were attributed to decreased recruitment, which was IFNγ-dependent (Ho et al., 2014). Furthermore, a decrease in patient MDSCs has been reported following BRAF inhibition. Schilling and colleagues demonstrated detectable populations of monocytic-MDSCs (moMDSCs) and granulocytic-MDSCs (grMDSCs) within the PBMCs of patients with progressive melanoma. These peripheral MDSC populations suppressed autologous T cell proliferation *in vitro.* Following Vemurafenib treatment, patients had decreased frequencies of MDSCs within the blood, although the effect on intratumoural MDSCs could not be assessed (Schilling et al., 2013). Collectively, these studies demonstrate that BRAF inhibition ameliorates tumour-mediated immune suppression by reducing the production of soluble suppressive mediators and neutralizing immunosuppressive cell types.

1.8 Combining Vemurafenib with immunotherapy

The improved immune recognition and targeting of tumours evoked by BRAF inhibitor therapy, and diminished immunosuppression, suggest it may be possible to achieve synergy when combining BRAF inhibition with immunotherapies. Enhanced anti-tumour responses with BRAF inhibition and immunotherapy have been demonstrated in a number of pre-clinical models of melanoma. Koya and colleagues investigated combination of Vemurafenib and ACT in the SM1 model, using both C57BL/6 splenocytes transduced with the OTI TCR, which is specific for ovalbumin (OVA), in the SM1.OVA model and gp100 specific "pmel" in T cells in non OVA-expressing SM1. With both types of ACT, combination with Vemurafenib provided significantly increased anti-tumour activity and prolonged survival when compared to single-agent treatments. The mechanism of synergy was investigated using pmel ACT, in combination with Vemurafenib there was no change detected in T cell distribution or expansion of adoptively transferred cells. Furthermore, no increase in tumour antigen expression was evident.

The increased efficacy of combination therapy was attributed to increased cytotoxic effector functions of TILs, with Vemurafenib treatment increasing antigen-specific IFNγ production by adoptively transferred cells (Koya et al., 2012). Hu-Lieskovan performed a similar study using the SM1 model and pmel ACT with the addition of BRAF inhibition using Dabrafenib. Combination of pmel ACT with Dabrafenib improved anti-tumour responses, as evidenced by a decrease in tumour growth. This combination therapy was associated with improved homing of effector T cells to the tumour and increased proportions of TILs. However, increased frequencies of intratumoural MDSCs, tumour associated macrophages and Tregs were also observed (Hu-Lieskovan et al., 2015). The benefit of Dabrafenib and pmel ACT combination was less striking than the synergy observed by Koya *et al.* with Vemurafenib. Perhaps the significant increase in suppressive cells within the tumour could have accounted for the sub-optimal efficacy of Dabrafenib combination. Combination of pmel ACT with PLX4720 was also investigated in xenograft models of human melanoma by Liu and colleagues, as previously mentioned. Combined therapy significantly enhanced anti-tumour activity resulting in reduced tumour size and prolonged survival. This increased efficacy was attributed to PLX4720 decreasing VEGF production by melanoma cells and inducing a less suppressive microenvironment. In patients, BRAF inhibition has also been demonstrated to cause downregulation of VEGF, which correlated with increased $CD8^+$ TIL (Liu et al., 2013).

Pre-clinical studies of BRAF inhibition with immunotherapy have not been limited to combination with adoptive T cell therapy: combined therapy with checkpoint blockade has also been examined. Cooper and colleagues developed a cell line from a tumour in an inducible $BRAF^{V600E}$ model, and investigated PLX4720 in combination with anti-PD-1 or anti-PD-L1. Both approaches improved therapy responses as measured by slowed tumour growth and significantly increased survival, with the benefit more pronounced when PLX4720 and anti-PD-L1 were administered together. In both combinations there was a significant increase of $CD3^+$ TILs, predominantly $CD8^+$ T cells, and this was accompanied by an improved ratio of CTLs to Tregs. With PLX4720 combination with anti-PD-1, but not anti-PD-

L1, increased CTL effector function was detected with increased proportions of $CD8^+$ T cells expressing Granzyme B, IFNγ and TNFα (Cooper et al., 2014).

With pre-clinical evidence suggesting BRAF inhibition may enhance anti-tumour immunity and independent mechanisms of action with minimal overlapping toxicities, Vemurafenib and Ipilimumab combination was progressed to a Phase I clinical trial. Initially the first six patients received both treatments at their maximum tolerated doses, with 960 mg of Vemurafenib given orally, twice daily and Ipilimumab delivered at 3 mg/kg every three weeks. However, this first cohort of patients experienced dose-limiting toxic effects involving grade 3 elevation of hepatic enzymes. The second cohort of patients was enrolled on a lower dose of Vemurafenib (720 mg twice daily, orally), with the Ipilimumab dose remaining the same as the original schedule. The first four patients treated in the second cohort also developed dose-limiting liver toxicities with grade 2 and grade 3 elevation in liver enzymes; thus the remaining two patients received single agent Vemurafenib. Following the significant hepatotoxicities associated with combination treatment the trial was closed to further patient accrual (Ribas et al., 2013). Despite the unanticipated, adverse side effects, there is some evidence that the combination of BRAF inhibition and anti-CTLA-4 synergized to achieve enhanced tumour-specific, immune responses. In addition to exploring BRAF inhibitor combination with checkpoint blockade in pre-clinical models, Cooper *et al.* analysed tumour biopsies from a single patient who received combination Ipilimumab and Vemurafenib as part of the phase I clinical trial. Combination treatment enhanced tumour infiltration of $CD8^+$ T cells, and achieved increased intratumoural $CD8^+$ T cell:Treg ratio. These parameters of improved anti-tumour immunity were detected out to 132 days after initiating Vemurafenib therapy, which was the final biopsy time point, indicating durable anti-tumour immune responses (Cooper et al., 2014). The immunological outcome of combination therapy in this patient supports the hypothesis that BRAF inhibitors may enhance immune cell function to synergize with checkpoint blockade. However, the severe, unexpected toxicities reinforce the need for rigorous pre-clinical investigation and carefully conducted clinical trials of BRAF inhibitor and immunotherapy combinations.

1.9 Aims

Collectively, the literature discussed so far demonstrates that while many recent breakthroughs have been made in the treatment of metastatic melanoma, further progress is required due to mutant-BRAF inhibitor resistance and low response rates to single-agent immunotherapy. Given the complementary mechanisms of action there is potential for mutant-BRAF inhibitors to synergize with immunotherapy, which provides a strong rationale for combination of these approaches. This potential has been realized in pre-clinical models combining adoptive cell transfer with BRAF inhibition, but has yet to be thoroughly investigated with other immunotherapeutic approaches. The unsuccessful attempt to combine checkpoint blockade and BRAF inhibition at maximum tolerated doses in clinical trial highlights the requirement for comprehensive pre-clinical investigation of combination therapies. There is a need for exploration of alternative immunotherapeutic approaches to be combined with BRAF inhibitors, with optimizing dose and sequence of treatments likely to play a pivotal role in the success of combination therapy. The variation reported in effects of BRAF inhibitors on T cell viability, proliferation and function also indicates the need for further clarification of the direct effects BRAF inhibitors have on immune cells.

1.9.1 Specific Aims

The research undertaken for this thesis sets out to achieve the following specific aims:

- To assess the effects of mutant BRAF inhibitors on both human and murine T cell viability and responses *in vitro.*

- To determine the effects of mutant BRAF inhibition on antigen-specific immune responses *in vivo*, and on anti-tumour immune responses *in vivo* in a BRAF wild-type model of melanoma.

- To optimize a mouse model of syngeneic, transplantable $BRAF^{V600E}$ melanoma, and develop a sub-optimal autologous whole tumour cell vaccine.

- To investigate whether vaccination can complement the anti-tumour effects of mutant BRAF-targeted inhibitors in a murine model of $BRAF^{V600E}$ melanoma. Subsequently, lymphocyte infiltration of tumours and local lymphoid tissues will be explored to determine the effects of therapy on immune cell populations.

CHAPTER 2: Materials and Methods

2.1 Materials

2.1.1 Labware

Product	Supplier/Distributor
Axygen Micro Tubes 1.7 mL	Axygen Scientific Inc., Union City, CA, USA
BD 1 mL tuberculin syringes	BD Biosciences, Bedford, MA, USA
BD Falcon 5 mL polystyrene round-bottom tubes with cell-strainer caps	BD Biosciences, Bedford, MA, USA
BD Falcon polypropylene 15 and 50 mL conical tubes	BD Biosciences, Bedford, MA, USA
BD Falcon tissue culture-treated 175 cm^2 Flasks	BD Biosciences, Bedford, MA, USA
BD Falcon Polystyrene tissue culture plates: 6, 12, 24 & 96-well plates and 96-well U-bottom plate	BD Biosciences, Bedford, MA, USA
Corning Costar 50 mL reagent reservoirs	Sigma-Aldrich, St. Louis, MO, USA
Corning Costar serological pipettes (5, 10 and 25 mL)	Sigma-Aldrich, St. Louis, MO, USA
Eppendorf tubes (0.5, 1.7 and 2 mL)	Sigma-Aldrich, St. Louis, MO, USA
Feeding needles 18 gauge (G)	Thermo Fisher Scientific, Auckland, NZ
Nunc™ cell culture-treated 25 cm^2 and 75 cm^2 Flasks	Thermo Fisher Scientific, Auckland, NZ
Nylon Cell Strainers (70 μM)	BD Biosciences, Bedford, MA, USA
Nylon Gauze (70 μM)	Sefar Filter Specialist, Nelson, NZ
Pasteur pipetters (Sterile, 1 mL)	Interlab, Wellington, NZ
PrecisionGlide™ Needles (25 and 27.5 G)	BD Biosciences, Bedford, MA, USA
Disposable carbon steel surgical blades	Swann-Morton, Sheffield, UK
Plastic 10 mL vaccutainers with spray-coated EDTA	BD Biosciences, Bedford, MA, USA

2.1.2 Reagents and Buffers

2.1.2.1 Cell culture reagents and buffers

Product	**Supplier/Distributor**
5-(and-6)-carboxyfluorescein diacetate, succinimidyl ester (CFSE)	Molecular Probes, Invitrogen, OR, USA
Brefeldin A	BioLegend, San Diego, CA, USA
Bovine serum albumin (BSA)	ICP Biologicals, New Zealand
Carboxymethylcellulose (CMC)	Sigma-Aldrich, St. Louis, MO, USA
Collagenase Type IV from *Clostridium histolyticum*	Sigma-Aldrich, St. Louis, MO, USA
CompBead anti-mouse Ig, κ /Negative Control Compensation Particles Set	BD Biosciences, Bedford, MA, USA
CompBead anti-rat/hamster Ig κ /Negative Control Compensation Particles Set	BD Biosciences, Bedford, MA, USA
Dimethyl sulfoxide (DMSO)	Sigma-Aldrich, St. Louis, MO, USA
Dimethylformamide (DMF)	Thermo Fisher Scientific, Auckland, NZ
DNase I	Sigma-Aldrich, St. Louis, MO, USA
UltraPure 0.5 M, pH 8.0 Ethylenediaminetetraacetic acid (EDTA)	Invitrogen, Life Technologies, Auckland, New Zealand
Foetal Calf Serum (FCS)	Sigma-Aldrich, St. Louis, MO, USA
Geneticin® Selective Antibiotic (G418)	GIBCO, Life Technologies, Auckland, New Zealand
Glacial Acetic Acid	Sigma-Aldrich, St. Louis, MO, USA
GlutaMAX™	GIBCO, Life Technologies, Auckland, New Zealand
Hanks Balanced Salt Solution (HBSS, 1.4 M NaCl, 5.3 mM KCl, 4.2 mM $NaHCO_3$, 0.44 mM KH_2PO_4, 0.34 mM NaH_2PO_4)	GIBCO, Life Technologies, Auckland, New Zealand
Human AB Serum – Heat Inactivated	GIBCO, Life Technologies, Auckland, New Zealand
Ionomycin	Sigma-Aldrich, St. Louis, MO,

	USA
Iscove's Modified Dulbecco's Medium (IMDM)	GIBCO, Life Technologies, Auckland, New Zealand
Liberase TL Research Grade	Roche, Mannheim, Germany
LymphoPrep	Axis-Shield, Norway
3-(4,5-dimethylthiazol-2-yl)-2,5-diphenyltetrazolium bromide (MTT)	Sigma-Aldrich, MO, USA
Mycoplasma PCR Detection Kit	Intron Biotechnology, Korea
M-Solution™ 1-2 Antibiotics	Intron Biotechnology, Korea
Ovalbumin (OVA)	Sigma-Aldrich, MO, USA
$OVA_{257-264}$ peptide (SIINFEKL)	GenScript, NJ, USA
Phorbol myristate acetate (PMA)	Sigma-Aldrich, MO, USA
Penicillin Streptomycin	Invitrogen, New Zealand
Dulbeccos Phosphate Buffered Saline (dPBS)	GIBCO, Life Technologies, Auckland, New Zealand
Red Blood Cell (RBC) lysis buffer	Sigma-Aldrich, MO, USA
RPMI-1640	GIBCO, Life Technologies, Auckland, New Zealand
Sodium Azide (NaN_3)	Sigma-Aldrich, MO, USA
Sodium dodecyl sulphate (SDS)	Sigma-Aldrich, St. Louis, MO, USA
Trypan blue (0.4% v/v)	GIBCO, Life Technologies, Auckland, New Zealand
TNFα	Peprotech, NJ, USA
Trypsin-EDTA (0.05%), phenol red	GIBCO, Life Technologies, Auckland, New Zealand

Complete IMDM (cIMDM)

IMDM was supplemented with 10% FCS, 2 mM Glutamax, 100 U/mL penicillin and 100 μg/mL streptomycin.

Complete RPMI (cRPMI)

RPMI was supplemented with 10% FCS, 2 mM Glutamax, 100 U/mL penicillin and 100 μg/mL streptomycin.

SDS lysing buffer

SDS and DMF were added to ddH_2O to concentrations of 10% SDS and 45% DMF. The pH was adjusted to 4.7 using glacial acetic acid. Lysing buffer solution was stored at room temperature.

Wurzburger buffer

EDTA, FCS and DNase I were added to 500 mL dPBS to give final concentrations of 1% FCS, 0.5 M EDTA and 0.02 mg/mL. Buffer was stored at 4 °C.

2.1.2.2 Enzymes

Collagenase IV

Lyophilized enzyme was reconstituted at 50 mg/mL in dPBS, aliquoted and stored at -20 °C.

DNase I

Lyophilized enzyme was resuspended in pre-warmed IMDM and agitated to reconstitute to a concentration of 10 mg/mL. Reconstituted enzymes were used stored at -80 °C.

Liberase TL

Lyophilized enzyme was stored at -20 °C for long-term storage. Prior to use enzymes were resuspended in pre-warmed IMDM and agitated to reconstitute to a concentration of 1 mg/mL. Reconstituted enzymes were used immediately or stored at -80 °C for up to three months.

2.1.2.3 Peptides/Antigens

α-Galactosylceramide (αGalCer)

αGalCer was manufactured by the Ferrier Research Institute, and was reconstituted in sterile dH2O at 0.5 mg/mL. Reconstituted αGalCer was stored a 4 °C.

OVA

OVA was reconstituted in sterile dH2O, creating a stock concentration of 50 mg/ml. Reconstituted stocks were stored in aliquots -80 °C.

SIINFEKL

SIINFEKL was dissolved in DMSO to give a stock concentration of 50 mM. Aliquots of reconstituted stocks were stored at -20 °C.

2.1.2.4 Cytokines

IFNγ

IFNγ was harvested from in-house X63-IFNγ hybridoma cultures and used neat.

Human recombinant Interleukin 2 (rIL-2)

rIL-2 under the brand name Proleukin was sourced from Prometheus Laboratories, Inc., San Diego, CA, USA. rIL-2 was aliquoted and stored at -80 °C.

TNFα

TNFα was reconstituted in dH_2O containing 0.1% BSA at 100 μg/mL. Aliquots were stored at -80 °C.

2.1.2.5 Purified Antibodies

Rat anti-mouse CD25 (Clone PC61)

Anti-mouse CD25 was affinity-purified in house from hybridoma culture supernatants using protein G-Sepharose columns.

Rat anti-mouse CD3 (Clone 2C11)

Anti-mouse CD3 was affinity-purified in house from hybridoma culture supernatants using protein G-Sepharose columns.

Rat anti-mouse CD16 (FcεRIII)/CD32 (FcεRII) (Clone 2.4G2)

Anti-mouse CD16 (FcεRIII)/CD32 (FcεRII) was affinity-purified in house from hybridoma culture supernatants protein G-Sepharose columns.

Hamster anti-mouse CD28 (Clone 37.51)

Anti-mouse CD28 was harvested from in house hybridoma cultures and used neat.

Mouse anti-human CD3ε

Lyophilized mouse anti-human CD3 epsilon MAb, clone UCHT1 (R&D systems, MN, USA) was reconstituted at 0.5 mg/mL in sterile dPBS and aliquoted. Aliquots were stored at 4 °C for short-term use (up to 1 month), or at -20 °C for long-term storage.

Mouse anti-human CD28

Lyophilized mouse anti-human CD28 MAb, clone 37407 (R&D systems, MN, USA) was reconstituted at 0.5 mg/mL in sterile dPBS and aliquoted. Aliquots were stored at 4 °C for short-term use (up to 1 month), or at – 20 °C for long-term storage.

2.1.2.6 Inhibitors

Etanercept

Etanercept (Enbrel®, Pfizer, NY, USA) was resuspended at 25 mg/mL in sterile water and stored at 4 °C in the dark.

PLX4720

PLX4720 was generously provided by Gideon Bollag, Plexxikon. PLX4720 powder was stored in the dark at room temperature long-term. For *in vitro* applications PLX4720 was dissolved in DMSO to give a stock solution of 100 mM, and aliquots were stored at -80 °C.

Sorafenib

Sorafenib (Sorafenib Tosylate, Selleck, TX, USA) was reconstituted in DMSO to give a stock solution of 100 mM and aliquots of stock were stored at -80 °C.

Vemurafenib

Vemurafenib was generously provided by Gideon Bollag, Plexxikon. Vemurafenib powder was stored in the dark at room temperature. For *in vitro* applications Vemurafenib was dissolved in DMSO to give a stock solution of 100 mM, aliquots were stored at -80 °C.

2.1.2.7 Flow cytometry reagents

Annexin V staining buffer

Annexin V 10x binding buffer (BD Biosciences, Bedford, MA, USA) was stored at 4 °C and diluted immediately prior to use 1:10 in dH_2O.

CFSE

CFSE was reconstituted at 10 mM in DMSO and stored at -20 °C.

DAPI

DAPI was reconstituted at 2 μg/mL in deionised (MilliQ) water, and vortexed to dissolve. DAPI was then aliquoted and stored at -20 °C for long-term storage, and at 4 °C for short-term storage.

Flow buffer (with Sodium Azide)

FCS, NaN_3 and EDTA were added to 500 mL dPBS to give final concentrations of 1% FCS, 0.01% NaN_3 and 2 mM EDTA. The buffer was stored at 4 °C.

Flow buffer (Sodium Azide free)

FCS was added to 500 mL dPBS to give a final concentration of 1%. The buffer was stored at 4 °C.

FoxP3 Transcription Factor Staining Set

The FoxP3 transcription factor staining set (Affymetrix, eBioscience San Diego, CA, USA) was stored at 4 °C. 4x Fixation/Permeabilization Concentrate was diluted 1:4 in Fixation/Permeabilization Diluent immediately prior to use. 10x Permeabilization Buffer was diluted 10-fold in dH_20 immediately prior to use, or diluted and stored at 4 °C.

2.1.2.8 Human flow cytometry antibodies

Specificity	Fluorophore	Clone	Supplier
CD3ε	APC-H7	SK7	BD Pharmingen
CD3	PE-Cy7	HIT3a	BioLegend
CD4	APC	RPA-T4	BioLegend
CD8	PE	HIT8a	BioLegend
CD69	AlexaFluor700 (AF700)	FN50	BioLegend
IgG isotype	-	-	Invitrogen

2.1.2.9 Murine flow cytometry antibodies

Specificity	Fluorophore	Clone	Supplier
Annexin V	APC	-	BD Pharmingen
CD1d	PE	1B1	BioLegend
CD3ε	BUV395	145-2C11	BD Horizon
CD3ε	FITC	145-2C11	BioLegend
CD3ε	PE	145-2C11	BD Horizon
CD3ε	PE-Cy7	145-2C11	EBioScience
CD4	APC-Cy7	GK1.5	BD Pharmingen
CD8α	Pacific Blue	53-6.7	BD Pharmingen
CD8α	PE-CF594	53-6.7	BD Horizon
CD11b	APC	M1/70	BioLegend
CD44	APC	IM7	BD Pharmingen

CD45	BV786	30-F11	BD Horizon
CD45.1	PE	A20	BioLegend
CD62L	PE	MEL-14	BD Pharmingen
CD279 (PD-1)	BV421	J43	BD Horizon
F4/80	BV605	BM8	BioLegend
FoxP3	FITC	FJK-16s	eBioscience
IFNγ	PE	XMG1.2	BioLegend
IgG1, κ, isotype control	BV421	RTK2071	BioLegend
I-A/I-E (MHC II)	PE-Cy7	M5/114.15.2	BioLegend
Ly6C	BV421	AL-21	BD Horizon
Ly6G	PE	1A8	BD Horizon
NK1.1	BV650	PK136	BD Horizon
PD-L1	BV711	MIH5	BD Horizon
TNFα	BV421	MP6-XT22	BioLegend
Vα2	APC	B20.1	BioLegend

2.1.2.10 Flow viability dyes

Name	**Source**
4',6-diamidino-2-phenylindole (DAPI)	Invitrogen, New Zealand
Live Dead Fixable Blue (LDFB)	Life Technologies

2.1.3 Cell lines

2.1.3.1 Human cell lines

The melanoma cells lines A375, SK-mel-5, LM-mel-15, LM-mel-34 and LM-mel-62 were obtained from frozen stocks of the Cancer Cell and Molecular Biology group, Malaghan Institute of Medical Research.

The LM-mel cell lines were originally obtained courtesy of the Ludwig Institute, Melbourne, Australia.

2.1.3.2 Murine cell lines

The melanoma cell lines B16 and B16.Ova were obtained from frozen stocks of the Cancer Cell and Molecular Biology Group, Malaghan Institute of Medical Research.

The primary murine melanoma cell lines YUMM1.1 and YUMM1.7 were generously provided by Associate Professor Marcus Bosenberg, Yale School of Medicine.

2.1.4 Mice

2.1.4.1 Maintenance and ethical approvals

Mice were either ordered from the Jackson Laboratory (Bar Harbour, ME, USA) or bred in the Biomedical Research Unit at the Malaghan Institute of Medical Research.

All mice were maintained in the Biomedical Research Unit of the Malaghan Institute of Medical Research.

Experimental procedures were performed with the approval of the Victoria University Animal Ethics Committee, and carried out according to institutional guidelines.

2.1.4.2 Mouse Strains

C57BL/6 mouse strain
C57BL/6 mice were from breeding pairs originally obtained from the Jackson Laboratory (Bar Harbour, ME, USA).

FoxP3 GFP mouse strain

The B6x(Foxp3$^{GFP\text{-}g2}$) mice, commonly referred to as FoxP3 GFP mice, have the eGFP construct knocked in to the first coding frame of the *Foxp3* gene. As a result this allele encodes a chimeric GFP-FoxP3 fusion protein (FoxP3^{GFP}) (Fontenot et al., 2005). These mice were from breeding pairs originally kindly provided by Prof. A Rudensky, University of Washington, USA.

B6.SJ-OTI mouse strain

The transgenic OTI mice (OT-I x B6.SJL-Ptprc^{a}Pepc^{b}/BoyJ) express the Vα2 Vβ5 T cell receptor designed to recognize OVA residues 257-264, rendering the majority of CD8^{+} T cells in the periphery OVA-specific (Hogquist et al., 1994). The breeding pairs for these mice were originally obtained with permission from of F. Carbone, Melbourne University, Australia.

B6Aa0 mouse strain

MHC Class II-deficient B6Aa^{0}/Aa^{0} (B6Aa0) mice initially generated by Köntgen and colleagues (Kontgen et al., 1993), were from breeding pairs originally obtained from the Biological Research Laboratories Ltd. Wolferstrasse 4, Switzerland.

TAP$^{-/-}$ mouse strain

TAP1 deficient (TAP$^{-/-}$) mice, which lack peptide transport to MHC Class I and thus are deficient in CD8^{+} T cell responses, were also used, and were initially generated by Van Kaer and colleagues (Van Kaer et al., 1992).

NOD/Scid mouse strain

NOD/Scid (severe combined immune deficiency on a non-obese diabetic background) mice, which have impaired T and B cell development (Schultz et al., 1995), were from breeding pairs initially obtained from the Hercus-Taieri Research Unit, University of Otago, New Zealand.

Mice strains were maintained by brother x sister mating. Mice between 6-14 weeks of age with gender-matched controls were used for all experiments.

2.2 Methods

2.2.1 Cell culture techniques

2.2.1.1 General cell culture

Cell culture took place in PC2 facilities at the Malaghan Institute of Medical Research, Wellington. Cell work was carried out in Class II (HERAsafe, Heraeus, Germany) biological safety cabinets with HEPA air filters. Cells were incubated in a humidified environment at 37 °C in 5% CO_2 (HERAcell incubator, Heraeus, Germany).

All tumour cell lines were grown cRPMI, except B16.Ova. B16.Ova cells were cultured in cIMDM containing 0.5 mg/mL Geneticin.

Tumour cells were passaged once they reached 70-80% confluence. Medium was removed and cells washed with sterile dPBS. To detach cells Trypsin-EDTA was added and cells were incubated for 2-4 minutes at 37 °C. Following detachment 7 mL complete medium was added to stop proteolysis and cells were washed and replated.

2.2.1.2 Harvesting adherent tumour cells

To harvest adherent tumour cells medium was removed from cultures and cells were washed with sterile dPBS. Trypsin-EDTA was added and incubated for 2-4 minutes at 37 °C. After cell detachment 7 mL medium was added to stop proteolysis. Cells were washed with complete medium and a single cell suspension was generated for subsequent use.

2.2.1.3 Mycoplasma testing

Cultured cells were tested every 3-6 months for mycoplasma contamination using the Intron Mycoplasma PCR Detection Kit, as per the manufacturer's

instructions. Cells were also tested for mycoplasma prior to freezing down to ensure frozen stocks were mycoplasma-free.

2.2.1.4 Mycoplasma treatment

Cell lines that tested positive for mycoplasma were treated with the M-Solution™ 1-2 Antibiotics, if no mycoplasma free stocks were available.

Cells were cultured in the presence of cRPMI containing M1 antibiotic (a Tiamutin-like antibiotic) for 4 days. Cells were then harvested, washed and replated in M2 antibiotic (a Minocycline derivative) for 3 days. This cycle was repeated twice. Cells were then cultured in antibiotic free media for a week before being re-tested. All contaminated cells were cleared through this process.

2.2.2 Cell isolation/purification

2.2.2.1 Isolation of human peripheral blood mononuclear cells (PBMCs) from whole blood

Blood was taken from healthy volunteers by a trained phlebotomist under the Malaghan Institute of Medical Research ethics approval. Blood was diluted 1:1 with sterile dPBS. Overlaying 8-10 mL of the diluted blood admixture on to 5 mL of Lymphoprep, in 50 mL conical tubes, isolated PBMCs. These overlays were centrifuged at 300 xg for 25 minutes with no brake at room temperature. The buffy coat was collected using transfer pipettes and transferred to 50 mL conical tubes. The buffy coat was washed by the addition of 20-40 mL serum-free RPMI (sfRPMI), after which it was centrifuged at 500 xg at room temperature for 5 minutes. The pellet was then washed twice with 10 mL sfRPMI.

PBMCs were frozen down in a 10% DMSO and 90% FCS solution, in a Nalgene® Mr. Frosty at -80 °C. PBMCs were then stored in liquid nitrogen.

2.2.2.2 Preparation of murine lymphocyte single cell suspensions

Blood

Lateral tail vein bleeding was performed on mice and 6-8 drops of blood were collected into 1.7 mL Eppendorf tubes containing 200 µL of dPBS with 10 mM EDTA. RBC lysis was performed; 500 µL of RBC lysis buffer was added and samples were incubated for 10-15 minutes at 37 °C. Samples were centrifuged at 400 xg for 5 minutes and washed once with dPBS.

Lymph Nodes (LN)

LN were harvested into cIMDM, then mashed through a 70 µM filter using a 1 mL syringe plunger. Cells were washed with dPBS if processing for flow cytometry or with Wurzburger buffer for sterile applications and centrifuged at 400 xg for 5 minutes. LN cells were then resuspended in the appropriate buffer or media for their application and kept on ice until further use.

Spleen

Spleens were harvested into cIMDM, then mashed through a 70 µM filter using a 1 mL syringe plunger. Cells were washed with dPBS if processing for flow cytometry or with Wurzburger buffer for sterile applications and centrifuged at 400 xg for 5 minutes. Splenocytes were resuspended in 2 mL of RBC lysis buffer and incubated at 37 °C for 5-10 minutes, RBC lysis was quenched with 8 mL cold cIMDM and washed once. Cells were resuspended in the appropriate buffer or media for their application, and kept on ice until further use.

2.2.2.3 Magnetic Cell Separation (MACs)

Lymphocyte suspensions were prepared from OTI spleens and lymph nodes (2.2.2.2) and enriched for $CD8^+$ T cells using the MACs Dynabead system.

Cells were resuspended at 1 x 10^8/mL in Wurzburger buffer and 50 µL of FlowComp anti-CD8 Antibody was added per 10^8 cells. The cell-antibody mixture was incubated at 4 °C for 10 minutes. Cells were washed with

Wurzburger buffer and resuspended in 1 mL of buffer. 150 μL of FlowComp Dynabeads was added per 10^8 cells and incubated at 4 °C for 15 minutes, mixing every 5 minutes. The tube was placed in the Dynabead magnet for at least 1 minute before removing the negative fraction. The cells were resuspended in 1 mL of buffer and the magnet step was repeated. The positive fraction was then resuspended in 1 mL FlowComp Release Buffer and incubated for 10 minutes at room temperature. The tube was again placed in the Dynabead magnet for at least 1 minute, following which the cells were collected.

2.2.3 Viability assays

2.2.3.1 Trypan blue exclusion

Cells were harvested as described in 2.2.1.2 to assay for viability. Following harvest cells were resuspended in complete media and 10 μL of cell suspension was mixed with 10-90 μL of Trypan blue. Within 5-10 minutes of mixing 10 μL of the cell and trypan blue mixture was loaded in a Neubauer haemocytometer (Hawksley, Lancing, UK). The cell numbers were counted using an inverted microscope (CK2; Olympus, PA, USA). To determine viability unstained (viable) and stained (dead) cells were counted, and percentage viability was calculated.

2.2.3.2 Annexin V apoptosis assays

Exponentially growing cells were harvested (2.2.1.2). Cells were then seeded at a density of 1 x 10^5 cells per well in a 12-well plate and were incubated at 37 °C in 5% CO_2 for 6 hours to adhere. BRAF inhibitors were added at a range of concentrations and the plates were incubated for a further 12-36 hours at 37 °C in 5% CO_2 for inhibitor action to take effect. 6 hours prior to harvesting plates 5 μM Staurosporine (diluted in cRPMI) was added to a control well, to provide a positive control for apoptosis.

Following drug treatment supernatant was collected from wells, and cells were harvested as described above. The supernatant and cells were combined, and centrifuged at 400 xg for 5 minutes. Annexin V staining for phosphatidylserine expression was undertaken (2.2.7.2) and cell expression was measured by flow cytometry (2.2.7.7).

2.2.4 MTT dye reduction assay

The colourimetric MTT assay was used to measure enzymatic reduction of MTT. The yellow MTT dye is reduced to blue formazan crystals by metabolically active cells, therefore the intensity of the blue colour was used as an indication of the number of live cells (Berridge et al., 1996).

Exponentially growing cells were harvested (2.2.1.2). Cells were then seeded at a density of 0.5-1 x 10^4 cells per well in a 96-well, flat-bottom plate and were incubated overnight at 37 °C in 5% CO_2 to adhere. Inhibitors were added at a range of concentrations and the plates were incubated for a further 48 hours at 37 °C in 5% CO_2 for inhibitor action to take effect. Dye reduction was initiated by adding 20 μL of 2.5 mg/mL MTT dissolved in HBSS to each well, plates were then incubated for 2 hours. Cells were lysed with 100 μL of SDS lysing buffer added to each well and incubated for 24 hours. MTT reduction was measured at an absorbance of 570 nm using a multi-well plate reader (FLUOstar Optima, BMG, Labtech, Australia).

2.2.5 Characterization of tumour cell surface markers

2.2.5.1 CD1d expression

Exponentially growing cells were harvested as described in 2.2.1.2. After generating a single cell suspension extracellular staining with α-CD1d-PE was performed (2.2.7.1) and expression was assessed by flow cytometry (2.2.7.7).

2.2.5.2 IFNγ and TNFα exposure and cell-surface marker expression

Exponentially growing cells were harvested (2.2.1.2) and seeded at a density of 5 x 10^4 cells per well in a 24-well plate. IFNγ was added to give final concentrations of 500 U/mL to 31.25 U/mL, or TNFα was added to give final concentrations of 100 ng/mL to 6.25 ng/mL. Control wells received complete medium alone. Cells were incubated in the presence or absence of cytokines for 48 hours. Subsequently, cells were again harvested (2.2.1.2) and extracellular staining with α-PDL1-BV711 and α-MHCII-PE-Cy7 was performed (2.2.7.1). Marker expression was assessed by flow cytometry (2.2.7.7).

2.2.6 Proliferation assays

2.2.6.1 One-way Mixed Lymphocyte Reaction

One-way mixed lymphocyte reactions combine allogeneic PBMCs, with the PBMCs from one donor sub-lethally irradiated to serve as stimulator cells while the other donor's PBMCs are labelled to allow proliferative responses to be measured.

PBMCs were either used fresh following isolation (2.2.2.1) or frozen PBMCs were thawed at 37 °C in the waterbath and transferred to 15 mL conical tubes containing pre-warmed cRPMI with 20% FCS. PBMCs were washed, resuspended in cRPMI and rested for 4 hours or overnight at 37 °C in 5% CO_2.

Stimulator PBMCs were washed and resuspended in serum-free RPMI then γ-irradiated with 30 Gray (Scheffer et al.) (Gammacell® 1000 Elite irradiator, Best Theratronics, Canada). Following irradiation cells were centrifuged at 500 xg for 5 minutes and resuspended at 4 x 10^6 cells/mL in cRPMI supplemented with 100 U/mL rIl-2.

Responder PBMCs were stained with 0.4 μM CFSE (2.2.7.3) before being washed twice with cRPMI and resuspended at 4 x 10^6 cells/mL in cRPMI

supplemented with 100 U/mL rIL-2. In a 96-well U-bottom tissue culture plate, 50 μL of responder and stimulator cells were added to each well to give 2 x 10^5 each cell type/well. PLX4720 or Vemurafenib was diluted to 2x the final desired concentration in cRPMI, and 100 μL of inhibitor or 0.2% DMSO control was plated out.

The plate containing PBMCs, a range of concentration of inhibitors, vehicle and unstimulated controls was incubated at 37 °C in 5% CO_2 for 7 days. Cells were then harvested and extracellular staining with α-CD3 PE-Cy7, α-CD4 APC and α-CD8 PE was performed (2.2.7.1). T cell proliferation was measured by flow cytometry (2.2.7.7).

2.2.6.2 α-CD3/28 assays

Human

PBMCs were either used fresh following isolation (2.2.2.1) or frozen PBMCs were thawed at 37 °C in the waterbath and transferred to 15 mL conical tubes containing pre-warmed cRPMI with 20% FCS. PBMCs were washed, resuspended in cRPMI and rested for 4 hours or overnight at 37 °C in 5% CO_2.

Antibodies to human CD3ε and CD28 were diluted to 3-5 μg/mL and 0.5 μg/mL respectively in dPBS. The diluted antibody mixture was distributed to the wells of a 96-well U bottom plate in 50 μL aliquots. Control wells for unstimulated samples received 50 μL of dPBS. The plate was incubated at 37 °C for 2-3 hours to facilitate antibody binding to the plate.

Following resting the PBMCs were washed and a small number were reserved on ice as unstained controls. The remaining PBMCs were stained with 0.4 μM CFSE (2.2.7.3). CFSE-stained PBMCs were resuspended in cRPMI supplemented with 40 U/mL rIL-2 at 1 x 10^6 cells/mL. The pre-coated 96-well plate was removed from the incubator and the antibody suspension discarded. α-CD3/28 coated wells were washed twice with dPBS to remove unbound antibody. PBMCs were plated out at 1 x 10^5 cells per well. PLX4720

or Vemurafenib was diluted to 2x the final desired concentration in cRPMI, and 100 μL of inhibitor or 0.2% DMSO control was plated out.

The plate containing PBMCs treated with a range of concentrations of inhibitors, as well as vehicle and unstimulated controls was incubated at 37 °C in 5% CO_2 for 3 days. Cells were then harvested, and extracellular staining with α-CD3 PE-Cy7, α-CD4 APC, α-CD8 PE and α-CD69 AF700 was performed (2.2.7.1). T cell proliferation and activation was measured by flow cytometry (2.2.7.7).

Murine

Murine CD3 antibody was diluted to 1 μg/mL in dPBS and distributed to the wells of a 96-well U bottom plate in 50 μL aliquots. Control wells for unstimulated samples received 50 μL of dPBS. The plate was incubated for 4 hours at 37 °C or overnight at 4 °C to facilitate antibody binding to the plate.

C57BL/6 mice were euthanized by CO_2 asphyxiation and spleens were harvested into 3mL IMDM and kept on ice. Single cell splenocyte suspensions were prepared from C57BL/6 spleens as described in 2.2.2.2. Splenocytes were then counted and 4 x 10^6 cells were resuspended in 2 mL cIMDM and kept on ice to be plated out as unstained, or single stained controls.

Splenocytes were stained with 0.4μM CFSE (2.2.7.3). Following CFSE staining splenocytes washed with cIMDM and counted. 2 x 10^6 cells were resuspended in 1 mL cIMDM as unstimulated controls. The remaining CFSE positive cells were resuspended at 2 x 10^6 cells/mL in cIMDM supplemented with murine α-CD28 at 1:50 and rIL-2 at 400 U/mL.

The pre-coated 96-well plate was removed from the incubator and the antibody suspension discarded. α-CD3 coated wells were washed twice with dPBS to remove unbound antibody. Splenocytes were plated out at 2 x 10^5 cells per well. PLX4720 or Vemurafenib was diluted to 2x the final desired concentration in cIMDM, and 100 μL of inhibitor or 0.2% DMSO control was plated out.

The plate containing splenocytes treated with a range of concentrations of inhibitors, as well as vehicle and unstimulated controls was incubated at 37 °C in 5% CO_2 for 3 days. Cells were then harvested and extracellular staining with α-CD3 PE-Cy7 and α-CD69 PE was performed (2.2.7.1). T cell proliferation and activation was measured by flow cytometry (2.2.7.7).

2.2.7 Fluorescent labelling of cells and analysis by flow cytometry

2.2.7.1 Staining for extracellular marker expression

Human

Single cell suspensions were prepared or harvested, washed once with flow buffer and resuspended in 50–200 μL flow buffer. The cell suspension was then distributed to the wells of a 96-well U bottom plate. Plates were centrifuged at 400 xg for 4 minutes and supernatants were tipped off by flicking once. Pellets were resuspended in residual volume by vortexing. 25 μL of flow buffer containing FC receptor blocking IgG antibody was added and samples were incubated on ice for 20 minutes. Following FC receptor blocking samples were again centrifuged, supernatants discarded and pellets resuspended as described above. 25 μL of flow buffer containing fluorescently-conjugated antibodies at the appropriate dilutions was added to samples and the plate was again vortexed, then incubated on ice for 20 minutes. After staining cells were washed once, then resuspended in 200 μL of flow buffer containing DAPI at 0.1 μg/mL for analysis by flow cytometry.

Murine

Single cell suspensions were prepared or harvested, washed once with flow buffer and resuspended in 50–200 μL flow buffer. The cell suspension was then distributed to either the wells of a 96-well U bottom plate or FACS tubes for staining. Samples were centrifuged at 400 xg for 4 minutes, and supernatants were tipped off plates by flicking once or aspirated from tubes. Pellets were resuspended in residual volume by vortexing. 50 μL of flow buffer containing FC receptor blocking 2.4G2 antibody at 10 μg/mL was

added, and samples were incubated on ice for 20 minutes. Samples were again centrifuged, supernatants discarded and pellets resuspended as described above. Cells were resuspended in 50 μL of flow buffer containing fluorescently-conjugated antibodies at the appropriate dilutions. Samples were incubated on ice for 20-30 minutes. Cells were then washed once with 200 μL flow buffer, then resuspended in 200 μL of flow buffer containing DAPI at 0.1 μg/mL, for analysis by flow cytometry, or progressed to intracellular staining.

Antibody titrations
All antibodies were titrated prior to use. Antibody titrations were performed on the cells or tissues that would be used experimentally, and under experimental conditions.

2.2.7.2 Detection of apoptosis markers

Cells were harvested (2.2.1.2 for adherent cells) and washed once with Annexin V Binding Buffer (binding buffer). The cell pellet was resuspended in 50 μL of Annexin V APC diluted at 1:100 in binding buffer, and cells were stained for 15 minutes at room temperature in the dark. After staining cells were washed once with binding buffer, then resuspended in 200 μL of flow buffer containing DAPI at 0.033 μg/mL, and transferred to FACS tubes for flow cytometry (2.2.7.7).

2.2.7.3 Labelling of cells with CFSE

CFSE is a non-toxic, fluorescent dye that readily crosses intact cell membranes and binds to intracellular proteins in live cells. As cells proliferate the CFSE is divided equally between daughter cells, and the resulting halving of fluorescence can be used to measure generations of cell division (Lyons and Parish, 1994).

Single cell suspensions were prepared, washed once with dPBS and resuspended in 2 mL of dPBS. 10 mM CFSE was thawed and diluted 1:20,000 in cold dPBS. 8 mL of diluted CFSE was added to the cell suspension and vortexed to ensure even staining with a final concentration of 0.4 μM CFSE. Cells were stained for 8 minutes in the dark at room temperature. The labelling reaction was then stopped with the addition of 10 mL of pre-warmed FCS and cells were centrifuged at 500 xg for 4 minutes. Following labelling cells were washed twice with complete media, counted and resuspended at the required concentration for the specific assay.

2.2.7.4 Intracellular transcription factor staining

Cells were stained with the viability dye Live Dead Fixable Blue (LDFB) at 1:1000 and blocked with 2.4G2 antibody at 10 μg/mL in 50 μL dPBS on ice for 30 minutes. 100-500 μL of flow buffer was then added and samples were centrifuged at 400 xg for 4 minutes. Surface staining was performed as described in 2.2.7.1, and cells were washed in flow buffer. Fixing and permeabilisation was performed using the FoxP3 Transcription Factor Staining Buffer Set to allow for intracellular staining. Cells were fixed by incubating in 200-500 μL of 1x Fix/Perm for 60 minutes to 18 hours at 4 °C in the dark. Without washing 200-500 μL of 1 x Perm Buffer was added and samples were centrifuged at 300-400 xg for 5 minutes. The cell pellet was resuspended in 50 μL of flow buffer containing anti-mouse FoxP3 FITC at 1:250.

2.2.7.5 Ex vivo restimulation

Prior to staining for intracellular cytokines, cells were plated out in 96- or 24-well plates at approximately 5 x 10^6 cells/mL in cIMDM. PMA and ionomycin were added to give final concentrations of 50 ng/mL PMA and 500 ng/mL Ionomycin. Cells were incubated at 37 °C, and after 2 hours 3 μg/mL of Brefeldin-A was added to prevent cytokine secretion. Cells were incubated for a further 2 hours after the addition of Brefeldin-A, then harvested, transferred to FACS tubes and washed in dPBS.

2.2.7.6 Detection of intracellular effector molecules

After re-stimulation, cells were stained with the viability dye LDFB at 1:1000 and blocked with 2.4G2 antibody at 10 μg/mL in 50 μL dPBS on ice for 30 minutes. 100-500 μL of flow buffer was then added and samples were centrifuged at 400 xg for 4 minutes. Cells were stained with antibodies to extracellular markers as described in 2.2.7.1, and then washed in flow buffer.

Fixing and permeabilisation was performed using the FoxP3 Transcription Factor Staining Buffer Set to allow for intracellular staining. Cells were fixed by incubating in 200-500 μL of 1x Fix/Perm for 60 minutes to 18 hours at 4 °C in the dark. Without washing 200-500 μL of 1 x Perm Buffer was added and samples were centrifuged at 300-400 xg for 5 minutes. The cell pellet was resuspended in 50 μL of flow buffer containing fluorescently-conjugated antibodies against intracellular markers at the appropriate dilutions. Following staining cells were washed once with flow buffer, and then resuspended for acquisition.

2.2.7.7 Acquisition

Samples were analysed on an LSR-II special order product (BD) with BD FACS Diva software. Cytometer set-up and tracking was performed daily to ensure calibration.

The LSR-II was equipped with the following lasers and detectors: Ultraviolet laser (355 nm) UV740/35, UV450/50 and UV379/28. Violet laser (405 nm) V780/60, V720/40, V660/20, V605/40, V560/40, V525/50 and V450/50. Blue laser (488 nm) B705/70, B515/20 and B488/10. Green laser (532 nm) G780/60, G610/20 and G575/26. Red laser (640 nm) R780/60, R710/50 and R670/14.

All fluorophores were detected using laser and detector combinations that best matched their emission and excitation profile.

2.2.7.8 Compensation

To allow accurate compensation, single stain controls were stained under the same conditions as experimental samples. Compensation beads were singly stained with the antibody-fluorophore conjugates used in the experimental staining panel. Unstained samples consisted of cells that had been cultured or isolated in the same conditions as experimental samples, and viability dye single stains were also performed on such cells. Compensation was automatically calculated and applied using the compensation wizard in FACS Dive software and manually checked at the time of analysis.

2.2.7.9 Flow cytometric data analysis

Following acquisition FCS files were analysed using the FlowJo software (Tree Star, San Carlos, CA, USA). Compensation was manually reviewed by observing single stain controls against all other channels used in the panel and confirming there was no under or over compensation applied.

Samples were always gated on singlet cells by gating on the diagonal in SSC-area against SSC-height and subsequently FSC-area against FSC-height. For the majority of gating strategies dead cells were excluded by gating on $DAPI^-$ or $LDFB^-$ cells, with the exception being in viability assays where data for both $DAPI^-$ and $DAPI^+$ populations were included. In multi-colour panels when gating on populations with no clear division between negative and positive cells fluorescence minus one (FMO) controls were used to determine background fluorescence, and thus confirm where gates should be set. For intracellular cytokine staining isotype controls were also used to confirm the validity of positive populations.

2.2.8 In vivo T cell assays

2.2.8.1 Adoptive T cell transfer

OTI T cells were isolated and adoptively transferred to C57BL/6 mice. B6.SJ-OTI mice were euthanized by CO_2 asphyxiation and LN and spleens were collected and processed to single cell suspensions (2.2.2.2). The CD8+ T cell population was the enriched by MACs Dynabead separation (2.2.2.3). Following enrichment the OTI T cells were washed with dPBS, and resuspended at 5 x 10^4 cells/mL in dPBS. C57BL/6 mice were then injected intravenously (IV) in to the lateral tail vein with 1 x 10^4 OTI T cells.

2.2.8.2 PLX4720 preparation and dosing

PLX4720 was dissolved in DMSO to give a 10x stock. For 20 mg/kg dosing at 8 mL/kg, 20 mg of PLX4720 was dissolved in 800 μL of DMSO. For 50 mg/kg dosing at 8 mL/kg, 50 mg of PLX4720 was dissolved in 800 μL of DMSO. 10x stocks were stored in the dark at room temperature for up to 7-10 days.

A solution of 1% CMC was prepared for use as the vehicle control. CMC was added to dH_2O at a ratio of 1 gram per 100 mL, the solution was agitated on a magnetic stirring platform for several hours until dissolved and solution was clear. 1% CMC was then stored at room temperature long term.

10x PLX4720 stock was added to 1% CMC at a 1:9 ratio and vortexed to produce a uniform suspension. This suspension was delivered intra-gastrically (IG) by oral gavage (IG) using a 1 mL syringe and feeding needle shortly after preparation. Fresh suspensions were prepared daily no more than 1 hour prior to delivery.

Control mice received a suspension of DMSO added to 1% CMC in a 1:9 ratio, also prepared fresh daily.

Mice were gavaged with control suspension or PLX4720 suspension daily, treatment was commenced on the day of OTI T cell transfer and continued until experiment completion.

2.2.8.3 Vaccination

OTI T cells were stimulated with the peptide OVA and the iNKT ligand αGalCer 7 days after adoptive transfer. OVA and αGalCer were resuspended at 500 μg/mL and 250 ng/mL respectively. C57BL/6 mice were injected IV with either 200 μL of OVA and αGalCer or with 200 μL of dPBS for control mice.

2.2.8.4 Analysis

The proportion of OTI T cells in the $CD8^+$ T cell compartment was analysed 7 days following vaccination. C57BL/6 mice were bled from the lateral tail vein and lymphocyte suspensions were isolated (2.2.2.2). Lymphocytes were stained for expression of the extracellular markers CD3, CD8, Vα2 and CD45.1 (2.2.7.1), and flow cytometry acquisition and analysis was performed (2.2.7.7). OTI T cells were identified as being $V\alpha2^+$ $CD45.1^+$.

2.2.9 Tumour challenge experiments

2.2.9.1 Tumour challenge

Mice were injected subcutaneously (SC) in the left flank with 1-4 x 10^5 YUMM1.1 cells, or 0.5-1 x 10^5 YUMM1.7 cells, or 1 x 10^5 B16.Ova cells. All YUMM1.1 and YUMM1.7 tumour experiments were performed in male mice, due to spontaneous tumour rejection observed in some female C57BL/6 mice (a phenomena also observed at Yale University; Katrina Meeth, personal communication).

Tumours in untreated control mice were palpable from approximately 4-7 days following tumour challenge. Once tumours were palpable they were measured every 2-3 days. Bisecting diameters were measured using Mitutoyo callipers. Mice were euthanized when tumour size reached 150 mm^2 or when tumours ulcerated.

2.2.9.2 Vaccine generation and delivery

Autologous tumour cells (YUMM1.1 or YUMM1.7) were passaged as previously described (2.2.2.1), and replated with cRPMI containing αGalCer at 200 ng/mL. Cells were incubated with αGalCer overnight, and then media was removed and cells were washed twice with dPBS. The αGalCer-loaded tumour cells were harvested (2.2.2.2), resuspended in serum free RPMI and delivered 150 Gy γ-irradiation (Gammacell®. 1000 Elite irradiator, Best Theratronics, Canada). Irradiated, αGalCer-loaded tumour cells were washed with dPBS and resuspended at 1 x 10^6 cells/mL. Mice were injected IV with 100-200 μL of vaccine, and control mice received 100-200 μL dPBS.

2.2.9.3 PLX4720 preparation and dosing

PLX4720 stocks were prepared as described in 2.2.8.2, with an additional 100 mg/kg 10 x stock prepared. For dosing at 8 mL/kg 100 mg of PLX4720 stock was dissolved in 800 μL DMSO.

10x PLX4720 was diluted with 1% CMC or DMSO with 1% CMC for control mice (2.2.8.2), and suspensions were prepared no more than 1 hour prior to delivery. Drug or control solution was delivered intra-gastrically using a 1mL syringe and feeding needle daily from 5 or 7 days post-tumour challenge.

2.2.9.4 Analysis of tumour infiltrating lymphocytes (TIL)

Mice were euthanized by CO_2 asphyxiation 14, 21 or 25 days post-tumour challenge. Tumours were harvested and transferred in to 3 mL IMDM in 15 mL falcon tubes on ice. Tumours were then manually disassociated in to roughly even sized small fragments, following which tumours were digested in IMDM containing 200 μg/mL of DNase and 1 mg/mL Collagenase IV at 37 °C for 60 minutes. After incubation in digestion media 0.5 M EDTA was added to give a final concentration of 10 μM and tissues were incubated for a further 5 minutes at 37 °C. Single cell tumour suspensions were then prepared by passing tissue fragments through an 18 G needle on a 5 mL

syringe approximately ten times. Tumour suspensions were then mashed through a 70 μM filter using a 1 mL syringe plunger. Tumour cells were resuspended in 2 mL RBC lysis buffer and incubated at 37 °C for 5-10 minutes; RBC lysis was quenched with 8 mL cold cIMDM and washed once. Following red blood cell lysis, cells for phenotyping were resuspended in flow buffer and extracellular and intracellular staining was performed as in 2.2.7.1 and 2.2.7.4 respectively. For cytokine analysis, cells were re-stimulated as described in 2.2.7.5 prior to extracellular and intracellular staining as detailed in 2.2.7.1 and 2.2.7.6.

2.2.9.5 Analysis of immune cell populations in peripheral lymphoid tissues

As described above, mice were euthanized 14, 21 or 25 days post-tumour challenge. Spleens and tumour draining inguinal lymph nodes were harvested and transferred in to 1-3 mL IMDM in 24- or 12-well plates on ice. Spleens were then manually disassociated into roughly even sized small fragments, following which tissues were digested in IMDM containing 100 μg/mL of DNase and 0.1 mg/mL Liberase at 37 °C for 30 minutes. After 30 minutes incubation in digestion media 0.5 M EDTA was added to give a final concentration of 10 μM, and tissues were incubated for a further 5 minutes at 37 °C. Single cell lymph node and splenocyte suspensions were then prepared as described in 2.2.2.2. Following the generation of single cell suspensions and red blood cell lysis of splenocytes, cells for phenotyping were resuspended in flow buffer and extracellular and intracellular staining was performed as in 2.2.7.1 and 2.2.7.4 respectively. For cytokine analysis, cells were re-stimulated as described in 2.2.7.5 prior to extracellular and intracellular staining as detailed in 2.2.7.1 and 2.2.7.6.

2.2.10 Statistical analyses

Statistical analysis and graphing of data was performed using Prism software (Graphpad Prism Version 5.0f for MacIntosh, GraphPad Software Incorporated, USA). Statistical analyses used are stated in figure legends and $p < 0.05$ was considered the threshold for significance. Analyses examining a

single parameter of two groups were performed using an unpaired T-test. Analyses examining a single parameter of three or more groups were undertaken using a one-way analysis of variance (ANOVA) with Bonferroni post-test. For experiments examining two or more parameters of three or more groups, two-way ANOVA with Bonferroni post-test was performed. MTT results were analysed to calculate the IC50 and generate a dose-response curve, using a non-linear regression model plotting log(inhibitor) versus normalised dose response. The number of experimental repeats performed is detailed in figure legends. Experimental data was not pooled across experiments using human cells due to individual-to-individual variation or for experiments with large flow cytometry panels due to slight changes to flow panels and machine set-up.

CHAPTER 3: Characterizing $BRAF^{V600E}$ melanoma models

3.1 Introduction

This thesis investigates the immunological effects of targeted BRAF inhibition and aims to optimize combination of BRAF inhibitors with immunotherapy. To undertake this research an *in vivo* model of $BRAF^{V600E}$ melanoma needs to be established, and the relevance of this model to human melanoma assessed.

Several different types of murine *in vivo* tumour models exist. Traditionally the most commonly used are xenograft models, which involve the transplantation of human tumour cells into severely immunocompromised mice (Budhu et al., 2014). Immune deficient mice are unable to reject non-autologous cells, allowing study of human tumour biology *in vivo* and providing the opportunity to generate patient-derived tumour models. However, the immune deficiencies that are essential to these models are also a key limitation, discounting the considerable contribution of the immune system to tumourigenesis and limiting the relevance of xenograft systems. Several immune competent alternatives have been developed, including transplantable models using syngeneic mouse cancer cell lines. Transplantable tumour models can be orthotopic with cells implanted directly into the tissue of origin, or ectopic most commonly with transplantation to a subcutaneous site. Of the two, orthotopic models are considered more clinically relevant, recapitulating the appropriate tumour microenvironment. However, they can be technically challenging and generally require imaging technology such as magnetic resonance imaging or fluorescent reporter imaging to assess tumour growth (Troiani et al., 2008). In contrast, subcutaneous models are widely used for their simplicity, reproducibility and ease of tumour measurement despite the disadvantage of not representing an appropriate tumour site (Killion et al., 1998). The most frequently used syngeneic, transplantable melanoma model is the B16 model, however this model lacks the genetic lesions found in many human melanomas, making it unsuitable for investigation of targeted therapies (Becker et al., 2010). Advances in the understanding of the genetic basis of tumour types and in genetic engineering have led to the derivation of transgenic mice with conditional, tissue specific oncogene expression or tumour suppressor inactivation modelled on human tumours. Of the mouse models available,

transgenic systems most faithfully recapitulate human cancers, but the caveat of this is phenotypic variability, lengthy experiments (a single experiment can take upwards of 6-12 months) and the need for expansion of the unique mouse colonies (Budhu et al., 2014).

For the research undertaken in this thesis the *BRaf*^{V600E}, *Pten*$^{-/-}$; *CDKN2a*$^{-/-}$ 'YUMM1.1' and 'YUMM1.7' cell lines were generously made available by Prof Marcus Bosenberg of Yale University. Whilst transgenic tumour models best exemplify human tumours, the lack of available imaging technology at the Malaghan Institute and lengthy experiment times make the inducible tumours of *Tyr::CreER; BRaf*^{CA}; *Pten*$^{lox5/lox5}$ mice unsuitable for use in this research. However, the transplantable cell lines developed from induced tumours recapitulate a mutational profile common to human melanoma tumours and have been derived from a C57BL/6 background. These tumours can be transplanted into fully immunocompetent, syngeneic mice. This makes the YUMM1.1 and YUMM1.7 tumour models good candidates for the study of the immunological effects of BRAF inhibitors and combination therapy. These are novel BRAF^{V600E} tumour lines, and effects of BRAF inhibition in these models will be assessed in comparison with human BRAF^{V600E} melanoma cells and BRAF^{WT} models. This will allow characterisation of the novel *BRaf*^{V600E}; *Pten*$^{-/-}$; *CDKN2a*$^{-/-}$ cell lines to be performed in the context of more widely used models.

Targeted mutant-BRAF inhibition will be investigated using the clinical compound Vemurafenib and the structural analogue PLX4720, which have kindly been provided by Dr Gideon Bollag of Plexxikon. The effects of these two inhibitors will be compared *in vitro*. *In vivo* experiments will be undertaken using PLX4720, which is the more appropriate compound for use in rodents as its pharmacokinetic profile is analogous to that of Vemurafenib in humans (Bollag et al., 2012). PLX4720 will be delivered by oral gavage *in vivo*, to accurately model the oral delivery of Vemurafenib to human patients. Additionally, targeted mutant-BRAF inhibitor profiles will be compared with those of the pan-RAF inhibitor Sorafenib to confirm mutant-BRAF specificity.

3.1.1 Aims

The experiments described in this chapter were performed to characterize novel $BRAF^{V600E}$ tumour lines and determine the relevance of these cell lines to human melanoma models, with overall aim of setting up an immunocompetent $BRAF^{V600E}$ melanoma model *in vivo.*

Specific aims were to:

- Determine the sensitivity of $BRAF^{V600E}$ and $BRAF^{WT}$ human and murine tumour cell lines to targeted BRAF inhibition and pan-RAF inhibition

- Examine the cytotoxicity of targeted BRAF inhibitors on $BRAF^{V600E}$ melanoma cell lines and establish the mechanism of cell death

- Characterize the effects of targeted BRAF inhibition on $BRAF^{V600E}$ melanoma-mediated immunosuppression

- Optimize *in vivo* models of $BRAF^{V600E}$ tumour growth in syngeneic C57BL/6 mice and determine PLX4720 sensitivity

3.2 Results

3.2.1 *In vitro* sensitivity of a range of human and murine cancer cell lines to BRAF inhibition

Initial experiments were performed to characterize the *in vitro* sensitivity of a range of human and murine cell lines to BRAF inhibition. Cells were treated with the targeted mutant-BRAF inhibitors PLX4720 and Vemurafenib (Figures 3.1 and 3.2), and the pan-RAF inhibitor Sorafenib (Figures 3.3 and 3.4). Inhibitor effects on cell viability were measured indirectly using MTT assays. Metabolically active cells will reduce the MTT tetrazolium salt to an insoluble formazan in a colourimetric reaction. This dye reduction is generally proportional to the number of viable cells in the exponential growth

phase, and thus can be used as an indirect measure of cell proliferation (Berridge et al., 2005). MTT reduction was plotted as a percentage of the DMSO (vehicle) treated controls, and the half maximal inhibitory concentration (IC50) was determined for each experimental repeat. The mean IC50 values for PLX4720 and Vemurafenib treatment of each cell line are detailed in Table 3.1, whilst IC50 values for Sorafenib treatment are summarized in Table 3.2. The MTT assay was subsequently validated as a measure of cell viability in Sections 3.2.2 and 3.2.3.

3.2.1.1 Human cell lines

Of the human cell lines profiled, the $BRAF^{V600E}$ homozygous A375 cells demonstrated the greatest sensitivity to targeted BRAF inhibition (Figure 3.1), with IC50 values of 333 nM for PLX4720 treatment and 82 nM for Vemurafenib treatment. However, these cells were approximately 10-fold less sensitive to pan-RAF inhibition, with Sorafenib treatment achieving an IC50 of 2.31 μM (Figure 3.2). In contrast, a second $BRAF^{V600E}$ human melanoma cell line, SK-mel-5, was relatively resistant to targeted BRAF inhibition. SK-mel-5 cells had IC50s of 10.82 μM with PLX4720 treatment and 48.37 μM with Vemurafenib treatment. Despite this insensitivity to targeted BRAF inhibition, SK-mel-5 cells were sensitive to broad-spectrum RAF inhibition, with an IC50 of 4.77 μM when treated with Sorafenib.

By way of comparison, the sensitivity of the human $BRAF^{WT}$ leukaemia cell line HL-60 was determined. HL-60 cells were shown to be insensitive to targeted BRAF inhibition with IC50s of greater than 20 μM. This cell line was, however, highly sensitive to inhibition with Sorafenib with a mean IC50 of 640 nM. These data demonstrate that HL-60 cells are susceptible to MAPK pathway blockade but as expected, not to selective inhibitors of mutant-BRAF.

Susceptibility to both targeted and broad-spectrum RAF inhibition was also established for human melanoma cell lines of unknown BRAF mutation status, with the aim of identifying a second cell line highly sensitive to mutant

BRAF inhibition. The cell lines LM-mel-15, LM-mel-34 and LM-mel-62 all demonstrated a lack of sensitivity to PLX4720 treatment with IC50s ranging from 23.32 μM to 59.8 μM, despite being relatively sensitive to Sorafenib. These results suggest that the three cell lines are likely BRAF wild-type, or heterozygous for the BRAF mutation and *de novo* resistant. Therefore, these cells were not included in any further work on targeted BRAF inhibition.

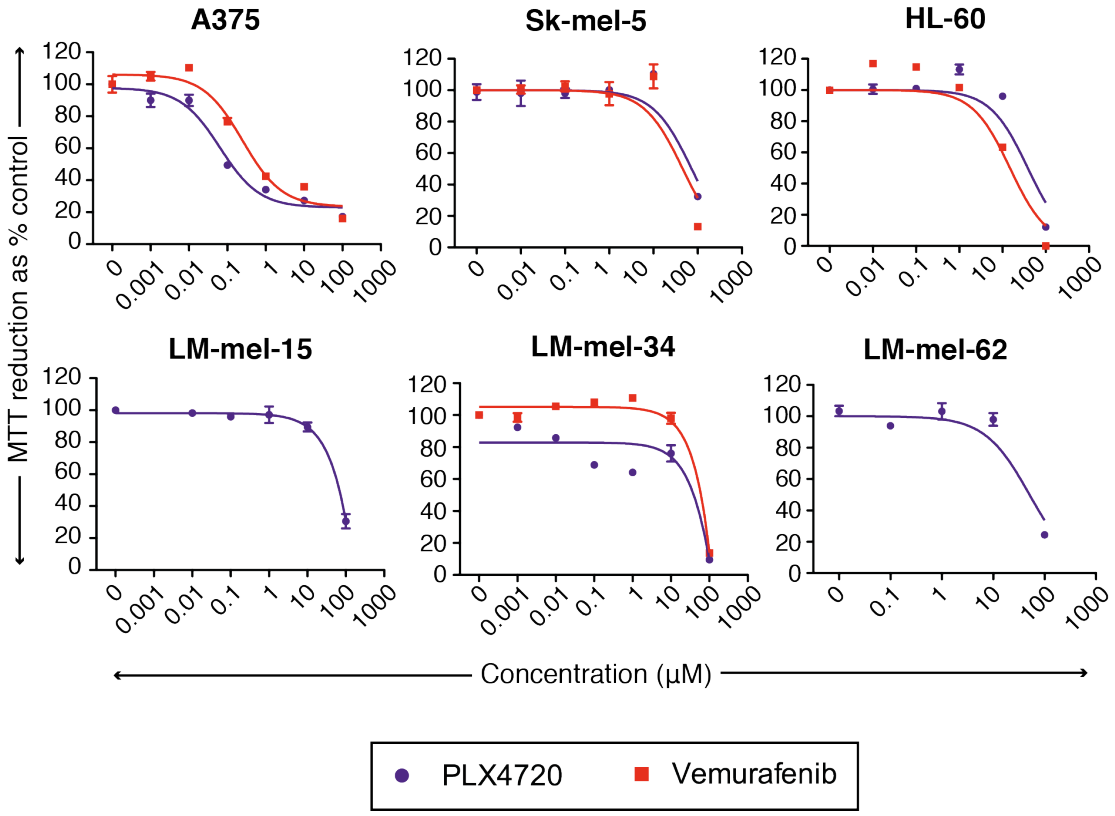

Figure 3.1: BRAF mutation status determines human melanoma cell line sensitivity to highly targeted BRAF inhibitors *in vitro*. Cells were treated with a range of concentrations (1nM-100μM) of PLX4720 or Vemurafenib for 48 hours. MTT reduction is shown as a percentage of DMSO treated control. Each symbol represents the mean of the triplicate; error bars are± S.D. Curves generated by non-linear regression analysis. Graphs are representative of at least two independent experiments.

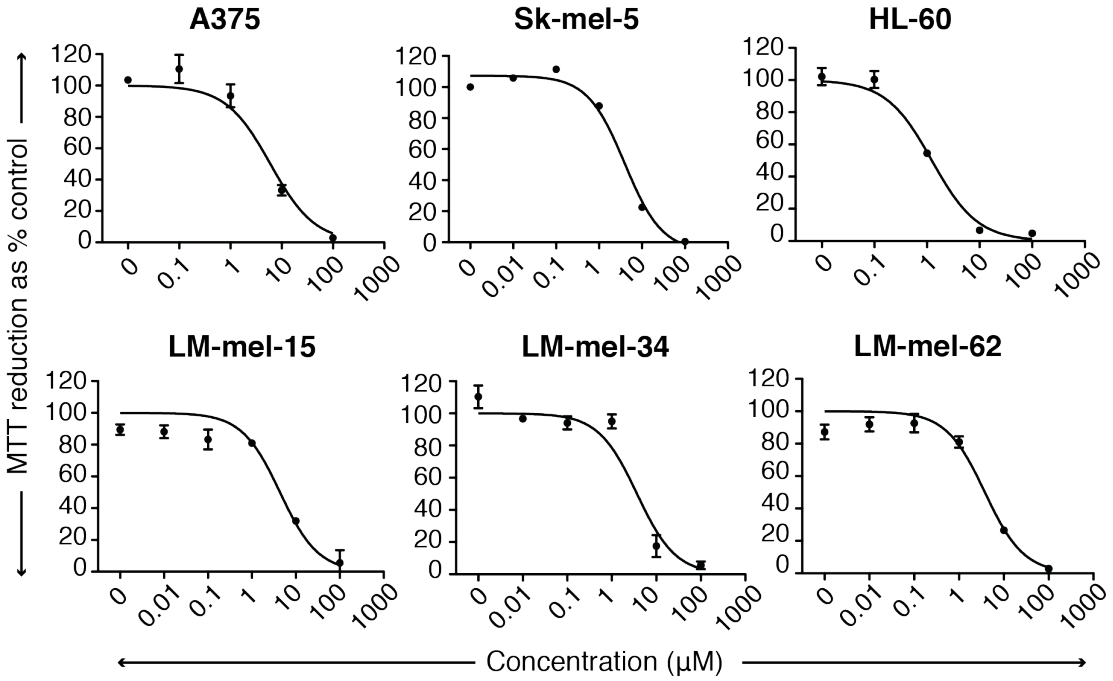

Figure 3.2: Human melanoma cell line sensitivity to broad spectrum RAF inhibition *in vitro* is not determined by BRAF mutation status. Cells were treated with a range of concentrations (10 nM-100 μM) of Sorafenib for 48 hours. MTT reduction is shown as a percentage of DMSO treated control. Each symbol represents the mean of the triplicate; error bars are ± S.D. Curves generated by non-linear regression analysis. Graphs are representative of at least two independent experiments.

3.2.1.2 Murine cell lines

Next, the sensitivities of murine $BRAF^{V600E}$ and $BRAF^{WT}$ melanoma cell lines were examined with both targeted BRAF inhibition (Figure 3.2 and Table 3.1) and broad-spectrum RAF inhibition (Figure 3.4 and Table 3.2).

The $BRAF^{V600E}$ YUMM1.1 and YUMM1.7 cells were moderately sensitive to targeted BRAF inhibition and had similar sensitivity to both PLX4720 and Vemurafenib. YUMM1.1 cells had an IC50 of 880 nM with PLX4720 and 1.53 μM with Vemurafenib treatment, while YUMM1.7 cells had IC50s of 1.44 μM and 1.26 μM with PLX4720 and Vemurafenib respectively. Despite the similar responses of both cell lines to targeted BRAF inhibition, YUMM1.1 cells were less sensitive to Sorafenib (mean IC50 of 16.75 μM) than YUMM1.7 cells

(mean IC50 of 5.58 μM). This discrepancy in sensitivity to broad spectrum MAP kinase inhibition may be related to differential proliferation rates, with YUMM1.7 cells proliferating more rapidly than YUMM1.1 (data not shown). As expected, the BRAF wild-type B16 cell line was highly resistant to targeted BRAF inhibition with IC50s of greater than 80 μM for both inhibitors. B16 cells were also one of the least sensitive cell lines to Sorafenib treatment, with an IC50 of 11.16 μM.

In summary, these data demonstrate that sensitivity to targeted BRAF inhibitors is dependent on BRAF mutation status, and confirms that PLX4720 and Vemurafenib have specificity for mutant BRAF. The human melanoma cell line A375 exemplified a highly sensitive $BRAF^{V600E}$ cell line, whilst SK-mel-5 cells showed *de novo* resistance to targeted BRAF inhibition. In comparison to the human melanoma cell lines, the murine $BRAF^{V600E}$ YUMM1.1 and YUMM1.7 cells were moderately sensitive to targeted BRAF inhibition. As expected, the response to broad-spectrum MAPK blockade with Sorafenib was not dependent on BRAF mutation status, and the cell lines assayed exhibited a narrower range of sensitivities to Sorafenib with IC50s ranging from 640 nM (HL-60 cells) to 17 μM (YUMM1.1 cells).

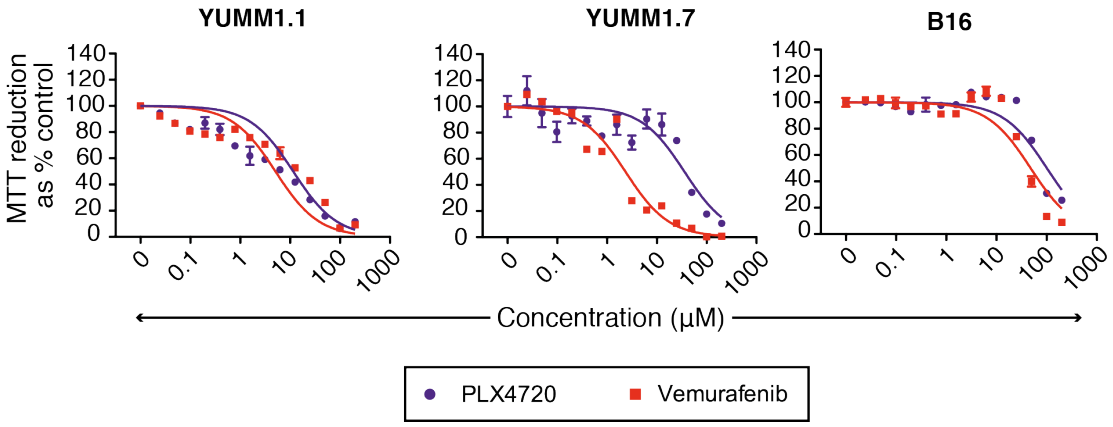

Figure 3.3: BRAF mutation status determines murine melanoma cell line sensitivity to highly targeted BRAF inhibitors treatment. Cells were treated with a range of concentrations (12 nM-200 μM) of PLX4720 or Vemurafenib for 48 hours. MTT reduction is shown as a percentage of DMSO treated control. Each symbol represents the mean of the triplicate; error bars are ± S.D. Curves generated by non-linear regression analysis. Graphs are representative of at least two independent experiments.

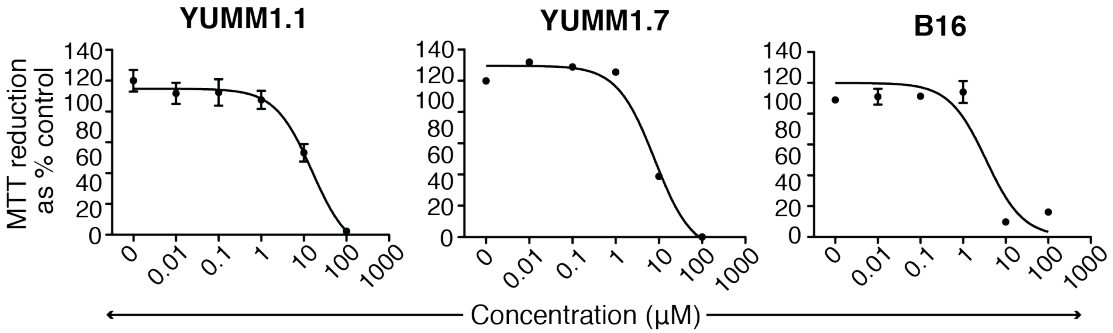

Figure 3.4: Murine melanoma cell line sensitivity to broad spectrum RAF inhibition *in vitro* is not determined by BRAF mutation status. Cells were treated with a range of concentrations (10 nM-100 μM) of Sorafenib for 48 hours. MTT reduction is shown as a percentage of DMSO treated control. Each symbol represents the mean of the triplicate; error bars are ± S.D. Curves generated by non-linear regression analysis. Graphs are representative of at least two independent experiments

Table 3-1: BRAF mutation status determines human and murine melanoma cell line sensitivity to targeted mutant BRAF inhibitors

Cell line	BRAF mutation	PLX4720		Vemurafenib	
		Number of tests	Average IC50	Number of tests	Average IC50
A375	V600E	4	333.15 nM	3	81.61 nM
YUMM1.1	V600E	3	880.23nM	2	1.53 μM
YUMM1.7	V600E	3	1.44 μM	4	1.26 μM
SK-mel-5	V600E	2	10.82 μM	2	48.37 μM
LM-mel-34	Unknown	2	23.32 μM	-	-
HL-60	WT	2	32.55 μM	2	20.92 μM
LM-mel-62	Unknown	4	48.65 μM	-	-
LM-mel-15	Unknown	2	59.8 μM	-	-
B16	WT	3	85.40 μM	2	80.91 μM

Table 3-2: Tumour cell line sensitivity to broad spectrum RAF inhibition *in vitro* is not determined by BRAF mutation status.

Cell line	BRAF	Number of tests	Average IC50
HL-60	WT	3	639.67 nM
A375	V600E	4	2.31 μM
LM-mel-34	Unknown	2	3.86 μM
LM-mel-62	Unknown	4	4.29 μM
LM-mel-15	Unknown	2	4.35 μM
SK-mel-5	V600E	2	4.77 μM
YUMM1.7	V600E	2	5.58 μM
B16	WT	3	11.16 μM
YUMM1.1	V600E	2	16.75 μM

3.2.2 BRAF inhibitors induce cell death in sensitive $BRAF^{V600E}$ cell lines in a time and concentration dependent manner

Having established that the $BRAF^{V600E}$ cell lines A375, YUMM1.1 and YUMM1.7 are susceptible to growth inhibition by targeted BRAF inhibitors *in vitro* as determined by MTT assay, direct effects on viability were investigated. To confirm that PLX4720 and Vemurafenib induce cell death rather than decreased metabolic activity, effects on viability were confirmed by fluorescent dye staining using flow cytometry. Cells were stained LDFB, a blue fluorescent stain which is excluded by live cells but can enter the compromised membranes of dead cells to irreversibly bind amines. This technique allowed cells to be fixed following staining, preventing ongoing cell death from occurring during processing and data acquisition. Melanoma cells were treated with a range of concentrations of PLX4720 or Vemurafenib for 12 to 72 hours. Following drug treatment cells were collected and the percentage of viable cells was determined, as shown in Figure 3.5 for A375, Figure 3.6 for YUMM1.1 and Figure 3.7 for YUMM1.7 cells. As expected, exposure to BRAF inhibitors resulted in cell death in all three cell lines, which occurred in a time and concentration dependent manner.

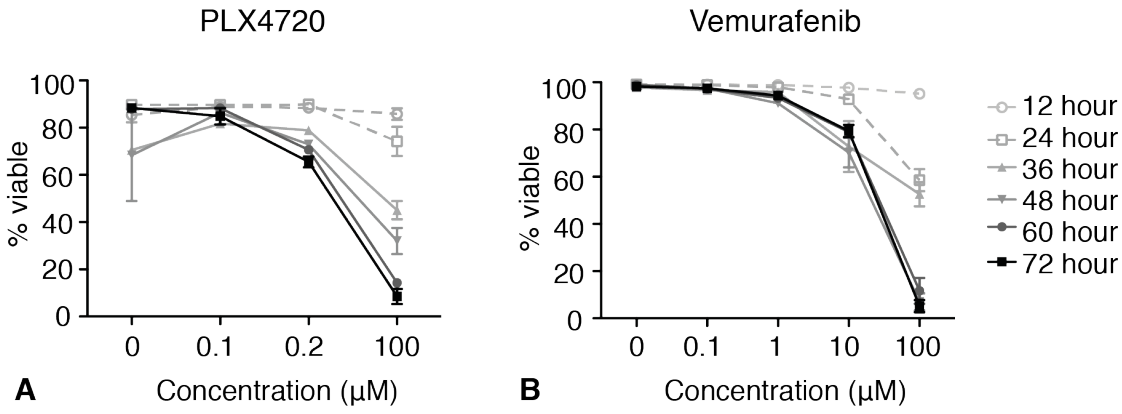

Figure 3.5: A375 sensitivity to PLX4720 and Vemurafenib is time and concentration dependent. Cells were treated with a range of concentrations (10 nM-100 μM) of PLX4720 or Vemurafenib for 12-72 hours. Cell viability was examined by flow cytometry. Each symbol represents the mean of the triplicate; error bars are ± S.D. Graphs are representative of two independent experiments.

More than 12 hours exposure to PLX4720 or Vemurafenib was required to induce A375 cell death (Figure 3.5A and B), with 20-40% loss of viability evident after 24 hours treatment with 100 μM PLX4720 or Vemurafenib. Treatment for 36 to 72 hours with PLX4720 induced up to 40% cell death at a concentration of 200 nM, and 50-95% cell death at 100 μM. While Vemurafenib treatment for 36 to 72 hours with 10 μM inhibitor resulted in 20% cell death. The highest concentration of Vemurafenib, 100 μM, induced 40% cell death at 36 and 48 hours, and close to 100% cell death with exposure of 60 hours or longer. Overall, A375 cells showed slightly increased susceptibility to PLX4720 treatment than Vemurafenib, with cell death observed at lower PLX4720 concentrations.

Similar to A375 cells, a concentration and time dependent effect was evident with PLX4720 treatment of YUMM1.1 cells (Figure 3.6A). Following 12 hours of exposure to PLX4720 YUMM1.1 cells remained viable at all drug concentrations used. Cell death was observed at concentrations of 10 μM with 24-36 hours exposure, at 2.5 μM after 48-60 hours and at 1 μM after 72 hours. Therefore, with increased treatment length YUMM1.1 cells were more sensitive to low concentrations of PLX4720. Additionally, increased cell death was observed at high drug concentrations with longer treatment times. After 24-36 hours treatment 100 μM PLX4720 induced 60% cell death, while 48 to 72 hours exposure to 100 μM resulted in 80-100% cell death.

This time dependent effect was less evident when YUMM1.1 cells were treated with Vemurafenib (Figure 3.6B). Following 12 hours exposure less than 10% cell death was observed at concentrations up to 25 μM, and 60% of cells died with 100 μM Vemurafenib treatment. However, with 24 to 72 hours treatment, Vemurafenib induced similar responses. Concentrations of 1 to 10 μM caused less than 20% cell death, at 25 μM approximately 60% cell death was evident and at 100 μM 90-100% of cells were dead. Largely, YUMM1.1 cells have similar sensitivity to both PLX4720 and Vemurafenib, however PLX4720 effects appear to be more closely linked to length of drug exposure.

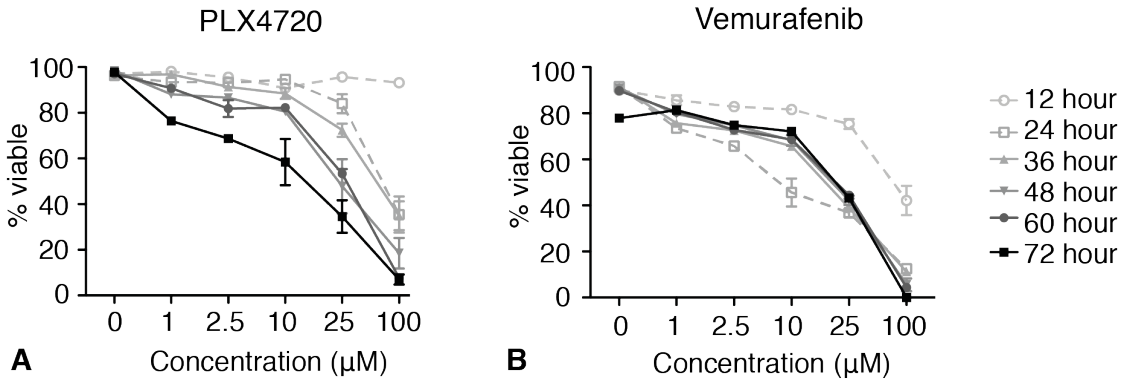

Figure 3.6: YUMM1.1 sensitivity to PLX4720 and Vemurafenib is time and concentration dependent. Cells were treated with a range of concentrations (1 μM-100 μM) of PLX4720 or Vemurafenib for 12-72 hours. Cell viability was determined by LDFB exclusion using flow cytometry. Each symbol represents the mean of the triplicate; error bars are ± S.D. Graphs are representative of at least two independent experiments.

Of the three cell lines analysed YUMM1.7 cells were the least sensitive to PLX4720 treatment. Concentrations of up to 25 μM PLX42720 failed to induce cell death of greater than 10% even after 72 hours of inhibitor exposure, and substantial cell death was not observed until YUMM1.7 cells were exposed to 100 μM PLX4720. Following 24 and 36 hours of 100 μM treatment around 30-40% cell death was evident, and after 48-72 hours exposure to 100 μM PLX4720 80-100% cell death was observed. In comparison, YUMM1.7 were slightly more sensitive to Vemurafenib. Treatment with 25 μM Vemurafenib for 24 to 72 hours caused 30-50% cell death. At 100 μM Vemurafenib induced 40-60% cell death after 12-24 hours, and greater than 90% cell death with treatment of 36 hours or longer.

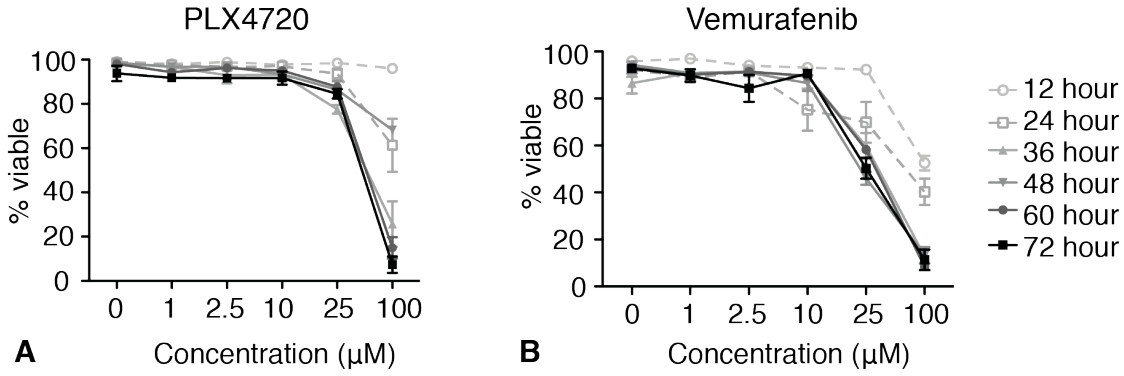

Figure 3.7: YUMM1.7 sensitivity to PLX4720 and Vemurafenib is time and concentration dependent. Cells were treated with a range of concentrations (1 μM-100 μM) of PLX4720 or Vemurafenib for 12-72 hours. Cell viability was examined by flow cytometry. Each symbol represents the mean of the triplicate; error bars are ± S.D. Graphs are representative of at least two independent experiments.

Collectively, these data confirm that BRAF inhibitors induce cell death of $BRAF^{V600E}$ cells, corroborating the conclusions drawn from the MTT assays (Section 3.2.1). All three cell lines showed a concentration and time dependent effect of targeted BRAF inhibitors on cell viability, although the length of inhibitor exposure had greater impact on A375 and YUMM1.7 cells. Overall, the cell lines had similar sensitivity to the two inhibitors, but A375 and YUMM1.1 cells showed slightly increased susceptibility to PLX4720 treatment while YUMM1.7 cells were slightly more sensitive to Vemurafenib.

3.2.3 $BRAF^{V600E}$ melanoma cells die by apoptosis following BRAF inhibitor treatment

In order to determine the mechanism by which targeted BRAF inhibitors induce $BRAF^{V600E}$ melanoma cell death, apoptosis assays were performed on A375, YUMM1.1 and YUMM1.7 cells following PLX4720 or Vemurafenib exposure. One of the earliest indications of apoptosis is loss of plasma membrane symmetry; this results in molecules such as phosphatidylserine being translocated from the inner to the outer surface of the cell membrane. Expression of phosphatidylserine was used a marker of apoptosis, and was detected with high-affinity fluorescently-conjugated Annexin V (AV) staining. Cell viability was determined using the nucleic acid binding dye DAPI, which

is excluded by live cells but can enter the compromised membranes of dead cells. Co-staining with AV and DAPI was used to resolve live, early apoptotic and late-stage apoptotic/necrotic cell populations. Live cells present as double negative for both AV and DAPI, while early apoptotic cells are AV positive and DAPI negative. As apoptosis progresses membrane integrity is lost and late-stage apoptotic cells present as double positive. Although double positive cells are often regarded as apoptotic, it is worth noting that due to the loss of membrane integrity with cell death necrotic cells may also appear double positive with AV labelling intracellular phosphatidylserine.

Exposure of A375 cells to PLX4720 or Vemurafenib for 18 or 24 hours resulted in minimal phosphatidylserine translocation or cell death, with greater than 90% of cells remaining viable (Figure 3.8). Treatment with 100 μM Vemurafenib for 18-24 hours induced early apoptosis in a small population of cells, and cell death in approximately 20% of cells. Following 36 hours of treatment, 25 μM PLX4720 or Vemurafenib resulted in approximately 20-30% early apoptosis and dead cells. The greatest proportion of apoptosis and cell death was detected with 100 μM inhibitor exposure for 36 hours. At this concentration it was evident that Vemurafenib induced apoptosis more effectively than PLX4720, with 20% and 70% of cells remaining viable respectively.

Overall, the distinct populations of AV^+ $DAPI^-$ A375 cells that were detected (Appendix A1) clearly demonstrate that PLX4720 and Vemurafenib induce A375 death through apoptosis. However, targeted BRAF inhibition caused fewer A375 cells to undergo early apoptosis or cell death than expected for a highly sensitive cell line. This discrepancy may be due to time dependent effects, with A375 cells requiring longer exposure to inhibitors to initiate apoptosis and undergo cell death, or passing through early apoptosis rapidly.

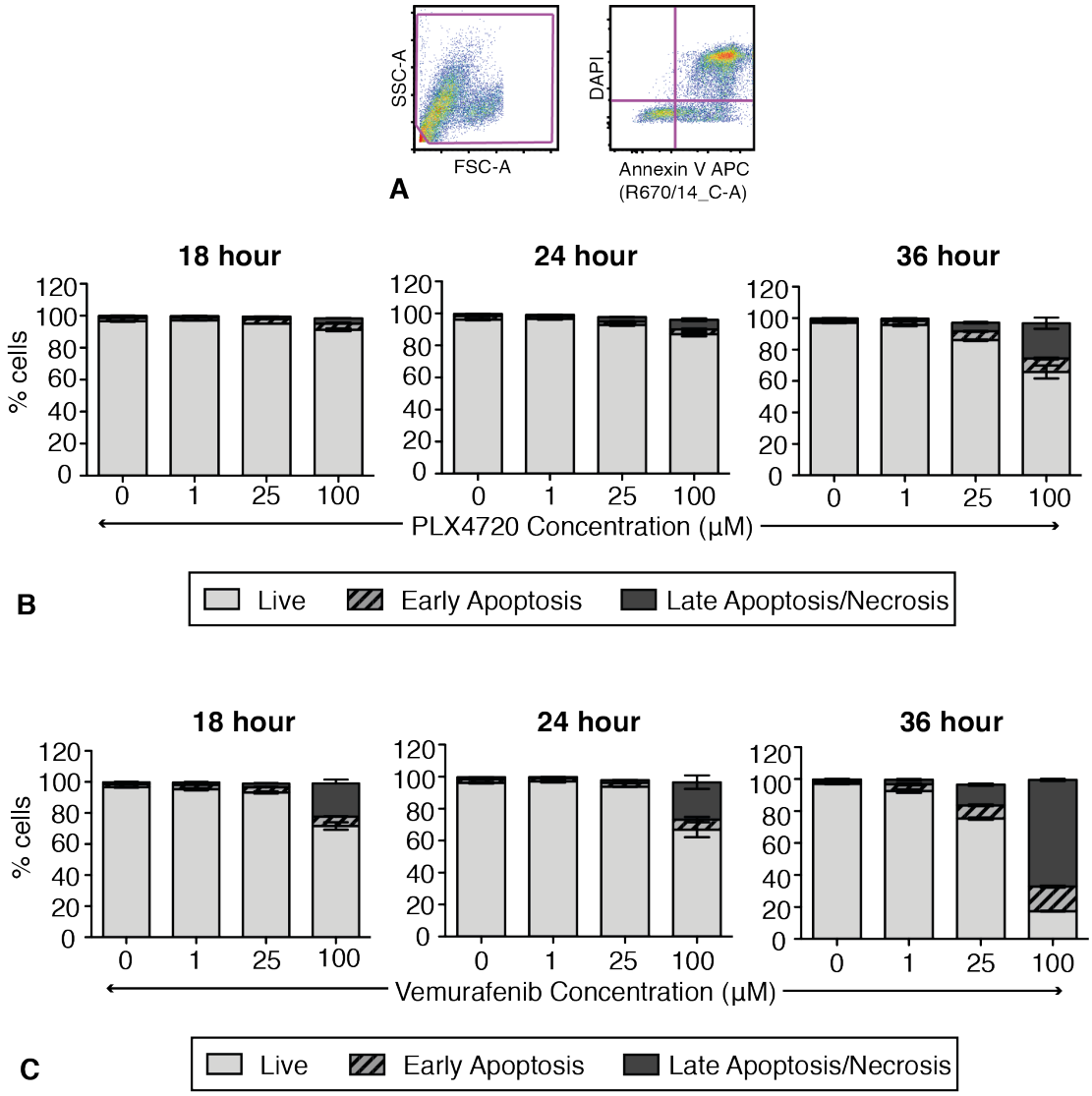

Figure 3.8: PLX4720 and Vemurafenib induce A375 cell death by apoptosis. Cells were treated with a range of concentrations of PLX4720 and Vemurafenib (1 μM-100 μM) for 18-36 hours. Cell viability and phosphatidylserine expression was then analysed by flow cytometry, with gating performed as shown in representative dot plots (**A**). Proportion of live ($DAPI^-$, AV^-), early apoptotic ($DAPI^-$, AV^+) and late apoptotic/necrotic ($DAPI^+$, AV^+) cells are shown with PLX4720 treatment (**B**) or Vemurafenib treatment (**C**). Each bar represents the mean of the triplicates and error bars are ± S.D. Data are representative of two independent experiments.

Similar results were obtained with YUMM1.1 cells (Figure 3.9). Treatment of YUMM1.1 cells with either PLX4720 or Vemurafenib for 18 hours resulted in little to no cells undergoing early apoptosis, and less than 20% cell death. This shows that generally YUMM1.1 cells require longer than 18 hours exposure to targeted BRAF inhibition for induction of apoptosis to occur. Furthermore, exposure of YUMM1.1 cells to 1 μM PLX4720 or Vemurafenib caused few cells to enter early apoptosis; even with 36 hours of treatment cell viability remained greater than 80%. However, at the higher concentrations of 25 and 100 μM PLX4720 and Vemurafenib induced early apoptosis and death when cells were exposed to inhibitors for 24-36 hours, with very similar effects observed with both inhibitors.

Comparatively, YUMM1.7 cells were more sensitive to BRAF inhibitor induced apoptosis. Unlike A375 or YUMM1.1 cells a 24 or 36 hour exposure to 1 μM PLX4720 or Vemurafenib treatment induced early apoptosis in YUMM1.7 cells. Additionally, Vemurafenib induced approximately 20% of YUMM1.7 cells to enter early apoptosis after only 18 hours of inhibitor treatment. Treatment with 25 and 100 μM PLX4720 or Vemurafenib for 18-36 hours clearly induced early apoptosis and death of YUMM1.7 cells, with 20-50% of cells shown to be AV^+ $DAPI^-$ and 20-40% of cells AV^+ $DAPI^+$. At all concentrations PLX4720 and Vemurafenib treatment results in greater apoptosis and death of YUMM1.7 cells than the other cell lines. Analogous to the effects seen with A375 cells, Vemurafenib was more effective than PLX4720 at inducing both YUMM1.1 and YUMM1.7 cell death.

Collectively, these data demonstrate that the targeted BRAF inhibitors PLX4720 and Vemurafenib induce death by apoptosis of both murine and human $BRAF^{V600E}$ melanoma cells. The proportion of cells undergoing apoptosis is time and concentration dependent, increasing with drug concentration and length of exposure. In all three cell lines Vemurafenib is more effective at inducing apoptosis than PLX4720, although both inhibitors showed similar trends.

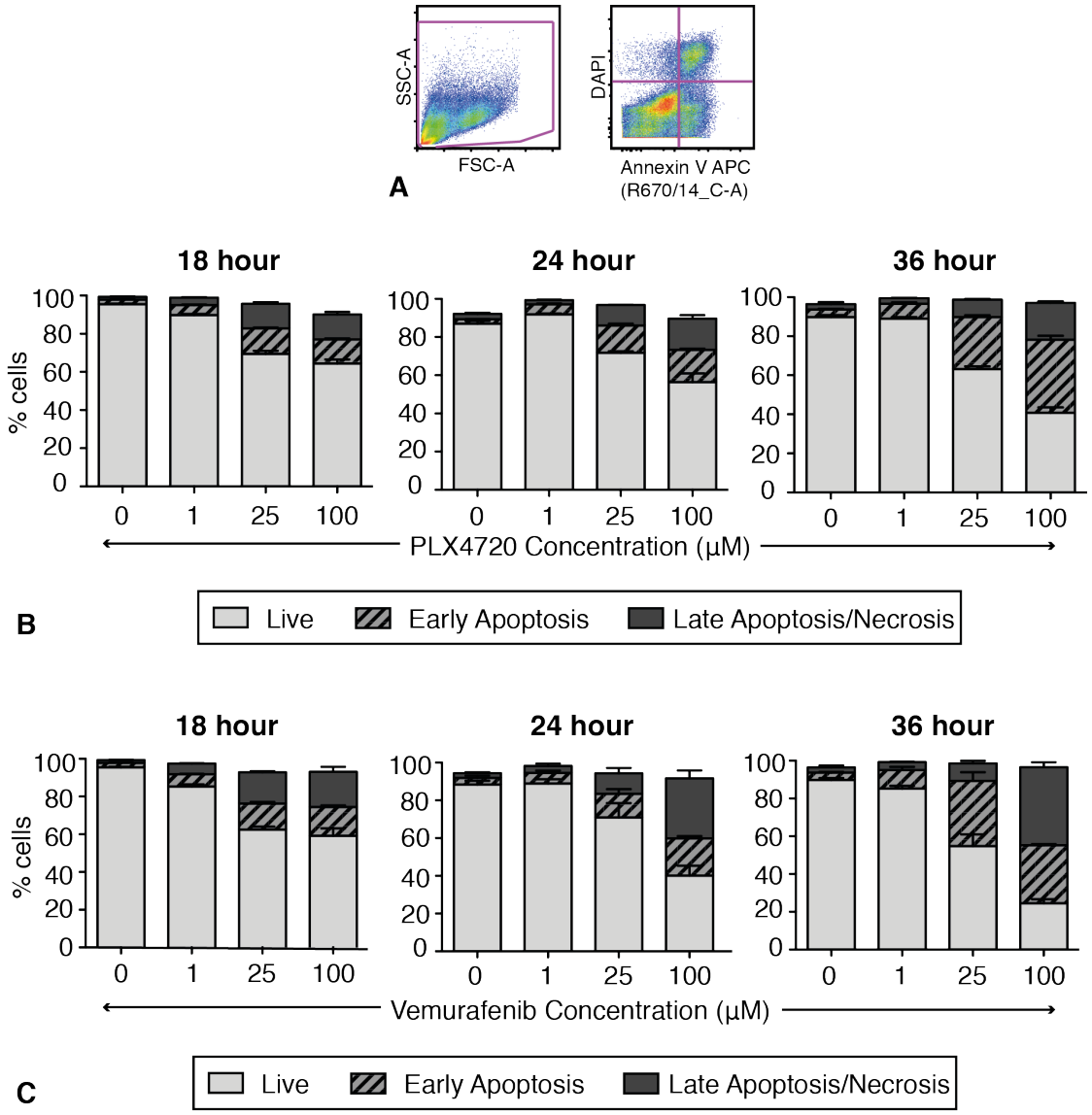

Figure 3.9: PLX4720 and Vemurafenib induce YUMM1.1 cell death by apoptosis. Cells were treated with a range of concentrations of PLX4720 and Vemurafenib (1 μM-100 μM) for 18-36 hours. Cell viability and phosphatidylserine expression was then analysed by flow cytometry, with gating performed as shown in representative dot plots (**A**). Proportion of live ($DAPI^-$, AV^-), early apoptotic ($DAPI^-$, AV^+) and late apoptotic/necrotic ($DAPI^+$, AV^+) cells are shown with PLX4720 treatment (**B**) or Vemurafenib treatment (**C**). Each bar represents the mean of the triplicates and error bars are ± S.D. Data are representative of two independent repeats.

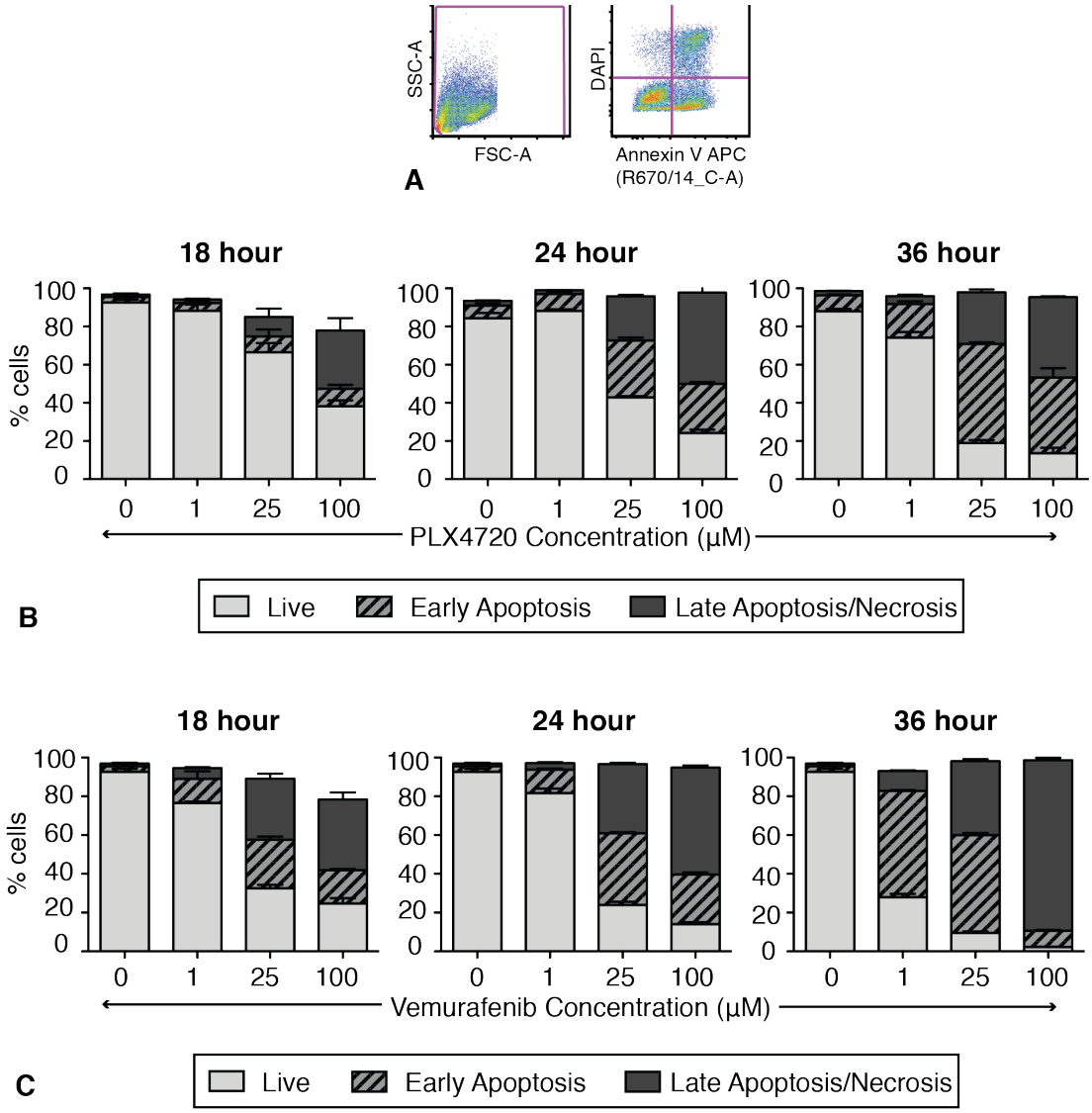

Figure 3.10 PLX4720 and Vemurafenib induce YUMM1.7 cell death by apoptosis. Cells were treated with a range of concentrations of PLX4720 and Vemurafenib (1 μM-100 μM) for 18-36 hours. Cell viability and phosphatidylserine expression was then analysed by flow cytometry, with gating performed as shown in representative dot plots (**A**). Proportion of live ($DAPI^-$, AV^-), early apoptotic ($DAPI^-$, AV^+) and late apoptotic/necrotic ($DAPI^+$, AV^+) cells are shown with PLX4720 treatment **(B)** or Vemurafenib treatment (**C**). Each bar represents the mean of the triplicates and error bars are ± S.D. Data are representative of two independent repeats.

3.2.4 Melanoma production of soluble immunosuppressive factors can be partially reversed by BRAF inhibition

The preceding experiments characterized the dynamics and mechanism of BRAF inhibitor induced cell death. Following on from this, the effects of BRAF inhibition on melanoma cells at non-cytotoxic concentrations were explored. Of particular interest was the effect of BRAF inhibition on melanoma-mediated immunosuppression. Initial experiments examined the ability of A375 cells to produce soluble immunosuppressive factors, and subsequently the effect of PLX4720 treatment on A375 immune suppression was investigated. Conditioned media was collected from A375 cell cultures (Figure 3.11A), and the effects of this conditioned media on human T cell proliferation *in vitro* were assessed. Peripheral blood mononuclear cells (PBMCs) were extracted from the blood of healthy human donors and were stimulated in a one-way mixed lymphocyte reaction with IL-2 (Figure 3.11B). T cell proliferation was determined by CFSE dilution as measured by flow cytometry (Figure 3.11C). The proportion of control T cell proliferation in the absence of conditioned media was determined, and T cell proliferation in presence of conditioned media was presented as a percentage of this control.

A375 conditioned media suppressed T cell proliferation significantly, with the proportion of cells proliferating reduced by approximately 50% (Figure 3.11D). Pre-treatment of A375 cells with 200 nM PLX4720 for 18 hours partially abrogated immunosuppression, with T cell proliferation increased by approximately 20-30%. Similarly, if A375 cells were exposed to 200 nM PLX4720 for 18 hours, then thoroughly washed and subsequently cultured in the absence of drug for 18 hours, the resulting conditioned media was also less immunosuppressive than that of untreated cells. These results demonstrate that PLX4720 was acting directly on the A375 cells, and the increased proliferation was not a result of residual drug in the conditioned media affecting T cell proliferation. Whilst PLX4720 abrogation of A375 mediated immunosuppression did not reach statistical significance this trend was consistent across five independent experiments performed using different donor PBMCs.

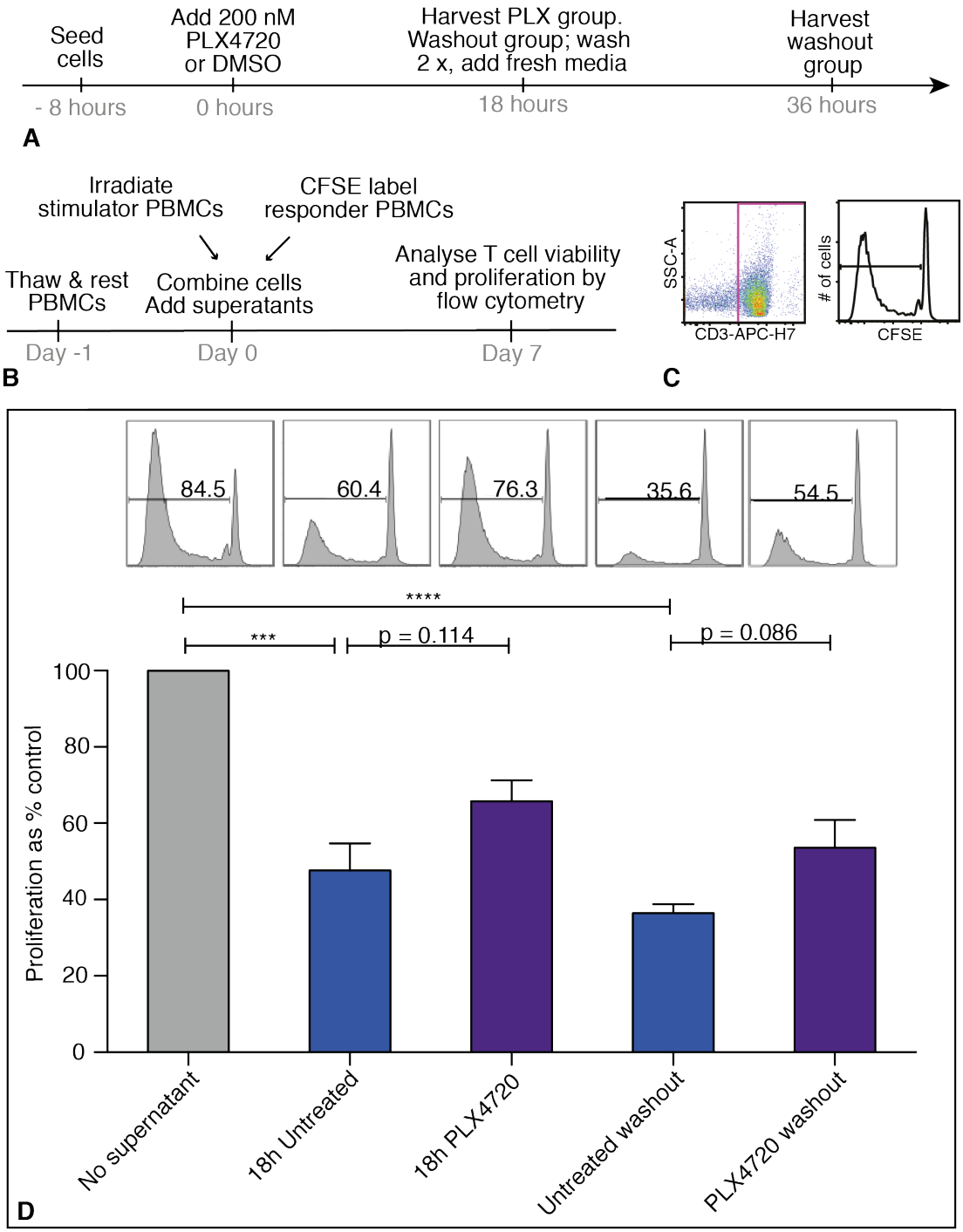

Figure 3.11: A375 supernatant suppression of T cell proliferation is partially reversed by PLX4720 treatment. A. Supernatants were collected from A375 cells treated with PLX4720 as described. **B.** Suppressive activity of these supernatants was then evaluated in a one-way mixed lymphocyte reaction. **C.** T cell proliferation was examined by flow cytometry, representative dot plots show the gating strategy used to identify T cells and measure proliferation. **D.** T cell proliferation is shown as a percentage of DMSO treated control. Each bar represents the mean of the triplicate. Error bars are ± S.D. NS = not significant, *** $p < 0.001$, **** $p < 0.0001$, one-way ANOVA with Bonferroni

post-test. Data are representative of 5 independent experiments, with concordant results.

Having established that PLX4720 abrogates immunosuppression mediated by $BRAF^{V600E}$ melanoma cells sensitive to targeted BRAF inhibition, the effect on *de novo* resistant SK-mel-5 cells was investigated. Similar to the experiments performed with A375 cells, SK-mel-5 production of immunosuppressive soluble factors in the presence and absence of BRAF inhibition was investigated. Conditioned media was collected from SK-mel-5 cells after 48 hours of culture with DMSO or varying concentrations of PLX4720 from 1 to 20 μM. PBMCs from healthy human donors were stimulated with anti-CD3, anti-CD28 and IL-2, and T cell proliferation was determined by CFSE dilution as measured by flow cytometry (Figure 3.12A and B). Again, T cell proliferation was presented as percentage of the untreated, control T cells (Figure 3.12C).

Similar to A375 cells, SK-mel-5 conditioned media suppressed T cell proliferation significantly (Figure 3.12C). Treatment of SK-mel-5 cells with 1 or 5 μM PLX4720 decreased the suppressive effects of the conditioned media. However, neither 10 nor 20 μM PLX4720 treatment reduced the immunosuppression of SK-mel-5 conditioned media. Direct treatment of T cells with 5 and 10 μM PLX4720 had no effect on T cell proliferation (as shown in Chapter 4). These data indicate that PLX4720 treatment of SK-mel-5 cells directly reduced SK-mel-5 production of soluble immunosuppressive factors, and that this effect only occurs at optimal drug concentration.

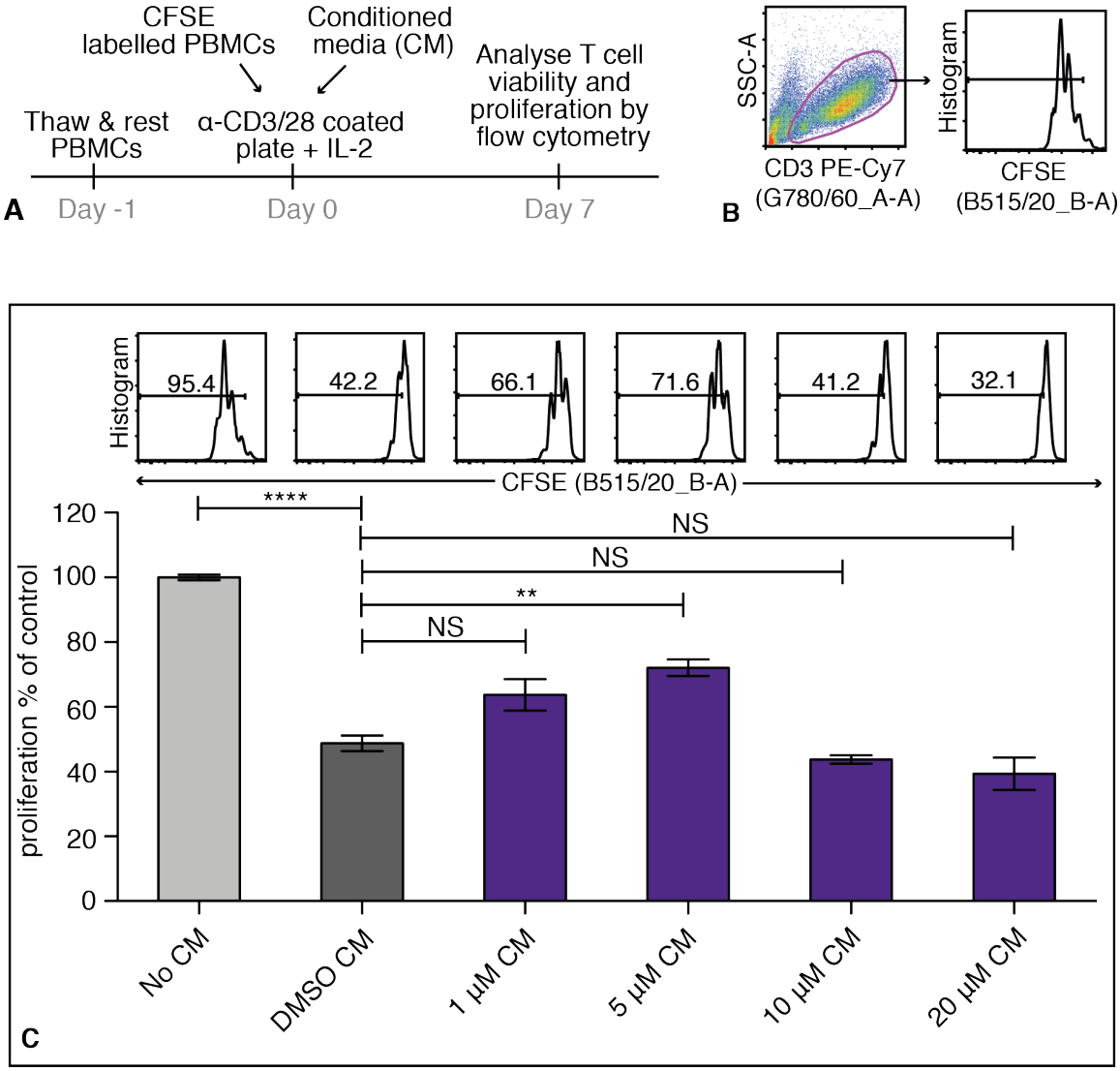

Figure 3.12: SK-mel-5 production of soluble immunosuppressive factors is abrogated by PLX4720 treatment. Conditioned media (CM) was harvested from SK-mel-5 cells following 48 hours of culture with DMSO or 1–5 μM PLX4720. A. Suppressive activity of CM was assessed with anti-CD3, anti-CD28 and IL-2 stimulation of PBMCs from healthy human donors. B. T cell proliferation was examined by flow cytometry, representative dot plots show the gating strategy used to identify T cells and measure proliferation. D. T cell proliferation is shown as a percentage of DMSO treated control. Each bar represents the mean of the triplicate. Error bars are ± S.D. NS = not significant, ** $p < 0.05$, **** $p < 0.0001$, one-way ANOVA with Bonferroni post-test. Data are representative of 2 independent experiments.

Finally, the immunosuppressive properties of YUMM cells were examined. Conditioned media was collected from YUMM1.1 or YUMM1.7 cells cultured at cell concentrations of 1 x 10^4 – 1 x 10^5 cells per well for 12 – 48 hours. C57BL/6 splenocytes were stimulated with anti-CD3, anti-CD28 and IL-2, and T cell proliferation was determined by CFSE dilution and activation by CD69 expression as measured by flow cytometry (Figure 3.13A and B). The proportion of T cells proliferating in control wells was determined, and T cell proliferation was presented as a percentage of control T cell proliferation. YUMM1.1 and YUMM1.7 conditioned media did not significantly suppress T cell proliferation or activation (Figure 3.13C and D). Experimental optimization was performed with cell numbers titrated, culture times varied and finally the addition of different dilutions of conditioned culture medium was tested (diluting from 1:1 to 1:4). None of these culture conditions or dilutions of conditioned media resulted in suppression of T cell proliferation or activation (data not shown). Therefore, it was concluded that the YUMM1.1 and YUMM1.7 cell lines did not produce soluble factors that directly suppressed T cell proliferation. With respect to this finding, the effect of PLX4720 on YUMM1.1 and YUMM1.7 production was unable to be assessed in these assays.

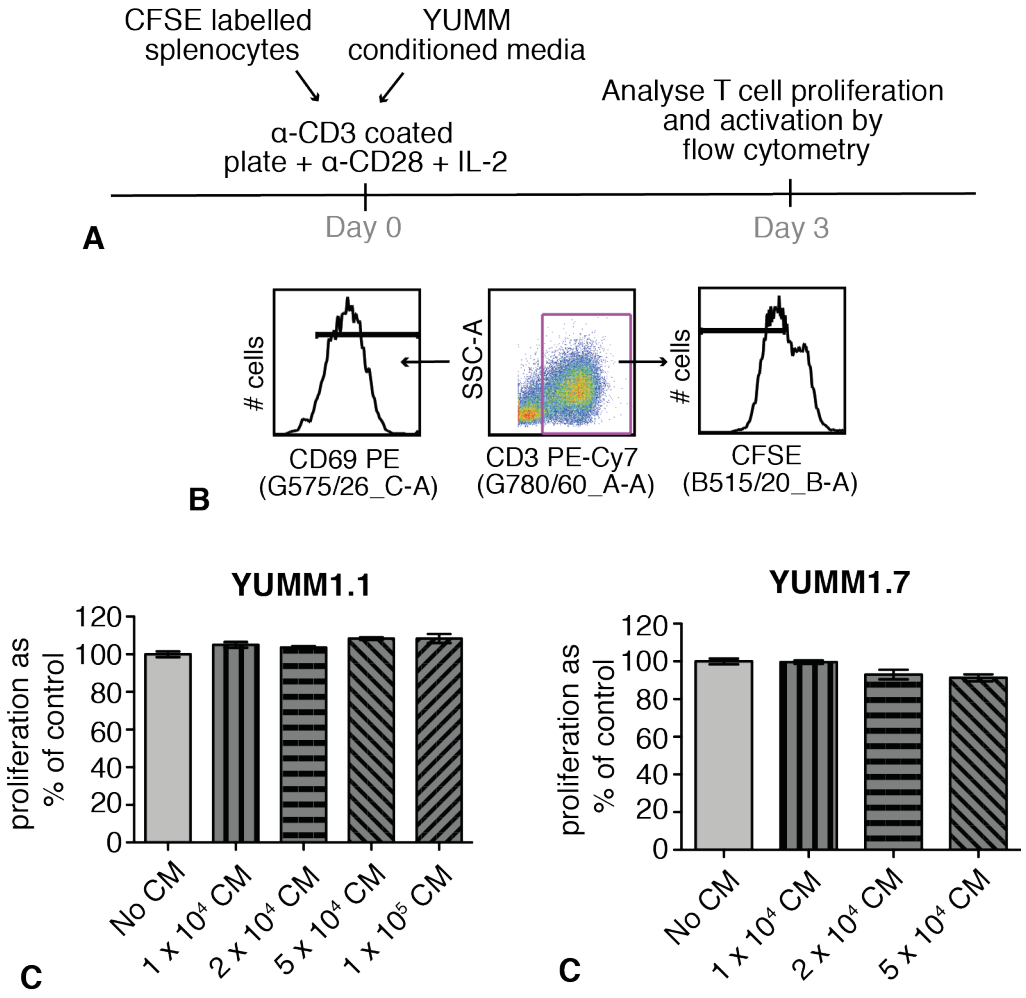

Figure 3.13: YUMM1.1 and YUMM1.7 cells do not produce soluble factors that suppress T cell proliferation. A. Conditioned media (CM) was harvested from YUMM1.1 or YUMM1.7 cells following 48 hours of culture at with varying cell numbers per well (1 x 10^4-1 x 10^5). Suppressive activity of CM was assessed with anti-CD3, anti-CD28 and IL-2 stimulation of C57BL/6 splenocytes. **B.** T cell proliferation was examined by flow cytometry with populations defined as shown, samples pre-gated on single and live cells. Neither YUMM1.1 **(C)** nor YUMM1.7 **(D)** conditioned media affected T cell proliferation.

3.2.5 PX4720 treatment slows YUMM1.1 and YUMM1.7 growth *in vivo* and increases survival

In order to investigate YUMM sensitivity to BRAF inhibitor treatment *in vivo*, the number of cells delivered during tumour challenge was optimized. Cell numbers for injection were based on a reported tumour growth rate of 1 cm^3 tumours 6 weeks after subcutaneous injection of 1 x 10^5 YUMM1.1 cells (personal communications; Katrina Meeth, Yale University), and the knowledge that YUMM1.7 cells have a faster doubling time *in vitro* (data not shown). Mice were injected subcutaneously with 2-4 x 10^5 YUMM1.1 cells, or 1-2 x 10^5 YUMM1.7 cells and tumour growth was monitored (Appendix B1). Similar rates of YUMM1.1 and YUMM1.7 tumour growth were seen with both cell numbers tested. YUMM1.1 growth was less variable with 2 x 10^5 cells, while YUMM1.7 tumours were less likely to ulcerate with 1 x 10^5 cells. Therefore, these cell numbers were used for tumour injections in the ensuing experiments.

Next, the effect of PLX4720 treatment on YUMM1.1 tumour growth and mouse survival was determined. C57BL/6 mice were challenged with 2 x 10^5 YUMM1.1 cells and seven days post-tumour challenge daily treatment with PLX4720 delivered by oral gavage was initiated (Figure 3.14A). Mice received doses of PLX4720 ranging from 5 mg/kg to 100 mg/kg with control mice receiving a vehicle solution, and tumour size was measured every two to three days. All PLX4720 treatments decreased average tumour growth, with a highly significant reduction in tumour size evident at Day 21 post tumour-challenge (the point at which the first control mouse had to be culled due to tumour size) (Figure 3.14B). Despite PLX4720 slowing tumour growth, delivery of the highest recommended drug concentration of 100 mg/kg (Dr Gideon Bollag, personal communications) did not result in tumour regression (Figure 3.14B and C). In addition to slowing tumour growth 5-100 mg/kg PLX4720 treatment significantly increased mouse survival relative to vehicle control treated mice (Figure 3.14D). The effects on tumour growth and survival were clearly dose dependent with increasing anti-tumour effects correlating with increased PLX4720 dose.

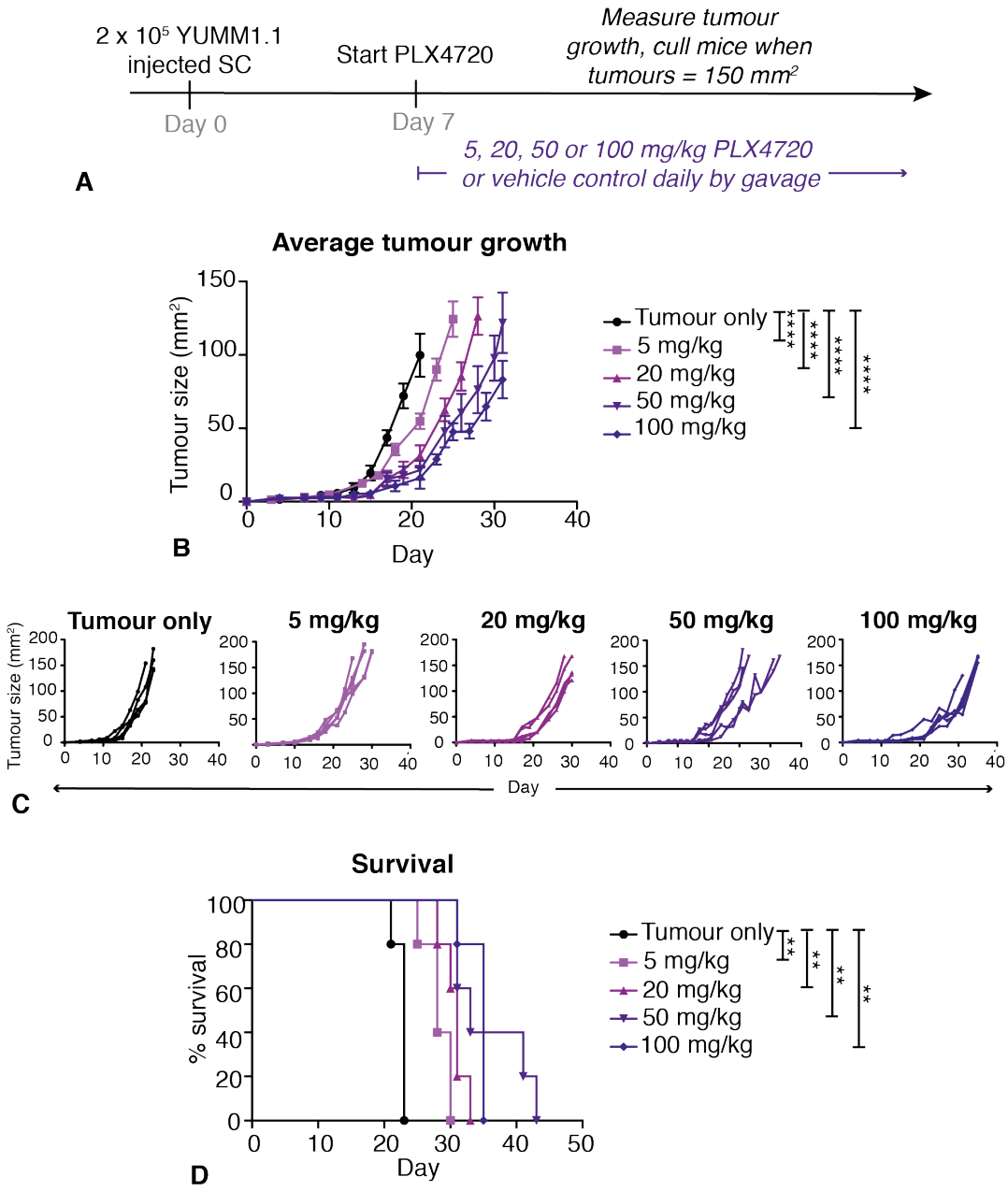

Figure 3.14: PLX4720 treatment slows YUMM1.1 growth *in vivo* and increases survival, but does not induce tumour regression. A. C57BL/6 mice were injected subcutaneously in the left flank with 2 x 10^5 YUMM1.1 cells. Daily drug treatment was begun 7 days post-tumour challenge with 5-100 mg/kg PLX4720 given by oral gavage. Tumour growth was monitored and size recorded. Mice were culled when tumours reached 150 mm^2, or when tumours ulcerated. **** $P \leq 0.0001$, 2-way ANOVA with Bonferroni post-test, statistics are shown for Day 21. **B.** Individual tumour growth is shown. Each symbol represents the mean growth of groups of 4-5 mice; error bars are ± SEM. **C.** Tumour growth for each treatment group. Each symbol represents one mouse. Graphs are representative of at least two independent experiments. **D.** Percent survival shown for groups of 4-5 mice. Treatment groups are compared to the vehicle treated control mice ** $P < 0.01$, Mantel-Cox test.

YUMM1.7 sensitivity to PLX4720 treatment *in vivo* was also examined using a similar experimental design. C57BL/6 mice were challenged with 1 x 10^5 YUMM1.7 cells and mice either received 5 or 20 mg/kg PLX4720 from seven days post-tumour challenge, while control mice received a vehicle solution (Figure 3.15A). Both 5 and 20 mg/kg PLX4720 significantly slowed tumour growth, relative to the vehicle treated control group, with statistics shown for Day 26 post-tumour challenge, when the first control mouse was culled due to tumour size (Figure 3.15B). A greater reduction in tumour growth was evident with 20mg/kg PLX4720 treatment than 5 mg/kg PLX4720, and 20 mg/kg also appeared to induce a more consistent response in tumours (Figure 3.15C). PLX4720 significantly increased survival at both doses, again the beneficial effect was more apparent at the higher dose of 20 mg/kg (Figure 3.15D). Comparable to the results observed in YUMM1.1 tumours, PLX4720 effects on YUMM1.7 tumour growth and mouse survival were also dose-dependent. However, YUMM1.7 tumours appear to be a lot more sensitive to PLX4720 treatment with 20 mg/kg dosing inducing a greater reduction in YUMM1.7 tumour growth than YUMM1.1 and proffering a greater survival advantage to mice with YUMM1.7 tumours.

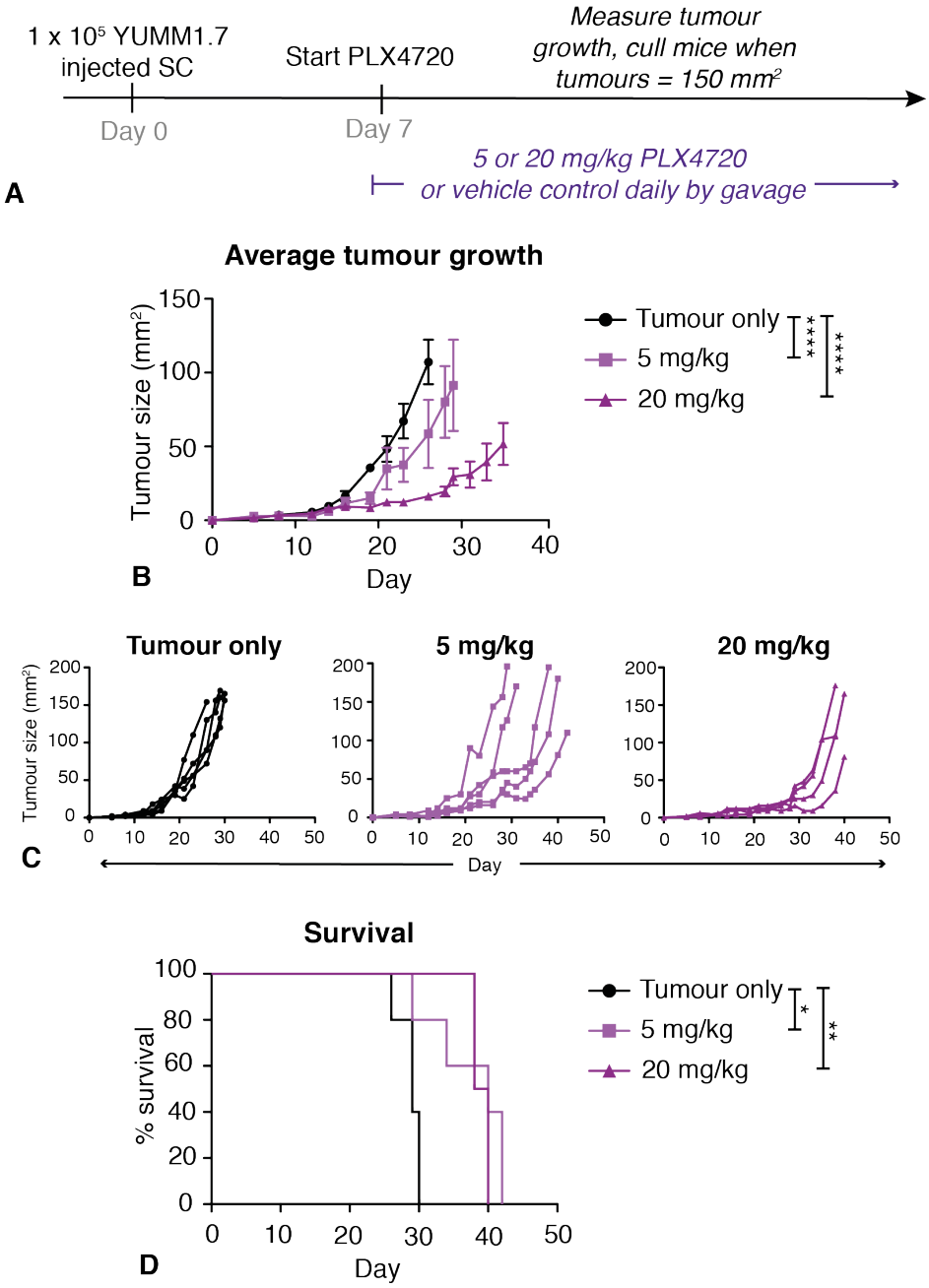

Figure 3.15: PLX4720 treatment slows YUMM1.7 growth *in vivo* and increases survival, but does not induce tumour regression. **A.** C57BL/6 mice were injected subcutaneously in the left flank with 1 x 10^5 YUMM1.7 cells. Daily drug treatment was begun 7 days post-tumour challenge with 5 or 20 mg/kg PLX4720 given by oral gavage. Tumour growth was monitored and size recorded. Mice were culled when tumours reached 150 mm^2, or when tumours ulcerated. **** $P \leq 0.0001$, 2-way ANOVA with Bonferroni post-test, statistics are shown for Day 26. **B.** Individual tumour growth is shown. Each symbol represents the mean growth of groups of 4-5 mice; error bars are ± SEM. **C.** Percent survival shown for groups of 4-5 mice. Treatment groups are compared to the vehicle treated control mice * $P \leq 0.05$ ** $P < 0.01$, Mantel-Cox test. **D.** Tumour growth for each treatment group. Each symbol represents one mouse. Graphs are representative of two independent experiments.

3.3 Discussion

In this chapter I have characterised novel *BRaf*^{V600E}; *Pten*$^{-/-}$; *CDKN2a*$^{-/-}$ murine melanoma cell lines. Both cytotoxic and non-cytotoxic effects of BRAF inhibition were investigated in these models, and responses were compared and contrasted with those of the widely used human BRAF^{V600E} A375 and SK-mel-5 cell lines. Additionally, responses of BRAF mutant cell lines have been compared with those of BRAF wild-type cell lines.

The mutant-BRAF targeted inhibitors PLX4720 and Vemurafenib were clearly demonstrated to be specific for cell lines with BRAF mutations, as expected. BRAF wild-type cell lines including B16 murine melanoma and HL-60 human leukaemia were resistant to PLX4720 and Vemurafenib, despite being sensitive to broad-spectrum MAP kinase blockade. The human BRAF^{V600E} cell line A375 was highly sensitive to BRAF inhibition, while human BRAF^{V600E} SK-mel-5 melanoma cells were relatively insensitive. These findings complement a previously published study showing SK-mel-5 cells to be *de novo* resistant to PLX4720 (Deng et al., 2012). Identification of two cell lines that represented different ends of the spectrum of BRAF^{V600E} melanoma sensitivity to PLX4720 and Vemurafenib provided a good framework for comparison of the novel *BRaf*^{V600E}; *Pten*$^{-/-}$; *CDKN2a*$^{-/-}$ YUMM1.1 and YUMM1.7 cell lines. These were demonstrated to be moderately sensitive cell lines *in vitro.* PLX4720-induced death of both these cell lines and of A375 cells was shown to occur by apoptosis.

Traditionally, immunogenic cell death has been associated with necrosis while apoptosis has been considered to be less immunostimulatory, or even tolerogenic (Zitvogel et al., 2008). However, it has become increasingly clear that this assumption does not always hold true. Under certain conditions, apoptosis of tumour cells can be immunostimulatory (Feng et al., 2002; Obeid et al., 2007; Restifo, 2000). Apoptosis is a non-uniform process that can occur either in a tolerogenic or immunogenic manner. Immunogenic apoptosis occurs when phagocytes engulf apoptotic cells in the presence of a danger signal (Steer et al., 2010). Commonly, in chemotherapy-induced immunogenic apoptosis this danger signal is the expression of calreticulin (Obeid et al.,

2007; Zitvogel et al., 2010). Vaccines using tumour cells have been shown to induce potent anti-tumour immune responses only if tumour cells were apoptotic, not necrotic (Scheffer et al., 2003). This study supports the idea that apoptotic tumour cell death is immunogenic in a context relevant to immunotherapy. Thus chemotherapy-induced apoptosis may be able to stimulate immune responses *in vivo*.

Unexpectedly, induction of YUMM1.1 and YUMM1.7 apoptosis by BRAF inhibition *in vitro* did not predict the outcome of BRAF inhibitor treatment of tumours *in vivo*. PLX4720 treatment *in vivo* significantly decreased tumour outgrowth, but did not cause tumour regression, implying a lack of significant tumour cell death. Irrespective of the absence of obvious tumour cell death *in vivo*, PXL4720 treatment of YUMM1.1 and YUMM1.7 tumours likely still generated an immunogenic phenotype. Previous studies have demonstrated that broad-spectrum chemotherapies do not necessarily need to induce cell death to render tumour cells more immunogenic. Sub-lethal chemotherapy has been shown to increase tumour cell immunogenicity, MHC class I expression and granzyme B permeability resulting in increased susceptibility to CTL-mediated killing (Fisk and Ioannides, 1998; Kaneno et al., 2011; Ramakrishnan et al., 2010). Furthermore, non-cytotoxic chemotherapy can cause downregulation of tumour anti-apoptotic genes and increased Fas expression, rendering cells more receptive to CTL-mediated Fas-dependent CTL lysis (Gameiro et al., 2011). Targeted BRAF inhibitors are likely to have similar effects, with non-cytotoxic concentrations of Vemurafenib and PLX4720 previously shown to enhance MHC expression, tumour antigenicity and decrease melanoma-mediated immunosuppression (Donia et al., 2012a; Frederick et al., 2013; Sapkota et al., 2013; Sumimoto et al., 2006).

There are several possible mechanisms that may underlie resistance to tumour cell death *in vivo*. This could be attributable to the PTEN-deficiency of the model, which has been strongly associated with resistance to BRAF inhibitor treatment (Deng et al., 2012; Paraiso et al., 2011; Xing et al., 2012; Ye et al., 2013). Although, there is variability in the degree of resistance conferred by PTEN loss. Resistance mediated by PTEN-loss may explain the decreased

sensitivity of YUMM cell lines compared with the highly sensitive, and PTEN wild-type, A375 cells (Chen et al., 2012). However, loss of PTEN alone would not account for the disparity between *in vitro* and *in vivo* cell death in the YUMM models. These contradictory findings may be reconciled by the presence of factors or interactions within the tumour microenvironment *in vivo*, which may confer a protective phenotype.

There is considerable evidence that tumour-associated fibroblasts, immune cells and vasculature can mediate a BRAF inhibitor resistant phenotype (Junttila and de Sauvage, 2013). Hepatocyte growth factor (HGF), produced by stromal cells, has been shown to induce $BRAF^{V600E}$ melanoma resistance to both Vemurafenib and PLX4720 (Filitis et al., 2015). In patients, both increased expression of the HGF receptor cMET by melanoma cells and stromal cell expression of HGF have been correlated with BRAF inhibitor resistance (Straussman et al., 2012). Additionally, Vemurafenib induced melanoma cells to produce TGFβ, causing fibroblast differentiation, and stimulating differentiated fibroblasts to produce HGF. This resulted in fibroblast- and HGF-mediated resistance to Vemurafenib treatment (Fedorenko et al., 2015). Independently, TGFβ was shown to induce Vemurafenib resistance through EGFR and PDGFRβ upregulation (Sun et al., 2014). Fibroblast-mediated resistance has also been demonstrated to occur through production of focal adhesion kinase (FAK) and integrinβ1, driving ERK activation and BRAF inhibitor resistance (Hirata et al., 2015). Finally, TNFα has been implicated in BRAF inhibitor resistance, through activation of nuclear factor-κB (NFκB), and macrophages are a likely source of TNFα within the tumour microenvironment (Gray-Schopfer et al., 2007; Menon et al., 2013; Shao et al., 2015). Therefore, a multitude of resistance mechanisms mediated by the tumour microenvironment can play a role in BRAF inhibitor resistance, some of which may be relevant to the YUMM1.1 and YUMM1.7 models.

In addition to effects of the tumour microenvironment, intra-tumoural heterogeneity is a well-established mechanism of resistance *in vivo*, where targeted drug treatment selects for the outgrowth of resistant phenotypes (Shi et al., 2014; Somasundaram et al., 2012). YUMM1.1 and YUMM1.7 are primary cell lines, containing a variety of distinct cell morphologies.

Treatment with PLX4720 *in vivo* may stimulate the outgrowth of drug-resistant populations, as shown previously in tumours with cell populations of mixed drug sensitivity (Obenauf et al., 2015). $BRAF^{V600E}$ melanomas sensitive to BRAF inhibition *in vitro* but refractory to treatment *in vivo* are becoming increasingly recognized. These models may represent the subset of patient BRAF-mutant melanomas that exhibit only limited, or short-term responsiveness to targeted BRAF inhibitors. With significant variability in the initial response of patients to BRAF inhibition, it is essential that research be carried out in models representing less responsive patients as well as in highly sensitive models (Chapman et al., 2011; Sosman et al., 2012).

PLX4720 induced reduction in A375- and SK-mel-5-mediated immunosuppression demonstrated in this chapter supports previously published data. Whilst the mediators of A375 and SK-mel-5 suppression were not investigated in this thesis, other studies using these cell lines have implicated the soluble factors TGFβ, IL-6, IL-10, VEGF, MICA/B and CCL22 as being key mediators of immunosuppression (Diaz-Valdes et al., 2011; Groh et al., 2002; Sumimoto et al., 2006; Yaguchi et al., 2011). These findings support the role for non-cytotoxic effects of BRAF inhibitors in creating a more favourable immune microenvironment in both BRAF inhibitor-sensitive and resistant melanoma cells. These effects were unable to be assessed in the YUMM1.1 and YUMM1.7 models, due to an absence of soluble factors that suppressed T cell proliferation. However, these cell lines likely generate an immunosuppressive microenvironment through one of a number of alternative mechanisms. Some melanoma cells have been previously shown to express immunosuppressive molecules on the cell surface, such as CD200 or members of the B7 family (such as PD-L1) (Yaguchi et al., 2011). Alternatively, YUMM cells may express molecules or produce soluble factors that induce the differentiation and migration of regulatory immune cell phenotypes.

3.3.1 Conclusions

In this chapter I have demonstrated that targeted BRAF inhibition induces both murine and human $BRAF^{V600E}$ melanoma cell death via apoptosis. At non-cytotoxic concentrations, BRAF inhibitors can partially abrogate

melanoma-mediated immune suppression, reducing the production of soluble immunosuppressive factors by melanoma cells. These findings support the hypothesis that BRAF inhibition will generate a tumour microenvironment more favourable to anti-tumour immunity and strengthen the justification for combining targeted BRAF inhibition with immunotherapy.

Two immunocompetent *in vivo* models of *BRaf^{V600E}; Pten$^{-/-}$; CDKN2a$^{-/-}$* murine melanoma have been optimized for further work. I have demonstrated that these models are only moderately sensitive to BRAF inhibition, and *in vivo* PLX4720 treatment reduced tumour growth but did not achieve tumour regression. This work has established a valuable model, which possesses key mutations genetically similar to many human melanomas and represents patients who are less sensitive to BRAF inhibition. This is a useful tool for further research into the combination of targeted BRAF inhibition and immunotherapy.

CHAPTER 4:
Direct effects of BRAF inhibitors on immune cells

4.1 Introduction

The previous chapter established that the targeted BRAF inhibitors PLX4720 and Vemurafenib had cytotoxic effects on $BRAF^{V600E}$ melanoma cells, inducing cell death via apoptosis, which is potentially immunogenic. In addition, targeted BRAF inhibition reversed $BRAF^{V600E}$ melanoma-mediated immunosuppression. These findings support investigation into combination of PLX4720 with immunotherapy. However, prior to attempting to combine BRAF inhibitors with T cell-mediated immunotherapy it is crucial that any direct immunological effects are elucidated. Therefore, this chapter examines the direct effects of targeted BRAF inhibitors on T cell responses.

When experimental research for this thesis commenced in 2012, it was widely assumed that targeted BRAF inhibitors would have no effect on immune cell viability or function due to their exceptional specificity for mutant BRAF over wild-type BRAF. Recently, several studies have investigated the effects of targeted BRAF inhibition on immune cells *in vitro* and *in vivo,* and the results have been contradictory (Callahan et al., 2014; Comin-Anduix et al., 2010; Gargett et al., 2015; Irving et al., 2013; Schilling et al., 2014). Both inhibitory and stimulatory effects of PLX4720 and Vemurafenib have been reported, and differential effects on T cell activation and function were observed. Despite study-to-study variation, clear detrimental effects of targeted BRAF inhibitors have been shown, questioning initial assumptions that PLX4720 and Vemurafenib would not affect immune cells. A major limitation of the studies published to date has been the concentration range of Vemurafenib and PLX4720 tested. Predominantly, doses of 50 μM or lower were tested, while patient plasma concentrations of Vemurafenib are often well in excess of this. Studies of patients receiving Vemurafenib have reported concentration ranges in patient plasma of 50-200 μM (Flaherty et al., 2010; Funck-Brentano et al., 2015). The mean plasma concentration in the Vemurafenib phase I clinical trial was 80 μM (Flaherty et al., 2010). Furthermore, meta-analysis of Vemurafenib clinical trials revealed that patient plasma concentrations often reached 300 μM, which was determined to be the optimally effective concentration for tumour regression (Bollag et al., 2012). Therefore, it is

essential that the effects of BRAF inhibitors on immune cells are assessed at concentrations of greater than 50 μM. In addition to the variability reported in *in vitro* studies, there also appears to be a discrepancy in the immunological effects of BRAF inhibitors observed between *in vitro* and *in vivo* studies. *In vivo* studies have reported less significant inhibitory effects and more commonly beneficial effects of targeted BRAF inhibitor treatment on immune cells compared with *in vitro* studies (Frederick et al., 2013; Ho et al., 2014; Irving et al., 2013; Schilling et al., 2014). This variability is likely a product of the considerable differences in *in vitro* and *in vivo* microenvironments, in particular the difference in drug bioavailability when considering serum binding proteins. While the absolute bioavailability of Vemurafenib is unknown, it is highly bound by human plasma proteins (in excess of 99% binding), possibly altering drug availability *in vivo* (da Rocha Dias et al., 2013).

To validate findings reported in the literature, the effects of PLX4720 and Vemurafenib on both human and murine T cells *in vitro* was assessed at physiologically relevant concentrations. Immunological effects were also established in *in vivo* models to determine the translational applicability of *in vitro* findings.

4.1.1 Aims

The following series of experiments were undertaken to determine the direct effects of targeted BRAF inhibitors on T cell responses. In particular, these experiments aimed to:

- Characterise the effects of targeted BRAF inhibition on human and murine T cells *in vitro*

- Determine the consequences of PLX4720 treatment on antigen-specific T cell responses *in vivo*

- Assess the relevance of BRAF inhibitor effects on T cell-mediated anti-tumour responses *in vivo*

4.2 Results

4.2.1 Human and murine T cells are susceptible to inhibition by targeted BRAF inhibitors *in vitro*

In order to establish the effects of targeted BRAF inhibitors on human T cell responses *in vitro,* PBMCs from healthy human donors were stimulated in a one-way mixed lymphocyte reaction and exposed to varying concentrations of PLX4720 or Vemurafenib (Figure 4.1A). Following seven days of stimulation and drug exposure cells were harvested and T cell viability and proliferation was assessed by flow cytometry. Unexpectedly, dose dependent effects were observed (Figure 4.1C). Below 1 μM neither PLX4720 nor Vemurafenib affected T cell proliferation or viability. However, at concentrations of greater than 1 μM inhibitory effects of drug treatment were evident with both viability and proliferation significantly reduced. Proliferative responses of T cells were more susceptible than viability to the detrimental effects of PLX4720 and Vemurafenib. Treatment with 12.5 μM PLX4720 reduced T cell proliferation by ~20% and viability by ~10% relative to controls. While 10 μM Vemurafenib had similar effects on viability (~10% reduction), the anti-proliferative effect was more substantial with a reduction in T cell proliferation of 60% relative to controls. Complete inhibition of T cell proliferation was observed with 200 μM PLX4720 or 100 μM Vemurafenib treatment, accompanied by decreases in viability of around 80% and 60% respectively.

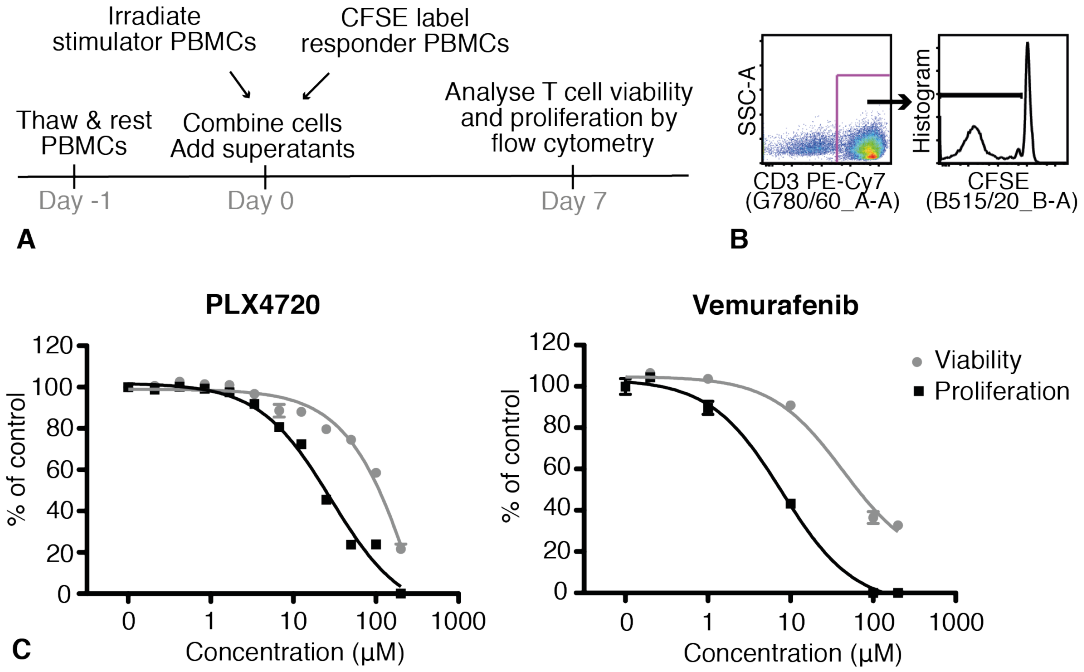

Figure 4.1: PLX4720 and Vemurafenib inhibit human T cell proliferation and viability *in vitro* in mixed lymphocyte cultures. A. PBMCs from healthy autologous donors were combined in a one-way mixed lymphocyte reaction. Stimulator cells received 30 Gy γ-irradiation and responder cells were CFSE labelled. Cells were combined and treated with a range of concentrations (24 nM-200 μM) of PLX4720 or Vemurafenib for 7 days. **B.** T cell proliferation was examined by flow cytometry. Representative dot plots show the gating strategy used to identify T cells and measure proliferation. **C.** Each symbol represents the mean of triplicates; error bars are ± S.D. Graphs are representative of at least 5 independent experiments using different donors, with similar results.

Results from the mixed lymphocyte reactions revealed a clear detrimental effect of targeted BRAF inhibitor treatment on both T cell viability and proliferation. However, with mixed cell populations present within the assay it is possible that impaired T cell proliferation resulted from diminished stimulatory capacity of antigen presenting cells rather than direct inhibitory effects on T cells. To determine if PLX4720 and Vemurafenib directly affect T cells, human PBMCs were stimulated for three days with anti-CD3 and anti-CD28 and treated with PLX4720 or Vemurafenib (Figure 4.2A). As seen in mixed lymphocyte reactions, T cell viability and proliferation were reduced with BRAF inhibitor treatment in a concentration dependent manner (Figure

4.2B). Trends were similar to those observed in previous experiments, with proliferation more sensitive than viability to both PLX4720 and Vemurafenib treatments. Concentrations of up to 6.75 μM PLX4720 and Vemurafenib did not effect T cell responses. However, treatment with 12.5 μM Vemurafenib reduced proliferation by approximately 25%, with viability remaining unaffected. Interestingly, PLX4720 treatment at the same concentration had no effect on T cells, again indicating a stronger inhibitory effect of Vemurafenib. At 50 and 100 μM both inhibitors almost completely abrogated T cell proliferation. PLX4720 had little effect on viability at 50 μM, but at 100 μM resulted in 20% reduction in viability. Vemurafenib reduced viability by approximately 20% and 50% with 50 μM and 100 μM treatments respectively.

The relative sensitivity of the two major subsets of T cells ($CD4^+$ and $CD8^+$) was then addressed by assessing the responses of sub-populations with anti-CD3/28 stimulation (Figure 4.3A). Both $CD4^+$ and $CD8^+$ T cells were equally inhibited by treatment with PLX4720 and Vemurafenib, and showed similar response profiles to those seen in previous experiments (Figure 4.3B).

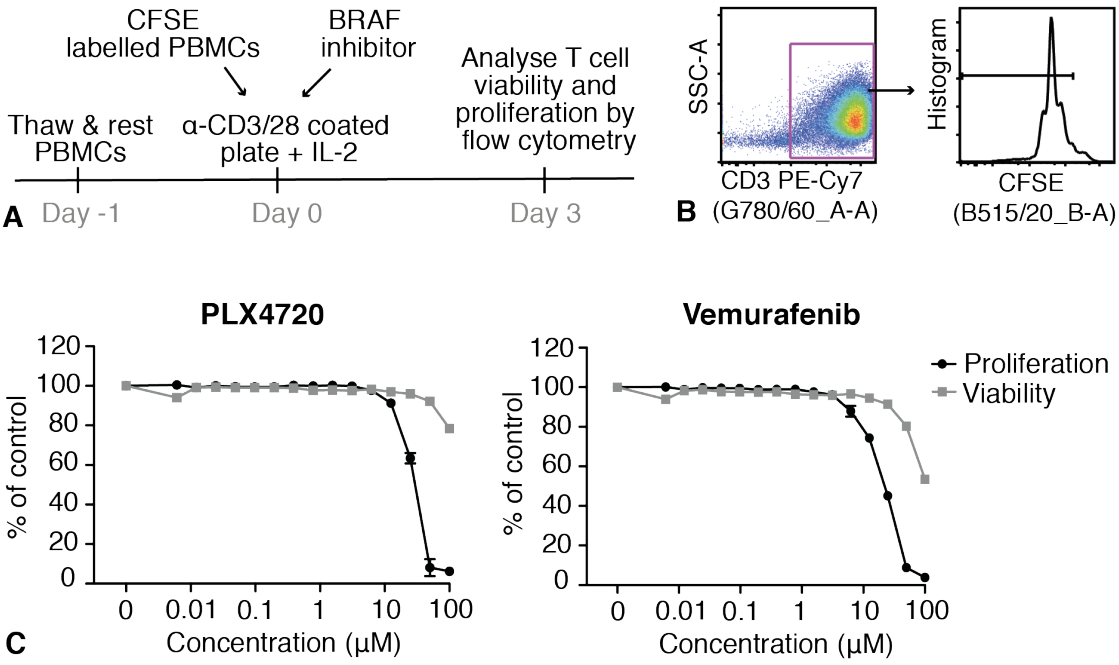

Figure 4.2: High concentrations of PLX4720 and Vemurafenib inhibit human T cell proliferation and viability *in vitro* with strong anti-CD3 and anti-CD28 stimulus. A. PBMCs from healthy human donors were stimulated for 3 days with 5 µg/mL anti-CD3, 0.5 µg/mL anti-CD28 and 20 U/mL IL-2. **B.** T cell proliferation was examined by flow cytometry. Representative dot plots show the gating strategy used to identify T cells and measure proliferation. **C.** Proliferation and viability are displayed as a percentage of DMSO control. Each symbol represents the mean of the triplicates. Error bars are ± S.D. Graphs are representative of 6 independent experiments using different donors, with similar results.

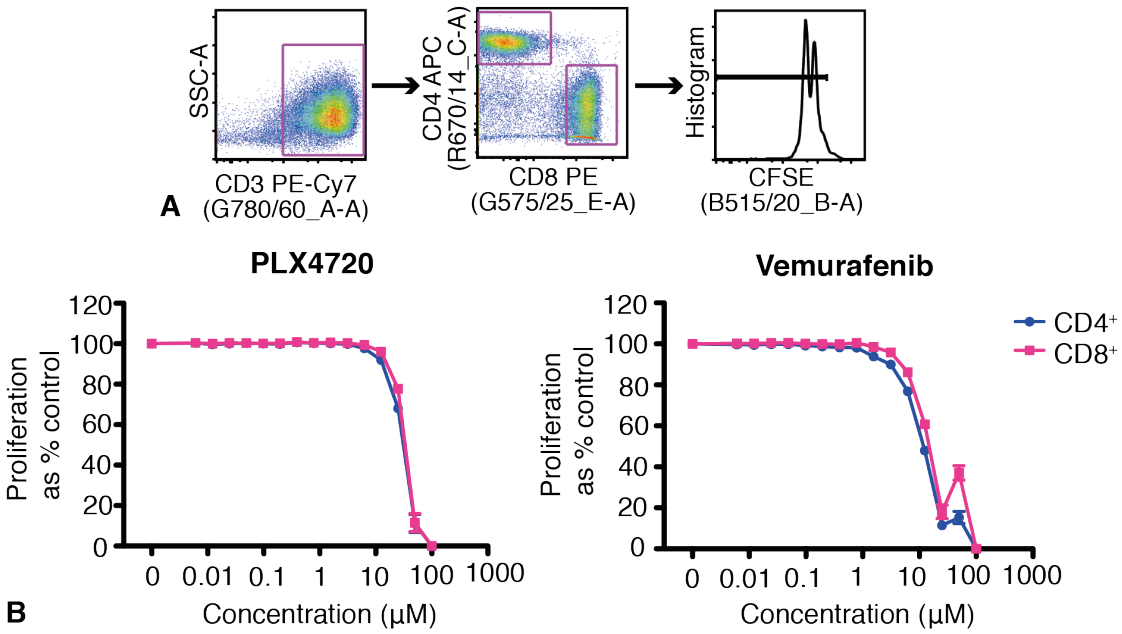

Figure 4.3: PLX4720 and Vemurafenib inhibit human CD4 and CD8 T cell proliferation following strong anti-CD3 and anti-CD28 stimulation. PBMCs were stimulated with anti-CD3, anti-CD28 and IL-2 as described in Figure 4.2A. **A**. T cell proliferation was examined by flow cytometry. Representative dot plots show the gating strategy used to identify $CD4^+$ and $CD8^+$ T cells and measure proliferation. **B.** Proliferation is displayed as a percentage of DMSO control. Each symbol represents the mean of the triplicates. Error bars are ± S.D. Graphs are representative of 3 independent experiments using different donors, with concordant results.

Having established the effects of BRAF inhibitors on human T cells, the effects on murine T cells *in vitro* were determined to allow direct comparison with human T cell responses. Splenocytes from naïve C57BL/6 mice were stimulated with anti-CD3 and anti-CD28, and treated with a range of concentrations of PLX4720 or Vemurafenib. (Figure 4.4A). After three days cells were harvested and T cell viability and proliferation assessed by flow cytometry (Figure 4.4B). Murine T cells showed dose-dependent inhibition following both PLX4720 and Vemurafenib exposure (Figure 4.4C). Again, with inhibitor treatment at low concentrations (up to 6.75 μM) T cell proliferation and viability remained unaffected. Exposure to PLX4720 and Vemurafenib at concentrations of 12.5 μM and above inhibited proliferation, with complete inhibition observed at 25 μM PLX4720 and 100 μM Vemurafenib. Again, effects on viability were observed at higher concentrations with PLX4720 reducing viability at concentrations of 50 μM or higher and Vemurafenib reduced viability at 100 and 200 μM. In contrast to human T cells, murine T cells appeared more susceptible to treatment with PLX4720.

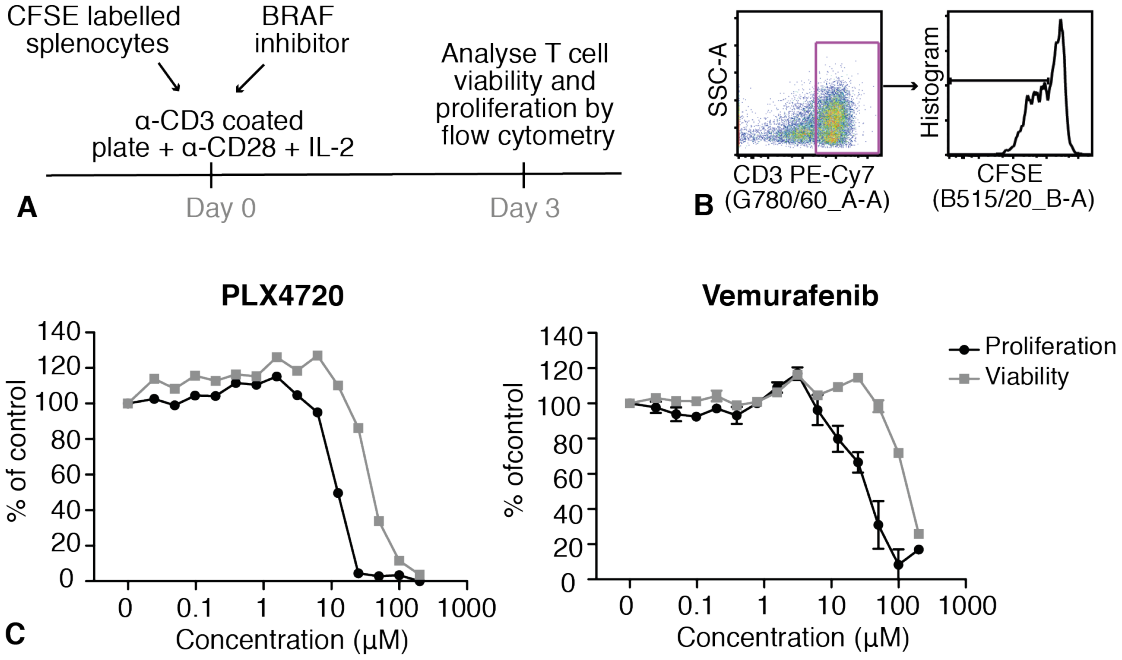

Figure 4.4: High concentrations of PLX4720 and Vemurafenib inhibit murine T cell proliferation and viability *in vitro* following strong anti-CD3 and anti-CD28 stimulation. A. Splenocytes from C57BL/6 mice were stimulated for 3 days with 1 μg/mL anti-CD3, 1:50 anti-CD28 and 100 U/mL IL-2. **B.** T cell proliferation was examined by flow cytometry. Representative dot plots show the gating strategy used to identify T cells and measure proliferation. **C.** Proliferation and viability are displayed as a percentage of DMSO control. Each symbol represents the mean of triplicates and error bars are ± S.D. Graphs are representative of 6 independent experiments using different donors, with similar results.

4.2.2 Serum protects T cells against detrimental effects of BRAF inhibitors *in vitro*

Previous experiments demonstrated that targeted BRAF inhibitors significantly impair both T cell proliferation and viability. Despite this, lymphopaenia is not an adverse event commonly associated with Vemurafenib treatment in patients. This suggests there is some protective mechanism *in vivo*, with sequestration of drug by plasma binding proteins a likely explanation.

To investigate the role of serum in sequestering BRAF inhibitors, human PBMCs were stimulated with anti-CD3/28 and exposed to PLX4720 at concentrations previously determined to inhibit T cell proliferation. Experiments were designed to assess the effects of PLX4720 on T cell proliferation in conditions of low serum (5%), normal serum (10%) or high serum (25-50%). Initial experiments were performed titrating FCS, to allow comparison with earlier data where FCS was the serum component used in cIMDM. These experiments revealed a clear role for serum concentration in modulating T cell susceptibility to PLX4720 inhibition of proliferative responses (Figure 4.5A). Increasing FCS concentrations provided protection against the detrimental effects of PLX4720 treatment. In low serum culture conditions, 25 μM PLX4720 impaired T cell proliferation, whilst in normal or high serum conditions 25 μM PLX4720 had less impact. The protective effects of higher serum culture conditions were observed at each drug concentration (Figure 4.5B).

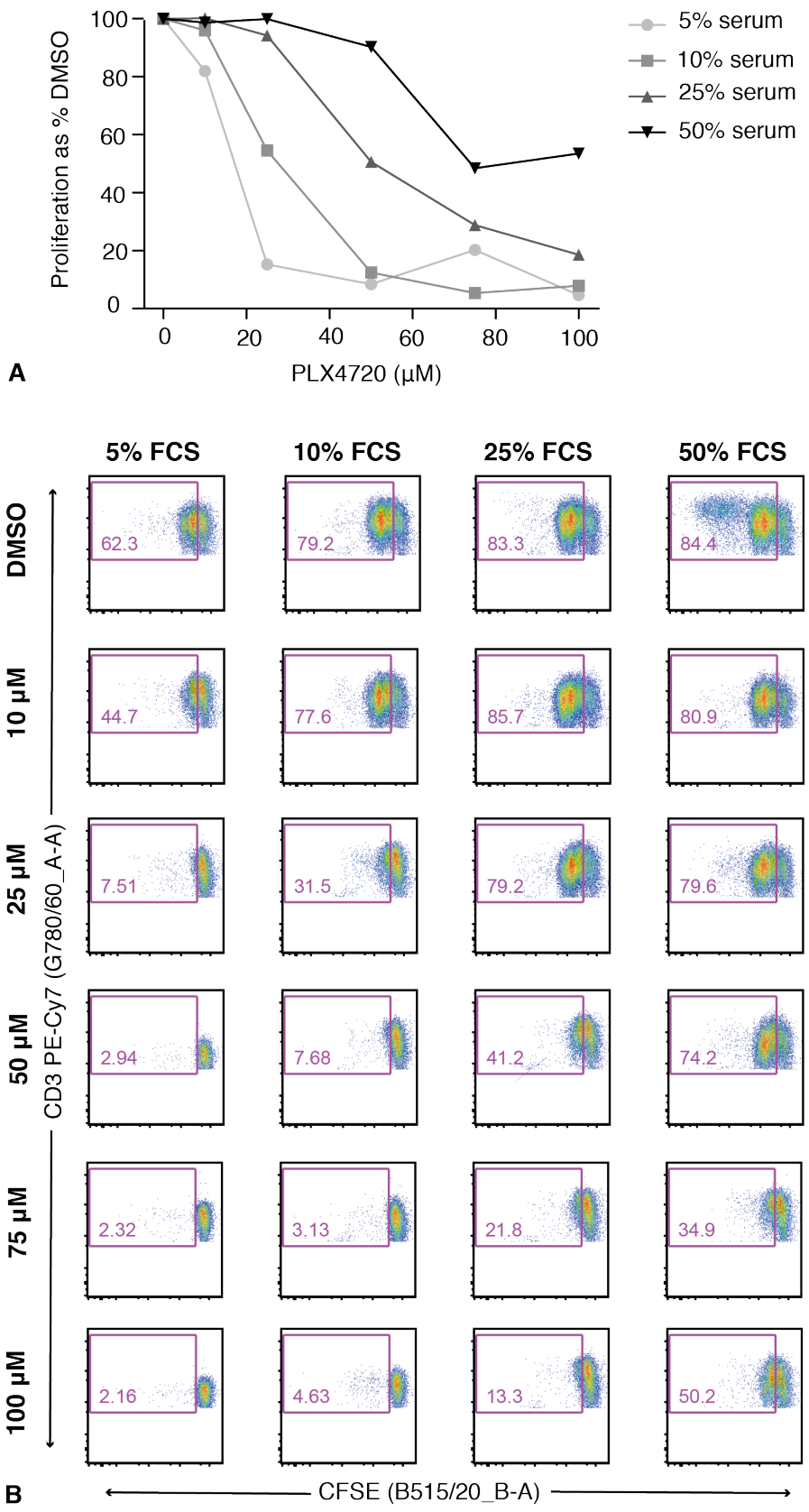
A
Proliferation as % DMSO
PLX4720 (µM)
5% serum
10% serum
25% serum
50% serum
B
5% FCS
10% FCS
25% FCS
50% FCS
DMSO
10 µM
25 µM
50 µM
75 µM
100 µM
CD3 PE-Cy7 (G780/60_A-A)
CFSE (B515/20_B-A)
62.3
79.2
83.3
84.4
44.7
77.6
85.7
80.9
7.51
31.5
79.2
79.6
2.94
7.68
41.2
74.2
2.32
3.13
21.8
34.9
2.16
4.63
13.3
50.2

Figure 4.5: Increasing concentrations of foetal calf serum (FCS) are partially protective against the inhibitory effects of PLX4720 *in vitro*. PBMCs from healthy human donors were stimulated for 3 days with 1 μg/mL anti-CD3, 0.1 μg/mL anti-CD28 and 20 U/mL IL-2 as described in Figure 4.2A. Cells were cultured in cIMDM with a range of FCS concentrations (5-50% FCS). Cells were treated with DMSO vehicle control or PLX4720 ranging from 10-100 μM. T cell proliferation was examined by flow cytometry as described in Figure 4.2B. **A.** Proliferation is shown relative to DMSO control. Each symbol represents the mean of triplicate. **B.** Representative dot plots illustrating T cell CFSE staining are shown. Data are representative of 3 independent experiments using different donors, with similar results.

To confirm the relevance of FCS findings to patients, similar experiments were performed using human AB serum. Again, human PBMCs were stimulated and the effects of PLX4720 treatment were assessed in conditions of low serum (5%), normal serum (10%) or high serum (25-50%). T cells exposed to PLX4720 in the presence of human AB serum exhibited strikingly reduced sensitivity to inhibition of T cell proliferation, with protection directly associated with serum concentration (Figure 4.6A). When compared with cultures containing FCS, all concentrations of human AB serum provided better protection against the detrimental effects of PLX4720 (Figure 4.6B). High human AB serum culture conditions were completely protective against PLX4720 effects. Interestingly, in the presence of 50% human AB serum 25 μM and 50 μM PLX4720 consistently stimulated T cell proliferation.

These data show that in high serum conditions the T cell inhibitory effects of PLX4720 are abrogated. This finding may explain the discrepancy between the severe inhibitory effects observed *in vitro* and the lack of clinical grade lymphopaenia reported in patients. Interestingly, there may be some capacity for PLX4720 to stimulate T cell proliferation, which is examined further in the next section.

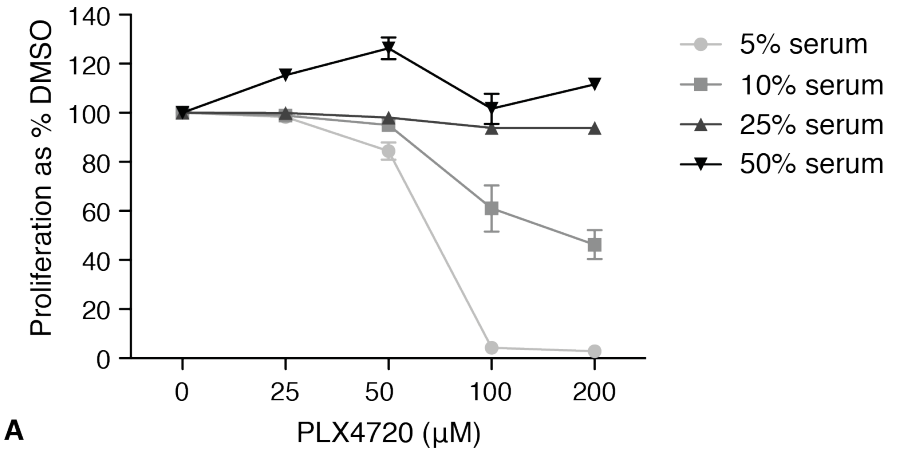
Proliferation as % DMSO
140
120
100
80
60
40
20
0
0
25
50
100
200
PLX4720 (µM)
5% serum
10% serum
25% serum
50% serum

A

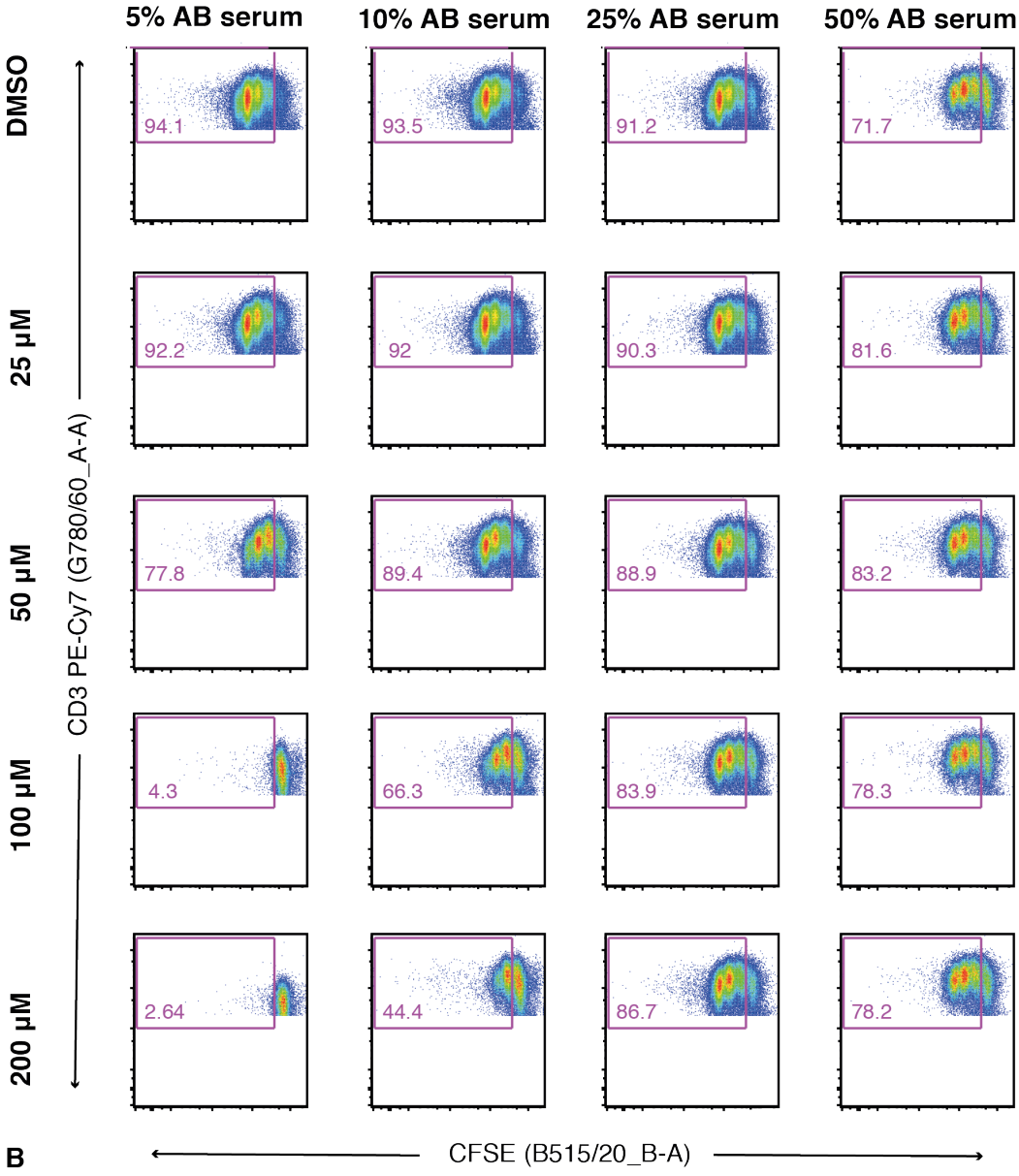
5% AB serum
10% AB serum
25% AB serum
50% AB serum
DMSO
25 µM
50 µM
100 µM
200 µM
94.1
93.5
91.2
71.7
92.2
92
90.3
81.6
77.8
89.4
88.9
83.2
4.3
66.3
83.9
78.3
2.64
44.4
86.7
78.2
CD3 PE-Cy7 (G780/60_A-A)
CFSE (B515/20_B-A)

B

Figure 4.6: Increasing concentrations of human AB serum abrogate the inhibitory effects of PLX4720 *in vitro*. PBMCs from healthy human donors were stimulated for 3 days with 1 μg/mL anti-CD3, 0.1 μg/mL anti-CD28 and 20 U/mL IL-2 as described in Figure 4.2A. Cells were cultured in cIMDM with a range of human AB serum (Scheffer et al.) concentrations (5-50%). Cells were treated with DMSO vehicle control or PLX4720 ranging from 10-100 μM. T cell proliferation was examined by flow cytometry as described in Figure 4.2B. **A.** Proliferation is shown relative to DMSO control. Each symbol represents the mean of triplicates, and error bars are ± S.D. **B.** Representative dot plots illustrating T cell CFSE staining are shown. Data are representative of 4 independent experiments using different donors, with similar results.

4.2.3 BRAF inhibitor treatment has paradoxical effects on sub-optimally stimulated human and murine T cells

To establish the capacity of BRAF inhibitors to stimulate T cell proliferation experiments were performed investigating the effects of PLX4720 and Vemurafenib on sub-optimally-stimulated T cells. Initial experiments were aimed at confirming the ability of BRAF inhibitors to stimulate human T cell proliferation *in vitro*. As with previous experiments healthy human PBMCs were stimulated with anti-CD3 and anti-CD28. Sub-optimal stimulation was achieved by decreasing the concentration of anti-CD3 from 5 μg/mL to 3 μg/mL. Both T cell proliferation, as measured by CFSE dilution, and T cell activation as determined by upregulation of CD69 expression were assessed by flow cytometry (Figure 4.7A). Treatment with Vemurafenib significantly augmented T cell proliferation at low concentrations, and some increased expression of the activation marker CD69 was also detected (Figure 4.7B and C). Conversely, at high concentrations, significant inhibition of T cell proliferation and non-significant decreases in CD69 expression were observed. These results confirm the concentration dependence of BRAF inhibitor effects on T cell functional parameters. Differential effects on proliferation compared with CD69 expression were observed. The strongest augmentation of T cell proliferation was seen at Vemurafenib concentrations between 50-500 nM, whilst concentrations of 5 μM and above clearly inhibited proliferation (Figures 4.7B and D). In contrast, concentrations of less than 500 nM Vemurafenib had little impact on CD69 expression, with optimal drug-

induced augmentation seen with 2 μM treatment (Figure 4.7C). Detrimental effects of Vemurafenib treatment on CD69 expression were also less marked. The discrepancies between the inhibitory effects on CD69 expression and proliferation may be a result of differences between temporal kinetics of both measures.

Subsequently, the stimulatory effects of BRAF inhibitors on murine T cells were assessed with a similar experimental design (Figure 4.8A). As with human T cells, murine T cell proliferation was increased with exposure to low concentrations of PLX4720 while high concentrations inhibited proliferation (Figure 4.8B). Stimulatory effects were most clearly observed between 50 nM and 2 μM PLX4720, and inhibition was evident at concentrations of greater than 5 μM (Figures 4.8B and D). No significant upregulation of CD69 expression was observed at low concentrations of PLX4720, although a consistent trend of small increases was observed and activation was clearly decreased with exposure to 5 and 20 μM (Figure 4.8C).

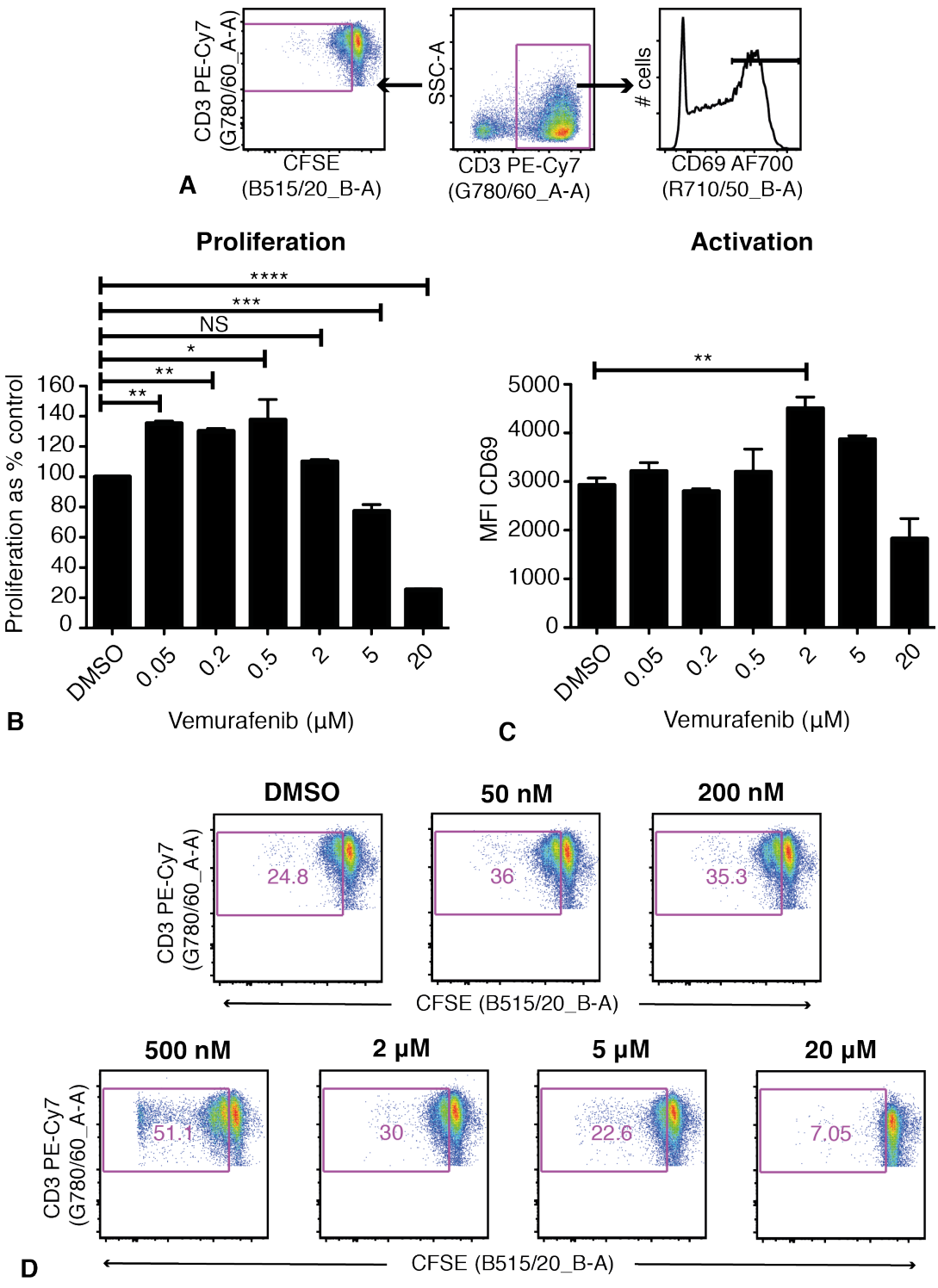
A
CD3 PE-Cy7 (G780/60_A-A)
CFSE (B515/20_B-A)
SSC-A
CD3 PE-Cy7 (G780/60_A-A)
cells
CD69 AF700 (R710/50_B-A)
Proliferation
Activation
****
***
NS
*
**
**
Proliferation as % control
160
140
120
100
80
60
40
20
0
DMSO
0.05
0.2
0.5
2
5
20
Vemurafenib (μM)
B
**
MFI CD69
5000
4000
3000
2000
1000
0
DMSO
0.05
0.2
0.5
2
5
20
Vemurafenib (μM)
C
DMSO
50 nM
200 nM
CD3 PE-Cy7 (G780/60_A-A)
24.8
36
35.3
CFSE (B515/20_B-A)
500 nM
2 μM
5 μM
20 μM
CD3 PE-Cy7 (G780/60_A-A)
51.1
30
22.6
7.05
CFSE (B515/20_B-A)
D

Figure 4.7: Low concentrations of Vemurafenib boost human T cell proliferation *in vitro* with sub-optimal anti-CD3 and anti-CD28 stimulation.PBMCs from healthy human donors were stimulated for 3 days with 3 μg/mL anti-CD3, 0.5 μg/mL anti-CD28 and 20 U/mL IL-2 as depicted in Figure 4.3A. **A.** T cell proliferation and activation (CD69 expression) was examined by flow cytometry. Representative dot plots show the gating strategy used to identify T cells. **B.** Proliferation is shown relative to the DMSO control. Each bar represents the mean of triplicates. Error bars are ± S.D. **C.** Each bar represents CD69 AlexaFluor700 average median fluorescence intensity (MFI) of triplicates. Error bars are ± S.D. **D.** Representative dot plots illustrating T cell CFSE staining are shown. NS = not significant, * $p < 0.05$, ** $p < 0.01$, *** $p < 0.001$, **** $p < 0.0001$, by one-way ANOVA with Bonferroni post-test. Data are representative of 3 independent experiments using different donors, with concordant results.

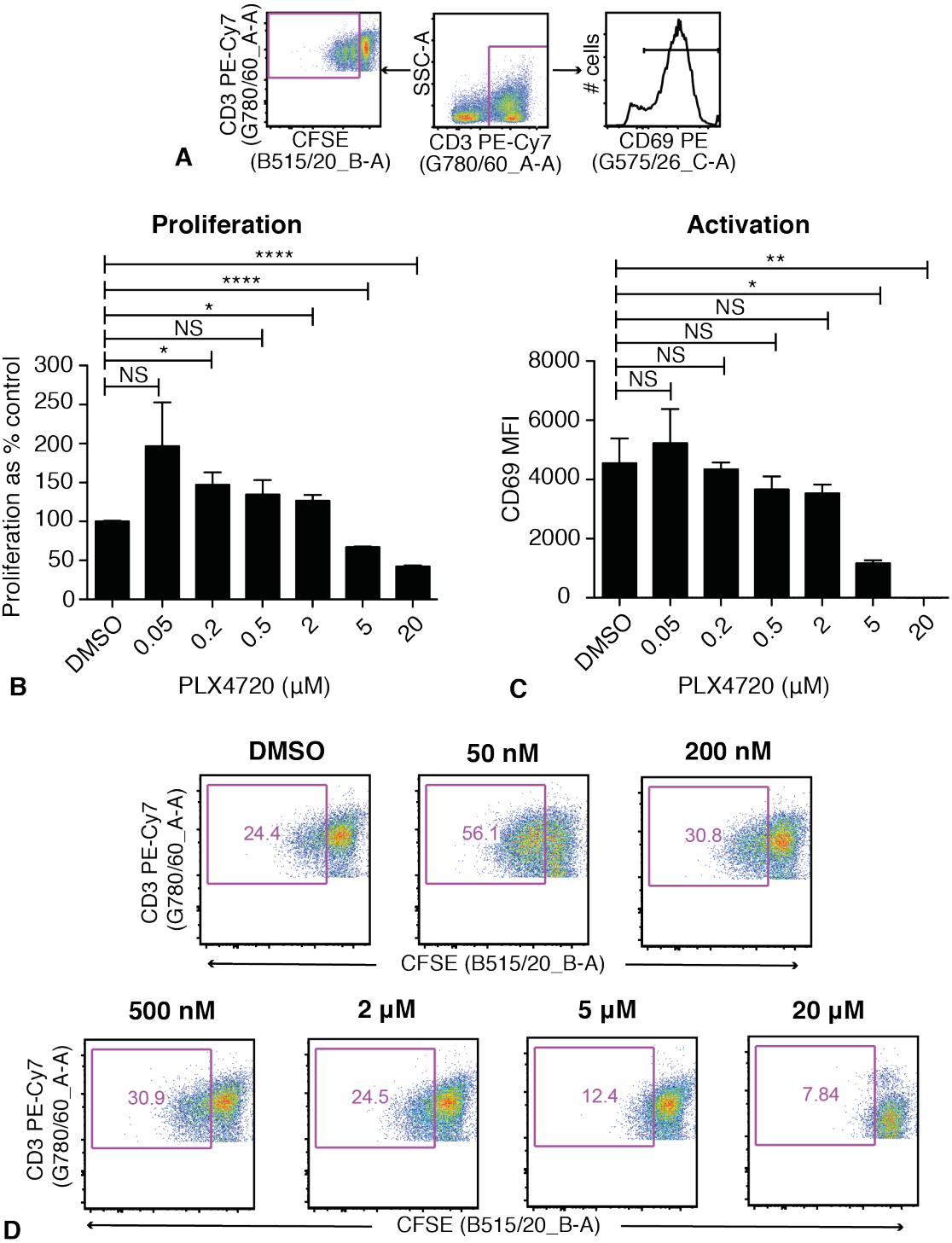
A
CD3 PE-Cy7 (G780/60_A-A)
CFSE (B515/20_B-A)
SSC-A
CD3 PE-Cy7 (G780/60_A-A)
cells
CD69 PE (G575/26_C-A)
Proliferation
Proliferation as % control
B
PLX4720 (μM)
Activation
CD69 MFI
C
PLX4720 (μM)
DMSO
50 nM
200 nM
24.4
56.1
30.8
500 nM
2 μM
5 μM
20 μM
30.9
24.5
12.4
7.84
D
CFSE (B515/20_B-A)

Figure 4.8: Low concentrations of PLX4720 and Vemurafenib boost murine T cell proliferation *in vitro* with sub-optimal anti-CD3 and anti-CD28 stimulation. Splenocytes from C57BL/6 mice were stimulated for 3 days with 0.6 μg/mL anti-CD3, 1:50 anti-CD28 and 100 U/mL IL-2 as shown in Figure 4.7A. **A.** T cell proliferation and activation (CD69 expression) was examined by flow cytometry. Representative dot plots show the gating strategy used to identify T cells. **B.** Proliferation is shown relative to the DMSO control. Each bar represents the mean of triplicates. Error bars are ± S.D. **C.** Each bar represents the average CD69 PE median fluorescence intensity (MFI) of triplicates. Error bars are ± S.D. **D.** Representative dot plots illustrating T cell CFSE staining are shown. NS = not significant, * $p < 0.05$, ** $p < 0.01$, **** $p < 0.0001$, one-way ANOVA with Bonferroni post-test. Data are representative of 4 independent experiments.

Building on the finding that BRAF inhibitors can stimulate T cell proliferation *in vitro,* the capacity of BRAF inhibitors to enhance antigen specific T cell proliferation *in vivo* was investigated. $CD8^+$ T cells specific for the ovalbumin peptide SIINFEKL ('OTI' T cells) were adoptively transferred to syngeneic C57BL/6 mice. PLX4720 treatment was initiated on the day of T cell transfer, with mice receiving either the recommended dose of 20 mg/kg PLX4720 or vehicle control by oral gavage daily (Dr Gideon Bollag, personal communication). BRAF inhibitor treatment was performed for seven days to allow plasma drug levels to stabilise prior to the intravenous challenge with OVA and αGalCer to stimulate OTI T cell expansion (Figure 4.9A). PLX4720 treatment continued following challenge and seven days later, at the expected peak of effector T cell responses, OTI T cell expansion was assessed by flow cytometry (Figure 4.9B). Without OVA and αGalCer challenge, OTI T cells were undetectable 14 days following adoptive transfer (Figures 4.9 C and D). Two different doses of OVA and αGalCer were delivered to achieve optimal and sub-optimal stimulation of OTI T cells. Previous work at the Malaghan Institute had identified that 200 μg OVA and 200 ng αGalCer optimally stimulates OTI T cell proliferation (Dr Taryn Osmond, personal communication). This was reduced to 100 μg OVA and 50 ng αGalCer to achieve sub-optimal stimulation. The lowered dose of antigen and adjuvant conferred an approximately two-fold reduction in the proportion of peripheral OTI T cells (Figures 4.9 C and D). PLX4720 treatment of mice that

received OTI T cells and 200 μg OVA with 200 ng αGalCer did not affect OTI T cell expansion, with a comparable proportion of OTI T cells detected seven days following challenge (Figure 4.9C). However, when OTI T cells were sub-optimally stimulated with 100 μg OVA and 50 ng αGalCer, PLX4720 treatment significantly increased the proportion of OTI T cells detected seven days following challenge (Figure 4.9D).

These *in vivo* results support the *in vitro* findings that targeted BRAF inhibitors can stimulate T cell proliferation. In addition to the concentration dependence of stimulatory effects observed *in vitro*, there also appears to be a role for stimulus strength in determining stimulatory capacity. This could be explained by the fact that maximally stimulated T cells are unable to proliferate further despite BRAF inhibitor treatment. The lack of inhibitory effects observed with strong stimulus of the OTI T cells supports the *in vitro* finding that a high serum environment (such as the blood) may be protective against the negative effects of BRAF inhibitors observed *in vitro*.

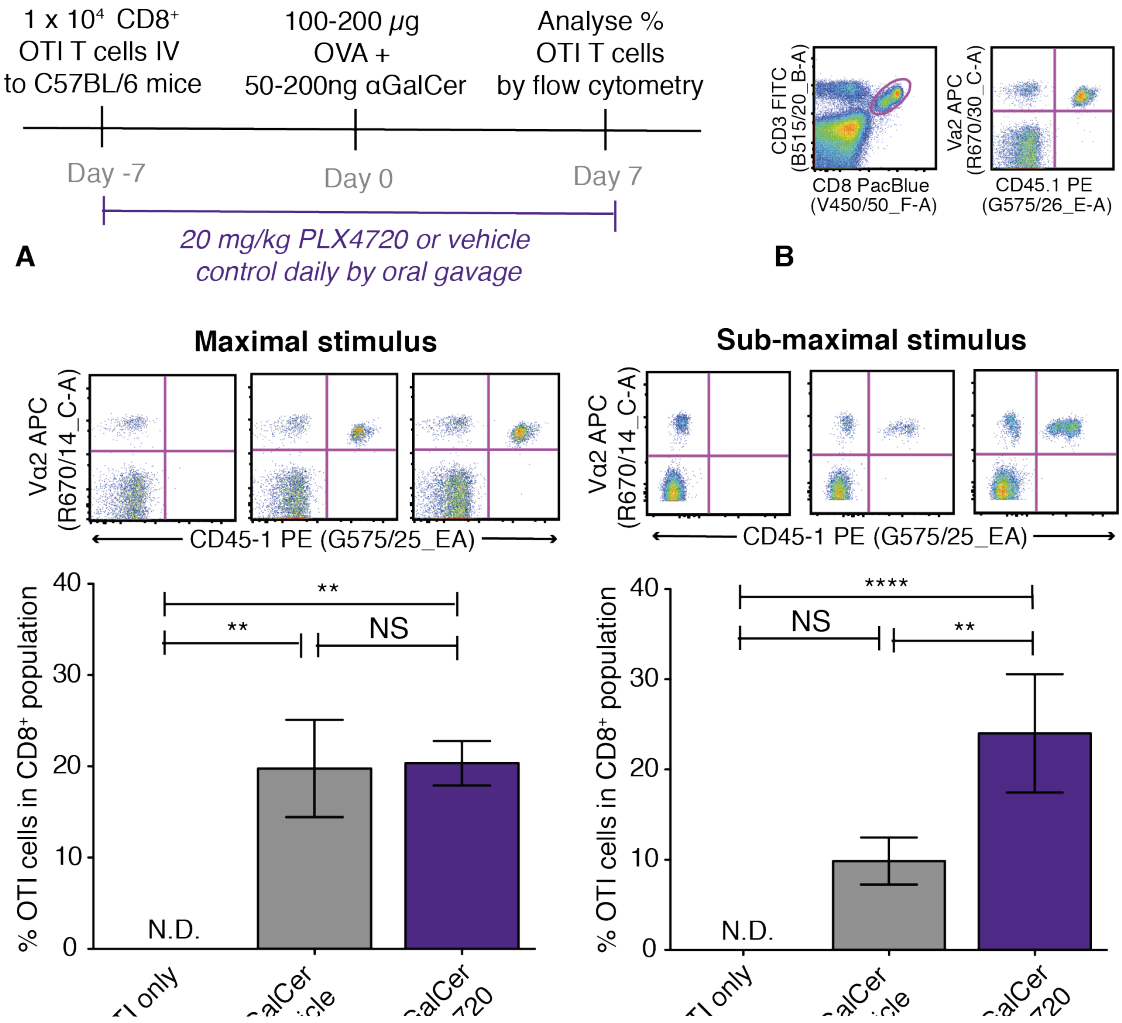

Figure 4.9: PLX4720 boosts sub-optimal, but not optimal, antigen specific stimulation of OTI T cells *in vivo*. A. 1 x 10^4 $CD8^+$ OTI T cells were adoptively transferred to naïve C57BL/6 mice. On the same day BRAF inhibitor treatment was initiated with 20 mg/kg PLX4720 given daily by oral gavage. 7 days post-adoptive transfer mice received 100-200 μg OVA + 50-200 ng αGalCer intravenously. 7 days later mice were bled via the lateral tail vein. **B.** The proportion of OTI T cells in the peripheral blood was analysed by flow cytometry. **C.** OVA was delivered at 200 μg and αGalCer at 200ng, deemed "maximal stimulus". **D.** Mice received 100 μg OVA and 50 ng αGalCer, deemed "sub-maximal stimulus". **C and D.** Each bar represents the mean of the group (5 mice), N.D. = non-detectable. Error bars are ± SEM. NS = not significant, ** $p < 0.01$, **** $p < 0.0001$, one-way ANOVA with Bonferroni post-test. Data are representative of 3 independent experiments, with concordant results.

4.2.4 Anti-tumour vaccination is unaffected by BRAF inhibition, while tumour growth is enhanced in a BRAF wild-type mouse model

Having established that BRAF inhibitors can stimulate T cell proliferation, experiments were designed to investigate the relevance of this finding to anti-tumour T cell responses. This required a melanoma tumour model insensitive to targeted BRAF inhibition, to allow inhibitor effects on T cell-mediated anti-tumour responses to be assessed without BRAF inhibition affecting tumour growth. Having previously established that the BRAF wild-type B16 melanoma cell line was highly resistant to PLX4720 and Vemurafenib treatment *in vitro* (Chapter 3), this tumour model was deemed suitable. It was also necessary to be able to induce effective anti-tumour T cell responses to investigate drug effects on tumour-specific T cells. Therefore, the B16.OVA tumour model was selected for these experiments; this model is derived from the B16 cell line and has been stably transfected to express ovalbumin as a model antigen (Moore et al., 1988).

Anti-tumour T cell responses were generated using a vaccine of 200 μg OVA with 200 ng of the adjuvant αGalCer to stimulate endogenous ovalbumin-specific T cells. Mice were injected with tumours and seven days later, at which point tumours were palpable, daily treatment with 20 mg/kg PLX4720 was initiated. The following day vaccination was delivered intravenously. Vaccination significantly slowed B16.OVA tumour growth (Figure 4.10B and C), which corresponded to significantly increased survival (Figure 4.10D) indicating effective anti-tumour T cell responses were elicited. As a control mice with B16.OVA tumours were treated with single agent 20 mg/kg PLX4720. Unexpectedly, PLX4720 treatment significantly increased tumour growth (Figure 4.10B), appearing to push tumours towards a more aggressive phenotype (Figure 4.10C). This increased growth rate of tumours corresponded with significantly decreased survival of mice treated with PLX4720 (Figure 4.10D).

The increased tumour growth seen with PLX4720 treatment confounded the experimental design. As a result of this, too many variables were affected by

PLX4720 treatment, which made it difficult to assess the direct effects of PLX4720 treatment on anti-tumour T cell responses. In an attempt to further elucidate the effects of PLX4720 on anti-tumour vaccine efficacy, survival benefit with vaccine or vaccine/PLX4720 combination was plotted relative to the appropriate control group, which were taken to be tumour only or PLX4720 only respectively (Figure 4.10E). In this way, the contribution of PLX4720 treatment to tumour growth could be assessed. Analysis showed no significant impact of PLX4720 on vaccine, and a non-significant but consistent trend towards increased vaccine efficacy across experimental repeats. However, due to the unexpected increase in tumour growth with single agent PLX4720 robust conclusions are unable to be drawn from these experiments.

To confirm the effects of targeted BRAF inhibition on BRAF wild-type melanoma growth, B16.OVA cells were treated with PLX4720 and Vemurafenib *in vitro*. Cellular reduction of MTT was used as an indirect measure of cell number, and thus proliferation. Concentration dependent effects of BRAF inhibitor treatment were observed (Figure 4.11). Low concentrations of ≤ 360 nM had no effect on B16.OVA tumour growth. However, at concentrations of 780 nM–1.56 μM, a stimulatory effect of PLX4720 treatment was repeatedly observed, which was not present with Vemurafenib treatment. PLX4720 at 6.25–50 μM significantly stimulated growth, and comparable concentrations of Vemurafenib reliably achieved small increases in B16.OVA growth. Growth was inhibited with 200 μM PLX4720 and 100–200 μM Vemurafenib.

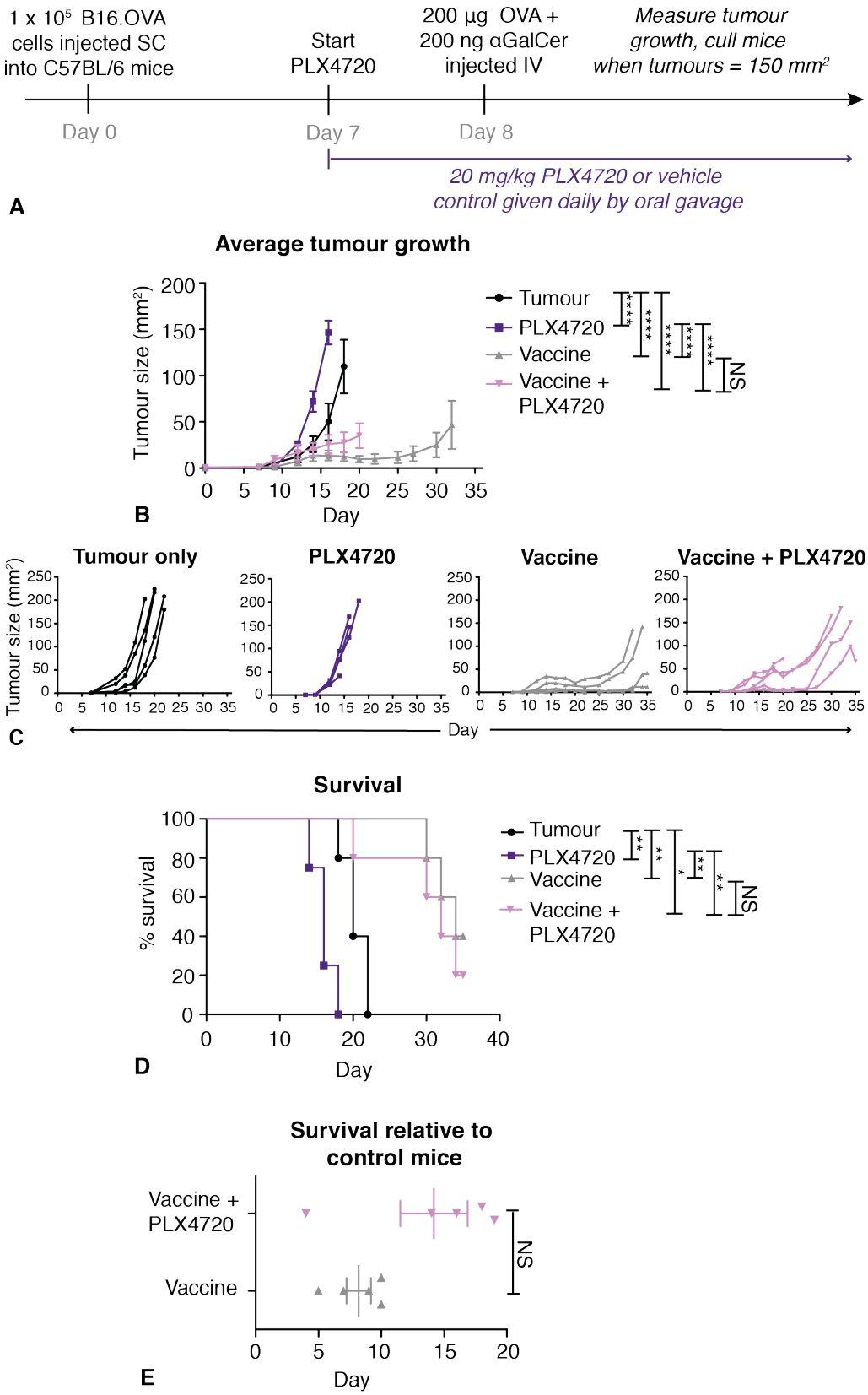
1 x 10⁵ B16.OVA cells injected SC into C57BL/6 mice
Start PLX4720
200 µg OVA + 200 ng αGalCer injected IV
Measure tumour growth, cull mice when tumours = 150 mm²
Day 0
Day 7
Day 8
20 mg/kg PLX4720 or vehicle control given daily by oral gavage
A
Average tumour growth
Tumour size (mm²)
Day
Tumour
PLX4720
Vaccine
Vaccine + PLX4720
****
****
****
***
****
NS
B
Tumour only
PLX4720
Vaccine
Vaccine + PLX4720
Tumour size (mm²)
Day
C
Survival
% survival
Day
Tumour
PLX4720
Vaccine
Vaccine + PLX4720
**
**
*
**
**
NS
D
Survival relative to control mice
Vaccine + PLX4720
Vaccine
NS
Day
E

Figure 4.10: PLX4720 has no effect on anti-tumour vaccination in a BRAF^{WT} B16.Ova tumour model, but directly stimulated BRAF^{WT} tumour growth. A. C57BL/6 mice were injected subcutaneously in the left flank with 1 x 10^5 B16.Ova cells. Daily drug treatment was initiated 7 days post-tumour challenge with 20 mg/kg PLX4720 given by oral gavage. The day after beginning drug treatment mice were vaccinated intravenously with 200 µg OVA + 200 ng αGalCer. Tumour growth was monitored and size recorded. Mice were culled when tumours reached 150 mm^2, or when tumours ulcerated. **B.** Average tumour growth is shown and each symbol represents the mean growth of 4-5 mice. Error bars are ± SEM. **C.** Individual tumour growth is shown. Each symbol represents one mouse. **D.** Percent survival shown for groups of 4-5 mice. Treatment groups are compared to vehicle-treated control mice * $P \leq 0.05$, ** $P < 0.01$, Mantel-Cox test. **E.** Overall survival shown relative to the survival of the appropriate control group, NS = not significant, unpaired t-test with Welch's correction. Graphs are representative of two independent experiments.

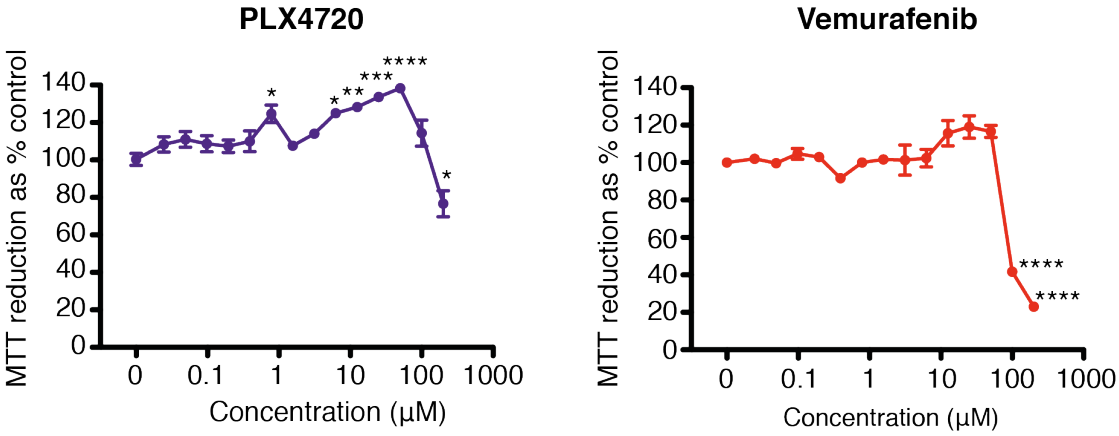

Figure 4.11: PLX4720 stimulates BRAF^{WT} B16.Ova melanoma growth *in vitro*. Cells were treated with a range of concentrations (24 nM-200 µM) of PLX4720 or Vemurafenib for 48 hours. Cell proliferation was measured by MTT reduction, and shown as a percentage of DMSO treated control. Each symbol represents the mean of the triplicates. Error bars are ± S.D. Curves were generated by non-linear regression analysis. Drug treated triplicates were compared to DMSO control by one-way ANOVA with Bonferroni post-test. Points for which no stars are shown differences were non-significant, * $P \leq 0.05$, ** $P < 0.01$, *** $P < 0.001$, **** $P < 0.0001$. Graphs are representative of at least four independent experiments.

4.3 Discussion

The focus of this chapter was to elucidate the effects of targeted BRAF inhibitors on T cell responses. I demonstrated that BRAF inhibition can either augment or inhibit T cell proliferation, depending on the setting and the inhibitor concentration. These results confirmed previously published work (Callahan et al., 2014; Comin-Anduix et al., 2010; Gargett et al., 2015). However this is the first time the contradictory effects have been reported together, indicating that the difference between inhibitory and stimulatory effects is not solely due to different inhibitors or culture conditions, as was previously suggested (Callahan et al., 2014). Furthermore, I have shown that high serum environments are protective against the detrimental effects of targeted BRAF inhibitors. This novel finding reconciles the contradictory effects observed in *in vitro* and *in vivo* studies.

The concentrations at which inhibitory effects on T cells were demonstrated *in vitro* fall within the range of patient plasma concentrations, which averaged 80 μmol/L in phase I clinical trial (Bollag et al., 2010; Flaherty et al., 2010). However, because Vemurafenib is more than 99% protein bound in serum, the free concentration of Vemurafenib should be less than 1% of the total plasma concentration (FDA, 2011). On this basis, immune cells within the circulation will be protected from inhibitory concentrations of free drug. This is supported by the protection I have demonstrated under high serum conditions *in vitro*. Nevertheless, the intratumoural concentration of Vemurafenib in patients, or mice, has not been well defined, and increased free drug concentrations may be possible. Daily dosing of mice with 100 mg/kg Vemurafenib generated peak plasma concentrations of greater than 100 μmol/L, and corresponding intratumour concentrations of 15 μmol/L (Yang et al., 2010). If this is free drug, intratumoural concentrations of inhibitors may approach concentrations at which growth inhibition and decreased viability of T cells have been observed *in vitro* in this study. However, both the data presented in this chapter and in the study by Comin-Anduix and colleagues show highly activated lymphocytes are more resistant to detrimental effects of BRAF inhibitors (Comin-Anduix et al., 2010). Thus, activated T cells within the tumour microenvironment are more likely to be

unaffected by high inhibitor concentrations, which would have significant effects on $BRAF^{V600E}$ melanoma cells. Collectively, these findings may explain the lack of clinical grade lymphopaenia observed in patients. However, the study by Schilling and colleagues reported decreased numbers of peripheral lymphocytes with Vemurafenib treatment, indicating that inhibitory effects may be occur *in vivo* and need to be considered when clinical dosing is being determined (Schilling et al., 2014).

The paradoxical stimulatory effects of BRAF inhibitors on T cell responses were demonstrated within a unique, and lower, dose range. Additionally, these effects were more apparent in settings of sub-maximal T cell stimulation. It is well established that activation of $BRAF^{WT}$ cells occurs due to inhibitor transactivation of RAF dimers, resulting in downstream ERK signalling (Callahan et al., 2014; Halaban et al., 2010; Hatzivassiliou et al., 2010; Heidorn et al., 2010; Poulikakos et al., 2010). Having demonstrated these effects *in vivo* with antigen-specific T cell proliferation highlights a possible capacity for augmentation of anti-tumour T cell responses. Unfortunately, as PLX4720 also increased wild-type BRAF melanoma proliferation the effects on anti-tumour T cell responses were unable to be fully assessed. The growth promoting consequences of BRAF inhibition in the $BRAF^{WT}$ B16.Ova tumours highlights the importance of rigorous tumour typing, and the risk of treating tumours with heterogeneous expression of $BRAF^{V600E}$. This represents a significant clinical problem, as both intratumour and intertumour polyclonality of the BRAF mutation has been shown in metastatic melanoma specimens. In two small but independent studies, heterogeneity of BRAF alleles was reported in 67-80% of primary tumour samples, whilst 26% of metastases were shown to have BRAF status discordant with the primary tumour type (Lin et al., 2011; Yancovitz et al., 2012). Therefore, it is likely that in a large proportion of patients who develop BRAF inhibitor resistance, initial treatment with a targeted BRAF inhibitor is selecting for $BRAF^{WT}$ tumour cell outgrowth. This strengthens the rationale for combination of targeted therapy with immunotherapy, which will target melanoma cells irrespective of their mutation status.

4.3.1 Conclusions

The results presented in this chapter have confirmed and extended previous studies demonstrating the paradoxical effects targeted BRAF inhibitors exert on T cell responses. I have provided strong evidence that PLX4720 can stimulate antigen-specific T cell responses *in vivo*, although it remains uncertain if anti-tumour T cell responses could be similarly augmented with targeted BRAF inhibitors. It is critical for success of combination BRAF inhibitor and immunotherapy that the direct effects of BRAF inhibitors on T cells are considered. Optimal combination therapy approaches may be able to harness the T cell stimulatory effects of BRAF inhibition, to achieve maximal augmentation of anti-tumour T cell responses. However, further elucidation of patient intratumoural inhibitor concentrations at clinically relevant doses would be required. This will also be necessary to ensure the elimination of detrimental effects on TILs.

CHAPTER 5: Developing an autologous vaccine for $BRAF^{V600E}$ tumours

5.1 Introduction

Recent advances in immunotherapy have transformed the treatment of metastatic melanoma. These breakthroughs have been driven by the development and clinical progression of antibodies against the checkpoint molecules CTLA-4 and PD-1. Targeting of immune checkpoints generates anti-tumour effects by blocking immunoinhibitory signals and unleashing existing tumour-specific immune responses. However, many patients do not respond to checkpoint blockade therapy. Meta-analysis of Ipilimumab (anti-CTLA-4) trials revealed approximately 20% of patients responded to treatment (Schadendorf et al., 2015b; Topalian et al., 2015), while the phase III clinical trial of Nivolumab (anti-PD-1) achieved responses in around 30% of patients (Robert et al., 2015a). Amongst the unresponsive patient cohort, it is likely that there are individuals who lack pre-existing anti-tumour immune responses (Delamarre et al., 2015). In these patients active immunization approaches, which promote the development of anti-tumour immune responses, may be more effective. Furthermore, when considering immunotherapy for combination with targeted BRAF inhibitors, checkpoint blockade may not represent the best immunotherapeutic strategy, as demonstrated by the unsuccessful phase I clinical trial combining Ipilimumab and Vemurafenib (Ribas et al., 2013). Other immunotherapeutic approaches may be more suitable for combination with BRAF inhibitors.

Autologous tumour cell vaccination is a form of active immunization that aims to generate anti-tumour immune responses. This approach delivers a full complement of tumour specific antigens, including undefined neoantigens, to stimulate cells of the innate and adaptive systems. The ability to stimulate responses to undefined neoantigens, which have been shown to drive potent anti-tumour effector T cell responses, is a major benefit of this approach (Carreno et al., 2015; Schumacher and Schreiber, 2015). To be effective the fundamental requirement of active immunotherapy is the stimulation of strong anti-tumour immune responses that generate long-lasting memory. However, without sufficient licensing of DCs upon activation, vaccination can have a tolerizing effect (Qiu et al., 2009; Steinman et al., 2000). The inclusion of an adjuvant promotes optimal DC activation, to

generate effector T cell responses. The glycolipid αGalCer has been shown to have potent adjuvant activity, stimulating iNKT cells to license dendritic cells, which has been demonstrated to be one of the most effective ways of inducing DC maturation (Fujii et al., 2003; Hermans et al., 2003b; Kawano et al., 1997; Liu et al., 2005). Initial attempts to use αGalCer in a tumour setting involved the infusion of soluble αGalCer. However, this approach was largely ineffective due to the induction of iNKT anergy (Parekh et al., 2005). DCs loaded with αGalCer have been more successful as a vaccine, inducing potent anti-tumour effects in several murine models, including the $BRAF^{WT}$ B16 melanoma model (Fujii et al., 2002). However, this approach faces technical hurdles with difficulty in extracting and expanding DCs from the peripheral blood mononuclear cells of patients. These limitations have driven the use of γ-irradiated, autologous tumour cells loaded with αGalCer as a preferable vaccine approach (Chung et al., 2007; Mattarollo et al., 2012; Shimizu et al., 2007b). Irradiation of tumour cells prior to vaccination prevents tumour cell growth when delivered intravenously, and increases the immunogenicity of tumour cells (Obeid et al., 2007). Further supporting the use of tumour cells over DCs as the cellular component of vaccine, αGalCer-loaded tumour cells have been shown to induce more effective T cell responses when compared to αGalCer-loaded DCs (Shimizu et al., 2007b).

Delivery of αGalCer-loaded, irradiated tumour cells should allow DCs to simultaneously acquire tumour antigens and αGalCer. Therefore, tumour-derived peptides could be presented on MHC molecules to T cells while αGalCer is simultaneously presented on CD1d to iNKT cells. DC and iNKT interactions promote CD40-CD40L signalling and lead to DC activation, increasing the capacity of DCs to stimulate tumour-specific effector T cell responses, as previously introduced (Chapter 1.5.5, Figure 1.3). Importantly, vaccines based on the administration of autologous tumour cells and αGalCer have been demonstrated to be highly effective in several murine tumour models including the B16 model (Gibbins et al., 2014; Hunn et al., 2012; Mattarollo et al., 2012; Shimizu et al., 2007b; Weinkove et al., 2013).

This approach has translational relevance, with autologous vaccination enabling targeting of patient-specific neoantigens. In addition, the use of αGalCer as an adjuvant has broad clinical application; as CD1d is not polymorphic, iNKT licensing of DCs is not dependent on HLA status. The iNKT population required for this approach has been shown to be present in late stage melanoma patients. Circulating iNKT cell populations were detected in patients prior to anti-CTLA-4 therapy and shown to be capable of eliciting strong anti-tumour immune responses (Ibarrondo et al., 2013).

5.1.1 Aims

The research undertaken in this chapter aimed to develop an active immunotherapeutic approach with anti-tumour efficacy against $BRAF^{V600E}$ melanoma. The following series of experiments were designed to develop and characterise an autologous, whole tumour cell vaccine. Specific aims were to:

- Determine the ability of an irradiated, αGalCer-loaded YUMM1.1 or YUMM1.7 tumour cell vaccine to induce an immune response
- Assess the anti-tumour efficacy of autologous vaccination
- Characterise the immune cell types involved in vaccine response

5.2 Results

5.2.1 Vaccination with irradiated, αGalCer-loaded YUMM1.1 and YUMM1.7 cells induces T cell-mediated immune responses

Initial experiments were performed to establish whether irradiated, αGalCer-loaded YUMM1.1 and YUMM1.7 cells could induce an immune response in naïve mice. To generate the whole tumour cell vaccine melanoma cells were pulsed with αGalCer overnight, washed to remove excess, unbound αGalCer and irradiated. Irradiation was performed to prevent tumour outgrowth and

to enhance immunogenicity. As iNKT cells are predominantly located in the spleen and liver, vaccine was delivered intravenously to provide access to these populations. Naïve mice received vaccine intravenously and control mice received PBS. Seven days later responses in peripheral lymphoid tissues were assessed (Figure 5.1A). Both the spleen and lung-draining mediastinal lymph node (mdLN) were collected for analysis as these tissues have previously been shown to be sites at which priming occurs with αGalCer-adjuvanted whole tumour cell vaccines (Gibbins et al., 2014; Hunn et al., 2012).

Vaccination with irradiated, αGalCer-loaded YUMM1.1 and YUMM1.7 cells resulted in an increase in the overall size of the spleens (Figure 5.1B and C) and mdLN. The increased size of these lymphoid tissues was associated with significantly increased absolute cell counts and numbers of $CD45^+$ immune cells (Figure 5.1D-G). Specific immune cell subsets were assessed by flow cytometry, with T cell, NK cell and NKT cell populations defined as shown in Figure 5.2A. As changes in lymphocyte numbers following vaccination reflected an overall increase in the number of $CD45^+$ immune cells, Data are presented as population frequencies. Although vaccination is likely to enhance iNKT cell responses, the frequency of general NKT cells within the spleen was relatively low and remained unchanged with both YUMM1.1 and YUMM1.7 vaccines (Figure 5.2B). Within the mdLN the NKT cell population comprised an even smaller proportion of the total $CD45^+$ immune cell population, and was decreased following vaccination (Figure 5.3B). Similarly, the NK cell populations within the mdLN and spleen were relatively small and remained largely unchanged following vaccination, although YUMM1.7 vaccine decreased the frequency of splenic NK cells (Figure 5.2C). The T cell population represented a large proportion of lymphocytes within the $CD45^+$ immune cell population in the mediastinal lymph node, and was unaltered with vaccination (Figure 5.3A). Within the spleen the frequency of total T cells was slightly decreased with YUMM1.1 vaccine and significantly decreased with YUMM1.7 vaccination.

Despite decreases in the overall T cell population in the spleen, the frequency of non-regulatory $CD4^+$ and $CD8^+$ T cells remained unchanged (Figure 5.2D

and F). In contrast, while there was no change in the overall T cell population within the mdLN both vaccines decreased the frequency of non-regulatory $CD4^+$ T cells and increased the frequency of $CD8^+$ T cells (Figure 5.3D and F). Interestingly, within both the spleen and mdLN, vaccination significantly reduced the proportion of Tregs (Figures 5.2E and 5.3E). The increased proportion of $CD4^+$ and $CD8^+$ T cells expressing the activation marker CD44 and down-regulating the lymph node-homing molecule CD62L were indicative of increased effector T cell populations within both tissues (Figures 5.2G&H, and 5.3G&H). Collectively, these changes in T cell populations resulted in significantly increased ratios of non-regulatory $CD4^+$ T cells and $CD8^+$ T cells to Tregs, as well as increased ratios of effector T cells to regulatory T cells, in both the spleen and mdLN (Figures 5.3 and 5.5).

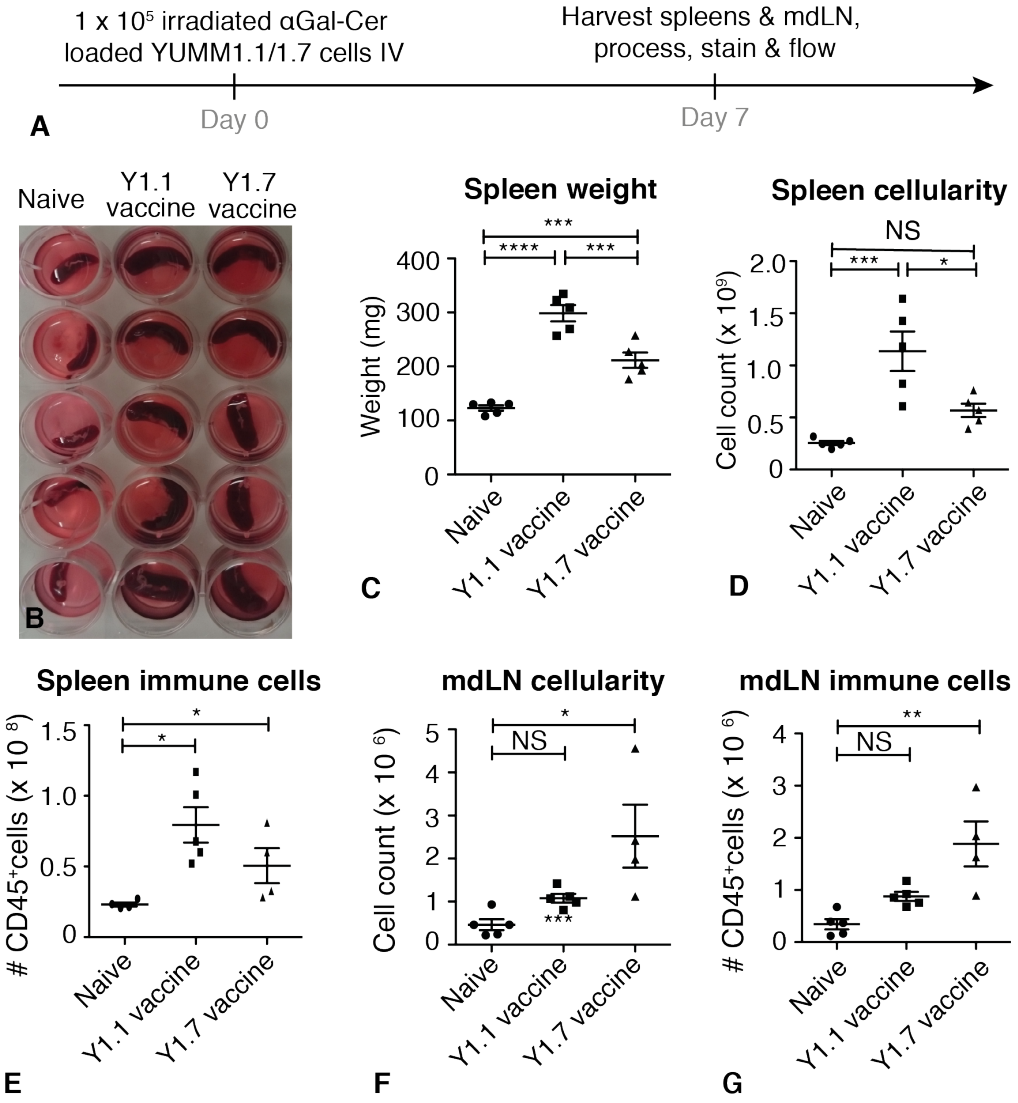

Figure 5.1: Whole tumour cell vaccination induces an immune response. A. Naïve C57BL/6 mice were intravenously administered vaccines consisting of irradiated, αGalCer-loaded YUMM1.1 or YUMM1.7 cells. Control mice received PBS. One week post-vaccination, mice were culled and spleens and mdLN were harvested. Cell counts were assessed by trypan blue exclusion and CD45 expression was determined by flow cytometric analysis (as shown in Figure 5.2A). The number of $CD45^+$ immune cells was calculated by multiplying the percentage of $CD45^+$ immune cells by the total number of single cells. Single cell numbers were determined by multiplying percentages of single cells by total number of live cells as determined by trypan blue exclusion. Vaccination resulted in gross splenomegaly (**B**), increased spleen weight (**C**) and increased spleen and mdLN cellularity (**D, F**). Numbers of $CD45^+$ immune cells were increased both in the spleen and mdlN (**E, G**). Each data point represents an individual mouse, with 4-5 mice used per group. Error bars are ± SEM. * $p \leq 0.05$, ** $p < 0.01$, *** $p < 0.001$, **** $p < 0.0001$, one-way ANOVA with Bonferroni post-test. Results are representative of two independent experiments.

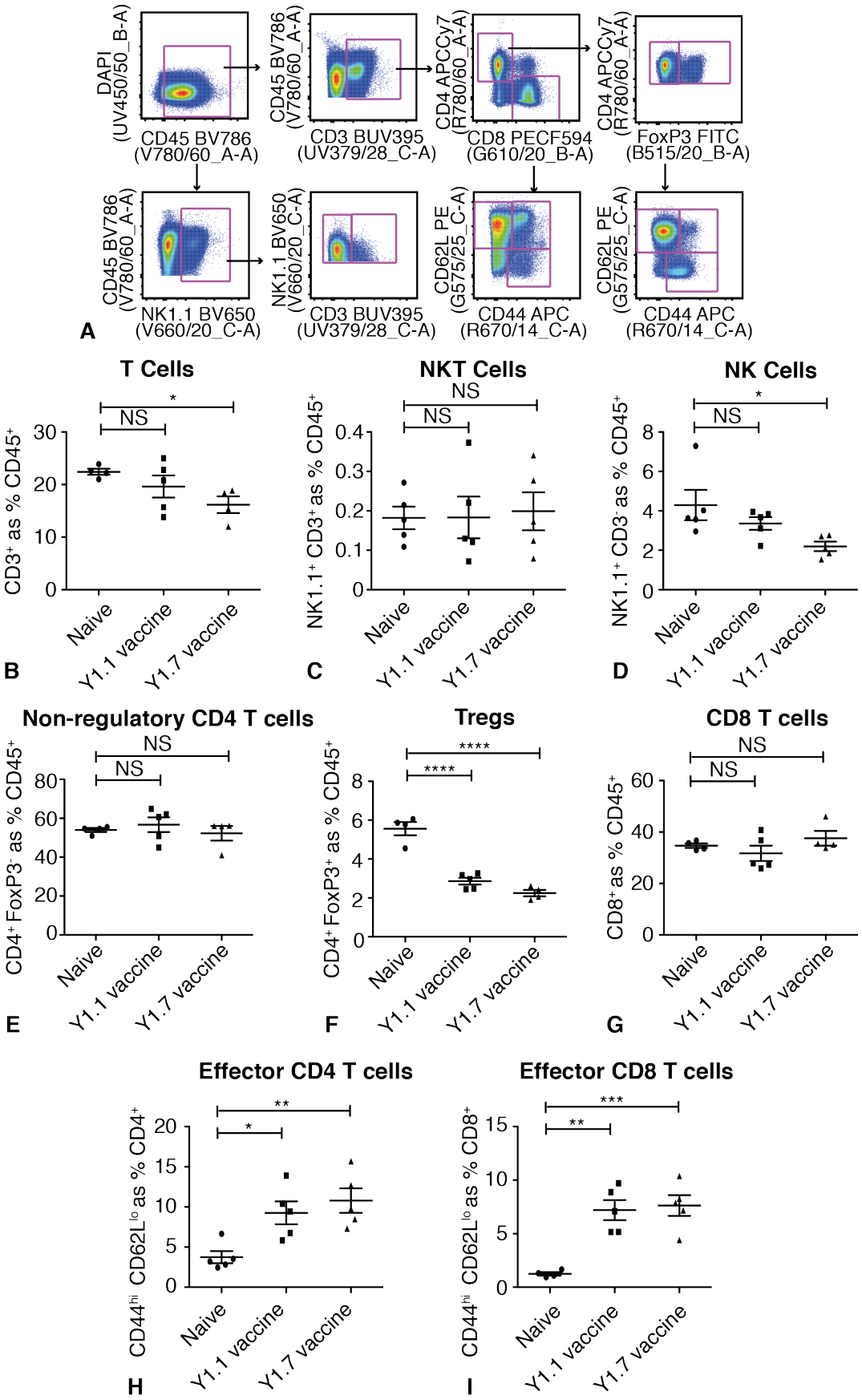
A
DAPI (UV450/50_B-A)
CD45 BV786 (V780/60_A-A)
CD3 BUV395 (UV379/28_C-A)
CD4 APCCy7 (R780/60_A-A)
CD8 PECF594 (G610/20_B-A)
FoxP3 FITC (B515/20_B-A)
NK1.1 BV650 (V660/20_C-A)
CD62L PE (G575/25_C-A)
CD44 APC (R670/14_C-A)
T Cells
NKT Cells
NK Cells
Non-regulatory CD4 T cells
Tregs
CD8 T cells
Effector CD4 T cells
Effector CD8 T cells
Naive
Y1.1 vaccine
Y1.7 vaccine
NS
B
C
D
E
F
G
H
I

Figure 5.2: Vaccination decreases frequencies of Tregs and increases frequencies of effector T cells within the spleen. C57BL/6 mice were vaccinated as described in Figure 5.1A. One week following vaccination spleens were harvested and immune cell frequencies assessed by flow cytometry. **A.** Gating strategy used to define splenic T cell, NK and NKT cell populations. Samples were pre-gated on live, single cells. Subsets were defined as follows: T cells = $CD3^+$; NKT cells = $NK1.1^+$, $CD3^+$; NK cells = $NK1.1^+$, $CD3^-$; Non-regulatory T cells = $CD3^+$, $CD4^+$, $FoxP3^-$; Tregs = $CD3^+$, $CD4^+$, $FoxP3^+$; CD8 T cells = $CD3^+$, $CD8^+$; Effector T cells = subset defined as previously described then $CD44^{hi}$, $CD62L^{lo}$. **B-I.** Frequencies of T cells, NK cells and NKT cells. Values represent individual mice, with 4-5 mice used per group. Error bars are ± SEM. * $p \leq 0.05$, ** $p < 0.01$, *** $p < 0.001$, **** $p < 0.0001$, one-way ANOVA with Bonferroni post-test. Results are representative of two independent experiments.

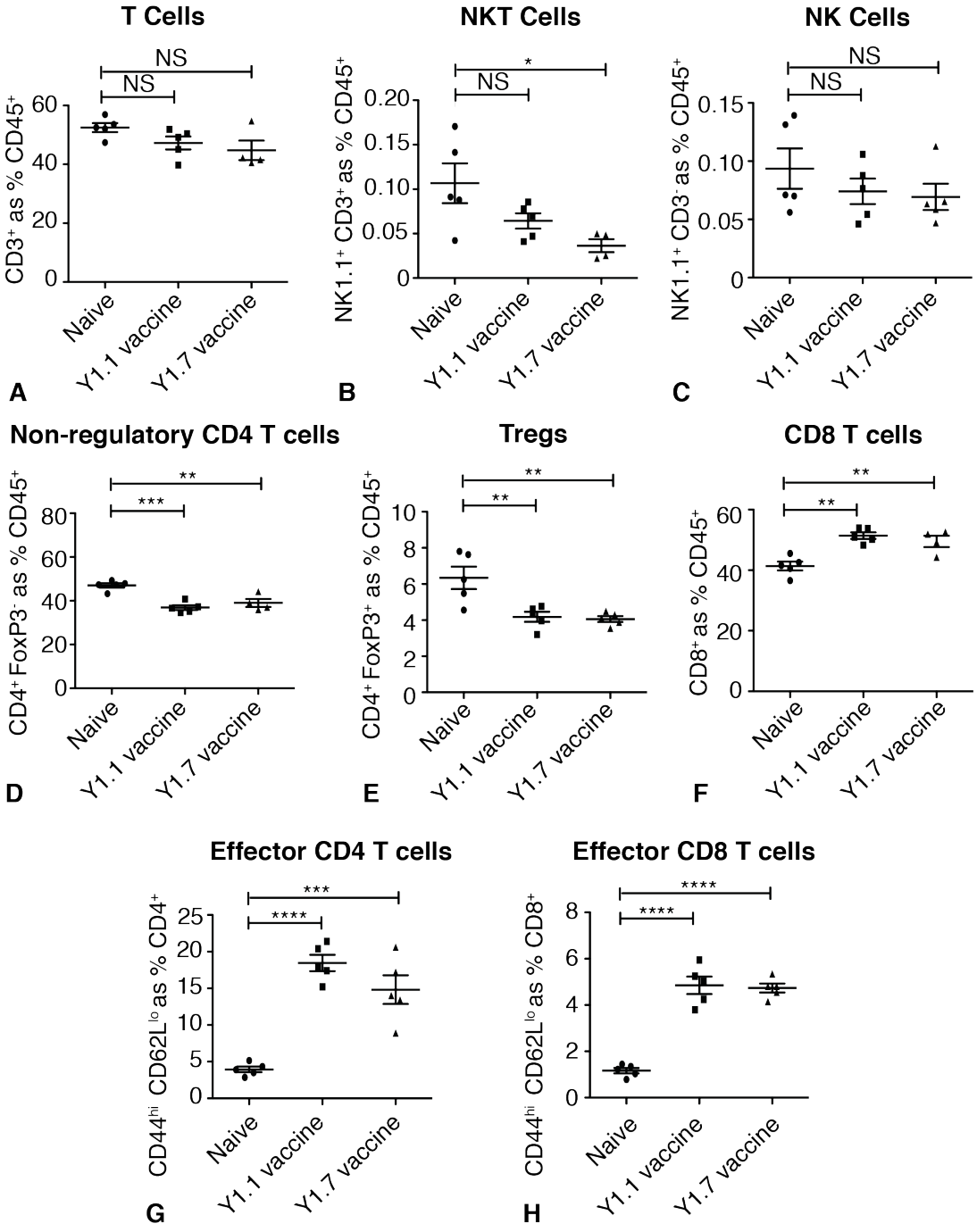

Figure 5.3: Vaccination decreases frequencies of both non-regulatory CD4$^+$ T cells and Tregs and increases frequencies of CD8 T cells and effector T cells within the mdLN. C57BL/6 mice were vaccinated as described in Figure 5.1A. One week following vaccination mdLN were harvested and immune cell frequencies assessed by flow cytometry. Samples were pre-gated on live, single cells and T cell, NK and NKT cell populations were defined as shown in Figure 5.2A. **A-H.** Frequencies of T cells, NK cells and NKT cells. Values represent individual mice, with 4-5 mice used per group. Error bars are ± SEM. * $p \leq 0.05$, ** $p < 0.01$, *** $p < 0.001$, **** $p < 0.0001$, one-way ANOVA with Bonferroni post-test. Results are representative of two independent experiments.

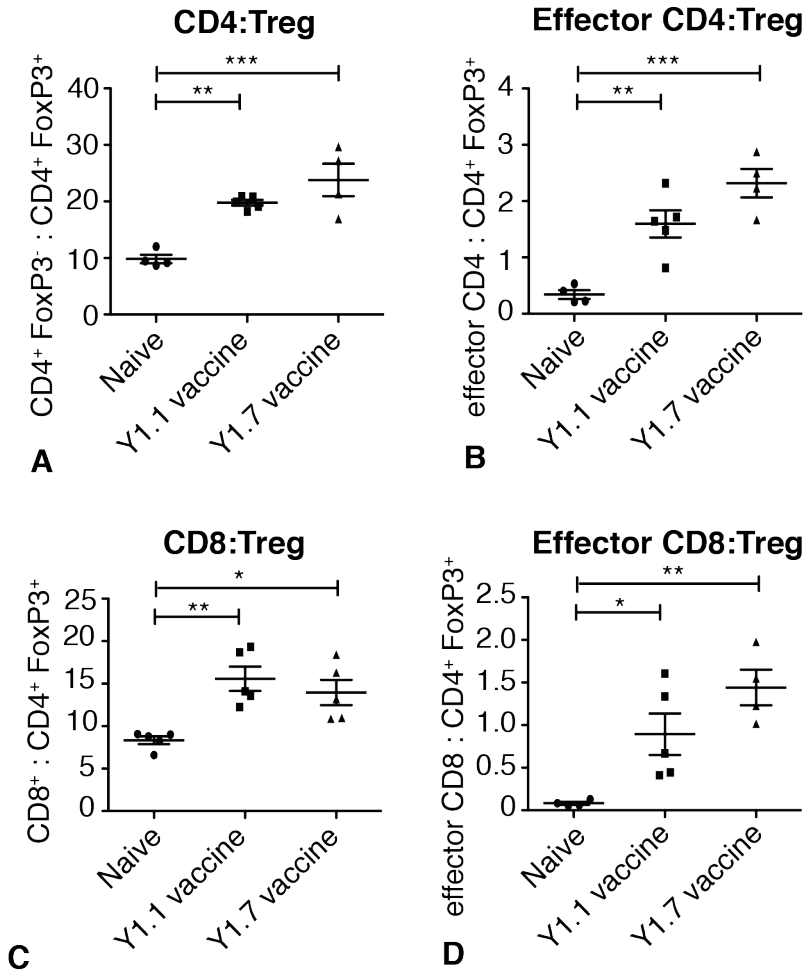

Figure 5.4: Vaccination favourably increases ratios of splenic non-regulatory and effector T cells to Tregs. C57BL/6 mice were vaccinated as described in Figure 5.1A. One week following vaccination spleens were harvested and immune cell frequencies assessed by flow cytometry. Samples were pre-gated on live, single cells and T cell, NK and NKT cell populations were defined as shown in Figure 5.2A. The number of specific T cells was calculated by multiplying the population percentage by the total number of cells in the preceding gate. Cell numbers within the initial single cell gate were determined by multiplying percentages of single cells by total number of live cells as determined by trypan blue exclusion. **A**. Ratio of non-regulatory $CD4^+$ $FoxP3^-$ cells to $CD4^+$ $FoxP3^+$ Tregs. **B.** Ratio of effector $CD4^+$ $FoxP3^-$ cells to Tregs. **C.** Ratio of $CD8^+$ cells to $CD4^+$ $FoxP3^+$ Tregs. **D.** Ratio of effector $CD8^+$ cells to Tregs. Values represent individual mice, with 4-5 mice used per group. Error bars are ± SEM. * $p \leq 0.05$, ** $p < 0.01$, *** $p < 0.001$, one-way ANOVA with Bonferroni post-test. Results are representative of two independent experiments.

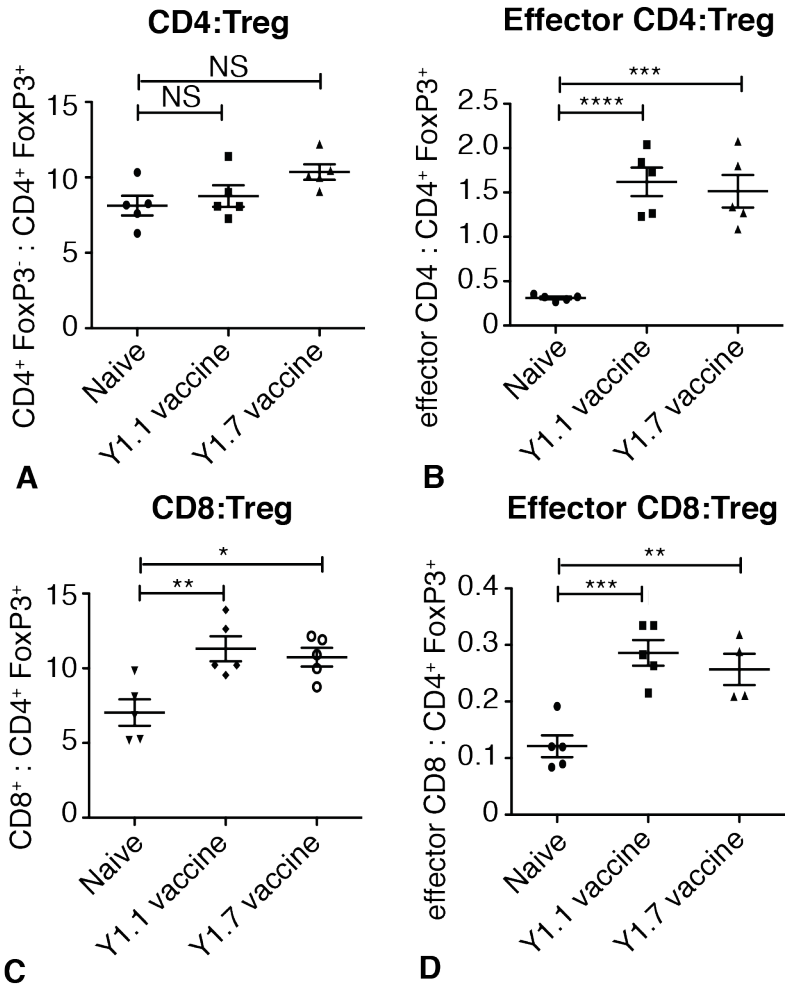

Figure 5.5: Vaccination favourably increases ratios of mdLN non-regulatory and effector T cells to Tregs. C57BL/6 mice were vaccinated as described in Figure 5.1A. One week following vaccination spleens were harvested and immune cell frequencies assessed by flow cytometry. Samples were pre-gated on live, single cells and T cell, NK and NKT cell populations were defined as shown in Figure 5.2A. The number of T cells was calculated by multiplying the population percentage by the total number of cells in the preceding gate. Cell numbers within the initial singlet cell gate were determined by multiplying percentages of single cells by total number of live cells as determined by trypan blue exclusion. **A**. Ratio of non-regulatory $CD4^+$ $FoxP3^-$ cells to $CD4^+$ $FoxP3^+$ Tregs. **B.** Ratio of effector $CD4^+$ $FoxP3^-$ cells to Tregs. **C.** Ratio of $CD8^+$ cells to $CD4^+$ $FoxP3^+$ Tregs. **D.** Ratio of effector $CD8^+$ cells to Tregs. Values represent individual mice, with 4-5 mice used per group. Error bars are ± SEM. * $p \leq 0.05$, ** $p < 0.01$, *** $p < 0.001$, **** $p < 0.0001$, one-way ANOVA with Bonferroni post-test. Results are representative of two independent experiments.

Taken together the data presented in this section show that both irradiated, αGalCer-loaded YUMM1.1 and YUMM1.7 cells can induce an immune response in naïve mice, which is predominantly T cell-mediated. Vaccination enhances effector T cell populations and reduces regulatory T cell frequency.

5.2.2 Autologous vaccination is partially protective against YUMM1.1 tumours but has minimal anti-tumour activity in YUMM1.7 tumours

Having ascertained that irradiated, αGalCer-loaded YUMM1.1 and YUMM1.7 cells induce an immune response, the anti-tumour efficacy of autologous vaccination was assessed in both a prophylactic setting and in mice with established tumours. C57BL/6 mice received vaccine either seven days prior to tumour challenge, to allow development of an effector T cell response, or five days after sub-cutaneous injection of 2×10^5 YUMM1.1 cells or 1×10^5 YUMM1.7 cells (Figures 5.6A and 5.7A). Tumour growth was monitored and size recorded every two to three days. Mice were culled when tumours reached 150 mm^2 or became severely ulcerated.

Vaccine provided protection in both prophylactic and therapeutic settings against YUMM1.1 tumours, with tumour growth significantly decreased (Figure 5.6B) and survival increased (Figure 5.6D). Although vaccination significantly delayed tumour growth, no tumour regression was seen indicating tumours were able to suppress or escape anti-tumour immune responses.

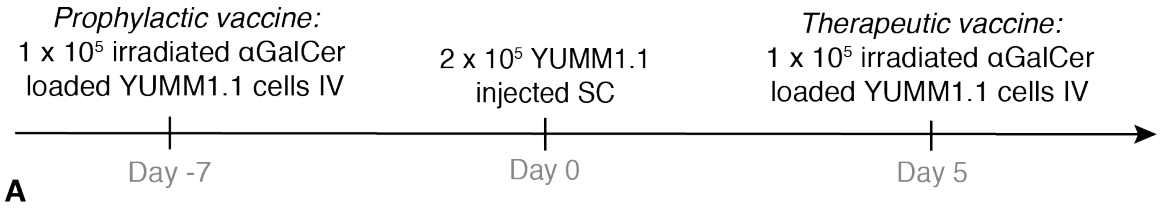
Prophylactic vaccine:
1 x 10⁵ irradiated αGalCer loaded YUMM1.1 cells IV
2 x 10⁵ YUMM1.1 injected SC
Therapeutic vaccine:
1 x 10⁵ irradiated αGalCer loaded YUMM1.1 cells IV
Day -7
Day 0
Day 5

A

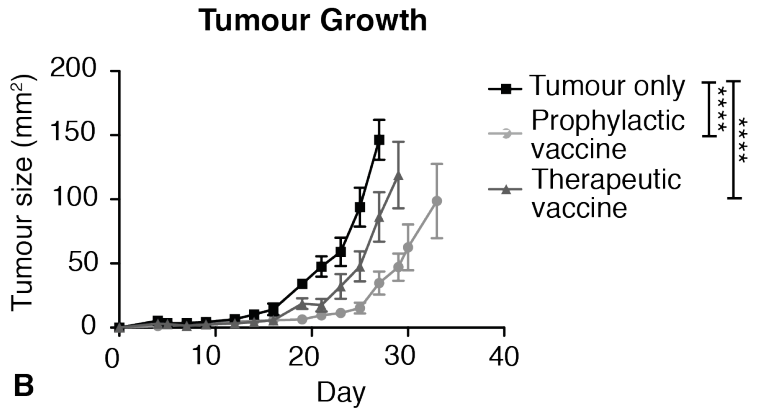
Tumour Growth
Tumour size (mm²)
Day
Tumour only
Prophylactic vaccine
Therapeutic vaccine
****
****

B

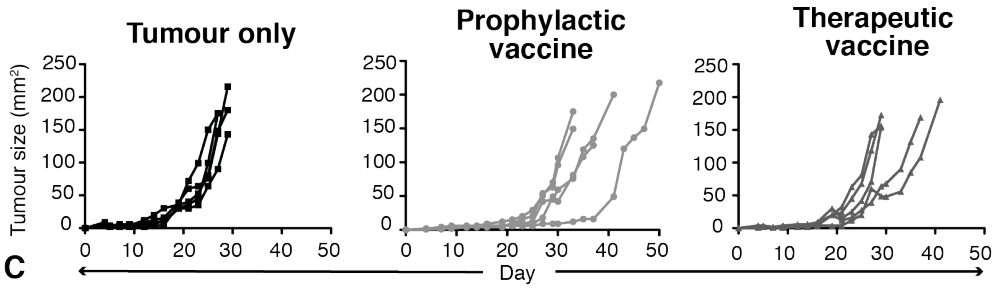
Tumour only
Prophylactic vaccine
Therapeutic vaccine
Tumour size (mm²)
Day

C

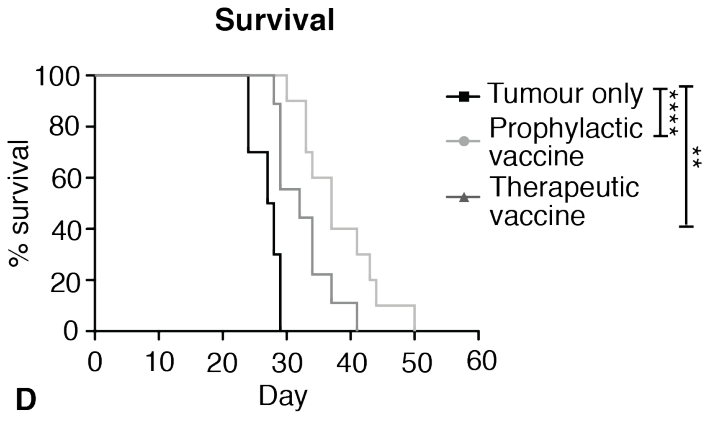
Survival
% survival
Day
Tumour only
Prophylactic vaccine
Therapeutic vaccine
****
**

D

Figure 5.6: Prophylactic and therapeutic autologous whole tumour cell vaccination slows YUMM1.1 growth and increases survival. A. C57BL/6 mice were vaccinated intravenously with irradiated, αGalCer-loaded YUMM1.1 cells either prophylactically seven days prior to tumour challenge, or therapeutically five days post-tumour challenge. Control mice received PBS. Mice were challenged sub-cutaneously with 2 x 10^5 YUMM1.1 cells. Tumour growth was monitored and size recorded. Mice were culled when tumours reached 150 mm^2, or when tumours ulcerated. **B.** Average tumour growth is shown, each symbol represents the mean growth of 4-5 mice, error bars are ± SEM. **** $P \leq 0.0001$, 2-way ANOVA with Bonferroni post-test, statistics shown for Day 27. **C.** Individual tumour growth, each data point represents one mouse. **D.** Percent survival is shown for 2 combined experiments each with 4-5 mice per group. Treatment groups are compared to control mice ** $P < 0.01$, **** $P < 0.0001$ Mantel-Cox test. Tumour growth is representative of two independent experiments (as tumours were measured on different days data was unable to be combined). Survival Data are pooled from two independent experiments.

In a prophylactic setting, vaccination slowed YUMM1.7 tumour growth significantly, although no tumour regression was induced (Figure 5.7B). Despite the effect of prophylactic vaccination on tumour growth, vaccination only conferred a small survival benefit, which was not statistically significant over control mice (Figure 5.7D). Vaccine efficacy was also tested in hosts with established YUMM1.7 tumours. Although the vaccine provided a small benefit in a prophylactic setting, in the therapeutic model no protection was evident. Following therapeutic vaccination both tumour growth and mouse survival were unchanged (Figures 5.7 B-D).

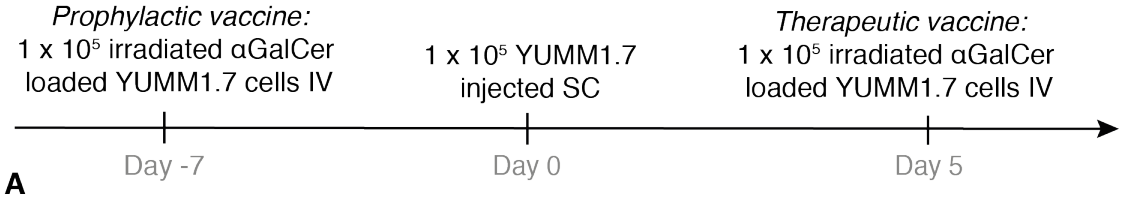
Prophylactic vaccine:
1 x 10⁵ irradiated αGalCer loaded YUMM1.7 cells IV
1 x 10⁵ YUMM1.7 injected SC
Therapeutic vaccine:
1 x 10⁵ irradiated αGalCer loaded YUMM1.7 cells IV
Day -7
Day 0
Day 5

A

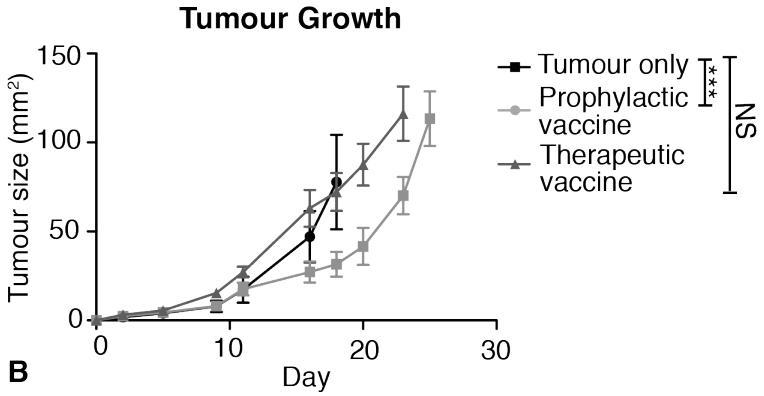
Tumour Growth
Tumour size (mm²)
Day
Tumour only
Prophylactic vaccine
Therapeutic vaccine
***
NS

B

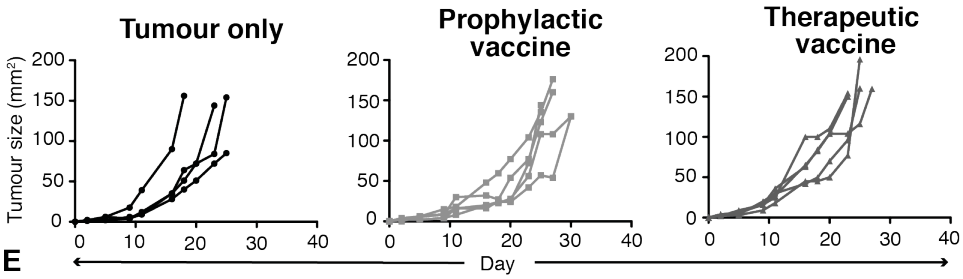
Tumour only
Prophylactic vaccine
Therapeutic vaccine
Tumour size (mm²)
Day

E

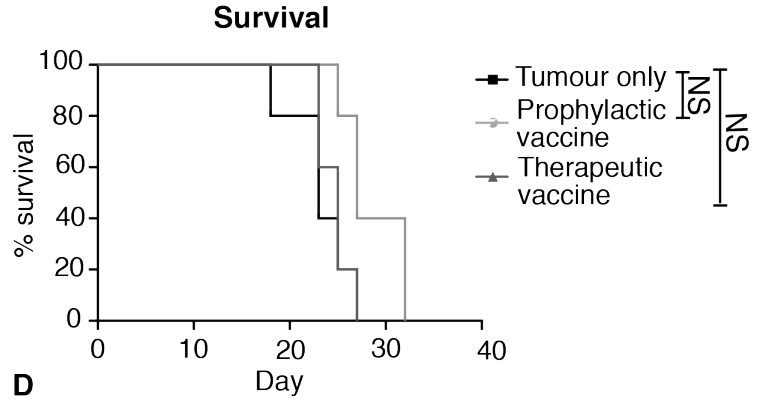
Survival
% survival
Day
Tumour only
Prophylactic vaccine
Therapeutic vaccine
NS
NS

D

Figure 5.7: Prophylactic but not therapeutic autologous whole tumour cell vaccination slows YUMM1.7 growth but does not increase survival. A. C57BL/6 mice were vaccinated intravenously with irradiated, αGalCer-loaded YUMM1.7 cells either prophylactically seven days prior to tumour challenge, or therapeutically five days post-tumour challenge. Control mice received PBS. Mice were challenged sub-cutaneously with 1 x 10^5 YUMM1.7 cells. Tumour growth was monitored and size recorded. Mice were culled when tumours reached 150 mm^2, or when tumours ulcerated. **B.** Average tumour growth is shown, each symbol represents the mean growth of 4-5 mice, error bars are ± SEM. *** $P < 0.001$, 2-way ANOVA with Bonferroni post-test, statistics shown for Day 27. **C.** Individual tumour growth. Each data point represents one mouse. **D.** Percent survival is shown for groups of 4-5 mice. Treatment groups are compared to control mice. NS= non-significant, Mantel-Cox test. Data are representative of two independent experiments.

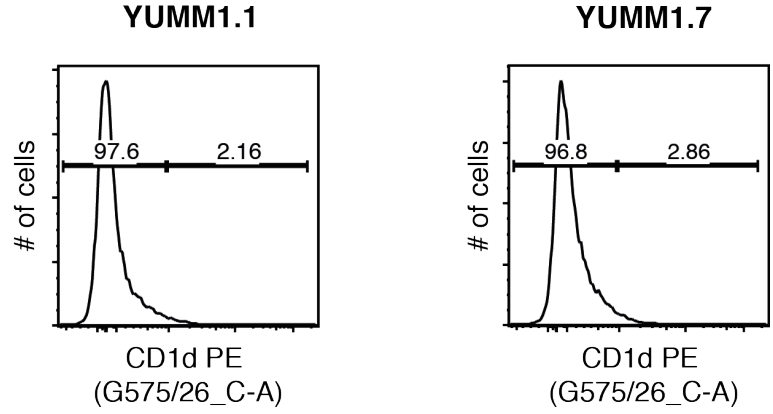

Figure 5.8: YUMM1.1 and YUMM1.7 cells do not express CD1d. Cells were cultured for 48 hours and subsequently harvested. CD1d expression was assessed in triplicate by flow cytometry. Plots are representative of two independent experiments.

Autologous whole tumour cell vaccination had greater efficacy in the YUMM1.1 model, than in the YUMM1.7 model. In both the prophylactic and therapeutic setting vaccination significantly decreased YUMM1.1 tumour growth and increased survival, while in the YUMM1.7 model only prophylactic vaccine showed an anti-tumour effect. CD1d expression was analysed to determine if either cell line could directly present αGalCer to iNKT cells. Results demonstrated that neither YUMM1.1 nor YUMM1.7 cells expressed CD1d (Figure 5.8), indicating that differential responsiveness to vaccine is not a result of a different mechanism of αGalCer association with tumour cells. Due to the increased efficacy of autologous vaccination against YUMM1.1 tumours, this model was used in subsequent experiments to investigate combination therapy approaches. While vaccination has significant anti-tumour activity in the YUMM1.1 model, the efficacy is only moderate as no tumour regression is evident. This "sub-optimal" form of immunotherapy is ideal to investigate combination therapy with PLX4720 because it will allow synergistic effects of targeted chemotherapy and immunotherapy to be determined.

5.2.3 YUMM1.1 vaccination of tumour-bearing mice alters the frequencies of T cell sub-populations but does not significantly change NK, NKT or myeloid populations

The preceding experiments established the YUMM1.1 tumour model as the preferable model for investigating vaccine and BRAF inhibitor combination therapy. In naïve mice YUMM1.1 vaccination induced effector T cell responses within the spleen and mdLN. Next, experiments were performed to define the immune cell populations within the tumour and peripheral lymphoid tissues of tumour bearing mice. The aim of these experiments was to identify immune cell subsets mediating anti-tumour effects of the vaccine. C57BL/6 mice were vaccinated either prophylactically or therapeutically with tumour challenge as previously described. Fourteen days post-tumour challenge, mice were culled and tumours, draining inguinal lymph node (iLN) and spleens were harvested (Figure 5.8A). Tissues were processed and flow cytometric analysis was performed with lymphoid and myeloid cell populations defined as shown in Figure 5.8 B and C respectively. As

previously described in Section 5.2.1 data are presented as population frequencies, because changes in cell number within subsets reflect the overall change in cell numbers within the tumours or lymphoid tissues following vaccination.

5.2.3.1 Tumour infiltrating lymphocytes

Intratumoural lymphocyte populations were assessed and it was found that the total frequency of $CD3^+$ T cells, approximately 40% of $CD45^+$ cells, did not change following vaccination (Figure 5.9A). There was also no change in the NKT population, while the frequency NK cells increased non-significantly from around 15% of $CD45^+$ to approximately 20% (Figure 5.9B and C). Despite the total T cell population remaining the same, the frequency of sub-populations changed with vaccine delivery. The proportion of non-regulatory $CD4^+$ T cells increased significantly, and correspondingly the frequency of Tregs decreased. No change was observed in the frequency of $CD8^+$ T cells (Figure 5.9D-F). Furthermore, both effector $CD4^+$ and $CD8^+$ T cells populations showed non-significant increases in frequency, while PD-1 expression decreased (Figure 5.9G-J). These data indicate that following vaccination there are decreases in intratumoural Tregs, and increases in $CD4^+$ and $CD8^+$ effector populations, along with decreased expression of the exhaustion marker PD-1. Changes in the frequency of T cell subpopulations were reflected in the significantly increased ratio of non-regulatory $CD4^+$ T cells to Tregs and $CD8^+$ T cells to Tregs (Figure 5.10 A and C). However, effector T cell to Treg ratios remained unchanged (Figure 5.10 B and D).

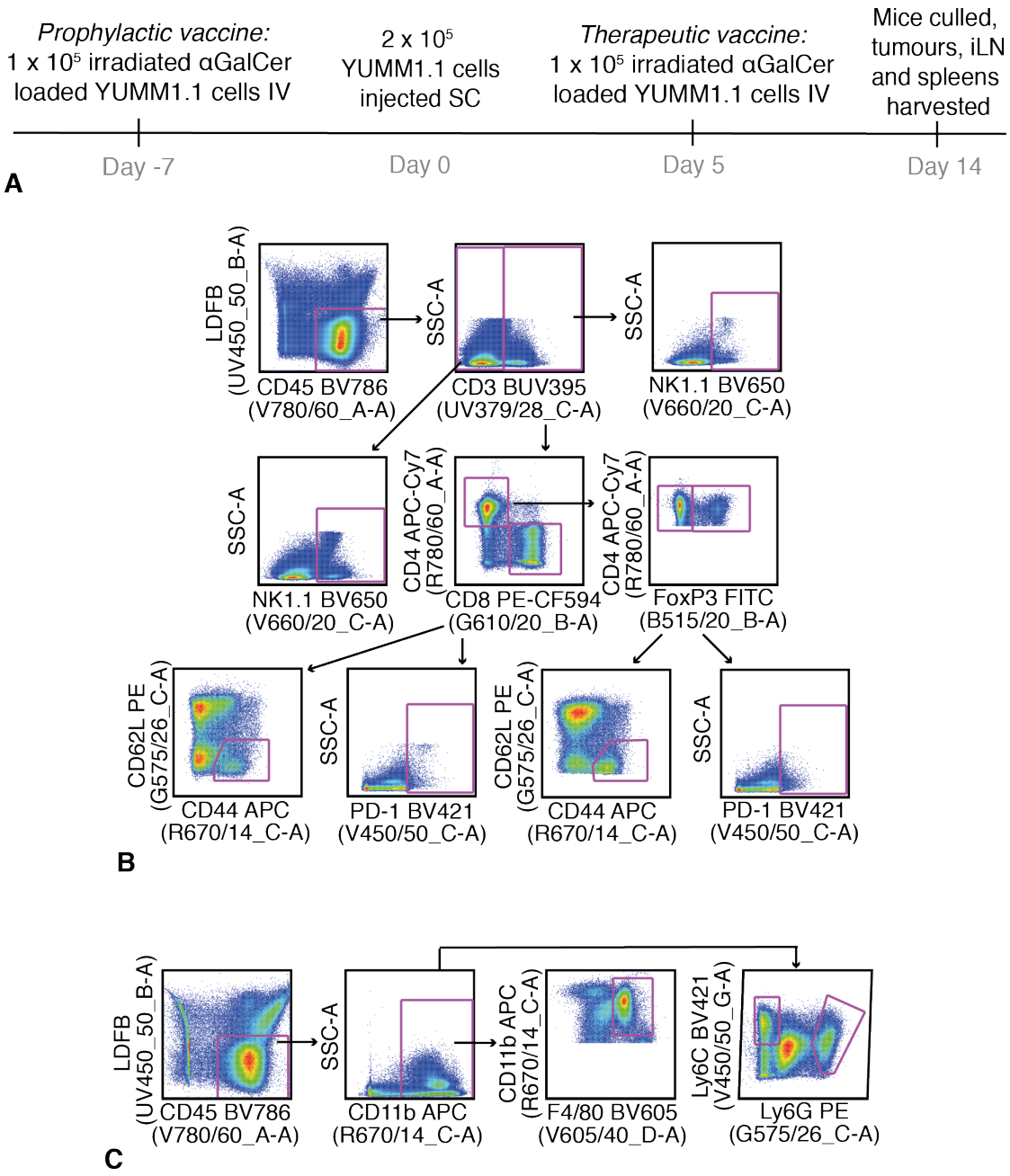

Figure 5.9: Flow cytometric gating strategy used to define lymphoid and myeloid populations within the tumour, spleen and draining iLN. A. C57BL/6 mice were vaccinated intravenously with irradiated, αGalCer-loaded YUMM1.1 cells either seven days prior to tumour challenge, or five days post-tumour challenge. Control mice received PBS intravenously. Mice were challenged sub-cutaneously with 2 x 10^5 YUMM1.1 cells. 14 days post-tumour challenge mice were culled and tumours, draining ilN and spleens harvested and processed for flow cytometric analysis. Samples were pre-gated on single cells. **B.** Gating strategy used to define T cell, NK and NKT cell populations. Subsets were defined as follows: T cells = $CD3^+$; NKT cells = $NK1.1^+$, $CD3^+$; NK cells = $NK1.1^+$, $CD3^-$; Non-regulatory T cells = $CD3^+$, $CD4^+$, $FoxP3^-$; Tregs = $CD3^+$, $CD4^+$, $FoxP3^+$; CD8 T cells = $CD3^+$, $CD8^+$; Effector T cells = subset defined as previously described then $CD44^{hi}$, $CD62L^{lo}$. **C.** Gating strategy used to define myeloid ($CD11b^+$), macrophage ($CD11b^+$, $F4/80^+$) and MDSC populations ($CD11b^+$, $Ly6C^{hi}$ and $Ly6G^{lo\ or\ hi}$).

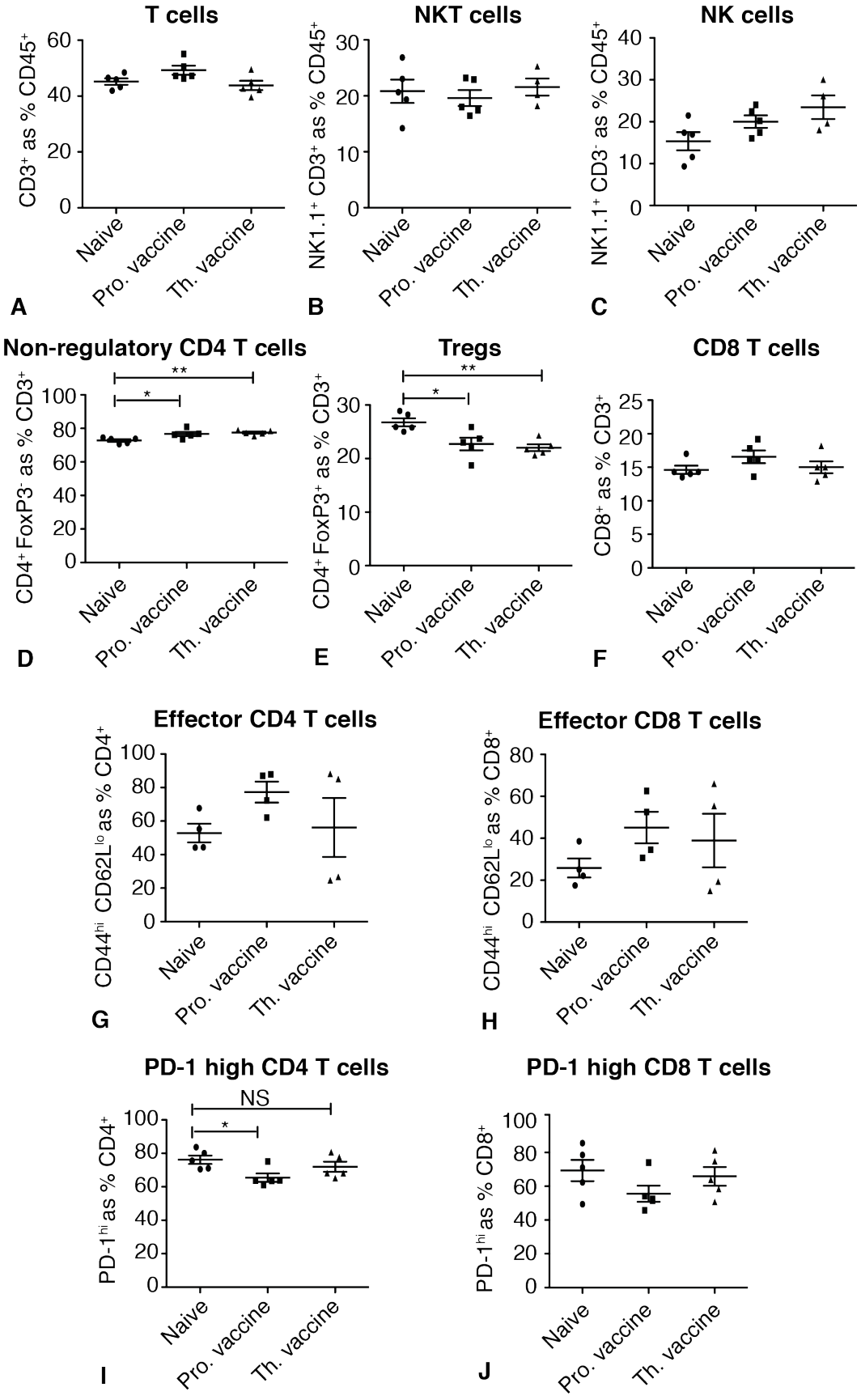
T cells
CD3+ as % CD45+
60
40
20
0
Naive
Pro. vaccine
Th. vaccine
A
NKT cells
NK1.1+ CD3+ as % CD45+
30
20
10
0
Naive
Pro. vaccine
Th. vaccine
B
NK cells
NK1.1+ CD3- as % CD45+
40
30
20
10
0
Naive
Pro. vaccine
Th. vaccine
C
Non-regulatory CD4 T cells
CD4+ FoxP3- as % CD3+
**
*
100
80
60
40
20
0
Naive
Pro. vaccine
Th. vaccine
D
Tregs
CD4+ FoxP3+ as % CD3+
**
*
30
20
10
0
Naive
Pro. vaccine
Th. vaccine
E
CD8 T cells
CD8+ as % CD3+
25
20
15
10
5
0
Naive
Pro. vaccine
Th. vaccine
F
Effector CD4 T cells
CD44hi CD62Llo as % CD4+
100
80
60
40
20
0
Naive
Pro. vaccine
Th. vaccine
G
Effector CD8 T cells
CD44hi CD62Llo as % CD8+
80
60
40
20
0
Naive
Pro. vaccine
Th. vaccine
H
PD-1 high CD4 T cells
PD-1hi as % CD4+
NS
*
100
80
60
40
20
0
Naive
Pro. vaccine
Th. vaccine
I
PD-1 high CD8 T cells
PD-1hi as % CD8+
100
80
60
40
20
0
Naive
Pro. vaccine
Th. vaccine
J

Figure 5.10: Vaccination increases frequencies of intratumoural non-regulatory CD4$^+$ T cells and decreases frequencies of Tregs. C57BL/6 mice were vaccinated as described in Figure 5.9A. One week following vaccination tumours were harvested and immune cell frequencies assessed by flow cytometry, lymphocyte populations were defined as shown in Figure 5.9B. **A-F.** Frequencies of T cells, NK cells and NKT cells. G-J. Frequencies of effector and exhausted CD4$^+$ and CD8$^+$ T cells. Values represent individual mice, with 5 mice used per group. Error bars are ± SEM. NS= non-significant, * $p \leq 0.05$, ** $p < 0.01$ one-way ANOVA with Bonferroni post-test. Results are representative of two independent experiments.

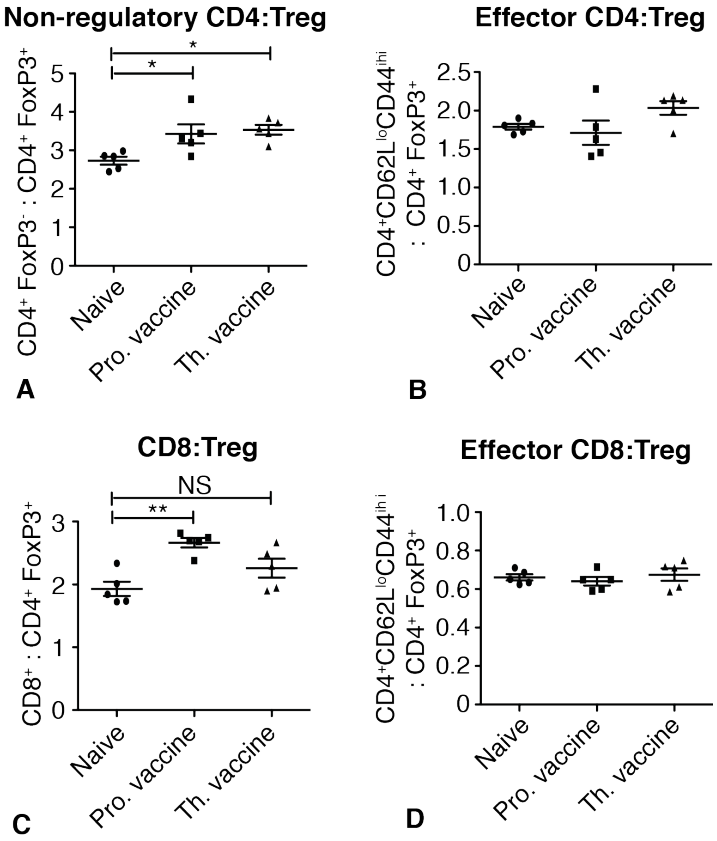

Figure 5.11: Vaccination increases intratumoural ratio of non-regulatory CD4$^+$ T cells and CD8$^+$ T cells to Tregs. C57BL/6 mice were vaccinated as described in Figure 5.9A. One week following vaccination tumours were harvested and immune cell frequencies assessed by flow cytometry, lymphocyte populations were defined as shown in Figure 5.9B. The number of T cells was calculated by multiplying the population percentage by the total number of cells in the preceding gate. Cells number within the initial singlet cell gate were determined by multiplying percentages of single cells by total number of live cells as determined by trypan blue exclusion. **A.** Ratio of non-regulatory CD4$^+$ FoxP3$^-$ cells to CD4$^+$ FoxP3$^+$ Tregs. **B.** Ratio of effector CD4$^+$ FoxP3$^-$ cells to Tregs**. C.** Ratio of CD8$^+$ cells to CD4$^+$ FoxP3$^+$ Tregs. **D.** Ratio of effector CD8$^+$ cells to Tregs. Values represent individual mice, with 5 mice used per group. Error bars are ± SEM. * $p \leq 0.05$, ** $p < 0.01$, one-way ANOVA with Bonferroni post-test. Results are representative of two independent experiments.

5.2.3.2 Tumour infiltrating myeloid cells

In addition to lymphoid cell populations, the effects of vaccination on intratumoural myeloid cell populations were assessed. Initial flow cytometric gating was on CD11b, which could include monocytes, moDCs, some conventional DCs, neutrophils, eosinophils, macrophages and MDSCs. These CD11b+ cells were shown to represent approximately 80% of the $CD45^+$ cells within the tumour. However, it is worth noting that the $CD45^+$ cells were pre-gated on FSC and SSC and these parameters were set at different voltages to those used in the lymphocyte panel (based on size and granularity of the target population). Thus, when considering frequencies of myeloid cells as a proportion of $CD45^+$ it should be considered that this $CD45^+$ gate may not include all lymphocytes. Following vaccination no change was seen in the total $CD11b^+$ cell population. Furthermore, there were no changes in the macrophage population (as defined by CD11b and F4/80 expression), which comprised the major subset of CD11b+ cells or in the monocytic MDSC (moMDSC) population, which accounted for approximately 15% of $CD11b^+$ cells. A small increase in the proportion of granulocytic MDSCs was observed, from around 1% of $CD11b^+$ cells to 2% in vaccinated mice, although this may not be biologically significant.

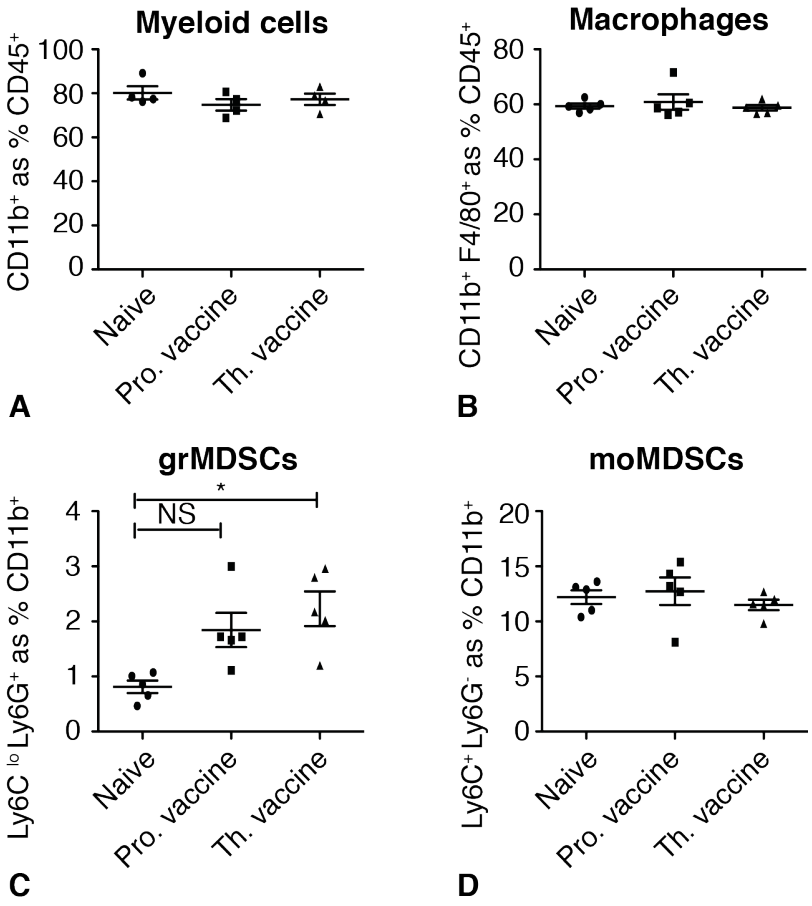

Figure 5.12: Vaccination does not alter intratumoural frequencies of myeloid, macrophage or moMDSCs, but may increase grMDSCs. C57BL/6 mice were vaccinated as described in Figure 5.9A. One week following vaccination tumours were harvested and immune cell frequencies assessed by flow cytometry. Myeloid populations were defined as shown in Figure 5.9C. **A-D.** Frequencies of $CD11b^{+,}$ macrophage and MDSC populations. Values represent individual mice, with 5 mice used per group. Error bars are ± SEM. NS= non-significant, * $p \leq 0.05$, ** $p < 0.01$ one-way ANOVA with Bonferroni post-test. Results are representative of two independent experiments.

5.2.3.3 Immune cell subsets within the spleen and tumour draining iLN

The frequency of immune cells within the spleen and tumour draining iLN were also analysed. Changes in splenic populations with vaccination reflected trends similar to those seen in tumour infiltrating immune cell subsets, while the draining iLN populations were largely unaffected by vaccination (Figures 5.13-5.17). Within the spleen no change was observed in the frequency of total T cells, and there were non-significant decreases in the proportion of NKT or NK cells. The frequency of non-regulatory $CD4^+$ or $CD8^+$ T cells also remained the same following vaccination. However, the proportion of Tregs decreased significantly. A small increase in the frequency of effector $CD4^+$ and $CD8^+$ T cells was observed, but these changes were largely non-significant. The changes in the frequency of Tregs and effector T cells were reflected in the ratios of non-regulatory or effector T cells to Tregs, which generally increased following vaccination. Similar to the intratumoural populations, the frequency of $CD4^+$ T cells expressing the exhaustion marker PD-1 decreased significantly with vaccination. In contrast to the tumour and spleen data, no significant changes were observed in the frequency of any of the lymphoid populations assessed within the tumour draining lymph node (Figure 5.14). Similarly, the effector function of populations as determined by CD44/CD62L expression and PD-1 expression remained largely unchanged.

Within the myeloid compartment of the spleen, $CD11b^+$ cells accounted for approximately 50% of $CD45^+$ cells, which was unaltered following vaccination, as was the frequency of macrophages. Splenic MDSC populations appeared to be skewed towards increased proportions of granulocytic MDSCs and decreased proportions of moMDSCs during vaccination, although as shown in other tissues, moMDSCs were present at much higher frequencies than grMDSCs (Figure 5.16). In the draining iLN a non-significant reduction in the frequency of total $CD11b^+$ cells was observed. However, the proportion of macrophages increased significantly following therapeutic vaccination whilst the frequency of MDSCs remained the same (Figure 5.17).

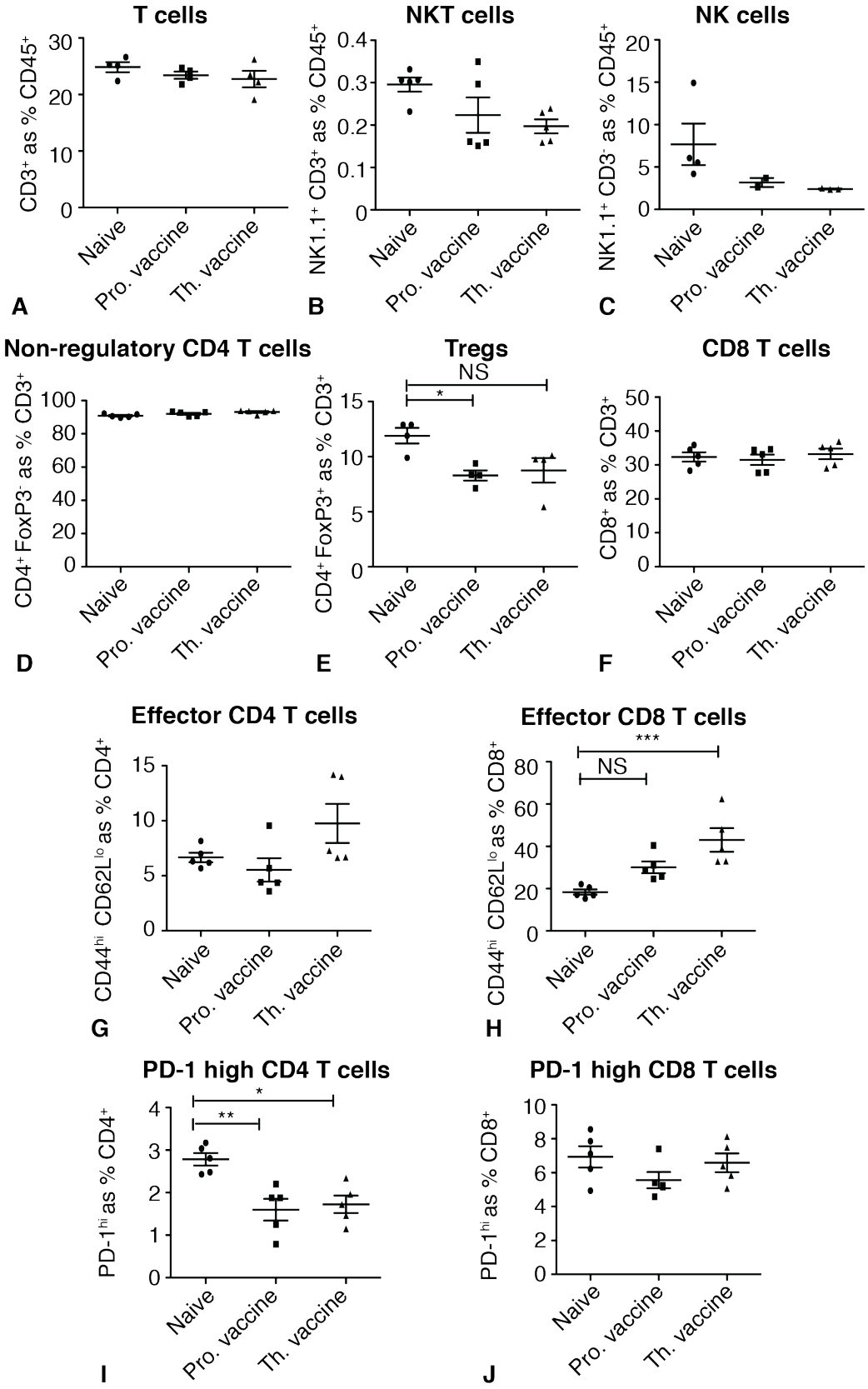
T cells
CD3+ as % CD45+
30
20
10
0
Naive
Pro. vaccine
Th. vaccine
A
NKT cells
NK1.1+ CD3+ as % CD45+
0.4
0.3
0.2
0.1
0
Naive
Pro. vaccine
Th. vaccine
B
NK cells
NK1.1+ CD3- as % CD45+
20
15
10
5
0
Naive
Pro. vaccine
Th. vaccine
C
Non-regulatory CD4 T cells
CD4+ FoxP3- as % CD3+
100
80
60
40
20
0
Naive
Pro. vaccine
Th. vaccine
D
Tregs
NS
*
CD4+ FoxP3+ as % CD3+
15
10
5
0
Naive
Pro. vaccine
Th. vaccine
E
CD8 T cells
CD8+ as % CD3+
50
40
30
20
10
0
Naive
Pro. vaccine
Th. vaccine
F
Effector CD4 T cells
CD44hi CD62Llo as % CD4+
15
10
5
0
Naive
Pro. vaccine
Th. vaccine
G
Effector CD8 T cells
***
NS
CD44hi CD62Llo as % CD8+
80
60
40
20
0
Naive
Pro. vaccine
Th. vaccine
H
PD-1 high CD4 T cells
*
**
PD-1hi as % CD4+
4
3
2
1
0
Naive
Pro. vaccine
Th. vaccine
I
PD-1 high CD8 T cells
PD-1hi as % CD8+
10
8
6
4
2
0
Naive
Pro. vaccine
Th. vaccine
J

Figure 5.13: Vaccination decreases frequencies of Tregs and of non-regulatory cells expressing PD-1 within the spleen. C57BL/6 mice were vaccinated as described in Figure 5.9A. One week following vaccination spleens were harvested and immune cell frequencies assessed by flow cytometry, lymphocyte populations were defined as shown in Figure 5.9B. **A-F.** Frequencies of T cells, NK cells and NKT cells. **G-J.** Frequencies of effector and exhausted $CD4^+$ and $CD8^+$ T cells. Values represent individual mice, with 4-5 mice used per group. Error bars are ± SEM. NS= non-significant, * $p \leq 0.05$, ** $p < 0.01$, *** $p < 0.001$ one-way ANOVA with Bonferroni post-test. Results are representative of two independent experiments.

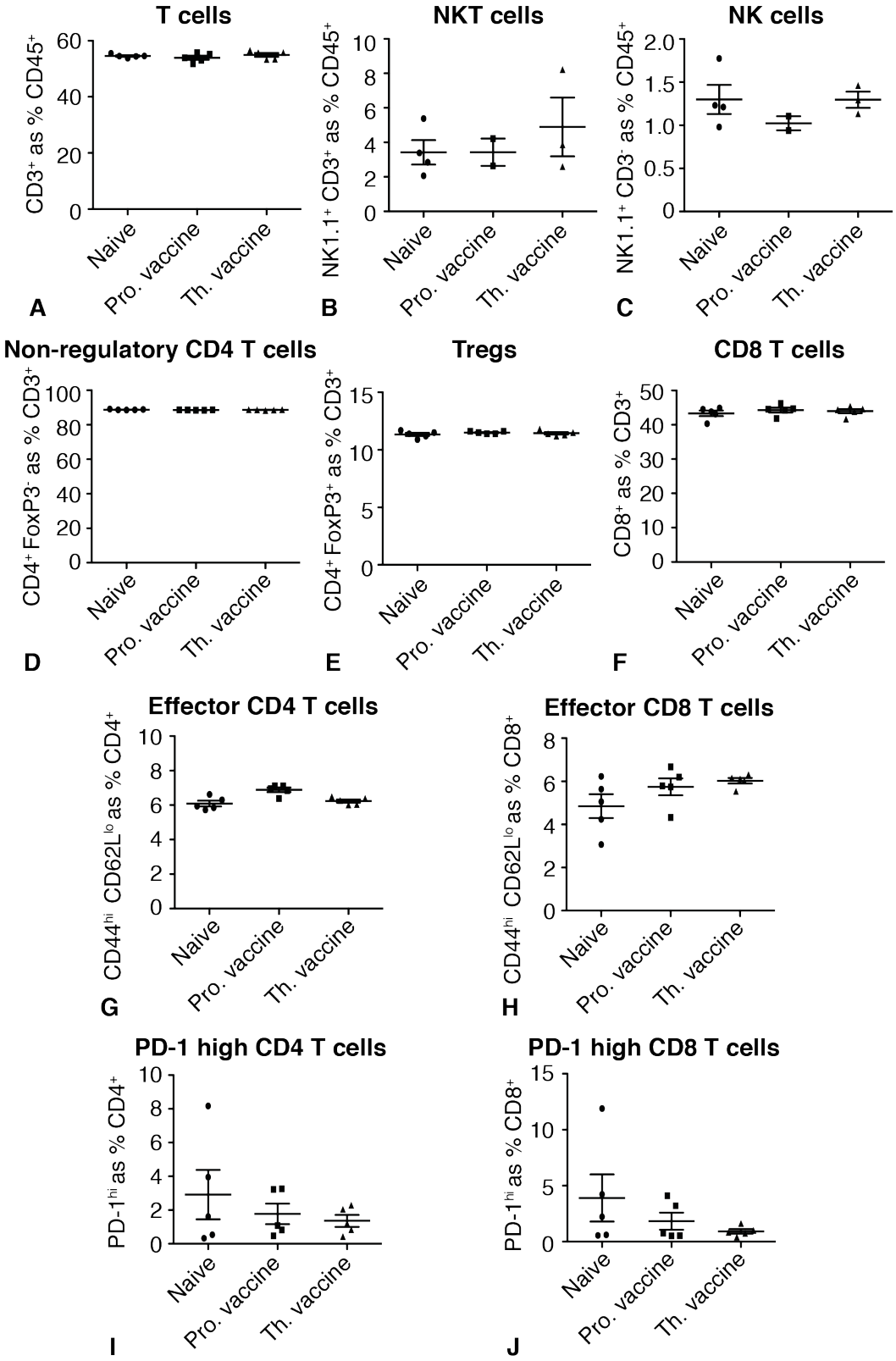
T cells
CD3+ as % CD45+
60
40
20
0
Naive
Pro. vaccine
Th. vaccine
A
NKT cells
NK1.1+ CD3+ as % CD45+
10
8
6
4
2
0
Naive
Pro. vaccine
Th. vaccine
B
NK cells
NK1.1+ CD3- as % CD45+
2.0
1.5
1.0
0.5
0
Naive
Pro. vaccine
Th. vaccine
C
Non-regulatory CD4 T cells
CD4+ FoxP3- as % CD3+
100
80
60
40
20
0
Naive
Pro. vaccine
Th. vaccine
D
Tregs
CD4+ FoxP3+ as % CD3+
15
10
5
0
Naive
Pro. vaccine
Th. vaccine
E
CD8 T cells
CD8+ as % CD3+
50
40
30
20
10
0
Naive
Pro. vaccine
Th. vaccine
F
Effector CD4 T cells
CD44hi CD62Llo as % CD4+
10
8
6
4
2
0
Naive
Pro. vaccine
Th. vaccine
G
Effector CD8 T cells
CD44hi CD62Llo as % CD8+
8
6
4
2
0
Naive
Pro. vaccine
Th. vaccine
H
PD-1 high CD4 T cells
PD-1hi as % CD4+
10
8
6
4
2
0
Naive
Pro. vaccine
Th. vaccine
I
PD-1 high CD8 T cells
PD-1hi as % CD8+
15
10
5
0
Naive
Pro. vaccine
Th. vaccine
J

Figure 5.14: Vaccination does not alter frequencies of lymphocyte populations within the draining iLN. C57BL/6 mice were vaccinated as described in Figure 5.9A. One week following vaccination mdLN were harvested and immune cell frequencies assessed by flow cytometry, lymphocyte populations were defined as shown in Figure 5.9B. **A-F.** Frequencies of T cells, NK cells and NKT cells. **G-J.** Frequencies of effector and exhausted $CD4^+$ and $CD8^+$ T cells. Values represent individual mice, with 4-5 mice used per group. One-way ANOVA with Bonferroni post-test was performed, however no differences were significant. Results are representative of two independent experiments

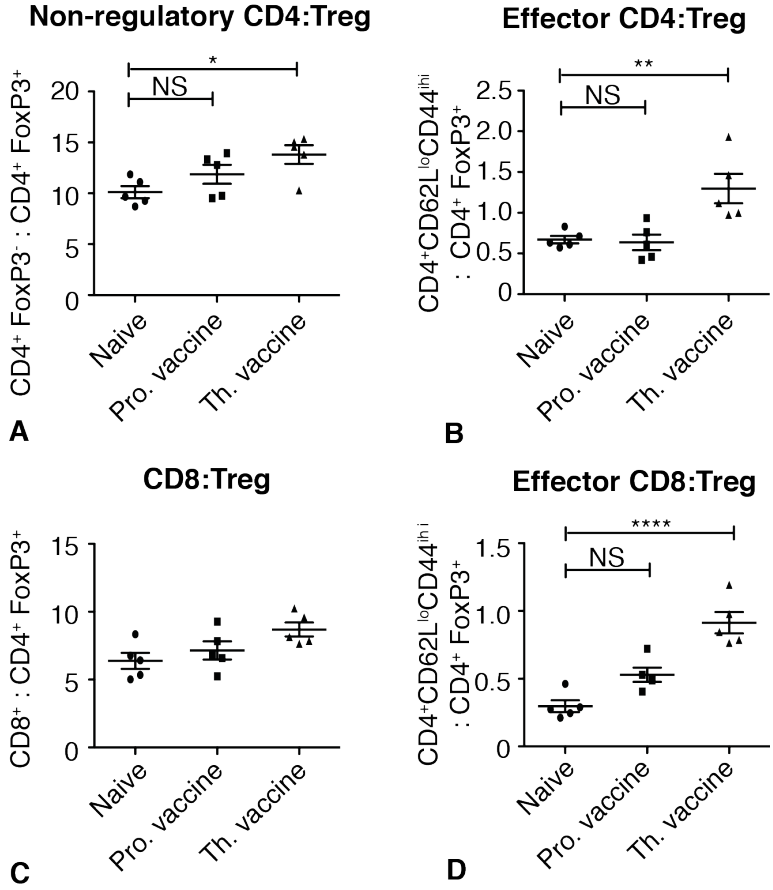

Figure 5.15: Vaccination increases splenic ratio of non-regulatory CD4 T cells and effector CD4 and CD8 T cells to Tregs. C57BL/6 mice were vaccinated as described in Figure 5.9A. One week following vaccination spleens were harvested and immune cell frequencies assessed by flow cytometry, lymphocyte populations were defined as shown in Figure 5.9B. The number of T cells was calculated by multiplying the population percentage by the total number of cells in the preceding gate. Cell numbers within the initial singlet cell gate were determined by multiplying percentages of single cells by total number of live cells as determined by trypan blue exclusion. **A**. Ratio of non-regulatory $CD4^+$ $FoxP3^-$ cells to $CD4^+$ $FoxP3^+$ Tregs. **B.** Ratio of effector $CD4^+$ $FoxP3^-$ cells to Tregs. **C.** Ratio of $CD8^+$ cells to $CD4^+$ $FoxP3^+$ Tregs. **D**. Ratio of effector $CD8^+$ cells to Tregs. Values represent individual mice, with 4-5 mice used per group. Error bars are ± SEM. * $p \leq 0.05$, ** $p < 0.01$, **** $p < 0.0001$ one-way ANOVA with Bonferroni post-test. Results are representative of two independent experiments.

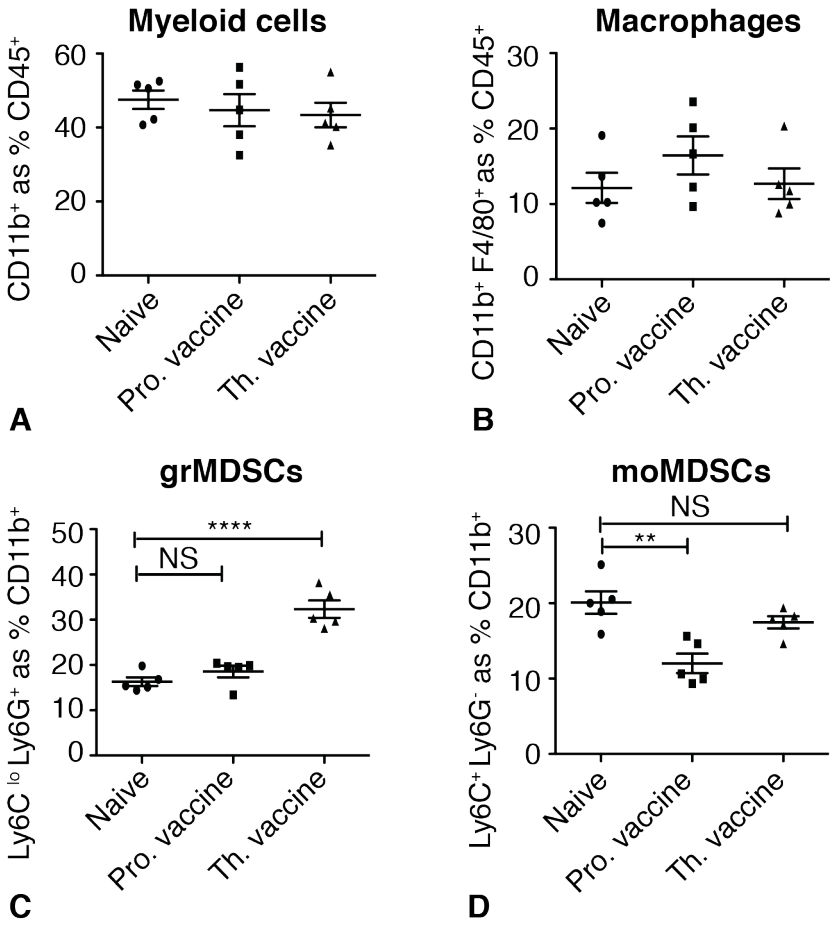

Figure 5.16: Vaccination does not alter splenic frequencies of myeloid cells or macrophages but may alter frequencies of MDSCs. C57BL/6 mice were vaccinated as described in Figure 5.9A. One week following vaccination spleens were harvested and immune cell frequencies assessed by flow cytometry, lymphocyte populations were defined as shown in Figure 5.9C. **A-D.** Frequencies of myeloid, macrophage and MDSC populations. Values represent individual mice, with 5 mice used per group. Error bars are ± SEM. ** $p < 0.01$ one-way ANOVA with Bonferroni post-test. Results are representative of two independent experiments.

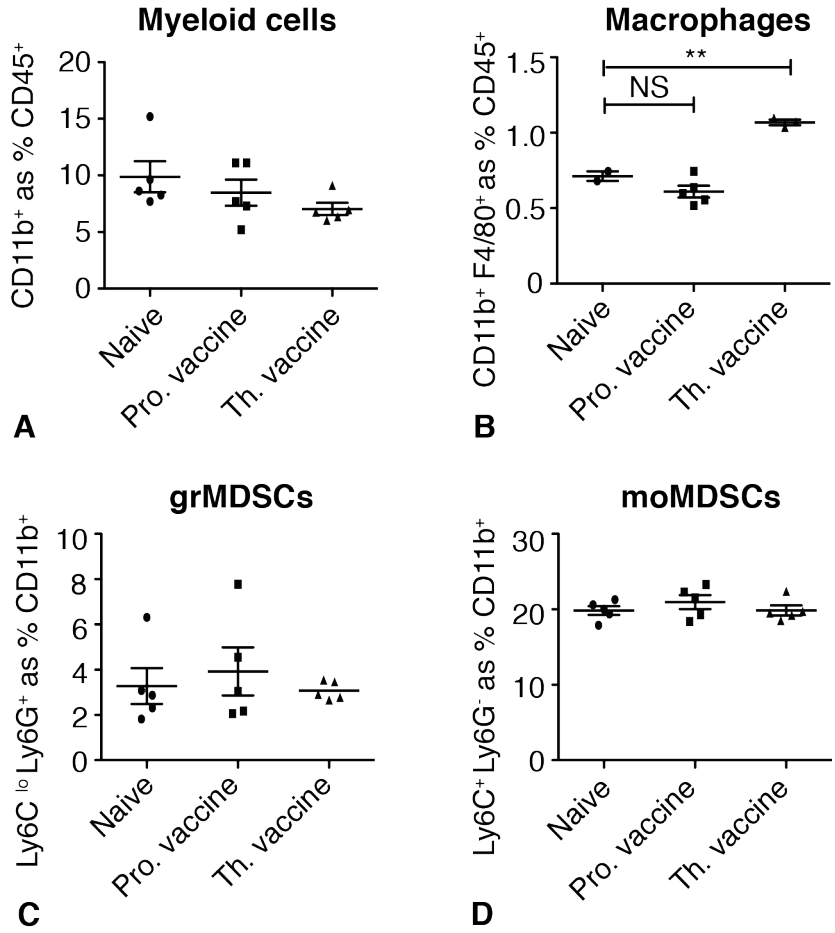

Figure 5.17: Vaccination does not alter frequencies of myeloid cells or MDSCs but can increases the frequency of macrophages within the draining iLN. C57BL/6 mice were vaccinated as described in Figure 5.9. One week following vaccination draining iLN were harvested and immune cell frequencies assessed by flow cytometry, lymphocyte populations were defined as shown in Figure 5.9C. **A-D.** Frequencies of myeloid, macrophage and MDSC populations. Values represent individual mice, with 5 mice used per group. Error bars are ± SEM. ** $p < 0.01$ one-way ANOVA with Bonferroni post-test. Results are representative of two independent experiments.

5.2.4 Vaccination does not significantly alter lymphocyte production of IFNγ and TNFα

Production of the cytokines IFNγ and TNFα by lymphocyte populations was assessed to evaluate the changes in immune cell function following vaccination. Both IFNγ and TNFα play significant roles in anti-tumour immune responses in many tumour types including melanoma. IFNγ is important for the elimination of tumour cells, and is required for the

development of Th1 responses and macrophage activation, in addition to having numerous other effects in tumour immune responses. The role of TNFα in tumours is more contentious. Similar to IFNγ, TNFα can also activate macrophages, and additionally acts on endothelial cells to increase migration of phagocytes into tissue, as well as being able to directly induce apoptosis of target cells such as tumour cells. However, continuous low exposure to TNFα has been demonstrated to promote tumour growth, invasion and metastasis (Szlosarek et al., 2006). The principal producers of IFNγ are $CD4^+$ and $CD8^+$ T cells, NK cells and NKT cells, while TNFα is primarily produced by $CD4^+$ and $CD8^+$ T cells, and macrophages. Therefore, effects of therapeutic vaccination on the production of IFNγ and TNFα by T cells, NK cells and NKT cells in the tumour, tumour draining iLN and spleen were assessed. C57BL/6 mice were challenged with 2 x $10^{\%}$ YUMM1.1 cells and vaccinated five days later as previously described. Mice were culled nine days after vaccination and tissues were harvested and assessed by flow cytometry. Cell populations and cytokine production were defined as shown in Figure 5.18.

5.2.4.1 IFNγ and TNFα production by TILs

Small proportions of tumour infiltrating lymphocytes (TILs) produced only IFNγ, (less than 10% of $CD4^+$ and $CD8^+$ T cells). In comparison, a greater frequency of T cells produced only TNFα; approximately 30% of $CD4^+$ and 40% of $CD8^+$ T cells. There was little change in the frequency of $CD4^+$ and $CD8^+$ T cells producing TNFα following vaccination. However, the percentage of $CD4^+$ and $CD8^+$ T cells producing both IFNγ and TNFα increased following vaccination, with the proportion of $CD4^+$ T cells producing both cytokines increasing from around 18% to 30% (Figure 5.19A-F). Intratumoural frequency of NK cells producing IFNγ was also low (~3%), while approximately 50% of NK cells produced TNFα and a small population (~5%) produced both cytokines. NK cell cytokine production was unchanged following therapeutic vaccination (Figure 5.19G-I). Only 1-2% of NKT cells produced IFNγ but this increased after vaccination, and high proportions (40-80%) of NKTs produced TNFα, which decreased non-significantly following vaccination (Figures 5.19J and K). The proportion of NKT cells producing

both cytokines increased from 10% to 20-40% following vaccination (Figure 5.19L). Together these results indicate that vaccination may alter production of cytokines by NKT cells, although the time point used may not be optimal for assessing vaccine effect on NKT cell cytokine production.

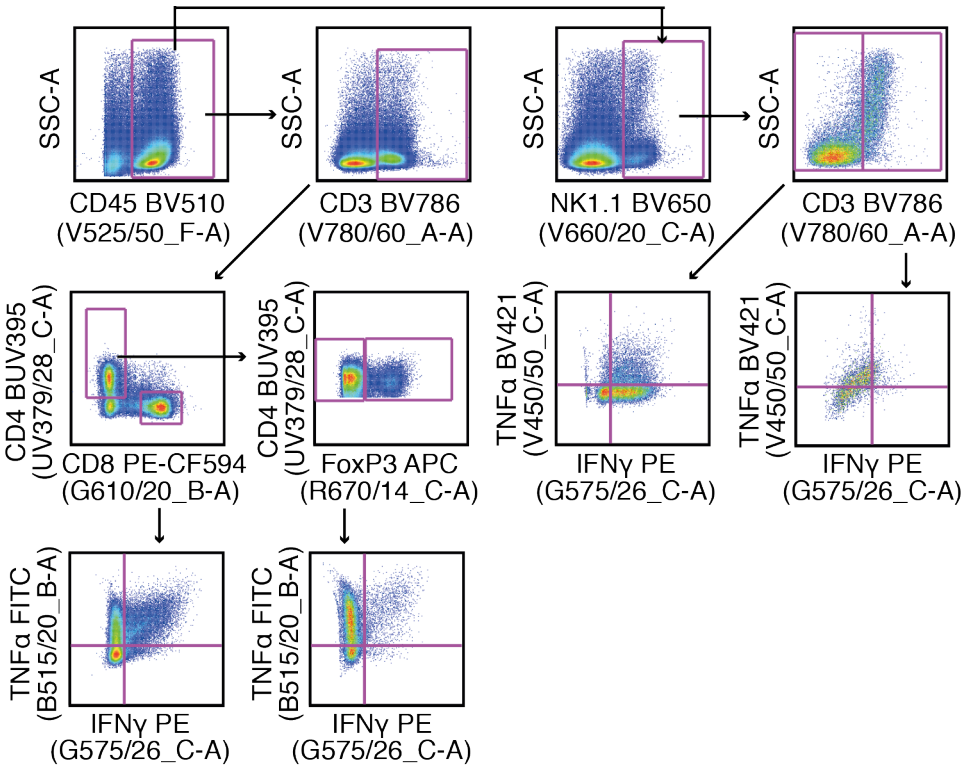

Figure 5.18: Flow cytometric gating strategy used to define IFNγ and TNFα producing lymphocytes within the tumour, spleen and draining iLN. Mice were tumour challenged and therapeutically vaccinated as described in Figure 5.8A. 14 days post-tumour challenge mice were culled and tumours, spleens and draining iLN harvested and processed for flow cytometric analysis. **A.** Gating strategy used to define T cell, NK and NKT cell production of IFNγ and TNFα. Samples were pre-gated on single, live cells. Subsets were defined as follows: T cells = $CD3^+$; NKT cells = $NK1.1^+$, $CD3^+$; NK cells = $NK1.1^+$, $CD3^-$; Non-regulatory T cells = $CD3^+$, $CD4^+$, $FoxP3^-$; Tregs = $CD3^+$, $CD4^+$, $FoxP3^+$; CD8 T cells = $CD3^+$, $CD8^+$; following which IFNγ and TNFα.

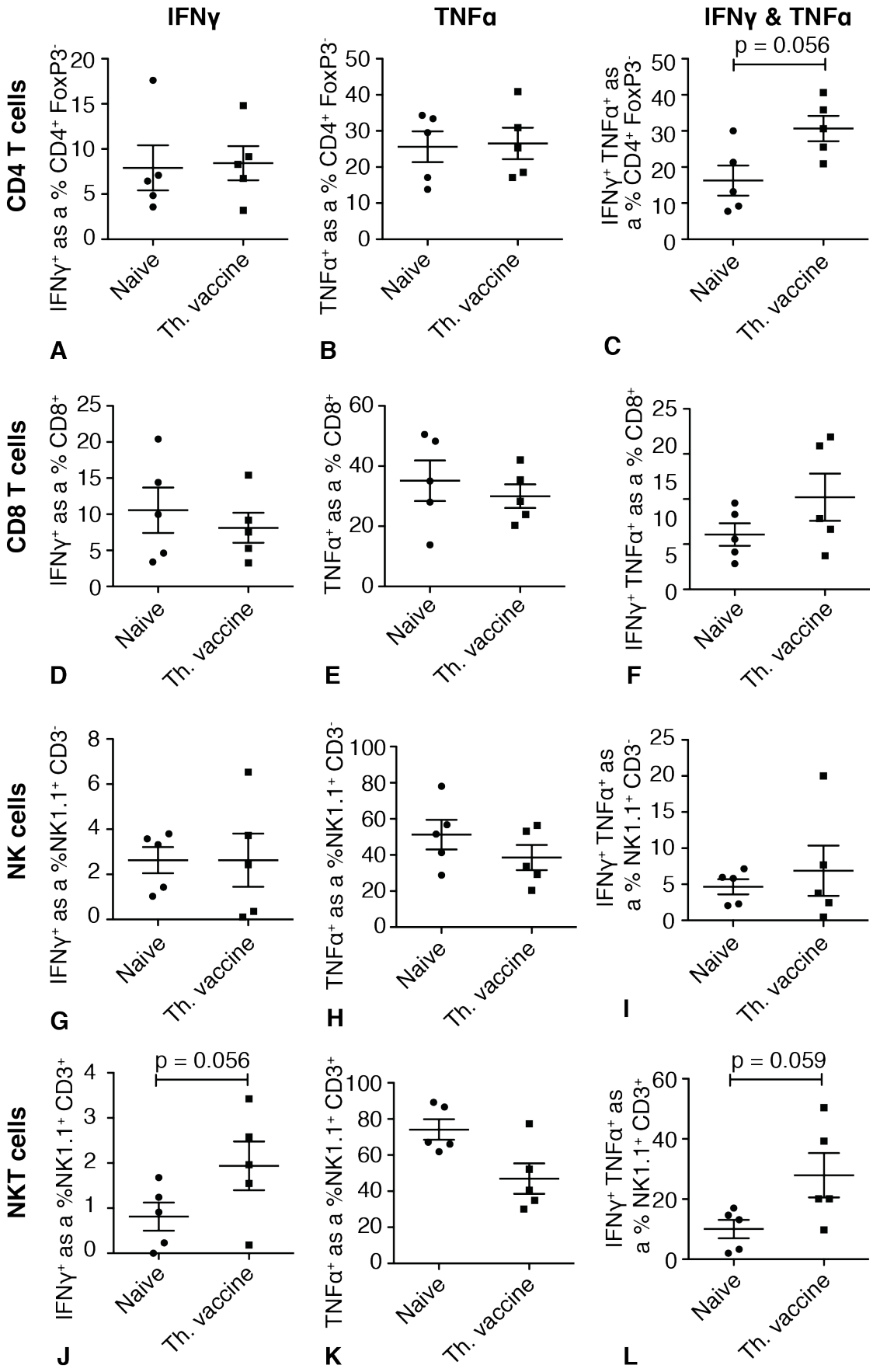
IFNγ
TNFα
IFNγ & TNFα
CD4 T cells
CD8 T cells
NK cells
NKT cells
p = 0.056
p = 0.056
p = 0.059
IFNγ+ as a % CD4+ FoxP3-
TNFα+ as a % CD4+ FoxP3-
IFNγ+ TNFα+ as a % CD4+ FoxP3-
IFNγ+ as a % CD8+
TNFα+ as a % CD8+
IFNγ+ TNFα+ as a % CD8+
IFNγ+ as a %NK1.1+ CD3-
TNFα+ as a %NK1.1+ CD3-
IFNγ+ TNFα+ as a % NK1.1+ CD3-
IFNγ+ as a %NK1.1+ CD3+
TNFα+ as a %NK1.1+ CD3+
IFNγ+ TNFα+ as a % NK1.1+ CD3+
Naive
Th. vaccine
A
B
C
D
E
F
G
H
I
J
K
L

Figure 5.19: Vaccination does not significantly alter tumour frequencies of T cells, NK cells or NKT cells producing IFNγ and/or TNFα. C57BL/6 mice were vaccinated as described in Figure 5.9A. One week following vaccination tumours were harvested and frequencies of IFNγ and TNFα producing lymphocytes were assessed by flow cytometry. Populations were defined as shown in Figure 5.12A. **A-C.** Frequencies of non-regulatory $CD4^+$ T cells producing IFNγ and TNFα. **D-F.** Frequencies of $CD8^+$ T cells producing IFNγ and TNFα. **G-I.** Frequencies of NK cells producing IFNγ and TNFα. **J-L.** Frequencies of NKT cells producing IFNγ and TNFα. Values represent individual mice, with 5 mice used per group. Error bars are ± SEM. Unpaired t-test was performed. Where no significance is stated differences are non-significant. For comparisons approaching significance p-values are stated. Results are representative of two independent experiments.

5.2.4.2 IFNγ and TNFα production by immune cells within the spleen and tumour draining iLN

IFNγ and TNFα production by lymphocytes within the spleen and draining iLN was also assessed, and showed trends similar to those observed in the tumour. Overall there was no major impact of vaccination on the production of the cytokines analysed within these lymphoid tissues. Less than 20% of all populations, $CD4^+$ and $CD8^+$ T cells, NK and NKT cells, were found to produce IFNγ within the spleen and draining iLN (Figures 5.20 and 5.21). Generally vaccination did not appear to alter the production of IFNγ by these populations, with the exception of splenic NKT cells, which significantly increased from approximately 2% to 6% of cells producing IFNγ with therapeutic vaccine (Figure 5.20J). As with intratumoural lymphocytes, spleen and iLN populations had a greater frequency of cells producing TNFα than IFNγ. In both the spleen and iLN 20-50% of CD4+ and CD8+ T cells produced TNFα alone, and similarly high proportions of NKT cells produced TNFα (20-40%), which was unaltered with vaccination except for a reduction in the frequency of CD8+ T cell producing TNFα. Again, relatively low proportions of T cells and NK cells produced both IFNγ and TNFα in naïve and vaccinated mice. Approximately 30% of NKT cells within the draining iLN produced both IFNγ and TNFα, which was slightly increased after vaccination, and the frequency of splenic NKTs producing both cytokines increased significantly from 5 to around 20% with vaccine delivery (Figure 5.20L and 5.21L).

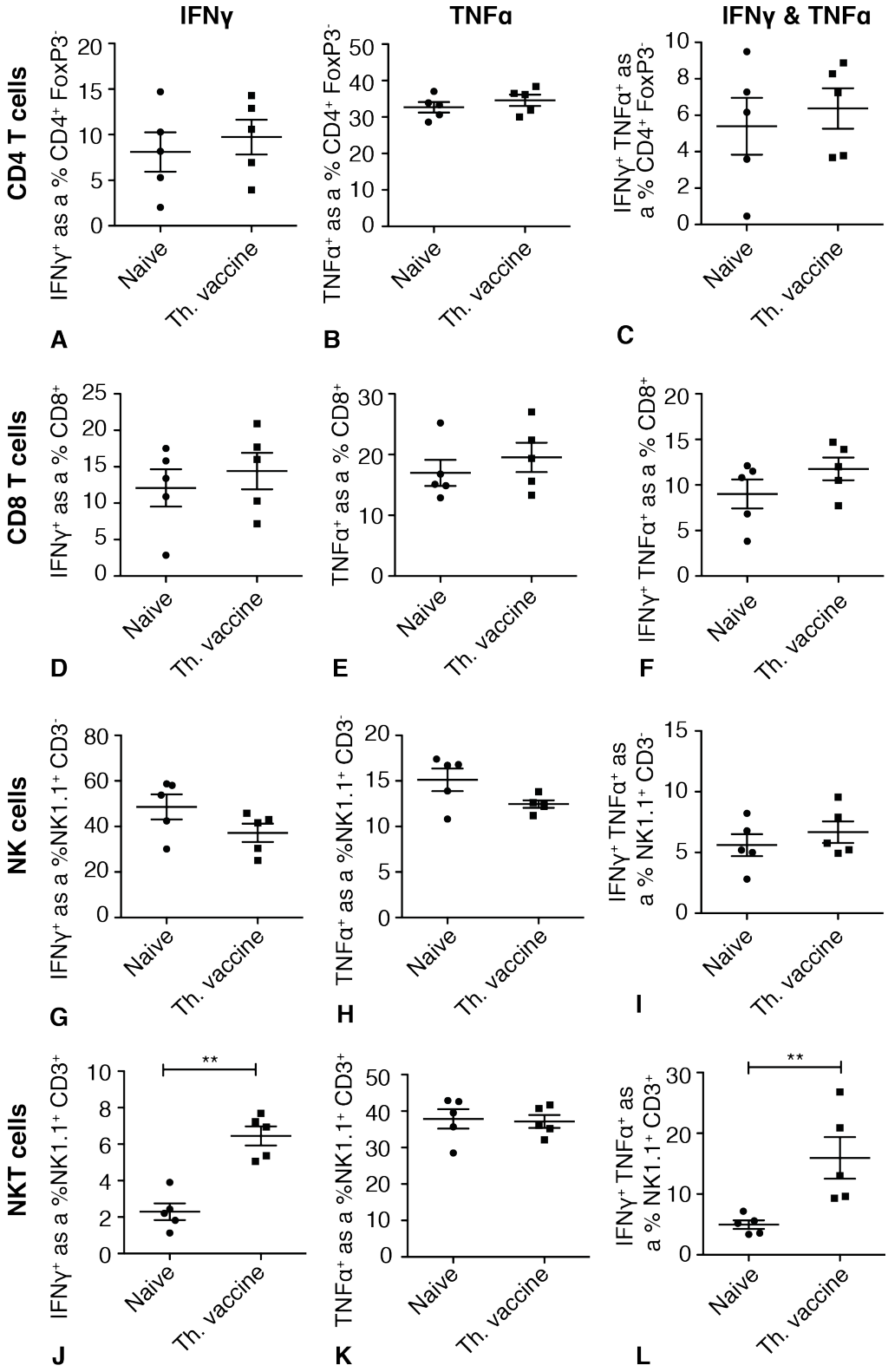
IFNγ
TNFα
IFNγ & TNFα
CD4 T cells
CD8 T cells
NK cells
NKT cells
IFNγ+ as a % CD4+ FoxP3-
TNFα+ as a % CD4+ FoxP3-
IFNγ+ TNFα+ as a % CD4+ FoxP3-
IFNγ+ as a % CD8+
TNFα+ as a % CD8+
IFNγ+ TNFα+ as a % CD8+
IFNγ+ as a %NK1.1+ CD3-
TNFα+ as a %NK1.1+ CD3-
IFNγ+ TNFα+ as a % NK1.1+ CD3-
IFNγ+ as a %NK1.1+ CD3+
TNFα+ as a %NK1.1+ CD3+
IFNγ+ TNFα+ as a % NK1.1+ CD3+
Naive
Th. vaccine
**
A
B
C
D
E
F
G
H
I
J
K
L

Figure 5.20: Vaccination does not significantly alter splenic frequencies of T or NK cells producing IFNγ and/or TNFα, but increases the percentage of NKT cells producing both IFNγ and TNFα. C57BL/6 mice were vaccinated as described in Figure 5.9A. One week following vaccination spleens were harvested and frequencies of IFNγ and TNFα producing lymphocytes were assessed by flow cytometry. Populations were defined as shown in Figure 5.12A. **A-C**. Frequencies of non-regulatory $CD4^+$ T cells producing IFNγ and TNFα. **D-F.** Frequencies of $CD8^+$ T cells producing IFNγ and TNFα. **G-I.** Frequencies of NK cells producing IFNγ and TNFα. **J-L.** Frequencies of NKT cells producing IFNγ and TNFα. Values represent individual mice, with 4-5 mice used per group. Error bars are ± SEM. ** $p < 0.01$, unpaired t-test was performed. Results are representative of two independent experiments.

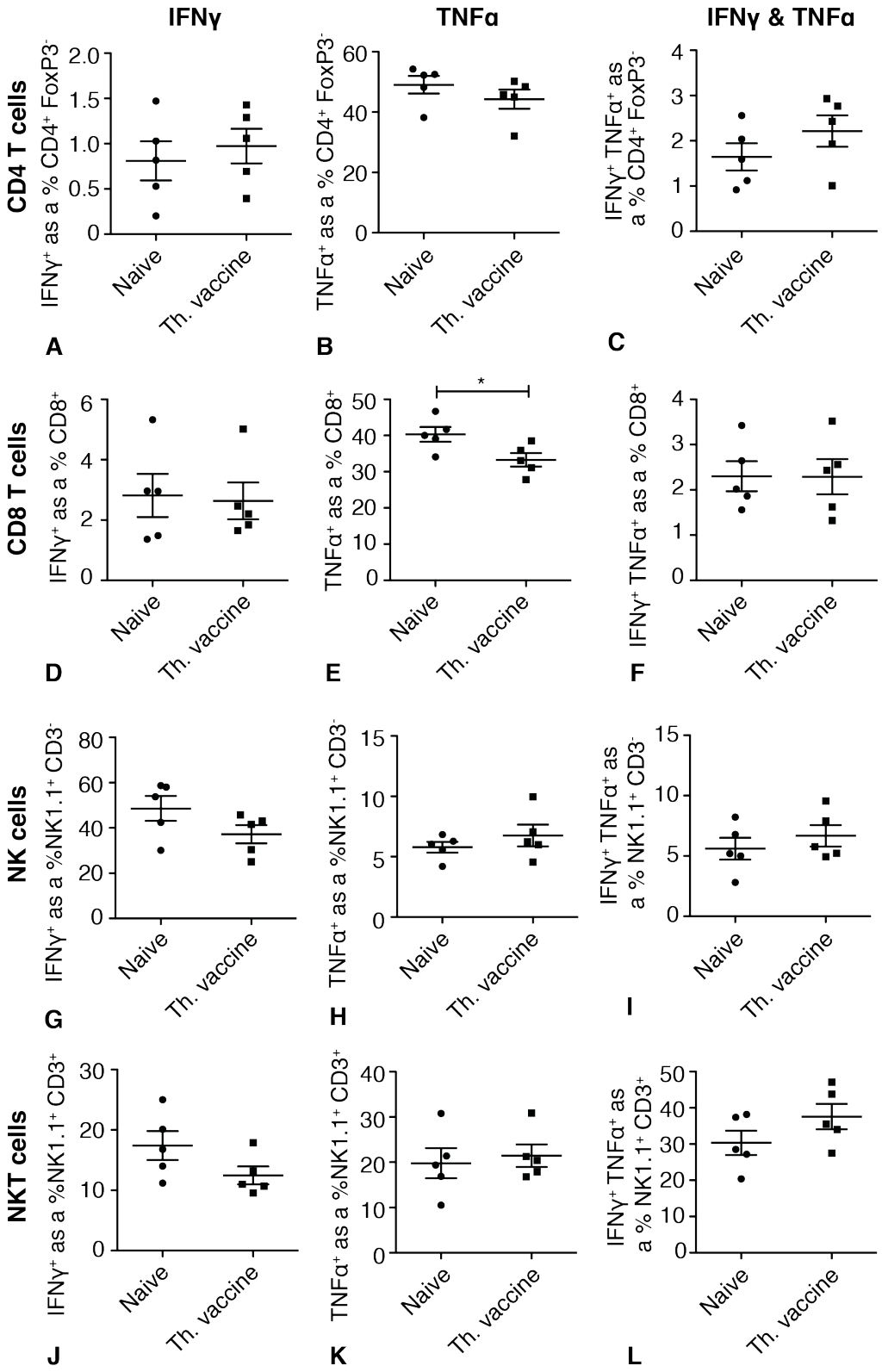
IFNγ
TNFα
IFNγ & TNFα
CD4 T cells
CD8 T cells
NK cells
NKT cells
IFNγ+ as a % CD4+ FoxP3-
TNFα+ as a % CD4+ FoxP3-
IFNγ+ TNFα+ as a % CD4+ FoxP3-
IFNγ+ as a % CD8+
TNFα+ as a % CD8+
IFNγ+ TNFα+ as a % CD8+
IFNγ+ as a %NK1.1+ CD3-
TNFα+ as a %NK1.1+ CD3-
IFNγ+ TNFα+ as a % NK1.1+ CD3-
IFNγ+ as a %NK1.1+ CD3+
TNFα+ as a %NK1.1+ CD3+
IFNγ+ TNFα+ as a % NK1.1+ CD3+
Naive
Th. vaccine
*
A
B
C
D
E
F
G
H
I
J
K
L

Figure 5.21: Vaccination does not significantly alter draining iLN frequencies of T cells or NK cells producing IFNγ and/or TNFα, but increases frequencies of NKT cells producing IFNγ alone or with TNFα. C57BL/6 mice were vaccinated as described in Figure 5.9A. One week following vaccination draining iLN were harvested and frequencies of IFNγ and TNFα producing lymphocytes were assessed by flow cytometry. Populations were defined as shown in Figure 5.12A. **A-C.** Frequencies of non-regulatory $CD4^+$ T cells producing IFNγ and TNFα. **D-F.** Frequencies of $CD8^+$ T cells producing IFNγ and TNFα. **G-I.** Frequencies of NK cells producing IFNγ and TNFα. **J-L.** Frequencies of NKT cells producing IFNγ and TNFα. Values represent individual mice, with 5 mice used per group. Error bars are ± SEM. Unpaired t-test was performed. Results are representative of two independent experiments.

5.2.4.3 IFNγ exposure causes YUMM1.1 and YUMM1.7 upregulation of PD-L1 expression, but not of MHC Class II expression.

The effect of IFNγ and TNFα exposure on YUMM1.1 surface marker expression was assessed *in vitro*. Untreated YUMM1.1 cells expressed neither PD-L1 nor MHC Class II (Figure 5.22A and B) but expressed high levels of MHC Class I, as expected (data not shown). Treatment with IFNγ resulted in massive upregulation of PD-L1, but no upregulation of MHC Class II. These effects were uniformly evident at all concentrations tested, from 31 U/mL to 500U/mL (highest concentration shown; Figure 5.22). In contrast, TNFα exposure had no effect on YUMM1.1 expression of PD-L1 or MHC Class II at with treatment of 6.25 ng/mL to 100 ng/mL (highest concentration shown; Figure 5.22). Exposure to IFNγ and TNFα had similar effects on YUMM1.7 cells; PD-L1 expression was upgregulated following IFNγ treatment, and no MHC II expression was detected on untreated, IFNγ or TNFα treated cells (Figure 5.22C and D).

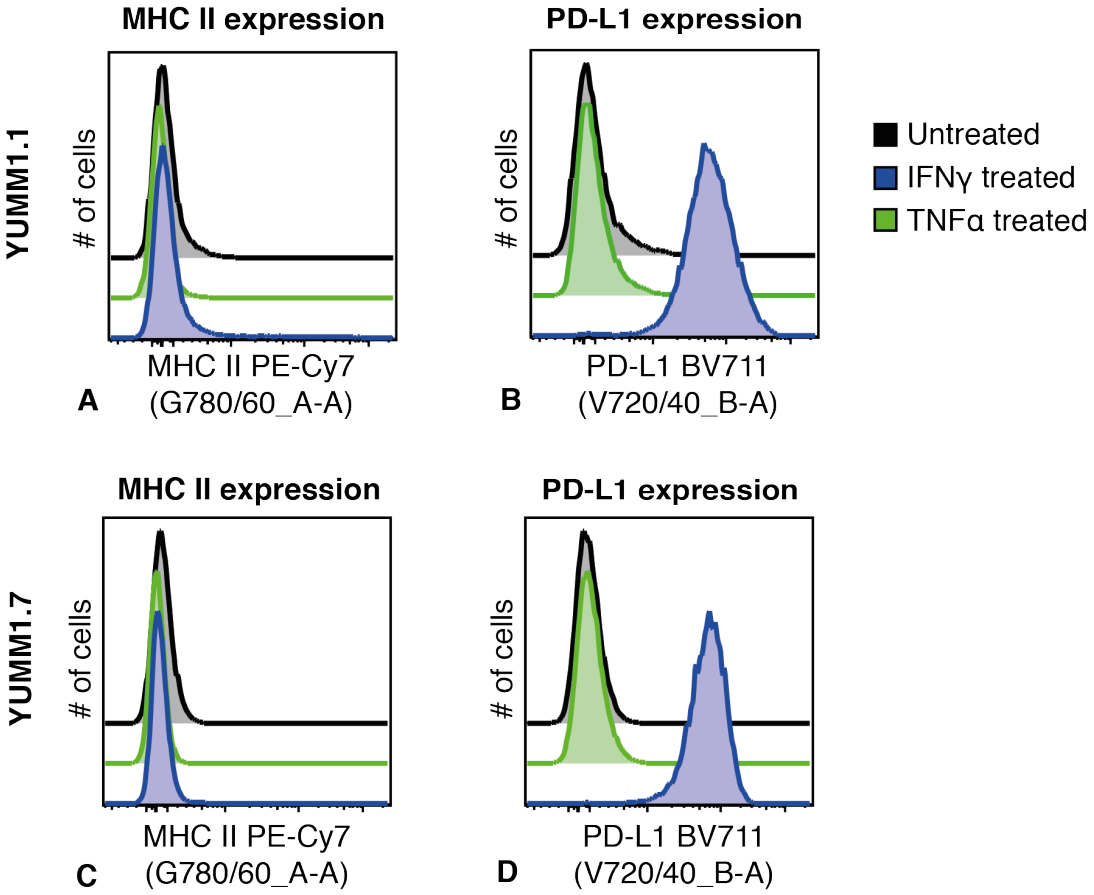

Figure 5.22: YUMM1.1 and YUMM1.7 cells upregulate expression of PD-L1, but not MHC Class II, following IFN γ exposure. Cells were cultured for 48 hours in the presence or absence of exogenous IFN γ at 500U/mL or 100ng/mL TNF α. MHC Class II and PD-L1 expression was assessed by flow cytometry. **A.** YUMM1.1 expression of MHC II and **B.** PD-L1. **C.** YUMM1.7 expression of MHCII, and **D.** of PD-L1. Plots are representative of two independent experiments, both carried out in triplicate.

5.2.5 Anti-tumour efficacy of YUMM1.1 vaccination is CD4$^+$ but not CD8$^+$ T cell dependent.

Given the increased frequency of non-regulatory CD4$^+$ and CD8$^+$ T cells following vaccination, the requirement of these cell types for vaccine efficacy was investigated using gene knockout mice. Experiments were conducted in B6AaO hosts deficient in MHC Class II, and thus in CD4$^+$ T cells, and in TAP1$^{-/-}$ mice, which lack stable MHC Class I expression and therefore lack CD8$^+$ T cells. Knockout mice were vaccinated either prophylactically or therapeutically and challenged with 2 x 10^5 YUMM1.1 cells (Figures 5.23A

and 5.24A). Tumour growth was monitored and vaccine protection against tumour growth and mouse survival assessed.

In $TAP^{-/-}$ mice vaccine significantly slowed tumour growth and increased survival (Figure 5.23B-D). Similar to the effects observed in wild-type C57BL/6 mice (Figure 5.6), vaccination had greater anti-tumour efficacy in a prophylactic model than in a therapeutic setting. These data show that vaccine protection was retained in the absence of $CD8^+$ T cells, indicating a lack of significant involvement of these cells in vaccine protection. In B6AaO mice, neither prophylactic nor therapeutic vaccination had any effect on tumour growth, and correspondingly did not improve mouse survival (Figure 5.24B and D). This complete loss of vaccine efficacy in the absence of $CD4^+$ T cells demonstrates a requirement for these cells in conferring protection. Whether $CD4^+$ T cells directly target tumour cells, as has been previously demonstrated, or activate a downstream effector cell remains to be determined.

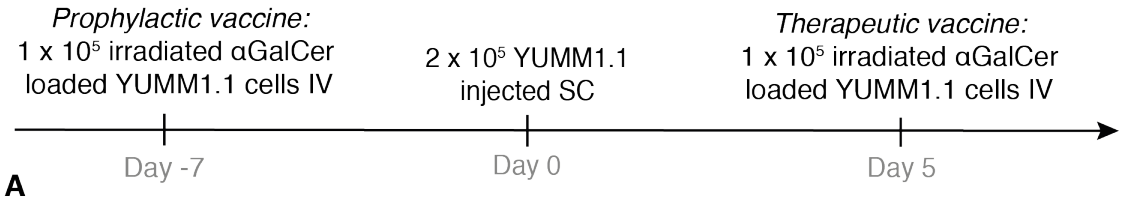
Prophylactic vaccine:
1 x 10^5 irradiated αGalCer loaded YUMM1.1 cells IV
2 x 10^5 YUMM1.1 injected SC
Therapeutic vaccine:
1 x 10^5 irradiated αGalCer loaded YUMM1.1 cells IV
Day -7
Day 0
Day 5

A

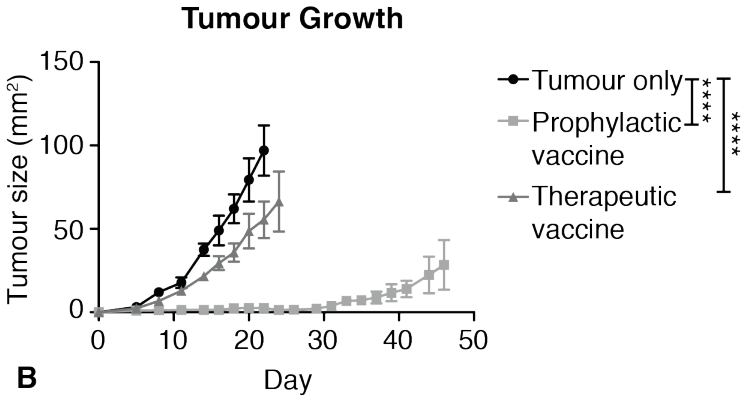
Tumour Growth
Tumour size (mm²)
Day
Tumour only
Prophylactic vaccine
Therapeutic vaccine
****
****

B

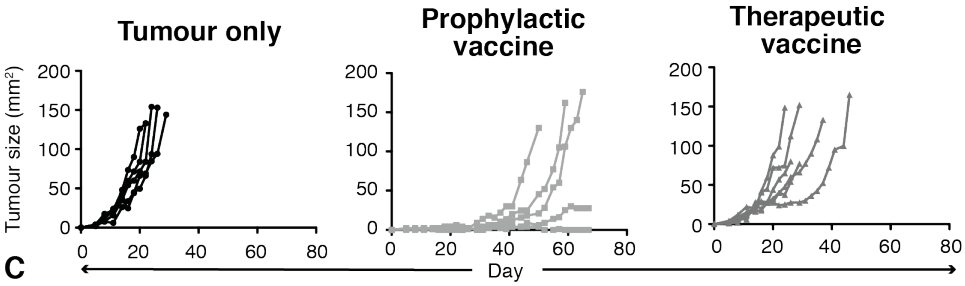
Tumour only
Prophylactic vaccine
Therapeutic vaccine
Tumour size (mm²)
Day

C

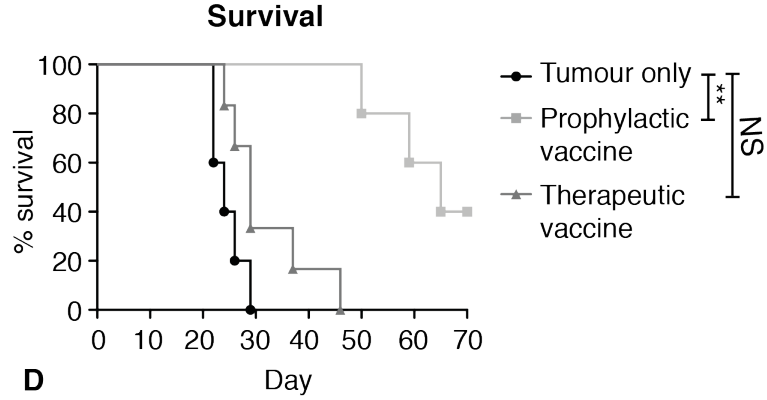
Survival
% survival
Day
Tumour only
Prophylactic vaccine
Therapeutic vaccine
**
NS

D

Figure 5.23: Autologous, whole tumour cell vaccination against YUMM1.1 tumours is not $CD8^+$ T cell-dependent. A. $TAP1^{-/-}$ mice were vaccinated intravenously with irradiated, αGalCer-loaded YUMM1.1 cells either prophylactically seven days prior to tumour challenge, or therapeutically five days post-tumour challenge. Control mice received PBS. Mice were challenged subcutaneously with 2 x 10^5 YUMM1.1 cells. Tumour growth was monitored and size recorded. Mice were culled when tumours reached 150 mm^2, or when tumours ulcerated. **B.** Average tumour growth is shown, each symbol represents the mean growth of 5-6 mice. Error bars are ± SEM. **** $P \leq 0.0001$, 2-way ANOVA with Bonferroni post-test, statistics shown for Day 23. **C.** Individual tumour growth. Each data point represents one mouse. **D.** Percent survival shown for groups of 5-6 mice. Treatment groups are compared to the control mice. NS = non-significant, ** $P < 0.01$, Mantel-Cox test. Data are representative of two concordant, independent experiments.

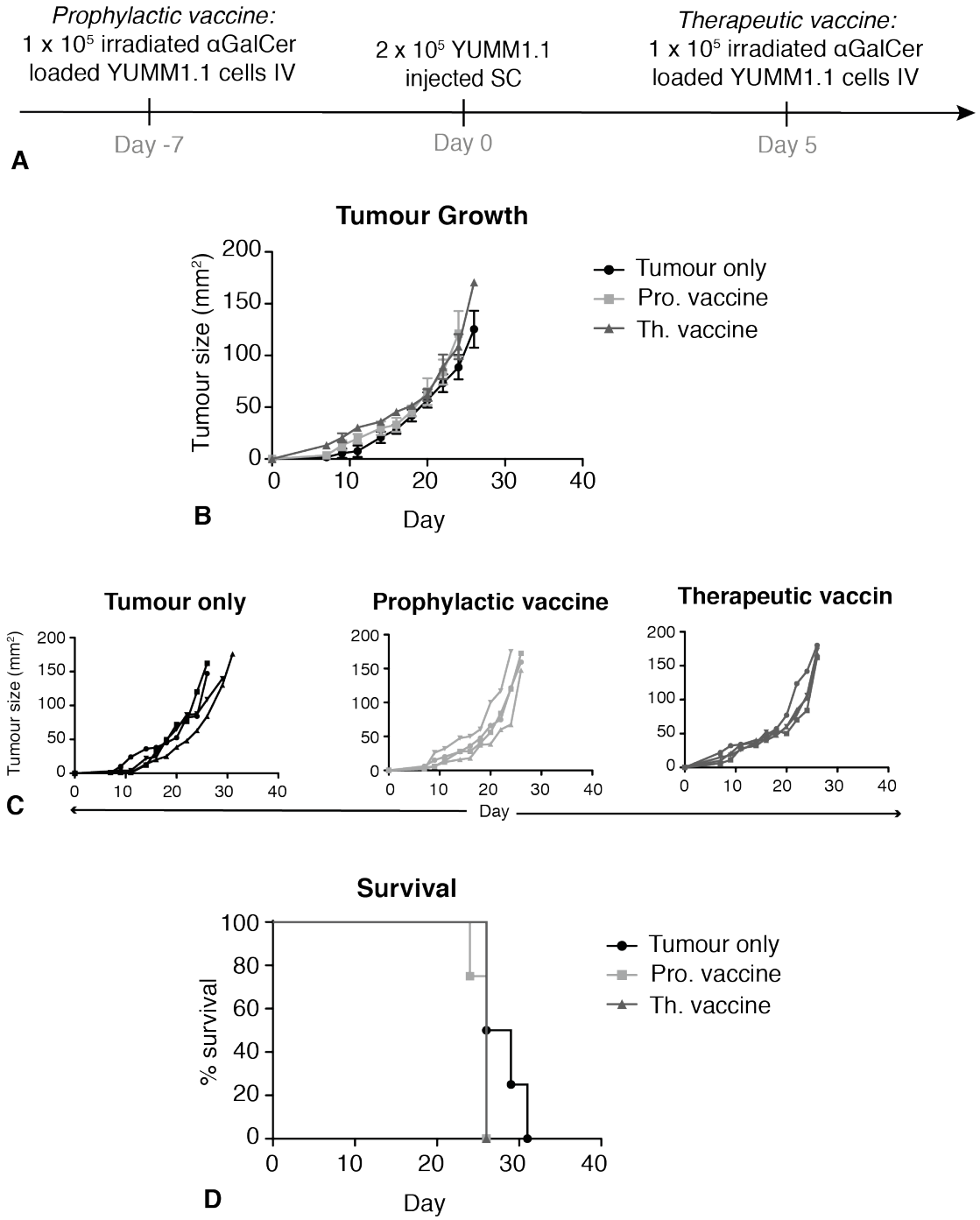

Figure 5.24: Autologous, whole tumour cell vaccination against YUMM1.1 tumours is CD4$^+$ T cell-dependent. A. B6AaO mice were prophylactically vaccinated intravenously with irradiated, αGalCer-loaded YUMM1.1 cells seven days prior to tumour challenge. Control mice received PBS. Mice were challenged sub-cutaneously with 2 x 10^5 YUMM1.1 cells. Tumour growth was monitored and size recorded. Mice were culled when tumours ≥ 150 mm^2, or when tumours ulcerated. **B.** Average tumour growth is shown. Each symbol represents the mean growth of 5 mice. Error bars are ± SEM. **C.** Individual tumour growth, each data point represents one mouse. **D.** Percent survival shown for groups of 5 mice. Treatment groups are compared to the control mice. NS = non-significant Mantel-Cox test. Data are representative of two concordant, independent experiments.

5.3 Discussion

The primary objectives of this chapter were to develop and characterize an immunotherapeutic approach with anti-tumour activity in a $BRAF^{V600E}$ melanoma model. I have generated a novel vaccine comprised of irradiated, autologous tumour cells loaded with the iNKT adjuvant αGalCer. This vaccine elicits a $CD4^+$ T cell response that has significant anti-tumour efficacy in the YUMM1.1 melanoma model.

The vaccine approach developed in this study utilised administration of whole tumour cells loaded with αGalCer, with aim of delivering both antigen and adjuvant to the same APC. This would achieve antigen presentation by optimally activated DCs, due to efficient iNKT cell licensing of DCs. The mechanism by which αGalCer becomes associated with the tumour cells in this vaccine is uncertain. As YUMM1.1 and YUMM1.7 cells do not express CD1d, the tumour cells do not directly present αGalCer. In the absence of CD1d expression it is likely that the lipophilic sphingosine tail of the αGalCer molecule becomes embedded in, or adheres to the plasma membrane of the tumour cell in an undefined way (Moody et al., 2002). A second possibility is that tumour cells sequester αGalCer in intracellular vesicles or phagosomes after endocytosis, which is then released upon tumour cell degradation *in vivo*. In both of these scenarioes only modest amounts of αGalCer are expected to be associated with tumour cells. It has been previously demonstrated that CD1d expression by the cellular component of an αGalCer-loaded vaccine is not required for vaccine efficacy (Petersen et al., 2011). However, CD1d expression may enhance vaccine efficacy. Direct comparison of αGalCer-loaded tumour cell vaccines showed increased anti-tumour effects when tumour cells were transfected to express CD1d (Shimizu et al., 2007a; Shimizu et al., 2007b). This would enable direct presentation of αGalCer by tumour cells to iNKT cells and may increase the amount of αGalCer incorporated by tumour cell.

The use of whole tumour cells as the cellular component of the vaccine has several advantages over DC or peptide-based vaccines. The delivery of a

range of tumour antigens including both known and undefined antigens, and MHC class I and II epitopes, will elicit polyclonal responses and reduce the risk of tumour immune escape. Additionally, a significant clinical benefit of this approach is that it is not HLA-type restricted. There are some safety issues surrounding the use of whole tumour cells but irradiation of tumour cells prior to their delivery nullifies concerns of tumour cell outgrowth from the vaccine. Although acute toxicity is a risk with intravenous infusion of irradiated, apoptotic tumour cells this has been well-tolerated in clinical trials using several tumour types (de Gruijl et al., 2008). Stimulating immune responses to a wide-range of uncharacterized antigens does raise concerns about generating autoimmunity. However, no evidence of this was seen in mice in this study. Autoimmune responses may represent a greater issue if immune regulation is further compromised with additional treatments, such as checkpoint blockade.

The delivery of irradiated, αGalCer-loaded YUMM1.1 and YUMM1.7 cells elicited vaccine-induced immune responses in both the spleen and mdLN. Splenic priming was anticipated with intravenous delivery of irradiated tumour cells, due to the well-known capacity of splenic APCs, in particular $CD8\alpha^+$ DCs, to take up antigen from circulating dying cells (Iyoda et al., 2002; Shimizu et al., 2007b). Although the mdLN is an unconventional site of vaccine priming, its involvement was investigated because it had previously been demonstrated as a site of priming with an αGalCer-loaded whole tumour cell vaccine in a glioma model (Hunn et al., 2012). It is postulated that following intravenous vaccination injected tumour cells may be trapped in the lung capillary bed and captured by lung-resident or circulating immune cells. Subsequent trafficking of tumour peptides and αGalCer to the lung-draining mdLN would result in mdLN priming.

Although both YUMM1.1 and YUMM1.7 cell-based vaccines induced effector T cell responses in naïve mice, autologous vaccination only gave significant protection against YUMM1.1 tumours. Both in the prophylactic and therapeutic setting minimal protection was conferred with autologous vaccination against YUMM1.7 tumours. There are several possible explanations for this difference. The higher growth rate of YUMM1.7 cells

may generate more aggressive tumours, or may facilitate YUMM1.7 escape from immune control. Additionally, it is likely the two tumour cell lines express different antigenic profiles; YUMM1.1 may express antigens that elicit stronger or more durable immune responses. The lack of vaccine efficacy against YUMM1.7 tumours does raise some concerns about the broad applicability of this vaccine approach. However, efficacy of irradiated αGalCer-loaded tumour cell vaccines has been demonstrated in several tumour types, in addition to YUMM1.1 tumours (Chung et al., 2007; Gibbins et al., 2014; Hunn et al., 2012; Mattarollo et al., 2012; Shimizu et al., 2007b). Therefore it is possible that YUMM1.7 represents an unusually immunosuppressive model.

Earlier results demonstrated that neither YUMM1.1 nor YUMM1.7 produced soluble T cell-suppressive factors (Chapter 3; Figure 3.13), however there is evidence of several other tumour-mediated immunosuppressive mechanisms present in these models. Exposure to IFNγ *in vitro* resulted in both YUMM1.1 and YUMM1.7 cells significantly upregulating PD-L1 expression. Similar tumour cell expression of PD-L1 likely occurs *in vivo*, as analysis of TILs in YUMM1.1 tumours showed subsets of cells producing IFNγ. PD-L1 is one of the two ligands for PD-1, which is expressed by activated T cells. PD-1/PD-L1 interactions negatively regulate T cell effector responses through suppression of proliferation, inhibition of cytokine production and even induction of apoptosis. In addition to YUMM cells expressing PD-L1, 60-80% of intratumoural T cells were shown to highly express PD-1 in the YUMM1.1 model. Vaccination reduced the frequency of T cells expressing high levels of PD-1, indicating that there is some amelioration of T cell exhaustion. However the majority of T cells still expressed high PD-1. Co-expression of the ligand and receptor, as occurs with YUMM1.1 tumours, has been widely implicated as a major mechanism of tumour immune resistance and immune evasion (Merelli et al., 2014; Topalian et al., 2012). PD-1/PD-L1 interactions can also promote the differentiation of $CD4^+$ $FoxP3^-$ T cells into $FoxP3^+$ Tregs (Amarnath et al., 2011; Francisco et al., 2009). This may account for the relatively large proportion of Tregs present within YUMM1.1 tumours, which appeared to increase with tumour progression (data not shown). Again vaccination had some impact on this mechanism of suppression, decreasing

the frequency of Tregs, but a large population of Tregs remained. Collectively, these data demonstrate a highly immunosuppressive microenvironment within YUMM1.1 tumours, which was partially reduced with vaccination. It is possible that the degree of immunosuppression present within the YUMM1.1 and YUMM1.7 tumours could differ. A more suppressive microenvironment in YUMM1.7 tumours could be a contributing factor towards the differential anti-tumour efficacy of vaccination in the two tumour models.

Interestingly, only $CD4^+$ T cells were required for vaccine efficacy, as indicated by the loss of vaccine protection in MHC Class II-deficient mice. While the retention of anti-tumour effects following vaccination in $TAP^{-/-}$ hosts indicates that $CD8^+$ T cells do not play a critical role in mediating vaccine efficacy. Nonetheless, there are limitations to these experiments that must be considered. MHC II-deficient mice lack cell surface expression of class II molecules. Thus $CD4^+$ T cell maturation in the thymus is compromised and these mice lack mature $CD4^+$ T cells and $CD4^+$ T cell-mediated responses (Grusby et al., 1991). However, a population of peripheral $CD4^+$ T cells have been detected. These cells do not express NK1.1 but have unusual reactivity, recognizing the CD1 molecule (Cardell et al., 1995). Nonetheless, the complete abrogation of vaccine efficacy in the absence of MHC II does demonstrate a requirement for $CD4^+$ T cells, which is not satisfied by this residual $CD4^+$ population. TAP-1 deficient mice lack peptide transport to MHC Class I molecules and therefore are deficient in MHC I-restricted antigen presentation. As a result, $TAP^{-/-}$ mice have a very low number of $CD8^+$ T cells in the periphery due to impaired positive selection (Van Kaer et al., 1992). Additionally there is some evidence that whilst these mice have normal numbers of NK cells, NK cell-mediated lysis is impaired (Ljunggren et al., 1994). Therefore, TAP deficient mice are not only defective in $CD8^+$ T cell responses, but also in other factors. However, as the vaccine is still effective in this model this does not change the conclusion that $CD8^+$ T cells are not required for efficacy.

Traditionally, $CD8^+$ T cells have been considered the primary effectors of T cell mediated tumour elimination, while the contribution of $CD4^+$ T cells has

been assumed to be in supporting and enhancing $CD8^+$ responses (Bevan, 2004). However, there is now substantial evidence that $CD4^+$ T cells exert more direct anti-tumour responses independently of $CD8^+$ T cells. In fact, $CD4^+$ T cells have been shown to eliminate tumour cells more effectively than $CD8^+$ T cells in a side-by-side comparison utilising MHC I or II-restricted TCR transgenic mice (Perez-Diez et al., 2007). Building on this, adoptive transfer of primed $CD4^+$ T cells has been shown to confer protection against tumour challenge, which was not dependent on host CTL responses (Greenberg, 1986). Several mechanisms have been implicated in direct $CD4^+$ T cell killing of tumour cells, including Granzyme B and perforin production and $CD4^+$ T cell FasL and tumour cell Fas interactions (Lundin et al., 2004, Quezada, 2010 #667). However, MHC class II expression by tumour cells has been demonstrated to be required for $CD4^+$ T cells to elicit direct cytolytic activity *in vivo*, although not *in vitro* (Lundin et al., 2004). Many tumour cells are induced to express MHC II in response to IFNγ exposure (Haabeth et al., 2014). However, YUMM cells expressed no detectable MHC II at baseline, and did not upregulate expression following 48 hours of exposure to IFNγ or TNFα. In the complete absence of MHC II expression $CD4^+$ T cell may indirectly induce tumour cell death through IFNγ anti-angiogenic effects or activation of tumouricidal macrophages to elicit cytotoxic effects (Corthay et al., 2005; Qin and Blankenstein, 2000).

Several of the effector functions of $CD4^+$ T cells depend on the presence of IFNγ including MHC II upregulation on tumours, anti-angiogenic effects and activation of macrophages. Analysis of lymphoid subsets producing IFNγ and TNFα revealed that the frequency of NKT cells producing IFNγ alone or both IFNγ and TNFα was increased in the spleen and tumour following vaccination. Additionally, $CD4^+$ T cell production of IFNγ within the tumour was augmented with vaccination. This demonstrates that vaccination is generating a tumour microenvironment supportive to $CD4^+$ T cell-mediated anti-tumour responses. Interestingly, in both untreated and vaccinated mice a larger proportion of T, NKT and NK cells produced TNFα than was expected. In the inducible $Braf^{V600E}$ $Pten^{-/-}$*CDKN2a* tumours, following similar harvest and restimulation, 5-30% of CD4+ T cells and less than 5% of CD8+ T cells

were shown to produce TNFα (Ho et al., 2014). Comparatively, the frequency of cells, and particularly $CD8^+$ T cells, producing TNFα in the YUMM1.1 model was much higher. This is noteworthy because TNFα has been previously implicated in mediating BRAF inhibitor resistance to apoptosis (Gray-Schopfer et al., 2007; Menon et al., 2013; Shao et al., 2015). However, the frequency of lymphocytes producing TNFα alone was not significantly increased following vaccination. Therefore vaccine is not impacting this possible mechanism of tumour microenvironment-mediated BRAF inhibitor resistance.

5.3.1 Conclusions

In this chapter I have generated a simple vaccine, which elicits effector $CD4^+$ T cell responses to decrease tumour growth and increase survival in a murine model of $BRAF^{V600E}$ melanoma. This vaccine possesses clinical relevance with the benefit of generating anti-tumour immunity to undefined neoantigens, and provides a strong foundation to investigate BRAF inhibitor combination with active immunotherapy in the next chapter.

CHAPTER 6: Combining autologous whole tumour cell vaccination and BRAF inhibitor therapy

6.1 Introduction

The rationale for combining BRAF inhibitors with immunotherapy is based on the potential for the mechanisms of action of these two approaches to work synergistically. In particular, targeted chemotherapy is expected to render the tumour microenvironment more favourable to anti-tumour immune responses. The induction of tumour cell death, which results in increased antigen availability, and reduced tumour mediated immune suppression are just some of the justifications that provide a strong basis for the combination of BRAF inhibition and immunotherapy. However, the results in Chapter 3 of this thesis demonstrate that whilst PLX4720 induces apoptosis of $BRAF^{V600E}$ melanoma cells *in vitro*, no tumour regression is seen with PLX4720 *in vivo*. This observation raises questions about whether significant tumour cell death is occurring *in vivo*. Despite this, non-cytotoxic effects of PLX4720 on $BRAF^{V600E}$ tumours *in vivo* may still be immunostimulatory. Previous studies have demonstrated that broad-spectrum chemotherapies do not necessarily need to induce cell death to render tumour cells more immunogenic (Fisk and Ioannides, 1998; Gameiro et al., 2011; Kaneno et al., 2011). Targeted BRAF inhibitors are likely to have similar effects, with non-cytotoxic concentrations of Vemurafenib and PLX4720 shown to enhance MHC expression, tumour antigenicity and decrease melanoma-mediated immunosuppression (Donia et al., 2012a; Frederick et al., 2013; Sapkota et al., 2013; Sumimoto et al., 2006).

Although it may not have major bearing on immunogenicity, the mechanism by which $BRAF^{V600E}$ melanoma cells are evading PLX4720-induced apoptosis *in vivo* remains of interest. Loss of PTEN, which is a characteristic of the YUMM1.1 and YUMM1.7 models, has been previously reported to decrease PLX4720 induced apoptosis (Hooijkaas et al., 2012b; Paraiso et al., 2011). However, as previously mentioned, this does not account for the inconsistency between the ability of BRAF inhibitors to induce apoptosis of YUMM1.1 and YUMM1.7 cells *in vitro* but not *in vivo*. It is likely that factors produced within the tumour microenvironment *in vivo* are playing a protective role. Interestingly, in Chapter 5 a high frequency of NK, NKT and T cells were shown to produce TNFα, which has previously been

demonstrated to confer resistance to apoptosis induced by BRAF inhibition (Gray-Schopfer et al., 2007; Menon et al., 2013; Shao et al., 2015). Exposure of $BRAF^{V600E}$ melanoma cell lines to TNFα reduced apoptosis induced by PLX4720, Vemurafenib and siRNA inhibition of mutant BRAF. In the studies by Gray-Schopfer and collegues, and Shao and colleagues the protective effect of TNFα was shown to be specific to mutant BRAF inhibition, and was associated with activation of NFκB, which is involved in a number of essential cellular functions, including cell survival. Similarly, Menon *et al.* attributed the protective effect of TNFα to increased levels of the anti-apoptotic protein Twist1. These findings are complementary as Twist1 is a downstream target of NFκB. Furthermore, the protective effect of TNFα is not dependent on PTEN mutation status. The models used in these studies were all $BRAF^{V600E}$ melanoma cell lines with varied PTEN mutation status (wild-type, heterozygous and homozygous loss of function), indicating TNFα mediated resistance can have diverse implications. Therefore, TNFα represents an interesting therapeutic target to consider in combination with BRAF inhibition.

Preclinical and clinical studies have revealed the importance of timing on the efficacy of combination therapy (Ascierto et al., 2012; Zitvogel et al., 2008). It is generally accepted that immunotherapy is more successful in a setting of minimal tumour burden, perhaps due to tumour-associated immunosuppression (Bilusic and Gulley, 2012). Therefore, a role for chemotherapy in combination therapy can be to reduce surgically inaccessible, or metastatic, tumour burden prior to immunotherapy. This induction of tumour cell death will also serve to augment anti-tumour immunity through previously described mechanisms including the release of tumour antigen. However, even in the absence of induced tumour cell death, chemotherapy prior to immunotherapy can increase the immunogenicity and decrease tumour-mediated immunosuppression. In addition to the direct tumour effects, pre-treatment with chemotherapy allows potentiation of the immune system to occur through immunomodulatory effects. Consistent with this, in most instances immunotherapy administered post-chemotherapy has been shown to be the most effective combination therapy strategy (Lake and Robinson, 2005). Despite this, there is evidence for the potentiation of

chemotherapy by prior immunotherapy. Retrospective analysis of the sequential use of Vemurafenib and Ipilimumab revealed that BRAF-mutant melanoma patients appeared to benefit from the administration of Ipilimumab prior to BRAF inhibitors rather than the delivery of therapies in the reverse order (Ascierto et al., 2012). Furthermore, delivery of vaccine-based immunotherapy followed by chemotherapy with cyclophosphamide has been shown to be more effective than either single agent in a B16 model of melanoma (Hermans et al., 2003a). Whilst algorithms have been devised to guide the sequencing of BRAF inhibitor and immunotherapy administration, the optimal timing of delivery requires further pre-clinical and clinical studies (Ascierto et al., 2012; Srivastava and McDermott, 2014).

6.1.1 Aims

There is a strong theoretical framework supporting the combination of immunotherapy and BRAF inhibitors. To date the majority of research into combination therapy has been pre-clinical, and the immunotherapeutic approaches utilised have focussed on checkpoint blockade or adoptive cell transfer. The experiments described in this chapter explore the combination of BRAF inhibition with active immunotherapy, using the whole tumour cell vaccine developed in Chapter 5.

In particular these experiments aimed to:

- Assess whether there is basal immune cell involvement in the anti-tumour effects of PLX4720 in a $BRAF^{V600E}$ tumour model

- Characterise the intratumoural, tumour draining lymph node and splenic immune milieu before and after PLX4720 treatment, to identify changes in immune cell populations associated with PLX4720 treatment

- Determine if TNFα inhibition improves PLX4720 induction of $BRAF^{V600E}$ melanoma cell death

- Investigate PLX4720 and vaccine combination therapy strategies, and the impact of Treg depletion on vaccine and combination therapy efficacy.

6.2 Results

6.2.1 The anti-tumour effects of PLX4720 in a $BRAF^{V600E}$ tumour model are partially dependent on host-mediated immunity

Prior to undertaking combination therapy experiments, the involvement of the immune system in PLX4720 anti-tumour efficacy was investigated with the aim of better informing combination strategies. To determine the involvement of the adaptive immune system in PLX4720 treatment, anti-tumour efficacy was compared between immunocompetent C57BL/6 and immunocompromised NOD/Scid mice. NOD/Scid mice are highly immunodeficient with impaired B and T lymphocyte development, and additional immunological dysfunction including reduced macrophage and NK cell function (Ito et al., 2002; Schultz et al., 1995). Mice were tumour challenged with 2 x 10^5 YUMM1.1 cells, and daily treatment with 20 or 50 mg/kg PLX4720 or vehicle control was initiated one week later (Figure 6.1A). Tumour growth was monitored, with size recorded every two to three days, and when tumours reached 150 mm^2 or ulcerated mice were culled and survival was recorded.

As seen previously, both 20 and 50 mg/kg PLX4720 treatment slowed YUMM1.1 tumour growth in C57BL/6 mice and increased survival significantly (Figure 6.1B-D). Strikingly, in NOD/Scid mice the anti-tumour efficacy of PLX4720 was reduced. Although PLX4720 still decreased tumour growth and increased survival significantly, PLX4720 treatment provided less protection against tumour growth and less of a survival advantage in immunocompromised hosts (Figure 6.1B-D). However, tumours of vehicle-treated control mice grew at different rates in the two hosts, with control tumour growth slower in NOD/Scid mice than in C57BL/6 mice (Figure

6.1B). In fact, when directly compared, the growth of control tumours in each strain differed significantly ($P > 0.0001$), as did survival ($P = 0.015$). As a result, direct comparisons of the effect of PLX4720 on growth and survival in the two different hosts were unable to be made. To allow comparison of the survival benefit whilst accounting for the difference in controls, the survival of treated mice relative to the vehicle control mice was determined. This data demonstrated that both 20 and 50 mg/kg PLX4720 were significantly more effective at prolonging survival in immunocompetent hosts than in immunocompromised hosts (Figure 6.1E). These results indicate that PLX4720, in the absence of any immunotherapy, involves host immune responses. PLX4720 anti-tumour effects may be T cell, B cell, NK cell or macrophage mediated, as functions of these cell populations are absent or compromised in NOD/Scid mice.

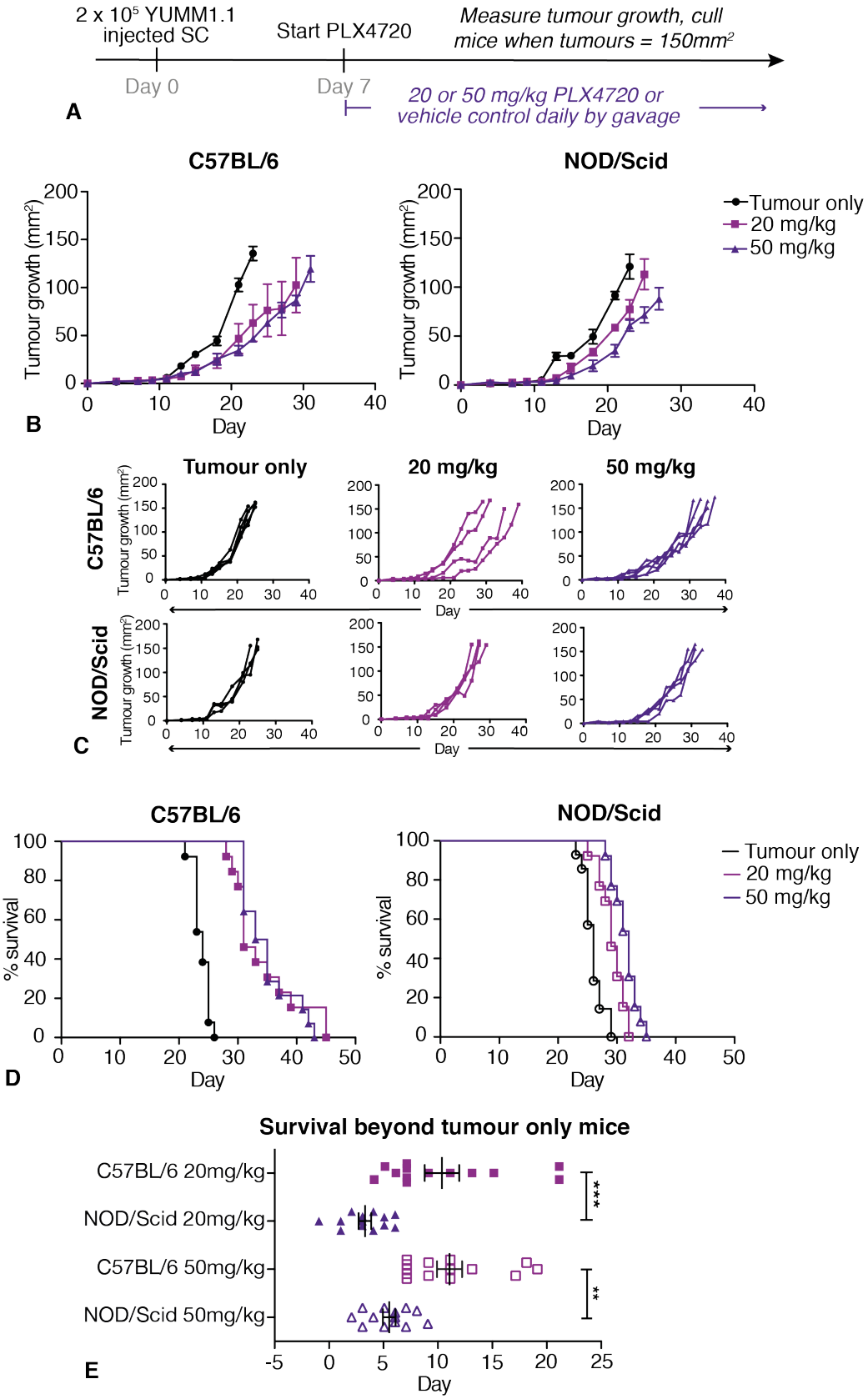
2 x 10⁵ YUMM1.1 injected SC
Start PLX4720
Measure tumour growth, cull mice when tumours = 150mm²
Day 0
Day 7
20 or 50 mg/kg PLX4720 or vehicle control daily by gavage
A
C57BL/6
NOD/Scid
Tumour only
20 mg/kg
50 mg/kg
Tumour growth (mm²)
Day
B
Tumour only
20 mg/kg
50 mg/kg
C57BL/6
NOD/Scid
C
C57BL/6
NOD/Scid
% survival
Day
D
Survival beyond tumour only mice
C57BL/6 20mg/kg
NOD/Scid 20mg/kg
C57BL/6 50mg/kg
NOD/Scid 50mg/kg
***
**
Day
E

Figure 6.1: PLX4720 treatment of YUMM1.1 tumours is partially dependent on host-mediated immunity. A. C57BL/6 or NOD/SCID mice were injected subcutaneously in the left flank with 2 x 10^5 YUMM1.1 cells. Daily drug treatment was begun 7 days post-tumour challenge with 20 or 50 mg/kg PLX4720 given by oral gavage, with control mice receiving a vehicle solution. Tumour growth was monitored and size recorded. Mice were culled when tumours reached 150 mm^2, or when tumours ulcerated. **B.** Average tumour growth is shown, each symbol represents the mean growth of 13-14 mice. Error bars are ± SEM. **C.** Individual tumour growth for each treatment group is shown, each data point represents an individual mouse. **D.** Kaplan-Meier plot showing survival. **E.** Effect of PLX4720 on survival relative to the particular mouse strain is shown. Relative survival was calculated by averaging the survival of control mice and subtracting this from the number of days survived following PLX4720 treatment. Data shown is combined from 3 independent experiments with concordant results. Each experiment had 4-5 mice per treatment group.

6.2.2 PLX4720 does not alter the frequency of immune cell subsets present within the tumour milieu

After establishing the dependence of PLX4720 on host-mediated immunity further experiments were designed to identify the immune cell subsets involved. C57BL/6 mice were tumour challenged and treatment with 20 mg/kg, 50 mg/kg PLX4720 or vehicle began one week later. After treating with drug or control for one week by daily oral gavage mice were culled and tumours, tumour draining iLN and spleens were harvested, processed and analysed by flow cytometry. Cell populations were defined as previously described in Chapter 5 (Figures 5.8 and 5.12). The frequency of several immune cell subsets, and functional properties of T cells, NK cells and NKT cells were investigated.

Within the tumour, no change was seen in the frequency of total T cells or any subsets examined including $CD4^+FoxP3^-$, $CD4^+FoxP3^+$ and $CD8^+$ T cells (Figure 6.2A, and D-F). Of note, within the tumour, $CD4^+FoxP3^+$ Tregs comprised a large proportion of the T cell population accounting for 40-50% of $CD4^+$ T cells. The proportions of T cells expressing the effector phenotype of $CD44^{hi}$ and $CD62L^{lo}$, and expressing the exhaustion marker PD-1 were also unchanged following therapy (Figure 6.2G-J). These results were reflected in

the ratio of non-regulatory $CD4^+$ and $CD8^+$ T cells to Tregs, and effector cells to Tregs, which also remained the same with PLX4720 treatment (Figure 6.3).

Intratumoural frequencies of NK and NKT cells, total $CD11b^+$ cells, macrophages and both grMDSCs and moMDSC were also assessed, and no changes were observed in the proportions of any of these populations (Figure 6.2B and C, Figure 6.4). Furthermore, the production of IFNγ and TNFα by T cells, NK cells and NKT cells was found to be unaltered with PLX4720 treatment of tumours. Interestingly, as was observed previously (Figure 5.13), a large proportion of all cell types produced TNFα, while the frequency of cells producing IFNγ was much lower. Approximately 60% of $CD4^+$ T cells, 10% of $CD8^+$ T cells and NK cells, and 20-40% of NKT cells produced TNFα, while less than 10% of all cell subsets produced IFNγ alone.

Similar to the results obtained with analysis of intratumoural immune cell subsets no differences were detected in the frequency of T, NK, or NKT cell, macrophage or MDSC populations within the tumour draining iLN or spleen (Appendices C1, C2, C5, C6). The expression of effector and exhaustion markers on T cells remained the same in vehicle treated or PLX4720-treated mice, as did the ratio of non-regulatory or effector T cells to Tregs (Appendices C1-C4). The production of IFNγ and TNFα by T cells, NK cells and NKT cells also did not change with PLX4720 treatment. Thus, the suggested role for host immune responses in the efficacy of PLX4720 could not be explained by differences in the frequency of immune cell subsets in the tissues examined. As no changes were detected in population frequency or effector function, the requirement for specific immune cell populations for PLX4720 efficacy was not further investigated.

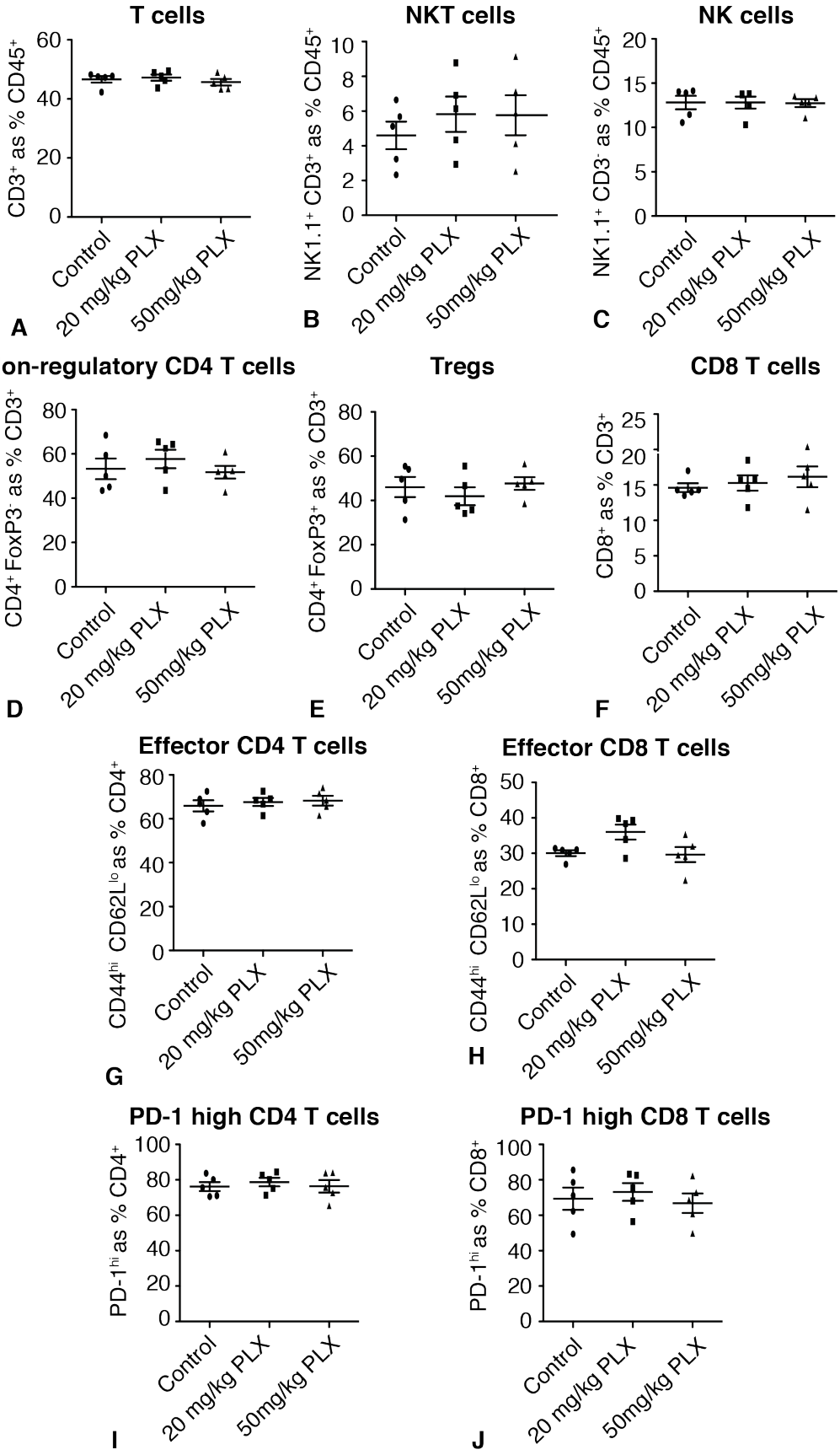
T cells
CD3+ as % CD45+
60
40
20
0
Control
20 mg/kg PLX
50mg/kg PLX
A
NKT cells
NK1.1+ CD3+ as % CD45+
10
8
6
4
2
0
Control
20 mg/kg PLX
50mg/kg PLX
B
NK cells
NK1.1+ CD3- as % CD45+
20
15
10
5
0
Control
20 mg/kg PLX
50mg/kg PLX
C
Non-regulatory CD4 T cells
CD4+ FoxP3- as % CD3+
80
60
40
20
0
Control
20 mg/kg PLX
50mg/kg PLX
D
Tregs
CD4+ FoxP3+ as % CD3+
80
60
40
20
0
Control
20 mg/kg PLX
50mg/kg PLX
E
CD8 T cells
CD8+ as % CD3+
25
20
15
10
5
0
Control
20 mg/kg PLX
50mg/kg PLX
F
Effector CD4 T cells
CD44hi CD62Llo as % CD4+
80
60
40
20
0
Control
20 mg/kg PLX
50mg/kg PLX
G
Effector CD8 T cells
CD44hi CD62Llo as % CD8+
50
40
30
20
10
0
Control
20 mg/kg PLX
50mg/kg PLX
H
PD-1 high CD4 T cells
PD-1hi as % CD4+
100
80
60
40
20
0
Control
20 mg/kg PLX
50mg/kg PLX
I
PD-1 high CD8 T cells
PD-1hi as % CD8+
100
80
60
40
20
0
Control
20 mg/kg PLX
50mg/kg PLX
J

Figure 6.2: PLX4720 treatment does not alter intratumoural frequencies of lymphocytes. C57BL/6 mice were treated with PLX4720 as described in Figure 6.1A. One week following initiation of PLX4720 treatment tumours were harvested and immune cell frequencies assessed by flow cytometry. Lymphocyte populations were defined as shown in Figure 5.8B. **A-F.** Frequencies of T cells, NK cells and NKT cells. **G-J**. Frequencies of effector and PD-1-high $CD4^+$ and $CD8^+$ T cells. Values represent individual mice, with 5 mice used per group. Error bars are ± SEM. Statistical analysis was performed using one-way ANOVA with Bonferroni post-test. No significant differences were identified. Results are representative of two independent experiments.

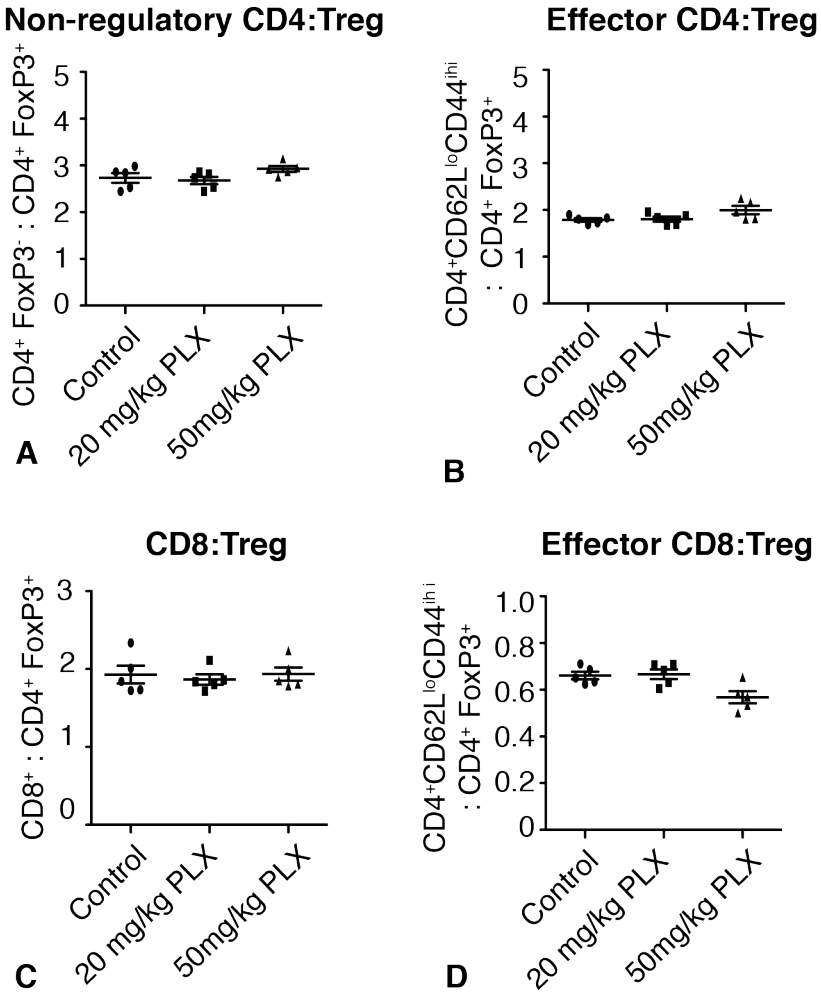

Figure 6.3: PLX4720 treatment does not alter the intratumoural ratio of Tregs to non-regulatory CD4 T cells or CD8 T cells, or effector T cells. C57BL/6 mice were treated with PLX4720 as described in Figure 6.1A. One week following initiation of PLX4720 treatment tumours were harvested and immune cell frequencies assessed by flow cytometry. Lymphocyte populations were defined as shown in Figure 5.8B. The number of T cells was calculated by multiplying the population percentage by the total number of cells in the preceding gate. Cell numbers within the initial singlet cell gate were determined by multiplying percentages of single cells by total number of live cells as determined by trypan blue exclusion. **A.** Ratio of non-regulatory $CD4^+$ $FoxP3^-$ cells to $CD4^+$ $FoxP3^+$ Tregs**. B.** Ratio of effector $CD4^+$ $FoxP3^-$ cells to Tregs. **C.** Ratio of $CD8^+$ cells to $CD4^+$ $FoxP3^+$ Tregs. **D.** Ratio of effector $CD8^+$ cells to Tregs. Values represent individual mice, with 5 mice used per group. Error bars are ± SEM. Statistical analysis was performed using one-way ANOVA with Bonferronis post-test. No significant differences were identified. Results are representative of two independent experiments.

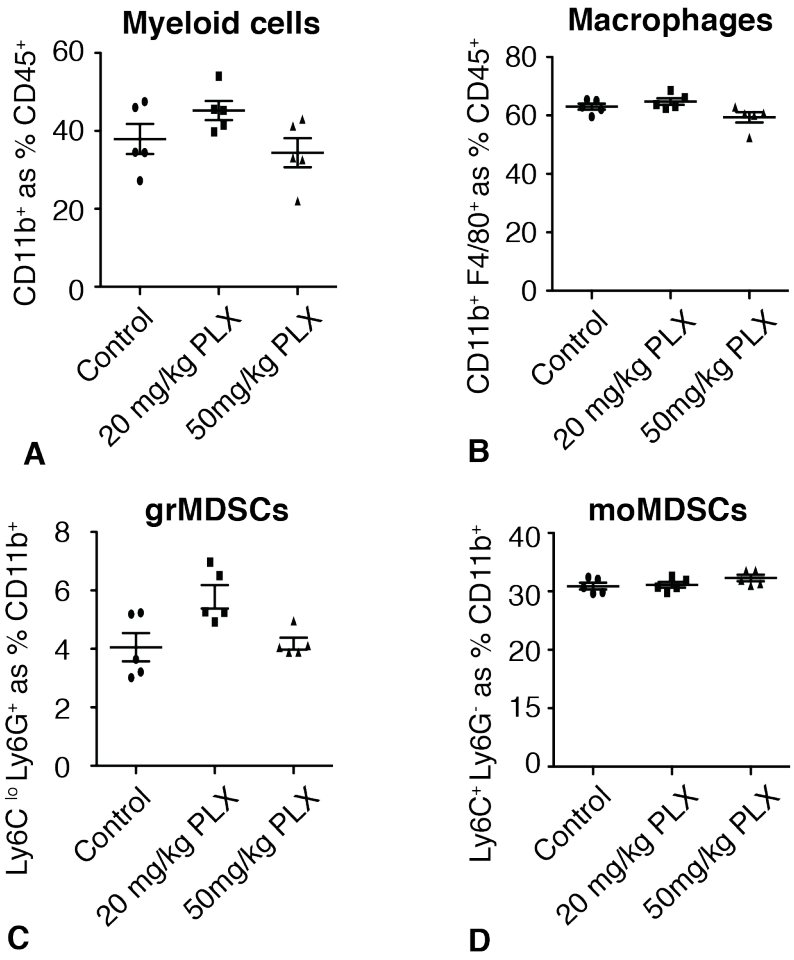

Figure 6.4: PLX4720 treatment does not significantly alter intratumoural frequencies of myeloid, macrophage or MDSCs. C57BL/6 mice were treated with PLX4720 as described in Figure 6.1A. One week following initiation of PLX4720 treatment tumours were harvested and immune cell frequencies assessed by flow cytometry. Myeloid populations were defined as shown in Figure 5.8C. **A-D.** Frequencies of CD11b+, macrophage and MDSC populations. Values represent individual mice, with 5 mice used per group. Statistical analysis was performed using one-way ANOVA with Bonferroni post-test. No significant differences were identified. Error bars are ± SEM. Results are representative of two independent experiments.

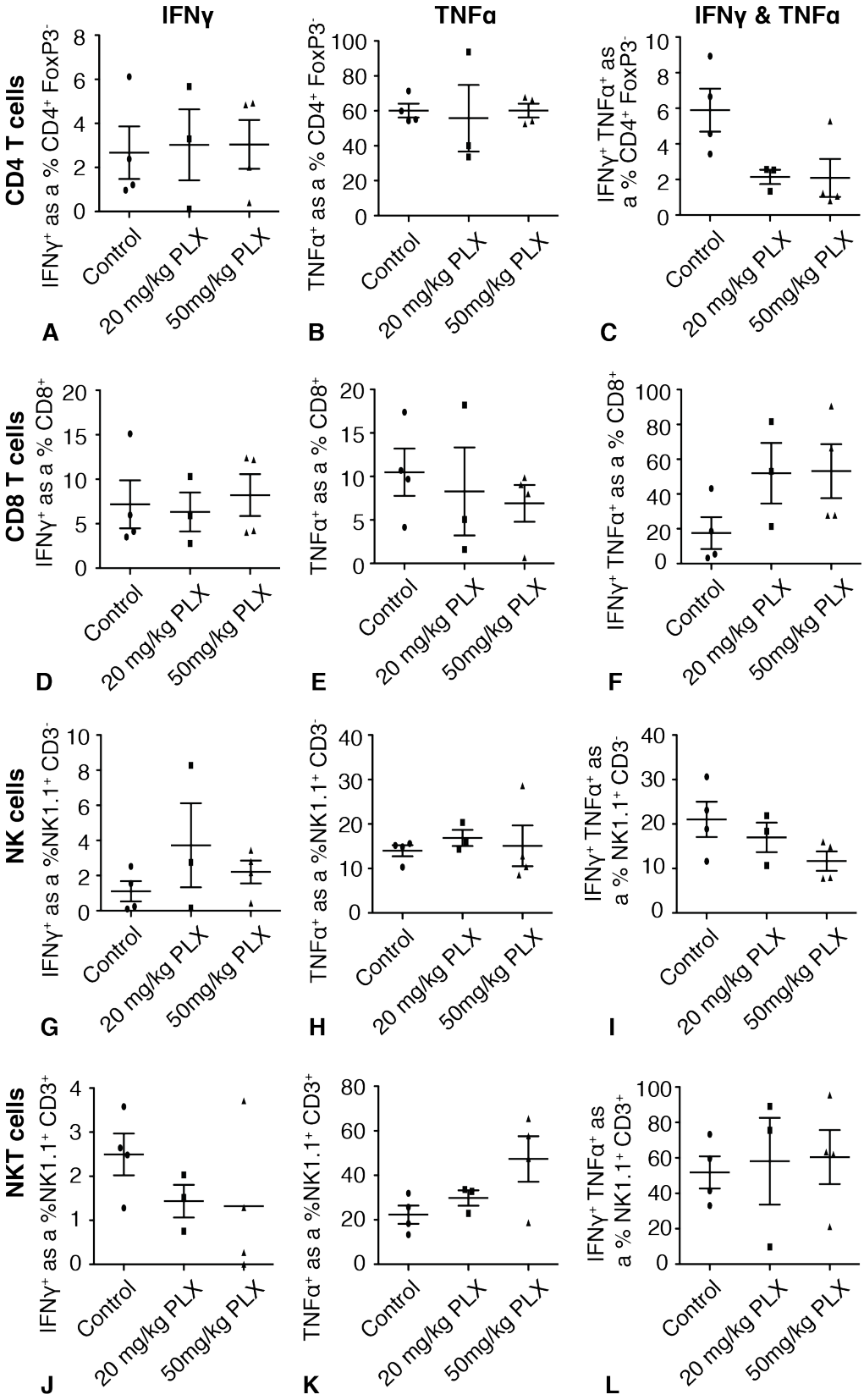
IFNγ
TNFα
IFNγ & TNFα
CD4 T cells
CD8 T cells
NK cells
NKT cells
IFNγ+ as a % CD4+ FoxP3-
TNFα+ as a % CD4+ FoxP3-
IFNγ+ TNFα+ as a % CD4+ FoxP3-
IFNγ+ as a % CD8+
TNFα+ as a % CD8+
IFNγ+ TNFα+ as a % CD8+
IFNγ+ as a %NK1.1+ CD3-
TNFα+ as a %NK1.1+ CD3-
IFNγ+ TNFα+ as a % NK1.1+ CD3-
IFNγ+ as a %NK1.1+ CD3+
TNFα+ as a %NK1.1+ CD3+
IFNγ+ TNFα+ as a % NK1.1+ CD3+
Control
20 mg/kg PLX
50mg/kg PLX
A
B
C
D
E
F
G
H
I
J
K
L

Figure 6.5: PLX4720 treatment does not significantly alter intra-tumoural frequencies of lymphocytes producing IFNγ and/or TNFα. C57BL/6 mice were treated with PLX4720 as described in Figure 6.1A. One week following initiation of PLX4720 treatment tumours were harvested and frequencies of IFNγ- and TNFα-producing lymphocytes were assessed by flow cytometry. Populations were defined as shown in Figure 5.12A. **A-C.** Frequencies of non-regulatory $CD4^+$ T cells producing IFNγ and TNFα. **D-F.** Frequencies of $CD8^+$ T cells producing IFNγ and TNFα. **G-I.** Frequencies of NK cells producing IFNγ and TNFα. **J-L.** Frequencies of NKT cells producing IFNγ and TNFα. Values represent individual mice with 5 mice used per group. Error bars are ± SEM. Statistical analysis was performed using one-way ANOVA with Bonferroni post-test. No significant differences were identified. Results are representative of two independent experiments.

6.2.3 TNFα inhibition does not augment the anti-tumour effects of PLX4720 treatment

Etanercept is an antagonistic inhibitor of human TNFα, originally developed for use in rheumatoid arthritis. It is now used in the treatment of several autoimmune and inflammatory diseases (Willrich et al., 2015). Etanercept is a recombinant fusion protein, which consists of human TNFα receptor proteins bound to human IgG1. In addition to inhibiting human TNFα, Etanercept has also been shown to effectively block murine TNFα and significantly reduce serum levels of TNFα in different strains of mice (Fries et al., 2008; Genovese et al., 2006; Liu et al., 2006; Popivanova et al., 2008).

C57BL/6 mice were tumour challenged, and six days later 100 μg of Etanercept or PBS was injected intraperitoneally and these injections were repeated every 3 days for the length of the experiment. As with previous experiments, daily gavage of PLX4720 at 50 mg/kg or vehicle control was initiated seven days after tumour challenge, and mice were monitored for tumour growth (Figure 6.11A). Inhibition of TNFα slightly decreased tumour growth and increased survival, however this effect was not significant. Consistent with previous experiments single agent PLX4720 significantly reduced tumour growth and increased survival, which did not result in tumour regression. When mice were treated with 50 mg/kg PLX4720 alongside TNFα inhibition, a non-significant reduction in tumour growth was observed in comparison to PLX4720 monotherapy. However, inhibition of

tumour growth did not translate to increased survival and no tumour regression was seen (Figure 6.11B-D).

A similar experiment was also performed once with just two doses of Etanercept; the first dose delivered six days after tumour challenge, and the second 18 hours later. PLX4720 treatment commenced six hours after the second dose of Etanercept. In this setting TNFα inhibition did not improve PLX4720 anti-tumour efficacy (data not shown).

These results clearly show that TNFα inhibition does not improve the anti-tumour effects of PLX4720. The absence of tumour regression (and thus significant tumour cell death) with TNFα inhibition and PLX4720 treatment suggests it is unlikely that TNFα is preventing PLX4720 from inducing apoptosis.

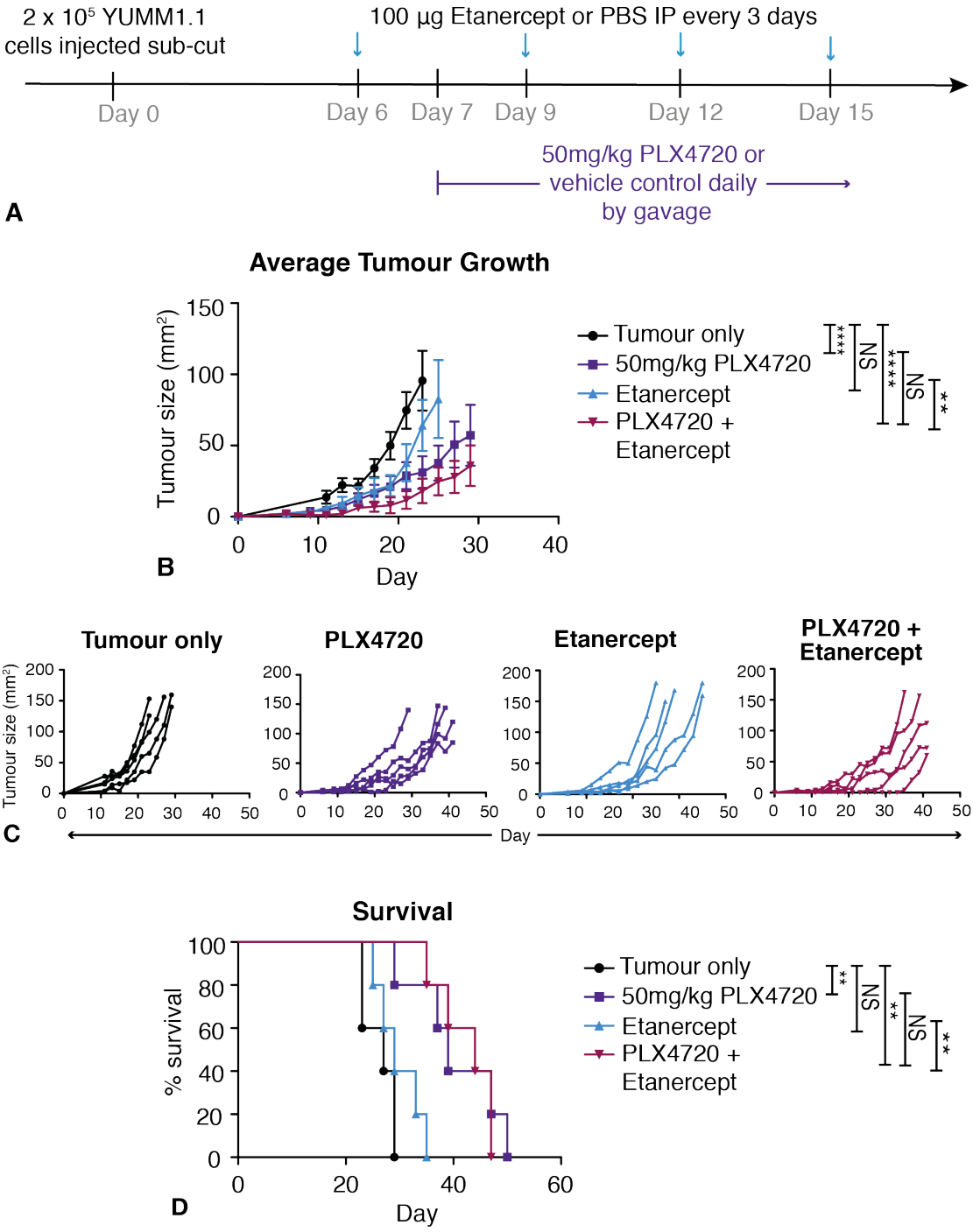
2 x 10⁵ YUMM1.1
cells injected sub-cut
100 µg Etanercept or PBS IP every 3 days
Day 0
Day 6
Day 7
Day 9
Day 12
Day 15
50mg/kg PLX4720 or
vehicle control daily
by gavage
A
Average Tumour Growth
Tumour size (mm²)
Day
Tumour only
50mg/kg PLX4720
Etanercept
PLX4720 +
Etanercept
****
NS
****
NS
**
B
Tumour only
PLX4720
Etanercept
PLX4720 +
Etanercept
Tumour size (mm²)
Day
C
Survival
% survival
Day
Tumour only
50mg/kg PLX4720
Etanercept
PLX4720 +
Etanercept
**
NS
**
NS
**
D

Figure 6.6: TNFα inhibition does not augment anti-tumour effects of PLX4720 treatment of YUMM1.1 tumours. A. C57BL/6 mice were injected subcutaneously in the left flank with 2 x 10^5 YUMM1.1 cells and given PC61 or PBS intraperitoneally. From six days post-tumour challenge mice received 100 μg Etanercept or PBS control injected intraperitoneally, every three days. Daily drug treatment with PLX4720 was initiated seven days post-tumour challenge. Mice received 50 mg/kg PLX4720 given by oral gavage, or a vehicle solution. Tumour growth was monitored and size recorded. Mice were culled when tumours reached 150 mm^2, or when tumours ulcerated. **B.** Average tumour growth is shown. Each symbol represents the mean growth of 5 mice, error bars are ± SEM. NS = non-significant, ** $P < 0.01$, **** $P < 0.0001$, 2-way ANOVA with Bonferroni post-test, statistics shown for Day 23. **C.** Individual tumour growth for each treatment group; each data point represents an individual mouse **D.** Kaplan-Meier plot showing survival for groups of 5 mice. NS = non-significant, ** $P < 0.01$, Mantel-Cox test. Data are representative of two independent experiments.

6.2.4 PLX4720 and autologous vaccination can be combined to achieve an additive, but not synergistic, anti-tumour effect

The final set of experiments for this thesis aimed to develop a strategy for combination of autologous vaccine and PLX4720 that improved the anti-tumour efficacy of either single-agent treatment.

The first combination therapy experiment involved initiation of PLX4720 treatment followed by therapeutic vaccination. The rationale for this approach was that PLX4720-induced tumour cell death would increase the release of tumour antigen to stimulate vaccine mediated anti-tumour responses. PLX4720 treatment was delivered at 20 mg/kg, as this dose has been previously identified to directly stimulate sub-optimal T cell proliferation *in vivo* (Chapter 4). Mice were tumour challenged, followed five days later by daily administration of 20 mg/kg PLX4720, and two days later mice were vaccinated (Figure 6.6A). Tumour growth was monitored and recorded, and mice were culled when tumours reached 150 mm^2 or ulcerated.

The efficacy of vaccine monotherapy, when delivered seven days after tumour challenge, was minimal. Tumour growth was not significantly reduced, while survival did not improve with therapeutic vaccination in this

setting (Figure 6.7B-D). In contrast, the single agent 20 mg/kg PLX4720 significantly slowed tumour growth and increased survival. Combination of PLX4720 and vaccine did not decrease tumour growth when compared to the protection afforded by PLX4720 alone (Figure 6.7B). However, when tumour growth of individual mice was assessed several mice had periods of tumour regression followed by aggressive tumour growth. This may indicate the development of an anti-tumour response, which was unable to overcome tumour-mediated immune suppression. Combination therapy did not improve the survival of mice significantly, although one mouse had significantly increased survival within the combination therapy treated group (Figure 6.7D). Overall, the sequential combination of PLX4720 followed by vaccine did not significantly improve anti-tumour efficacy of these monotherapies. This may be a result of the vaccine failing to induce sufficient anti-tumour responses when delivered seven days post-tumour challenge.

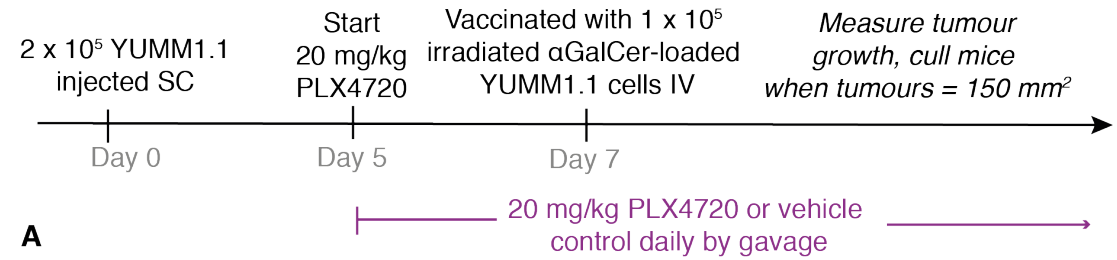
2 x 10⁵ YUMM1.1 injected SC
Start 20 mg/kg PLX4720
Vaccinated with 1 x 10⁵ irradiated αGalCer-loaded YUMM1.1 cells IV
Measure tumour growth, cull mice when tumours = 150 mm²
Day 0
Day 5
Day 7
20 mg/kg PLX4720 or vehicle control daily by gavage

A

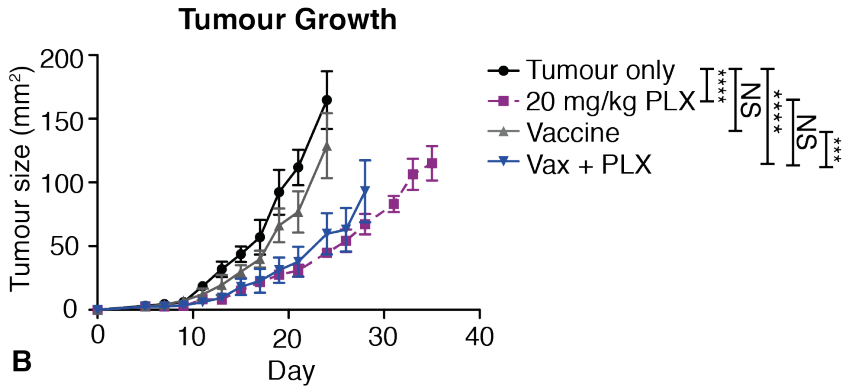
Tumour Growth
Tumour size (mm²)
Day
Tumour only
20 mg/kg PLX
Vaccine
Vax + PLX
****
NS
****
NS
***

B

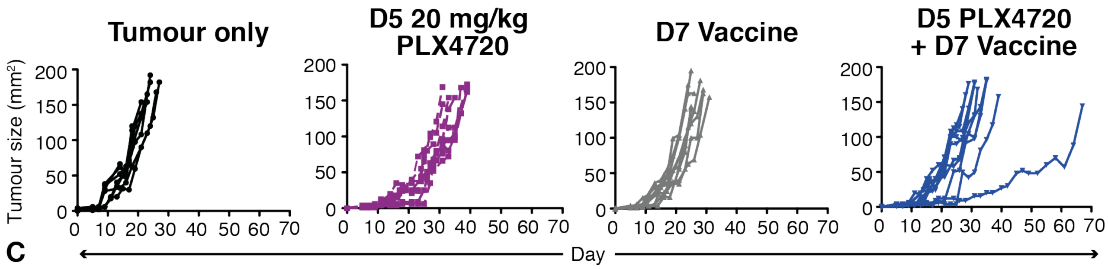
Tumour only
D5 20 mg/kg PLX4720
D7 Vaccine
D5 PLX4720 + D7 Vaccine
Tumour size (mm²)
Day

C

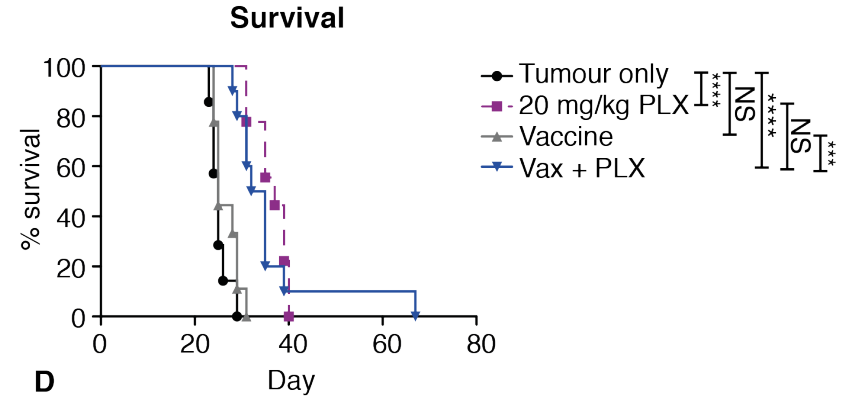
Survival
% survival
Day
Tumour only
20 mg/kg PLX
Vaccine
Vax + PLX
***
NS
****
NS
***

D

Figure 6.7: Combination therapy with 20 mg/kg PLX4720 followed by vaccination does not significantly improve anti-tumour efficacy. A. C57BL/6 mice were injected subcutaneously in the left flank with 2 x 10^5 YUMM1.1 cells. Daily drug treatment was begun five days post-tumour challenge with 20 mg/kg PLX4720 given by oral gavage, and control mice receiving a vehicle solution. Seven days post-tumour challenge mice were vaccinated intravenously with irradiated, αGalCer-loaded YUMM1.1 cells. Control mice received PBS. Tumour growth was monitored and size recorded. Mice were culled when tumours reached 150 mm^2, or when tumours ulcerated. **B.** Average tumour growth is shown. Each symbol represents the mean growth of 4 - 5 mice. Error bars are ± SEM. NS = non-significant, *** $P < 0.001$ **** $P < 0.0001$, 2-way ANOVA with Bonferroni post-test, statistics shown for Day 23. Tumour growth is representative of three independent experiments (as tumours were measured on different days data was unable to be combined). **C.** Individual tumour growth for each treatment group is shown. Each data point represents an individual mouse **D.** Kaplan-Meier plot showing survival for 2 combined experiments each with 4-5 mice per group. NS = non-significant, *** $P < 0.001$ **** $P < 0.0001$, Mantel-Cox test.

Based on the previous findings (Figure 6.7), the optimal timing for therapeutic vaccine in this model was considered to be no later than five days post-tumour challenge. The next strategic approach delivered therapeutic vaccine five days post-tumour challenge, and PLX4720 treatment was initiated two days later (Figure 6.8A). Both therapeutic vaccine and PLX4720 as single-agent therapies significantly slowed tumour growth and increased survival (Figure 6.8B-D). However, the combination of these two treatments in this sequence also did not improve the anti-tumour efficacy over monotherapies (Figure 6.8B-D).

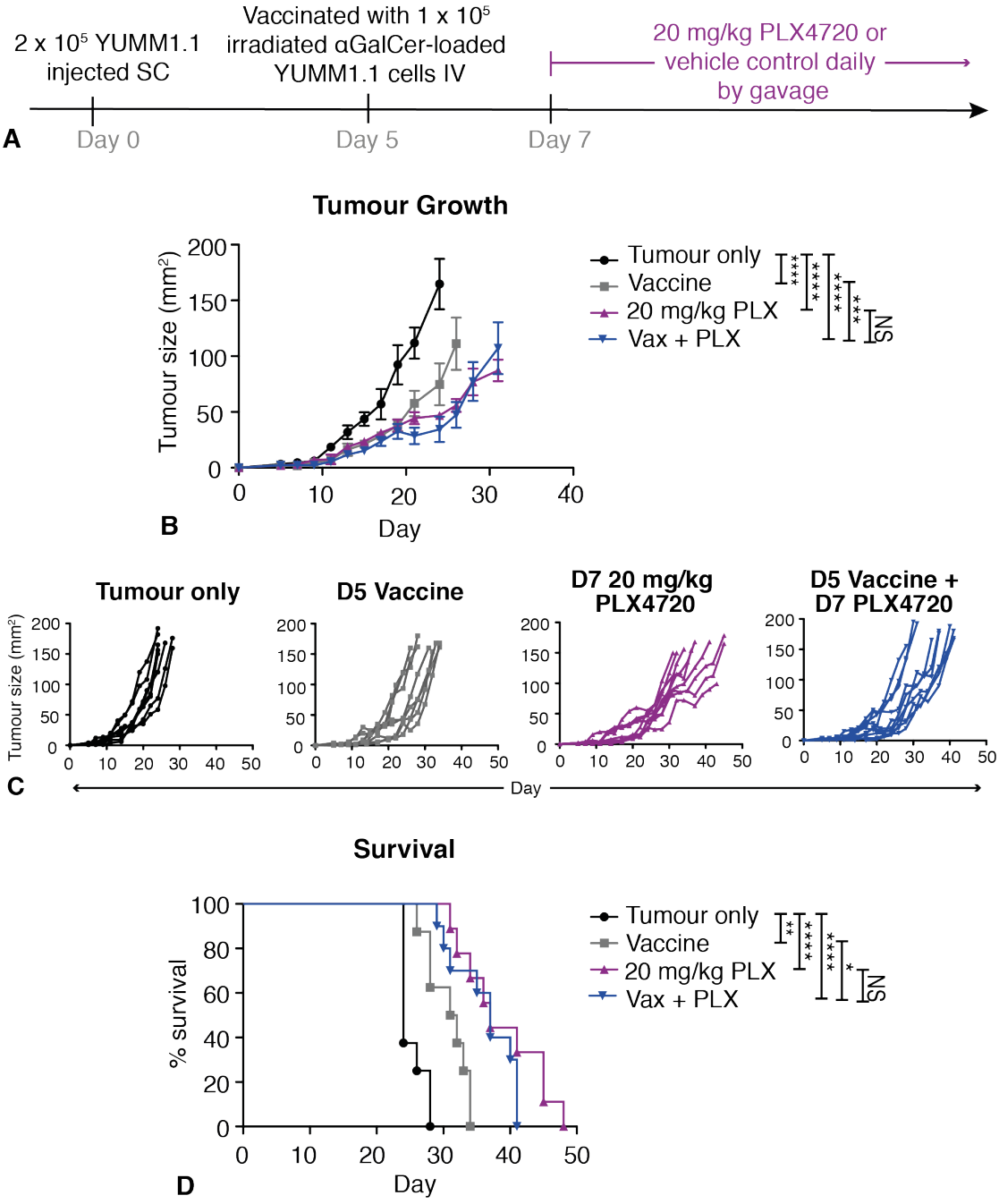
2 x 10⁵ YUMM1.1 injected SC
Vaccinated with 1 x 10⁵ irradiated αGalCer-loaded YUMM1.1 cells IV
20 mg/kg PLX4720 or vehicle control daily by gavage
A
Day 0
Day 5
Day 7
Tumour Growth
Tumour size (mm²)
Day
Tumour only
Vaccine
20 mg/kg PLX
Vax + PLX
****
****
****
***
NS
B
Tumour only
D5 Vaccine
D7 20 mg/kg PLX4720
D5 Vaccine + D7 PLX4720
Tumour size (mm²)
Day
C
Survival
% survival
Day
Tumour only
Vaccine
20 mg/kg PLX
Vax + PLX
**
****
****
*
NS
D

Figure 6.8: Combination therapy with vaccination followed by 20 mg/kg PLX4720 does not significantly improve anti-tumour efficacy. A. C57BL/6 mice were injected subcutaneously in the left flank with 2 x 10^5 YUMM1.1 cells. Five days post-tumour challenge mice were vaccinated intravenously with irradiated, αGalCer-loaded YUMM1.1 cells or PBS. Two days later, daily treatment was initiated with 20 mg/kg PLX4720 given by oral gavage, and control mice receiving a vehicle solution. Tumour growth was monitored and size recorded. Mice were culled when tumours reached 150 mm^2, or ulcerated. **B.** Average tumour growth is shown. Each symbol represents the mean growth of 4 - 5 mice. Error bars are ± SEM. NS = non-significant, *** $P < 0.001$ **** $P < 0.0001$, 2-way ANOVA with Bonferroni post-test, statistics shown for Day 24. Tumour growth is representative of three independent experiments (as tumours were measured on different days data was unable to be combined). **C.** Individual tumour growth for each treatment group is shown. Each data point represents an individual mouse **D.** Kaplan-Meier plot showing survival for 2 combined experiments each with 4-5 mice per group. NS = non-significant, * $P \leq 0.05$, ** $P < 0.01$, **** $P < 0.0001$, Mantel-Cox test.

The third and final strategy assessed the effect of higher dose PLX4720 in combination therapy. Therapeutic vaccination was delivered five days after tumour challenge and two days later 50 mg/kg PLX4720 treatment commenced (Figure 6.9A). Again, vaccine or 50 mg/kg PLX4720 monotherapy slowed tumour growth and improved survival significantly (Figure 6.9B-D). Combination therapy significantly reduced tumour growth and improved survival significantly when compared with single agent treatments (Figure 6.9B-D). The increased benefit observed with the sequential combination of vaccine and 50 mg/kg PLX4720 appeared to be additive rather than synergistic. Additionally, tumour regression remained elusive and long-term survival was only achieved in 10% of mice, with all hosts eventually culled due to tumour size or ulceration.

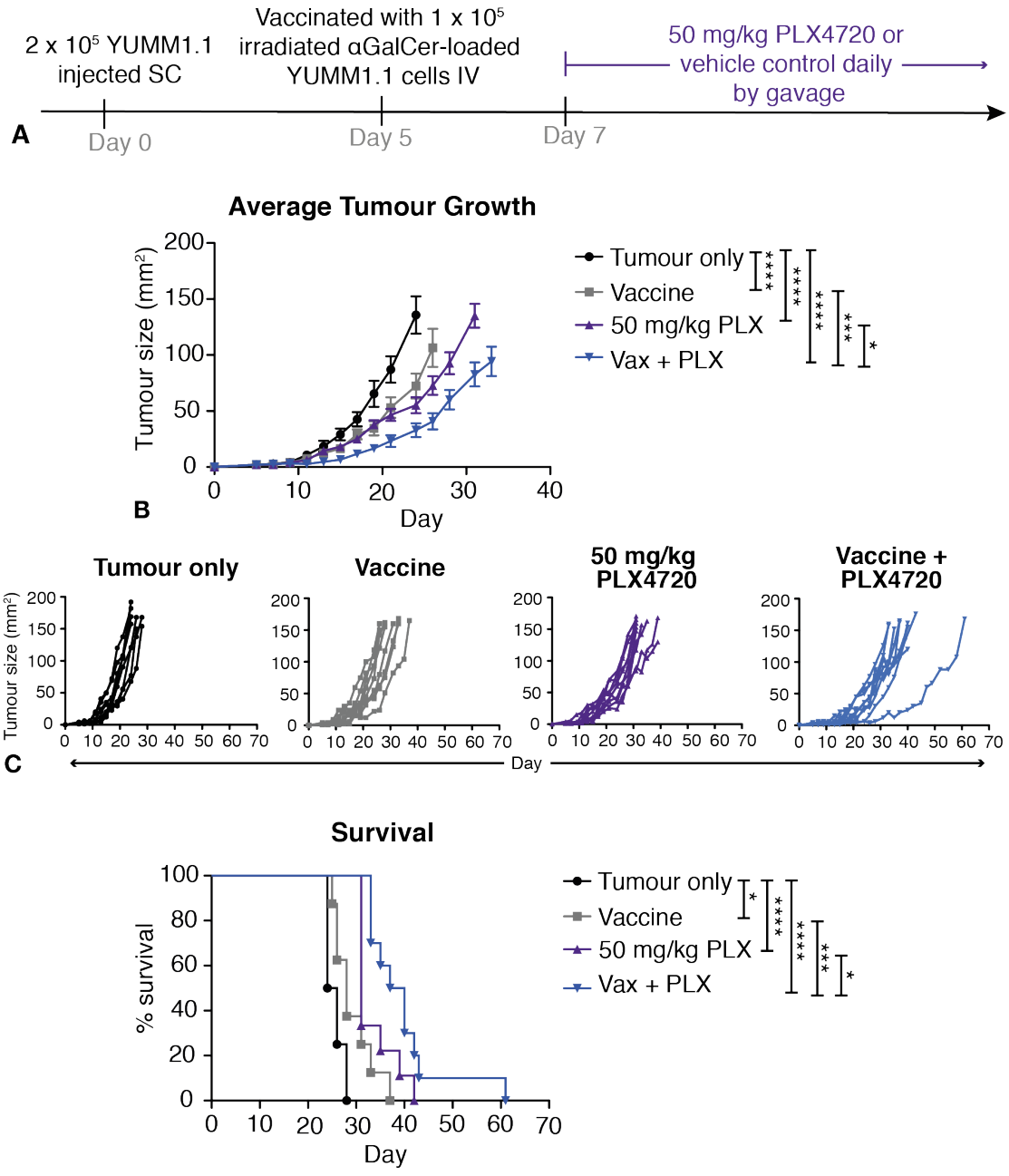
2 x 10⁵ YUMM1.1 injected SC
Vaccinated with 1 x 10⁵ irradiated αGalCer-loaded YUMM1.1 cells IV
50 mg/kg PLX4720 or vehicle control daily by gavage
A
Day 0
Day 5
Day 7
Average Tumour Growth
Tumour size (mm²)
Day
Tumour only
Vaccine
50 mg/kg PLX
Vax + PLX
B
Tumour only
Vaccine
50 mg/kg PLX4720
Vaccine + PLX4720
C
Survival
% survival

Figure 6.9: Combination therapy with vaccination followed by 50 mg/kg PLX4720 significantly improves anti-tumour efficacy. A. C57BL/6 mice were injected subcutaneously in the left flank with 2 x 10^5 YUMM1.1 cells. Five days post-tumour challenge mice were vaccinated intravenously with irradiated, αGalCer-loaded YUMM1.1 cells. Control mice received PBS. Daily drug treatment was begun seven days post-tumour challenge with 50 mg/kg PLX4720 given by oral gavage, and control mice receiving a vehicle solution. Tumour growth was monitored and size recorded. Mice were culled when tumours reached 150 mm^2, or when tumours ulcerated. **B.** Average tumour growth is shown. Each symbol represents the mean growth of 4 - 5 mice. Error bars are ± SEM. * $P \leq 0.05$, *** $P < 0.001$ **** $P < 0.0001$, 2-way ANOVA with Bonferroni post-test, statistics shown for Day 23. Tumour growth is representative of two independent experiments (as tumours were measured on different days data was unable to be combined). **C.** Individual tumour growth for each treatment group is shown. Each data point represents an individual mouse **D.** Kaplan-Meier plot showing survival for 2 combined experiments each with 4-5 mice per group. * $P \leq 0.05$, *** $P < 0.001$ **** $P < 0.0001$, Mantel-Cox test.

Collectively these data demonstrate that it is possible to achieve increased anti-tumour efficacy by combining therapeutic vaccination and PLX4720. However, both drug dose and the sequence of therapy must be optimized. The benefit achieved with the combination therapy strategy developed still leaves room for improvement.

6.2.5 Treg depletion does not improve vaccine, PLX4720 or combination therapy efficacy

The suppressive capacity of Tregs presents a major hurdle to effective immunotherapy. Due to the high frequency of Tregs present in YUMM1.1 tumours it is possible that these cells are limiting both vaccine, and combination therapy efficacy. Experiments were undertaken to establish whether depletion of Tregs could improve the benefit achieved with these therapies.

PC61 (anti-CD25 depleting antibody) depletion of Tregs within peripheral blood was assessed with each batch of antibody used. Naïve FoxP3 GFP mice were injected with 250 μg of PC61 intraperitoneally and peripheral blood was collected and analysed by flow cytometry (Appendix B2). PC61 significantly

reduced the proportion of Tregs present within the peripheral blood $CD4^+$ T cell population, with depletion maintained for at least seven days after antibody delivery (Appendix B2).

The effect of Treg depletion on vaccine monotherapy or vaccine and PLX4720 combination therapy was assessed. Mice were tumour challenged, and on the day of tumour implantation received either 250 μg of PC61 or PBS delivered intraperitoneally. Tumour challenge and Treg depletion were performed on the same day to maximise the effect of depletion on the suppressive tumour microenvironment, and to maximum ensure Treg depletion at the time of vaccination. Five days later mice were vaccinated intravenously, and two days after vaccination daily treatment with PLX4720 or vehicle control was commenced (Figures 6.10A and 6.11A). Depletion of Tregs by PC61 did not improve vaccine or combination therapy efficacy, with the effect of therapy on tumour growth and survival remaining unchanged (Figures 6.10B-D and 6.11B-D). As a control, the effect of Treg depletion on PLX4720 monotherapy was also assessed and found to have no impact on treatment efficacy (Appendix B3).

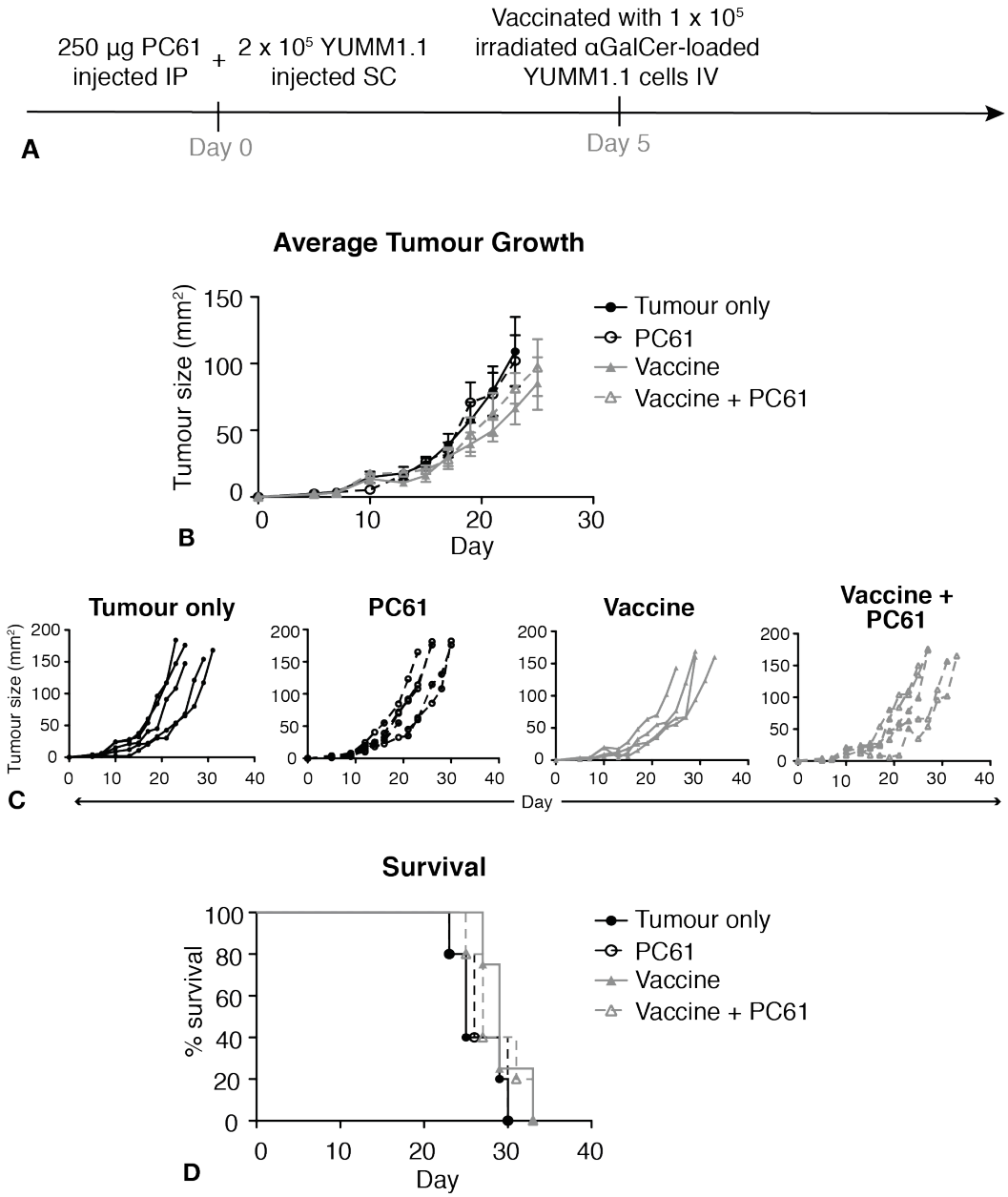

Figure 6.10: Depletion of Tregs does not augment anti-tumour effects of therapeutic vaccination against YUMM1.1 tumours. A. C57BL/6 mice were challenged sub-cutaneously with 2 x 10^5 YUMM1.1 cells, and given PC61 or PBS intraperitoneally. Mice were vaccinated intravenously with irradiated, αGalCer-loaded YUMM1.1 cells therapeutically five days post-tumour challenge. Control mice received PBS. Tumour growth was monitored and size recorded. Mice were culled when tumours reached 150 mm^2, or when tumours ulcerated. **B.** Average tumour growth is shown, each symbol represents the mean growth of 4-5 mice. Error bars are ± SEM. 2-way ANOVA with Bonferroni post-test was performed with no significant differences between groups. **C.** Individual tumour growth is shown. Each data point represents one mouse. **D.** Kaplan-Meier plot showing survival with 4-5 mice per group. Treatment groups are compared to control mice. Statistical analysis with the Mantel-Cox test revealed no significant differences between groups. Data are representative of two concordant, independent experiments.

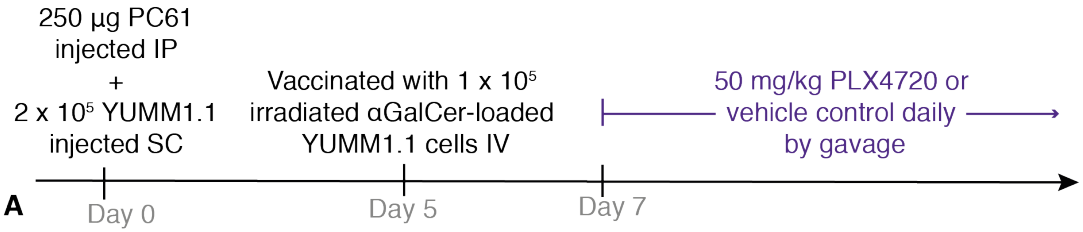
250 µg PC61
injected IP
+
2 x 10⁵ YUMM1.1
injected SC
Vaccinated with 1 x 10⁵
irradiated αGalCer-loaded
YUMM1.1 cells IV
50 mg/kg PLX4720 or
vehicle control daily
by gavage
A
Day 0
Day 5
Day 7

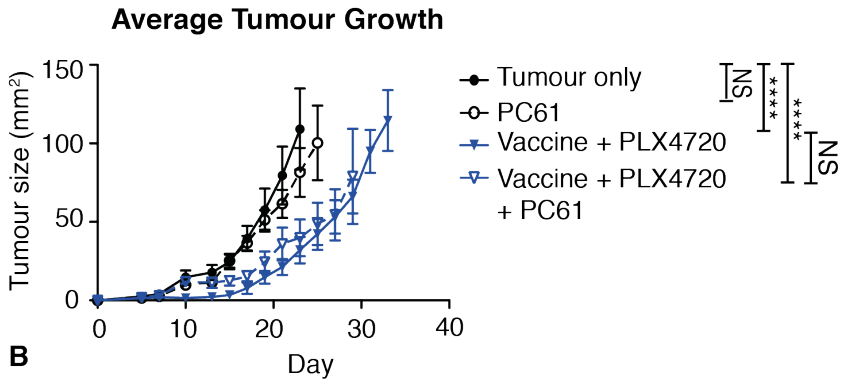
Average Tumour Growth
Tumour size (mm²)
150
100
50
0
0
10
20
30
40
Day
B
Tumour only
PC61
Vaccine + PLX4720
Vaccine + PLX4720
+ PC61
NS
****
****
NS

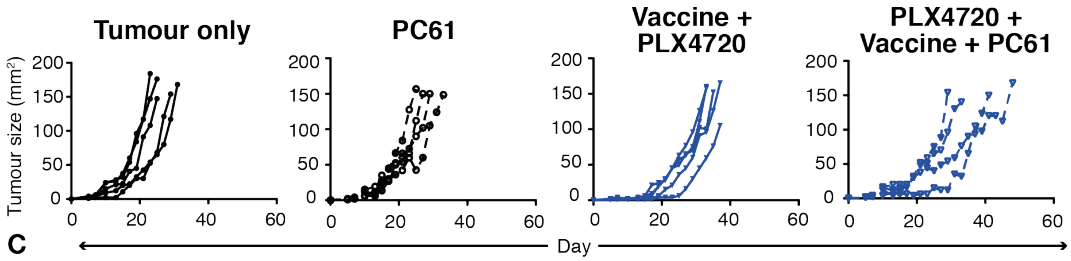
Tumour only
PC61
Vaccine +
PLX4720
PLX4720 +
Vaccine + PC61
Tumour size (mm²)
200
150
100
50
0
0
20
40
60
Day
C

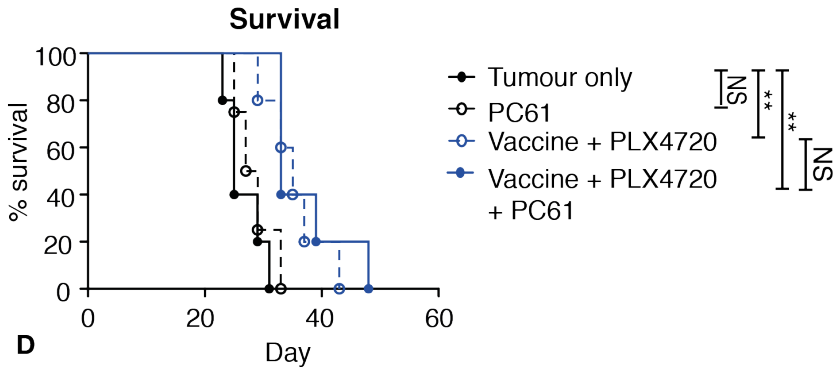
Survival
% survival
100
80
60
40
20
0
0
20
40
60
Day
D
Tumour only
PC61
Vaccine + PLX4720
Vaccine + PLX4720
+ PC61
NS
**
**
NS

Figure 6.11: Depletion of Tregs does not augment anti-tumour effects of combination PLX4720 and vaccine therapy. A. C57BL/6 mice were injected subcutaneously in the left flank with 2 x 10^5 YUMM1.1 cells, and given PC61 or PBS intraperitoneally. Five days post-tumour challenge mice were vaccinated intravenously with irradiated, αGalCer-loaded YUMM1.1 cells. Control mice received PBS. Daily drug treatment was begun seven days post-tumour challenge with 50 mg/kg PLX4720 given by oral gavage, with control mice receiving a vehicle solution. Tumour growth was monitored and size recorded. Mice were culled when tumours reached 150 mm^2, or when tumours ulcerated. **B.** Average tumour growth is shown. Each symbol represents the mean growth of 4 - 5 mice. Error bars are ± SEM. NS= non-significant, **** $P < 0.0001$, 2-way ANOVA with Bonferroni post-test, statistics shown for Day 23. **C.** Individual tumour growth for each treatment group is shown. Each data point represents an individual mouse **D.** Kaplan-Meier plot showing survival for groups of 4-5 mice. NS = non-significant, ** $P < 0.01$, Mantel-Cox test. This experiment was performed only once as neither single agent treatment demonstrated benefit of Treg depletion.

6.3 Discussion

The primary aims of the work described in this chapter were to determine if host-mediated immune responses contributed to PLX4720 anti-tumour efficacy, and to devise an effective strategy to combine PLX4720 and vaccine to improve therapy outcomes. Additionally, targeting of potential mediators of therapy resistance was explored, with the aim of increasing tumour sensitivity to PLX4720 and vaccine.

Comparison of PLX4720 anti-tumour efficacy in the immunocompetent C57BL/6 mice and immunocompromised NOD/Scid mice revealed a clear role for host immune responses in anti-tumour effects of BRAF inhibitors. The use of NOD/Scid mice is a potential limitation of this study, as these mice have a different genetic background to the C57BL/6 mice for which YUMM1.1 tumours are syngeneic. In this context syngeneic Rag-1 deficient mice may have been a better choice. However, NOD/Scid mice were used as they exhibit not only defective T and B lymphoyctes (a commonality shared with Rag-1-deficient mice), but also have defective NK and macrophage responses (Shultz et al., 1995). Diminished NK cell and macrophage responses were desirable as these cells can be important mediators of anti-tumour immunity, and NK cells have been previously implicated in BRAF inhibitor-mediated anti-tumour efficacy (Ferrari de Andrade et al., 2014). Additionally, NOD/Scid mice have been shown to be the preferable model for xenotransplantation, with a 100% engraftment rate for many human tumours (Hudson et al., 1998), indicating that the difference in genetic background of the tumours should not be a major issue. Whilst delayed YUMM1.1 growth was observed in NOD/Scid mice compared to C57BL/6 mice this was attributed to a technical problem. The skin of NOD/Scid mice was "leakier" than that of C57BL/6 mice. Consequently, following subcutaneous injection of tumour cells a greater volume of cell suspension seeped from the tumour injection site. Slow, careful injection minimized this but did not completely stop seepage.

The finding that BRAF inhibitors require host immunity to be fully effective supports a growing body of literature demonstrating that these inhibitors

enhance anti-tumour immune responses. In melanoma patients, Vemurafenib treatment has been shown to increase $CD4^+$ and $CD8^+$ T cell infiltration of tumours, which has been associated with increased expression of melanoma antigens and upregulation of MHC Class I expression (Frederick et al., 2013; Sapkota et al., 2013; Wilmott et al., 2012). Similarly, in the inducible model of *Braf*^{V600E} *Pten*$^{-/-}$ *Cdkn2a*$^{-/-}$ tumours PLX4720 treatment increased $CD4^+$ $FoxP3^-$ and $CD8^+$ T cell infiltration of tumours, and reduced the frequency of $FoxP3^+$ Tregs (Ho et al., 2014). The associated increased IFNγ production and CD40L expression by non-regulatory $CD4^+$ T cells, was shown by specific blockade to be required for optimal PLX4720 anti-tumour efficacy. However, the immunological effects or requirements of BRAF inhibitor treatment do vary between patients and between models. In the SM1 model of $BRAF^{V600E}$ melanoma PLX4720 and Vemurafenib treatment increased ratios of $CD8^+$ T cells to Tregs, but also significantly increased NK cell infiltration of tumours (Knight et al., 2013). Furthermore, in this model PLX4720 augmented NK cell function, and NK cells were required for PLX4720 anti-tumour efficacy in a perforin-dependent manner (Ferrari de Andrade et al., 2014).

Despite the requirement for host-mediated immune responses for PLX4720 efficacy, further characterisation of the tumour milieu following PLX4720 treatment did not reveal any of the previously reported augmented antitumour responses. T, NK and NKT cell, macrophage and MDSC frequencies, ratios, and numbers (data not shown) were unaffected by PLX4720 treatment. Evidently, the PLX4720 induced tumour infiltration demonstrated in other models does not occur in YUMM1.1 tumours. Effector T cells, T cell expression of PD-1, and IFNγ and TNFα production by T, NK and NKT cells were also unchanged with BRAF inhibition. Therefore, although PLX4720 efficacy requires host-immunity, in the YUMM1.1 model it does not appear to specifically enhance tumour infiltration or effector function of any of the immune cell populations previously shown to be important in other models. The immune mediated component of PLX4720 efficacy may be a consequence of PLX4720 treatment changing the equilibrium within the YUMM1.1 tumour microenvironment, allowing existing host immune responses to achieve greater efficacy. One such mechanism may be through BRAF inhibitor-mediated attenuation of

melanoma-mediated immunosuppression, or reduction of stromal cell production of suppressive factors. Diminished immunosuppression would allow cell populations already infiltrating the tumour to mediate greater anti-tumour effects. Although a specific effector population was unable to be identified, these data demonstrate that anti-tumour immune responses develop against YUMM1.1 tumours, which are associated or possibly augmented with PLX4720 treatment.

The role for host-immunity in PLX4720 anti-tumour efficacy and PLX4720 augmentation of T cell responses (Chapter 4) provided strong support for the combination of PLX4720 and vaccine. Three combination strategies were investigated, with permutations in PLX4720 dose and timing of delivery of the two therapies. Surprisingly, of these three strategies only one yielded improved anti-tumour efficacy. No advantage was achieved when vaccine was combined with PLX4720 at a dose of 20 mg/kg. The 20 mg/kg dose of PLX4720 was initially favoured for combination therapy T cell stimulatory effects were achieved at this dose *in vivo* (Figure 4.9) and this dose offered a greater survival advantage when responses in C57BL/6 and NOD/Scid mice were compared (Figure 6.1). Despite this, combination of 20 mg/kg PLX4720 and vaccine did not improve efficacy over 20 mg/kg PLX4720 monotherapy regardless of which treatment was given first. However, when vaccine was followed by 50 mg/kg PLX4720 treatment, increased anti-tumour efficacy was achieved, with a benefit that appears to be additive.

Initially, PLX4720 followed by vaccination was anticipated to be the preferable combination strategy, as it would allow PLX4720-induced cell death to potentiate anti-tumour vaccine immune responses. However, the greatest benefit was achieved when vaccine was followed by PLX4720. Theoretically, this setting would still allow for PLX4720 potentiation of vaccine immune responses, when the effects are considered temporally. The tumour specific $CD4^+$ T cell response elicited with vaccination would be expected to peak approximately seven days after vaccine delivery. PLX4720 would be expected to reach peak, stable plasma concentration after 48 hours and begin to have either cytostatic or cytotoxic effects on melanoma cells within 36-48 hours of initiating drug treatment. Therefore, if PLX4720

treatment is commenced shortly after vaccine delivery, PLX4720 is likely to begin to have anti-tumour effects, which are expected to potentiate immune responses, prior to the peak of the vaccine effector response. However, the benefit achieved in this model with vaccine and 50 mg/kg PLX4720 was an additive effect, indicating that synergy of the two mechanisms of action did not occur.

Interestingly, PLX4720 as a monotherapy or in combination with immunotherapy did not induce regression of YUMM1.1 tumours *in vivo*, even at the maximum recommended dose of 100 mg/kg daily (Dr Gideon Bollag, personal communication). Despite this, YUMM1.1 cells were relatively sensitive to PLX4720 induced apoptosis *in vitro*, indicating that factors within the tumour microenvironment are conferring some *in vivo* resistance. The relatively high frequency of lymphocytes producing TNFα alongside previous reports of TNFα-mediated resistance to BRAF inhibition prompted investigation of the role of TNFα in YUMM1.1 . However, in the YUMM1.1 model TNFα inhibition did not improve the anti-tumour efficacy. Etanercept was delivered at a dose of 100 μg, which is well established to reduce serum TNFα levels, but the efficacy of this dose at inhibiting intratumoural TNFα is unknown. Therefore, it is possible that either TNFα is not a key mediator of resistance to BRAF inhibition in the YUMM1.1 model, or alternatively that the dose of Etanercept used was insufficient to inhibit intratumoural TNFα. Nonetheless, the dose of Etanercept commonly used for inflammatory diseases did not improve PLX4720 anti-tumour effects *in vivo*.

Next, depletion of Tregs was investigated with the aim of augmenting vaccine efficacy. Tregs are widely acknowledged to present a significant hurdle to immunotherapy, suppressing the development of effective anti-tumour immune responses through immunoregulatory functions. Additionally, Tregs can promote tumour progression through the production of factors such as VEGF. In the inducible model of *Braf*^{V600E} *Pten*$^{-/-}$ *Cdkn2a*$^{-/-}$ melanoma accumulation of intratumoural Tregs, as well as MDSCs, was shown to drive tumour growth and suppress T cell-mediated anti-tumour effector responses (Ho et al., 2014). Within YUMM1.1 tumours, Tregs represent a significant population, accounting for approximately 30-40% of the total CD4^{+} T cell

population at Day 14 post-tumour challenge. Depletion of Tregs improved endogenous tumour responses in a number of murine tumour models, and has been shown to improve efficacy of a range of vaccine strategies in mouse models of melanoma (Klages et al., 2010; Shimizu et al., 1999; Steitz et al., 2001; Tan et al., 2013). Furthermore, Treg depletion significantly enhanced efficacy of an autologous irradiated, αGalCer-loaded vaccine in a mouse model of glioma (Hunn et al., 2012). Surprisingly, depletion of Tregs with the anti-CD25 depleting antibody PC61 did not improve the efficacy of vaccination in the YUMM1.1 tumour model. There was no benefit in combining Treg depletion with vaccine monotherapy, or with vaccine and PLX4720 combination therapy. Despite this, PC61 significantly reduced the peripheral Treg populations for at least seven days after delivery, indicating efficacy of antibody depletion. However, this peripheral depletion does not demonstrate that effective depletion was achieved intratumourally. Thus, it is possible that factors produced by melanoma cells caused persistent differentiation of inducible Tregs, which were not sufficiently depleted by PC61. To more definitively deplete Tregs the DEREG mice could be used, these mice have DTR-eGFP under control of the FoxP3 gene locus allowing diphtheria toxin depletion of $FoxP3^{+}$ Tregs (Lahl, 2007 #1005). Alternatively, given the plethora of immunosuppressive mechanisms present within established tumours, such as MDSCs, tumour-associated macrophages and direct melanoma-mediated immunosuppression, it is possible that depletion of only one suppressive subset did not adequately reduce the overall immunosuppression by the tumour microenvironment.

6.3.1 Conclusions

The anti-tumour effects of PLX4720 incorporate endogenous host immune responses. However, there was no evidence of potentiation of a specific effector response following treatment, indicating that drug therapy may be unleashing pre-existing anti-tumour immunity. Investigation of three different strategies of vaccine and PLX4720 combination revealed an approach that achieved increased anti-tumour efficacy over single agent therapies. The success of this combination therapy was shown to be dependent on drug dose and timing of therapy delivery, emphasizing the

need for robust investigation of combination strategies. Despite achieving increased anti-tumour efficacy with PLX4720 and vaccine combination, lack of tumour regression leaves room for improvement of this therapeutic strategy. Inhibiting potential mediators of therapy resistance, TNFα and Tregs, was unsuccessful at improving PLX4720 or vaccine efficacy, respectively.

CHAPTER 7:
General Discussion

Metastatic melanoma is an aggressive form of skin cancer that presents a serious clinical issue, and has increased significantly in incidence over the past few decades (Giblin and Thomas, 2007; Siegel et al., 2014). Recent breakthroughs in treatment with the approval of targeted BRAF inhibition and checkpoint blockade immunotherapy have improved the prognosis of patients with advanced disease. Despite these advances, treatment resistance and non-responsiveness remains an issue in a large proportion of patients. Combination therapy is widely expected to be the way forward. The research undertaken in this thesis was motivated by the need for greater understanding of the immunological effects of BRAF inhibition and pre-clinical investigation of combination therapy strategies.

7.1.1 Modelling BRAF^{V600E} melanoma and BRAF inhibitor responses in mice

The investigation of targeted BRAF inhibitors and immunotherapy, either as single agents or in combination, required a murine melanoma model that recapitulates genetic mutations common to human melanomas in an immunocompetent system. Two novel *BRaf^{V600E}*, *Pten$^{-/-}$*; *CDKN2a$^{-/-}$* murine melanoma cell lines were generously provided by Prof. Marcus Bosenberg of Yale University. These cell lines were derived from inducible tumours of *Tyr::CreER; BRaf^{CA}*; *Pten$^{lox5/lox5}$* mice. The genetic profile of these cells represents mutations common to human melanomas. The BRAF^{V600E} mutation is found in 40 to 70% of human melanomas (Davies et al., 2002; Lee et al., 2011; Long et al., 2011), while loss of PTEN is observed in 38% of primary melanomas and 58% of metastases (Birck et al., 2000). Finally, loss of CDKN2a has been demonstrated to occur in 56% of primary melanomas (Young et al., 2014). The C57BL/6 background of these cell lines allowed transplantation to immunocompetent, syngeneic mice. However, it must be acknowledged that within this thesis tumour implantation was performed subcutaneously to allow ongoing measurement of tumour size. Therefore, tumours are growing at an ectopic site, not within the tissue of origin, the epidermis. Although not without their limitations, these cell lines meet the key requirements of a suitable model for preclinical assessment of targeted therapy and immunotherapy.

Initial experiments revealed that YUMM cell lines were not highly sensitive to BRAF inhibition in comparison with the highly sensitive human $BRAF^{V600E}$ melanoma cell line A375. PTEN status is an important difference between these two models as it has been associated with BRAF inhibitor resistance (Deng et al., 2012; Paraiso et al., 2011; Xing et al., 2012; Ye et al., 2013). A375 express functional PTEN, whereas the YUMM cells have homozygous *Pten* inactivation. This likely contributes to the inherent insensitivity of YUMM cells to BRAF inhibitor targeting. Additionally, tumour heterogeneity and acquired resistance may contribute to the outgrowth of YUMM1.1 and YUMM1.7 tumours *in vivo* during PLX4720 treatment.

The development of BRAF inhibitor resistance was investigated in a recent study, with proteomic and genetic analysis performed on tumour samples at baseline, during BRAF inhibitor responsiveness and after the development of drug resistance (Kwong et al., 2015). Known resistance-conferring mutations, such as loss of PTEN, were identified in 50% of patients. Protein expression allowed categorization of patient resistance into three subsets, two of which were defined by reactivation of the MAPK pathway and a third was MAPK-independent. Interestingly, in this study, a mouse model that recapitulates the resistance phenotype seen in patients was generated. This mouse model has inducible $Braf^{V600E}$, conditional loss of *Pten* and constitutive knockout of *Cdkn2a.* This mouse model shared not only mutations similar to those in resistant patients but also a similar protein expression pattern to that identified in patients tumour samples. When treated with PLX4720, tumour growth was effectively inhibited for a median of 32 days, after which tumour growth increased. At this point the tumours were considered to have developed a fully resistant phenotype. The model developed in that study has the same mutational profile as that of the $BRAF^{V600E}$ models utilised in this thesis, and also shares similarities in drug responsiveness. In the YUMM1.1 and YUMM1.7 models, PLX4720 treatment appears to control tumour outgrowth efficiently until 20 to 30 days post-tumour challenge, dependent on drug dose, at which point tumour growth rapidly increases. Taken together this supports the conclusion that YUMM tumours are also representative of BRAF inhibitor resistant patients. Given that virtually all patients treated with targeted BRAF inhibitors develop resistance, with an

average onset of only eight months after commencement of treatment, this model is highly clinically relevant.

Combination of PLX4720 and vaccine could only be investigated in one of the two *BRaf*^{V600E}, *Pten*$^{-/-}$; *CDKN2a*$^{-/-}$ models, due to time and resource limitations. Although the YUMM1.1 and YUMM1.7 cell lines exhibited similar sensitivity to PLX4720 treatment *in vitro* and *in vivo*, the efficacy of autologous vaccination differed between the models. Vaccines comprised of both YUMM1.1 and YUMM1.7 cells, irradiated and αGalCer loaded, induced immune responses in naïve mice demonstrating that both cell lines were, to some extent, immunogenic. Despite this, autologous vaccination only demonstrated protection in the YUMM1.1 model. On the basis of vaccine efficacy, the YUMM1.1 model was used for further investigation of combination therapy approaches, and exploration of the immune interactions of PLX4720.

7.1.2 Immune interactions of targeted BRAF inhibitors

Elucidating immunological interactions of BRAF inhibitors is of utmost importance to fully understand the effects of this treatment, and is critical in informing uptake of combination therapy. The research carried out in this thesis supports the prediction that BRAF inhibitor therapy will generate a tumour microenvironment favourable to effective anti-tumour immune responses. Indirectly, BRAF inhibitors can modulate immune responses by reducing immunosuppression mediated by melanoma-produced soluble factors. This was demonstrated in both BRAF inhibitor-sensitive and *de novo* resistant human BRAF^{V600E} cell lines, but YUMM cells were not shown to be immunosuppressive in this manner. Previous studies have reported similar effects of BRAF inhibition, indicating reduction of melanoma-mediated immunosuppression, through soluble factors or other mechanisms, is a widespread phenomenon (Frederick et al., 2013; Ho et al., 2014; Schilling et al., 2013; Steinberg et al., 2014; Sumimoto et al., 2006).

BRAF inhibitors have paradoxical effects on T cell responses and viability, inhibiting or enhancing T cell proliferation and activation in a concentration

and stimulus dependent manner. The protective effect of high serum environments indicates that inhibitory effects will be limited *in vivo*, although decreased peripheral lymphocyte numbers in Vemurafenib-treated patients cautions against ignoring the potential detrimental effects of BRAF inhibition (Schilling et al., 2014). The stimulatory effects of BRAF inhibition on lymphocyte proliferation were demonstrated to occur in an *in vivo* antigen-specific setting, supporting the concept that in a similar manner, BRAF inhibition could strengthen anti-tumour T cell responses. However, the effects of BRAF inhibitors on tumour-directed T cell responses were difficult to assess. Investigation of this required a BRAF wild-type melanoma model, however in this setting BRAF inhibitor treatment significantly increased the rate of tumour growth. This strengthens the evidence for BRAF inhibitor stimulation of BRAF wild-type cell proliferation but confounded assessment of efficacy of vaccine-induced anti-tumour T cell responses.

The finding that BRAF inhibitor efficacy is reliant on host anti-tumour immunity complements clinical reports that immune activation correlates with improved BRAF inhibitor responses. A gene expression profile marking tumour infiltration by activated T cells has been shown to positively correlate with Vemurafenib-induced tumour regression (Kwong et al., 2015). Similarly, immune serum markers, including decreased IL-8 and increased IFNγ, TNFα and macrophage inflammatory protein-1β, were associated with BRAF inhibitor responses (Wilmott et al., 2014). Collectively, these data demonstrate a strong role for host immunity in BRAF inhibitor efficacy and suggest that pre-existing anti-tumour immune responses are predictive of patient responses to BRAF inhibition. This may be very important clinically for patient stratification for therapy. Interestingly, the association of anti-tumour immune responses with outcome of metastatic melanoma patients is not limited to those undergoing BRAF inhibitor treatment. Generally, micro-array-based signatures of tumour immune infiltration positively correlate with metastatic melanoma patient survival (Bogunovic et al., 2009; Mandruzzato et al., 2006; Mann et al., 2013).

7.1.3 Active immunotherapy for BRAF^{V600E} melanoma

Immunotherapeutic treatment, and to some extent research on metastatic melanoma, is currently focussed on blockade of immune checkpoints, fuelled by recent approval of Ipilimumab, Pembrolizumab and Nivolumab. Following many years of relatively discouraging clinical results with immunotherapies, checkpoint blockade antibodies have reinvigorated enthusiasm for immunotherapy as a viable treatment for cancer. There are many benefits of checkpoint blockade, most notably the durable response rates, which can achieve progression-free survival of up to ten years in some patients. However, these treatments are not without limitations, the most significant of which are low response rates and side effects. Ipilimumab has a response rate of only 20%, while Nivolumab and Pembrolizumab response rates range from 20-40% (Hamid et al., 2013; Robert et al., 2015a; Robert et al., 2014; Schadendorf et al., 2015a; Topalian et al., 2015; Topalian et al., 2014). As has been previously discussed, checkpoint blockade allows pre-existing immune responses to be released from suppression by regulatory molecules. Thus, it is probable that in some non-responsive patients there is minimal pre-existing anti-tumour immunity. Active immunotherapy with cancer vaccines has the potential to address this by generating anti-tumour responses. Historically, vaccines have achieved disappointing outcomes, however, increased understanding of the immune system will facilitate design of more effective vaccines.

Recent studies have revealed that neoantigens can drive potent T cell anti-tumour immunity, with neoantigen-specific CD8$^+$ T cells highly effective at targeting tumours (Rizvi et al., 2015; Rooney et al., 2015; Schumacher and Schreiber, 2015; Snyder et al., 2014). Information supporting a critical role of neoantigens in immune control of tumours is continuing to build. This knowledge when applied to cancer vaccine design could significantly improve the efficacy of vaccines. Supporting this concept, a Phase I clinical trial by Carreno *et al* demonstrated DC-based vaccines loaded with neoantigen-derived peptides generated a highly diverse melanoma-specific T cell repertoire (Carreno et al., 2015). Assessment of T cell responses was the primary readout of the trial, and results indicated vaccination increased the

breadth of anti-tumour T cell responses, as well as increasing T cell cytotoxic activity and type 1 cytokine production. Because patients underwent surgical resection prior to vaccination, tumour regression was unable to be monitored. However vaccination against neoantigens appears to be safe with patients experiencing no autoimmune adverse events and patient survival is ongoing (Carreno et al., 2015). The key limitation of the approach undertaken in this study is the technical difficulty associated with defining patient-specific, immunogenic neoantigens. For each patient several hundred mutant peptides were identified and screened based on MHC I affinity and mRNA expression level. One-third of peptides were found to be non-immunogenic, and of the remaining candidates seven were selected for each patient based on MHC I binding. This approach involves an extremely complex manufacturing process, which is time-consuming and requires high throughput sequencing and data analysis that would make it difficult to carry out for a large patient cohort. Ongoing technological development will markedly reduce costs and time associated with these approaches making patient-specific vaccines increasingly feasible, as will progress towards defining optimal target antigens (Boisguerin et al., 2014). As an alternative, autologous tumour cell vaccines can circumvent these difficulties whilst providing a broad range of patient-specific neoantigens.

The vaccine design used in this thesis has several advantages, in addition to including neoantigens it provides both $CD4^+$ and $CD8^+$ T cell epitopes, and has the practical benefits of avoiding the need to identify and select neoantigens, or generate autologous DCs *ex vivo*. As many patients will undergo surgical resection of primary tumours prior to immunotherapy the acquisition of patient tumour material would not be difficult. Furthermore, the incorporation of cell-associated αGalCer enables strong adjuvant activity whilst limiting the potential for induction of iNKT cell anergy, which occurs when soluble αGalCer is delivered (Parekh et al., 2005). Infusion of αGalCer-loaded DCs retains iNKT responsiveness to a subsequent delivery of vaccine 30 days later (Fujii et al., 2002). Therefore, by using cell-associated αGalCer it may be feasible to deliver multiple doses of vaccine in a prime-boost regime without developing iNKT anergy. However, further research into the efficacy of such a regime is required.

The anti-tumour responses induced by vaccination slowed tumour growth, but did not control tumour outgrowth in the long term or induce regression, indicating tumour escape from immune responses occurred. Despite this, YUMM1.1 cells appear to be immunogenic, based on the contribution of endogenous anti-tumour immune responses to PLX4720 efficacy and the induction of immune responses following intravenous injection of irradiated, αGalCer-loaded cells into naïve mice. Therefore, it is likely that vaccine efficacy was limited by the establishment of a highly immunosuppressive tumour microenvironment, which is characteristic of melanoma. Although YUMM cells did not directly produce immunosuppressive soluble factors *in vitro*, there was evidence of several other suppressive mechanisms including tumour cell expression of PD-L1, TIL expression of PD-1, accumulation of Tregs and a sizable population of MDSCs within the $CD11b^+$ compartment. Vaccination decreased the frequency of PD-1 high $CD4^+$ T cells, and increased ratios of non-regulatory T cells to Tregs. However, this was only a partial effect. The presence of multiple suppressive mechanisms within the YUMM tumour model may have contributed to the lack of therapeutic benefit achieved with Treg depletion. Despite this highly suppressive environment, vaccination did drive the development of effector T cell responses with significant anti-tumour activity, which appeared to be augmented in a combination therapy regime.

Interestingly, the anti-tumour efficacy of vaccination was determined to be $CD4^+$ T cell mediated, with no requirement for $CD8^+$ T cells observed. $CD4^+$ T cells can exert anti-tumour effects in a number of CTL-independent ways, including direct cytotoxic targeting of tumour cells, recruitment and promotion of cytotoxic functions of innate immune cells and anti-angiogenic effects of IFNγ and TNFα (Corthay et al., 2005; Haabeth et al., 2014; Lundin et al., 2004; Qin and Blankenstein, 2000). In this model tumour cells did not upregulate MHC Class II expression following IFNγ exposure. Thus $CD4^+$ T cells are unlikely to be killing tumour cells through granzyme- and perforin-mediated mechanisms, which are MHC II dependent (Quezada et al., 2010). It is possible that $CD4^+$ T cells are indirectly eliciting tumour cell cytotoxicity, through activation of tumouricidal macrophages. Although, direct $CD4^+$ T cell killing in this model cannot be completely excluded as $CD4^+$ T cells may be

able to induce cytotoxicity of MHC II-negative tumour cells through Fas-FasL interactions (Lundin et al., 2004). The broader implications of a $CD4^+$ T cell-mediated vaccine are positive. One of the major benefits of an autologous, whole tumour cell vaccine is the stimulation of immune responses against a complement of neoantigens. Recently, $CD4^=$ T cells have been demonstrated to recognise neoantigens and elicit neoantigen-targeted anti-tumour responses (Linnemann et al., 2015; Tran et al., 2014). Vaccination of a patient with advanced epithelial cancer with neoantigen-reactive $CD4^+$ T cells led to long-term tumour regression, which appeared to be mediated by direct cytolytic activity of effector memory $CD4^+$ T cells (Tran et al., 2014). This highlights the potential clinical efficacy of immunotherapeutic strategies, such as the one devised in this thesis, which boost $CD4^+$ T cell responses against neoantigens.

7.1.4 Combining targeted BRAF inhibition with immunotherapy

The combination of BRAF inhibitors with immunotherapy is widely touted as being the way forward for treatment of metastatic melanoma. The combination of these therapies is expected to increase response rates and circumvent the development of BRAF inhibitor resistance. Moreover, a key requirement of combination therapies is to improve efficacy whilst keeping toxicity at a clinically manageable level. As has been previously discussed, the only clinical trial to date that has investigated combination of immunotherapy with BRAF inhibition combined Ipilmumab with Vemurafenib and resulted in significant toxicities (Ribas et al., 2013). Despite attempts to limit the serious adverse events with decreased drug doses, patient enrolment was halted early. There is a precedent for chemotherapy and immunotherapy combination resulting in increased toxicity but failing to achieve increased benefit. A Phase III clinical trial for metastatic melanoma investigated chemotherapy, comprised of Tamoxifen, Cisplatin, and Dacarbazine, in combination with subsequent IL-2 and IFNα2b therapy (Rosenberg et al., 1999). The outcome for patients randomized to combination therapy was significantly increased toxicities, and no improvement in overall survival. These results led the trial investigators to recommend combination of chemo-

and immunotherapy should be undertaken with caution, and on the basis of well-designed pre-clinical studies demonstrating clear benefit. Despite this, there have been some encouraging trial results of combination chemo- and immunotherapy. A phase III clinical trial combining Ipilimumab and Dacarbazine achieved significantly improved overall survival and higher one-year survival rates with combination therapy, although toxicity issues were still present (Robert et al., 2011). Grade 3-4 adverse events were reported in 56.3% of combination therapy patients compared with only 27.5% of patients receiving dacarbazine alone. Interestingly, the most commonly increased adverse event in patients receiving combination therapy was immune-related compromised liver-function, which the trial authors deemed unexpected based on previous studies. This is analogous to the adverse events observed with Vemurafenib and Ipilimumab combination (Ribas et al., 2013), and the reason for these events warrants further investigation.

When considering concerns surrounding toxicity of combined chemo- and immunotherapy, the combination strategy devised in this thesis holds considerable promise. The primary safety concern with vaccination comprised of autologous tumour cells is the induction of autoimmunity arising from stimulation of immune responses against normal self-peptides. No evidence of autoimmune events was observed in mice following the delivery of autologous vaccine against either YUMM1.1 or YUMM1.7 tumours. Furthermore, neither vaccination alone or in combination with BRAF inhibition was associated with obvious toxicity. This is supported by clinical trials of similar vaccine strategies incorporating αGalCer or using autologous melanoma cells, which reported minimal toxicities of low grade, with no reports of autoimmunity (Baars et al., 2000; Berd et al., 2004; Chang et al., 2005).

In addition to minimal toxicities, the combination of vaccination with BRAF inhibition has much to recommend it. Vaccine induction of $CD4^+$ T cell responses is advantageous for combination with BRAF inhibitor therapy. Previous reports of increased tumour infiltrating lymphocytes following BRAF inhibitor treatment have primarily demonstrated increased $CD8^+$ T cell infiltration (Frederick et al., 2013; Liu et al., 2013), with only one report of

increased $CD4^+$ T cell infiltration (Wilmott et al., 2012). Therefore, if vaccination is eliciting $CD4^+$ T cell anti-tumour responses, and BRAF inhibition drives $CD8^+$ T cell anti-tumour immunity, combining these therapies may induce a range of T cell effector responses against multiple independent epitopes, ensuring broad immune targeting of the tumour. This would be particularly beneficial when considering the propensity melanoma has for escaping anti-tumour immune responses, and for developing resistance to targeted therapies. Furthermore, the combination therapy approach devised in this thesis had the ability to achieve significant anti-tumour efficacy in a model that is resistant to BRAF inhibitor-induced cell death *in vivo*. This is an encouraging result, which demonstrates the potential of combination targeted BRAF inhibition with immunotherapy in overcoming therapy resistance.

7.2 Conclusions

In conclusion, the results presented in this thesis demonstrate that targeted BRAF inhibition, in the right conditions, can enhance T cell proliferation and activation, which translate into augmented antigen-specific T cell responses *in vivo*. In a tumour setting, BRAF inhibitor responses were shown to involve host immunity, demonstrating beneficial immunological effects of targeted BRAF inhibitors. Furthermore, BRAF inhibition reduced melanoma-mediated immune suppression implicating a role for BRAF inhibitors in creating a microenvironment more favourable to anti-tumour immunity. The development of a novel $CD4^+$ T cell-mediated, autologous tumour cell vaccine lead to a successful combination of active immunotherapy and targeted BRAF inhibition. The combination therapy approach devised in this study achieved significant anti-tumour efficacy in a model of BRAF inhibitor-resistant melanoma, an exciting finding that highlights the potential of combination BRAF inhibitor and immunotherapy to achieve improved outcomes for therapy-resistant patients.

7.3 Future Directions

The research in this thesis assessed immunological interactions of BRAF inhibitors and generated an autologous tumour cell vaccine and BRAF inhibitor combination therapy with significant anti-tumour efficacy in a therapy-resistant melanoma model. Below I outline experiments and strategies that may improve the specific approaches used in this study, and may benefit combination therapy approaches more broadly to achieve increased treatment efficacy in metastatic melanoma.

A key finding of this thesis was the requirement for host-mediated immunity in PLX4720 efficacy. Although it was demonstrated that PLX4720 does not enhance tumour infiltration by T cells, NK cells or cells of $CD11b^+$ lineage, further characterisation of the requirement for these cell subsets could be a productive question to address. This could be achieved by assessing anti-tumour efficacy of PLX4720 in mice deficient in the aforementioned cell subsets, either through antibody depletion or the use of knockout mice. Further understanding of the cell types involved in BRAF inhibitor responsiveness may facilitate development of improved combination therapy approaches.

In addition to further characterizing the cell types involved in the anti-tumour efficacy of BRAF inhibitors, the effects of BRAF inhibition on T cells could be explored in more detail. The effects of BRAF inhibitors on T cell proliferation and viability were assessed in Chapter 4, and these experiments revealed paradoxical effects of BRAF inhibition. T cell proliferation could be inhibited or augmented depending on the stimulus and drug concentration. To further understand the effects of BRAF inhibitors on T cells it would be of interest to perform experiments assessing effects on more functional parameters, such as specific killing and cytokine production.

The vaccine developed in this thesis elicited anti-tumour immune responses *in vivo*. However, these responses were only partially protective against established tumours, even when combined with targeted BRAF inhibition. There are several additional strategies that could be explored to enhance both

vaccine and combination therapy efficacy. Autologous tumour cells incorporated in the vaccine could be transduced to stably express CD1d. This would be expected to increase the amount of αGalCer associated with tumour cells, and would allow iNKT cells to directly recognize αGalCer presented by the tumour cells. Secondly, a prime-boost approach could be investigated. As αGalCer is cell-associated upon intravenous injection iNKT cells would be expected to remain responsive to a second vaccination. However, this would require testing and the optimal timing of a second vaccination would need to be assessed, especially in combination with BRAF inhibitors.

The impact of checkpoint blockade on the combination therapy regime devised in this thesis would also be of interest. There is significant risk of toxicity associated with α-CTLA-4 when combined with BRAF inhibitors. One potential approach to reduce toxicities would be to deliver minimal doses of checkpoint blockade antibody. In support of this, colleagues at the Malaghan Institute have recently demonstrated that delivery of a single dose of α-CTLA-4 in combination with an αGalCer-loaded tumour cell vaccine achieves long-term protection in a murine model of glioma (Cameron Field, personal communication). Additionally, other forms of checkpoint blockade therapy may result in less toxicity when combined with BRAF inhibition. As both PD-1 and PD-L1 are expressed in the tumour microenvironment in YUMM1.1 tumours, inhibitors of these checkpoints may prove most effective in this model. Additionally, investigation of newer checkpoint blockade therapies, such as α-LAG-3 or α-TIM-3, would be worthwhile as the differential expression of these targets will likely confer different efficacy and toxicity profiles that may make them more complementary for combination therapy.

Combining vaccination with chemotherapies other than PLX4720/Vemurafenib may also be worthwhile exploring. One alternative that would be interesting to investigate is second-generation BRAF inhibitors, such as PLX PB-3, which are currently in development. Early reports suggest these inhibitors do not induce paradoxical activation of the MAPK pathway, have higher specificity for mutant-BRAF and may overcome some mechanisms of acquired BRAF-inhibitor resistance (Dr Gideon Bollag, personal communication). Combining second-generation BRAF inhibitors

with immunotherapy may have important implications for both efficacy and toxicities. As well as considering next generation targeted chemotherapies for combination with vaccine, low-dose delivery of traditional cytotoxics, such as Cisplatin or Dacarbazine, could also be considered.

For future pre-clinical investigation of combination therapy approaches appropriate models must be used. Mouse models that recapitulate both the genetic mutations and therapy responsiveness of patients should be selected. On this basis, the YUMM1.1 and YUMM1.7 models are a good choice. Although it is difficult to achieve therapeutic benefit in such models, they more accurately represent clinical challenges. However, the use of an inducible, transgenic system with tumours growing in the tissue of origin would be ideal. This would require imaging technology to accurately monitor tumour responses to therapy. In such models it would also be pertinent to investigate tumour resection followed by therapy, to reflect clinical scenarios.

Ultimately, there is unlikely to be a single therapy or combination therapy regime that is effective for all patients. As the number of available therapeutic options increases the identification of molecular or genetic signatures to predict therapy responsiveness is going to be critical to improving patient outcomes. Stratification of patients with pre-existing anti-tumour immune responses may predict outcomes with BRAF inhibitor treatment and checkpoint blockade therapy. In patients with an absence of existing anti-tumour immunity an αGalCer-loaded, whole tumour cell vaccine in combination with either BRAF inhibition, checkpoint blockade therapy or both could conceivably be a highly effective therapeutic regime. Nevertheless, it should be emphasized that complex combination therapy regimes must be well grounded in pre-clinical evidence.

References

Alegre, M. L., Frauwirth, K. A., and Thompson, C. B. (2001). T-cell regulation by CD28 and CTLA-4. Nat Rev Immunol *1*, 220-228.

Amaravadi, R. K., Schuchter, L. M., McDermott, D. F., Kramer, A., Giles, L., Gramlich, K., Carberry, M., Troxel, A. B., Letrero, R., Nathanson, K. L., *et al.* (2009). Phase II Trial of Temozolomide and Sorafenib in Advanced Melanoma Patients with or without Brain Metastases. Clin Cancer Res *15*, 7711-7718.

Amarnath, S., Mangus, C. W., Wang, J. C., Wei, F., He, A., Kapoor, V., Foley, J. E., Massey, P. R., Felizardo, T. C., Riley, J. L., *et al.* (2011). The PDL1-PD1 axis converts human TH1 cells into regulatory T cells. Sci Transl Med *3*, 111ra120.
Anguille, S., Smits, E. L., Lion, E., van Tendeloo, V. F., and Berneman, Z. N. (2014). Clinical use of dendritic cells for cancer therapy. Lancet Oncology *15*, E257-E267.

Ascierto, P. A., Simeone, E., Giannarelli, D., Grimaldi, A. M., Romano, A., and Mozzillo, N. (2012). Sequencing of BRAF inhibitors and ipilimumab in patients with metastatic melanoma: a possible algorithm for clinical use. J Transl Med *10*, 107.

Atkins, M. B., Lotze, M. T., Dutcher, J. P., Fisher, R. I., Weiss, G., Margolin, K., Abrams, J., Sznol, M., Parkinson, D., Hawkins, M., *et al.* (1999). High-dose recombinant interleukin 2 therapy for patients with metastatic melanoma: Analysis of 270 patients treated between 1985 and 1993. Journal of Clinical Oncology *17*, 2105-2116.

Avruch, J., Khokhlatchev, A., Kyriakis, J. M., Luo, Z., Tzivion, G., Vavvas, D., and Zhang, X. F. (2001). Ras activation of the Raf kinase: tyrosine kinase recruitment of the MAP kinase cascade. Recent Prog Horm Res *56*, 127-155.

Baars, A., Claessen, A. M., van den Eertwegh, A. J., Gall, H. E., Stam, A. G., Meijer, S., Giaccone, G., Meijer, C. J., Scheper, R. J., Wagstaff, J., *et al.* (2000).

Skin tests predict survival after autologous tumor cell vaccination in metastatic melanoma: experience in 81 patients. Ann Oncol *11*, 965-970.

Balch, C. M., Gershenwald, J. E., Soong, S. J., Thompson, J. F., Atkins, M. B., Byrd, D. R., Buzaid, A. C., Cochran, A. J., Coit, D. G., Ding, S., *et al.* (2009). Final version of 2009 AJCC melanoma staging and classification. J Clin Oncol *27*, 6199-6206.

Becker, J. C., Houben, R., Schrama, D., Voigt, H., Ugurel, S., and Reisfeld, R. A. (2010). Mouse models for melanoma: a personal perspective. Exp Dermatol *19*, 157-164.

Beeram, M., Patnaik, A., and Rowinsky, E. K. (2005). Raf: a strategic target for therapeutic development against cancer. J Clin Oncol *23*, 6771-6790.

Berd, D., Sato, T., Maguire, H. C., Jr., Kairys, J., and Mastrangelo, M. J. (2004). Immunopharmacologic analysis of an autologous, hapten-modified human melanoma vaccine. J Clin Oncol *22*, 403-415.

Berridge, M. V., Herst, P. M., and Tan, A. S. (2005). Tetrazolium dyes as tools in cell biology: New insights into their cellular reduction. Biotechnology Annual Review *11*, 127-152.

Berridge, M. V., Tan, A. S., McCoy, K. D., and Wang, R. (1996). The biochemical and cellular basis of cell proliferation assays that use tetrazolium salts. Archiv Biochem Biophys *163*, 474–482

Bevan, M. J. (2004). Helping the CD8(+) T-cell response. Nat Rev Immunol *4*, 595-602.

Bilusic, M., and Gulley, J. L. (2012). Endpoints, patient selection, and biomarkers in the design of clinical trials for cancer vaccines. Cancer Immunol Immunother *61*, 109-117.

Birck, A., Ahrenkiel, V., Zeuthen, J., Hou-Jensen, K., and Guldberg, P. (2000). Mutation and allelic loss of the PTEN/MMAC1 gene in primary and metastatic melanoma biopsies. J Invest Dermatol *114*, 277-280.

Biselli, R., Matricardi, P. M., D'Amelio, R., and Fattorossi, A. (1992). Multiparametric flow cytometric analysis of the kinetics of surface molecule expression after polyclonal activation of human peripheral blood T lymphocytes. Scand J Immunol *35*, 439-447.

Bogunovic, D., O'Neill, D. W., Belitskaya-Levy, I., Vacic, V., Yu, Y. L., Adams, S., Darvishian, F., Berman, R., Shapiro, R., Pavlick, A. C., *et al.* (2009). Immune profile and mitotic index of metastatic melanoma lesions enhance clinical staging in predicting patient survival. Proc Natl Acad Sci U S A *106*, 20429-20434.

Boisguerin, V., Castle, J. C., Loewer, M., Diekmann, J., Mueller, F., Britten, C. M., Kreiter, S., Tureci, O., and Sahin, U. (2014). Translation of genomics-guided RNA-based personalised cancer vaccines: towards the bedside. Br J Cancer *111*, 1469-1475.

Bollag, G., Hirth, P., Tsai, J., Zhang, J., Ibrahim, P. N., Cho, H., Spevak, W., Zhang, C., Zhang, Y., Habets, G., *et al.* (2010). Clinical efficacy of a RAF inhibitor needs broad target blockade in BRAF-mutant melanoma. Nature *467*, 596-599.

Bollag, G., Tsai, J., Zhang, J., Zhang, C., Ibrahim, P., Nolop, K., and Hirth, P. (2012). Vemurafenib: the first drug approved for BRAF-mutant cancer. Nat Rev Drug Discov *11*, 873-886.

Boni, A., Cogdill, A. P., Dang, P., Udayakumar, D., Njauw, C. N., Sloss, C. M., Ferrone, C. R., Flaherty, K. T., Lawrence, D. P., Fisher, D. E., *et al.* (2010). Selective BRAFV600E inhibition enhances T-cell recognition of melanoma without affecting lymphocyte function. Cancer Res *70*, 5213-5219.

Boomer, J. S., and Green, J. M. (2010). An enigmatic tail of CD28 signaling. Cold Spring Harb Perspect Biol *2*, a002436.

Boon, T., and Van Pel, A. (1978). Teratocarcinoma cell variants rejected by syngeneic mice: protection of mice immunized with these variants against other variants and against the original malignant cell line. Proc Natl Acad Sci *75*, 1519-1523 .

Bosenberg, M., Muthusamy, V., Curley, D. P., Wang, Z., Hobbs, C., Nelson, B., Nogueira, C., Horner, J. W., 2nd, Depinho, R., and Chin, L. (2006). Characterization of melanocyte-specific inducible Cre recombinase transgenic mice. Genesis *44*, 262-267.

Budhu, S., Wolchok, J., and Merghoub, T. (2014). The importance of animal models in tumor immunity and immunotherapy. Curr Opin Genet Dev *24*, 46-51.

Burnet, F. M. (1970). The concept of immunological surveillance. Prog Exp Tumor Res *13*, 1-27.

Butterfield, L. H. (2015). Cancer vaccines. BMJ *350*, h988.

Callahan, M. K., Masters, G., Pratilas, C. A., Ariyan, C., Katz, J., Kitano, S., Russell, V., Gordon, R. A., Vyas, S., Yuan, J., *et al.* (2014). Paradoxical activation of T cells via augmented ERK signaling mediated by a RAF inhibitor. Cancer Immunol Res *2*, 70-79.

Cardell, S., Tangri, S., Chan, S., Kronenberg, M., Benoist, C., and Mathis, D. (1995). CD1-restricted CD4+ T cells in major histocompatibility complex class II-deficient mice. J Exp Med *182*, 993-1004.

Carreno, B. M., Magrini, V., Becker-Hapak, M., Kaabinejadian, S., Hundal, J., Petti, A. A., Ly, A., Lie, W. R., Hildebrand, W. H., Mardis, E. R., and Linette, G. P. (2015). Cancer immunotherapy. A dendritic cell vaccine increases the

breadth and diversity of melanoma neoantigen-specific T cells. Science *348*, 803-808.

Cerundolo, V., Silk, J. D., Masri, S. H., and Salio, M. (2009). Harnessing invariant NKT cells in vaccination strategies. *9*, 28-38.

Chang, D. H., Osman, K., Connolly, J., Kukreja, A., Krasovsky, J., Pack, M., Hutchinson, A., Geller, M., Liu, N., Annable, R., *et al.* (2005). Sustained expansion of NKT cells and antigen-specific T cells after injection of alpha-galactosyl-ceramide loaded mature dendritic cells in cancer patients. J Exp Med *201*, 1503-1517.

Chapman, P. B. (2013). Mechanisms of resistance to RAF inhibition in melanomas harboring a BRAF mutation. Am Soc Clin Oncol Educ Book.
Chapman, P. B., Hauschild, A., Robert, C., Haanen, J. B., Ascierto, P., Larkin, J., Dummer, R., Garbe, C., Testori, A., Maio, M., *et al.* (2011). Improved survival with vemurafenib in melanoma with BRAF V600E mutation. N Engl J Med *364*, 2507-2516.

Chen, B., Tardell, C., Higgins, B., Packman, K., Boylan, J. F., and Niu, H. (2012). BRAFV600E negatively regulates the AKT pathway in melanoma cell lines. PLoS One *7*, e42598.

Chomez, P., De Backer, O., Bertrand, M., De Plaen, E., Boon, T., and Lucas, S. (2001). An overview of the MAGE gene family with the identification of all human members of the family. Cancer Res *61*, 5544-5551.

Chong, H., Vikis, H. G., and Guan, K. L. (2003). Mechanisms of regulating the Raf kinase family. Cell Signal *15*, 463-469.

Chung, Y., Qin, H., Kang, C. Y., Kim, S., Kwak, L. W., and Dong, C. (2007). An NKT-mediated autologous vaccine generates CD4 T-cell dependent potent antilymphoma immunity. Blood *110*, 2013-2019.

Coley, W. B. (1893). The treatment of malignant tumors by repeated inoculations of erysipelas: with a report of ten original cases. Am J Med Sci *105*, 487-510.

Coley, W. B. (1910). The Treatment of Inoperable Sarcoma by Bacterial Toxins (the Mixed Toxins of the Streptococcus erysipelas and the Bacillus prodigiosus). Proc R Soc Med *3*, 1-48.

Comin-Anduix, B., Chodon, T., Sazegar, H., Matsunaga, D., Mock, S., Jalil, J., Escuin-Ordinas, H., Chmielowski, B., Koya, R. C., and Ribas, A. (2010). The oncogenic BRAF kinase inhibitor PLX4032/RG7204 does not affect the viability or function of human lymphocytes across a wide range of concentrations. Clin Cancer Res *16*, 6040-6048.

Comis, R. L. (1976). DTIC (NSC-45388) in malignant melanoma: a perspective. Cancer Treat Rep *60*, 165-176.

Cooper, Z. A., Juneja, V. R., Sage, P. T., Frederick, D. T., Piris, A., Mitra, D., Lo, J. A., Hodi, F. S., Freeman, G. J., Bosenberg, M. W., *et al.* (2014). Response to BRAF inhibition in melanoma is enhanced when combined with immune checkpoint blockade. Cancer Immunol Res *2*, 643-654.

Corthay, A., Skovseth, D. K., Lundin, K. U., Rosjo, E., Omholt, H., Hofgaard, P. O., Haraldsen, G., and Bogen, B. (2005). Primary antitumor immune response mediated by CD4+ T cells. Immunity *22*, 371-383.

Coulie, P. G., Van den Eynde, B. J., van der Bruggen, P., and Boon, T. (2014). Tumour antigens recognized by T lymphocytes: at the core of cancer immunotherapy. Nat Rev Cancer *14*, 135-146.

Croce, C. M. (2008). Oncogenes and cancer. N Engl J Med *358*, 502-511.

Curtin, J. A., Fridlyand, J., Kageshita, T., Patel, H. N., Busam, K. J., Kutzner, H., Cho, K.-H., Aiba, S., Bröcker, E.-B., LeBoit, P. E., *et al.* (2005). Distinct sets of genetic alterations in melanoma. *353*, 2135-2147.

Curtsinger, J. M., Schmidt, C. S., Mondino, A., Lins, D. C., Kedl, R. M., Jenkins, M. K., and Mescher, M. F. (1999). Inflammatory cytokines provide a third signal for activation of naive CD4+ and CD8+ T cells. J Immunol *162*, 3256-3262.

da Rocha Dias, S., Salmonson, T., van Zwieten-Boot, B., Jonsson, B., Marchetti, S., Schellens, J., Giuliani, R., and Pignatti, F. (2013). The European Medicines Agency review of vemurafenib (Zelboraf®) for the treatment of adult patients with BRAF V600 mutation-positive unresectable or metastatic melanoma: summary of the scientific assessment of the Committee for Medicinal Products for Human Use. Eur J Cancer *49*, 1654-1661.

Dankort, D., Curley, D. P., Cartlidge, R. A., Nelson, B., Karnezis, A. N., Damsky, W. E., Jr., You, M. J., DePinho, R. A., McMahon, M., and Bosenberg, M. (2009). Braf(V600E) cooperates with Pten loss to induce metastatic melanoma. Nat Genet *41*, 544-552.

Dankort, D., Filenova, E., Collado, M., Serrano, M., Jones, K., and McMahon, M. (2007). A new mouse model to explore the initiation, progression, and therapy of BRAFV600E-induced lung tumors. Genes Dev *21*, 379-384.

Dardalhon, V., Awasthi, A., Kwon, H., Galileos, G., Gao, W., Sobel, R. A., Mitsdoerffer, M., Strom, T. B., Elyaman, W., Ho, I. C., *et al.* (2008). IL-4 inhibits TGF-beta-induced Foxp3+ T cells and, together with TGF-beta, generates IL-9+ IL-10+ Foxp3(-) effector T cells. Nat Immunol *9*, 1347-1355.

Daum, G., Eisenmann-Tappe, I., Fries, H. W., Troppmair, J., and Rapp, U. R. (1994). The ins and outs of Raf kinases. Trends Biochem Sci *19*, 474-480.

Davies, H., Bignell, G. R., Cox, C., Stephens, P., Edkins, S., Clegg, S., Teague, J., Woffendin, H., Garnett, M. J., Bottomley, W., *et al.* (2002). Mutations of the BRAF gene in human cancer. Nature *417*, 949-954.

de Gruijl, T. D., van den Eertwegh, A. J., Pinedo, H. M., and Scheper, R. J. (2008). Whole-cell cancer vaccination: from autologous to allogeneic tumor- and dendritic cell-based vaccines. Cancer Immunol Immunother *57*, 1569-1577.

DeGrendele, H. C., Estess, P., and Siegelman, M. H. (1997). Requirement for CD44 in activated T cell extravasation into an inflammatory site. Science *278*, 672-675.

Delamarre, L., Mellman, I., and Yadav, M. (2015). Cancer immunotherapy. Neo approaches to cancer vaccines. Science *348*, 760-761.

Deng, W., Gopal, Y. N., Scott, A., Chen, G., Woodman, S. E., and Davies, M. A. (2012). Role and therapeutic potential of PI3K-mTOR signaling in de novo resistance to BRAF inhibition. Pigment Cell Melanoma Res *25*, 248-258.

Dezfouli, S., Hatzinisiriou, I., and Ralph, S. J. (2003). Enhancing CTL responses to melanoma cell vaccines in vivo: synergistic increases obtained using IFNgamma primed and IFNbeta treated B7-1+ B16-F10 melanoma cells. Immunol Cell Biol *81*, 459-471.

Diamond, M. S., Kinder, M., Matsushita, H., Mashayekhi, M., Dunn, G. P., Archambault, J. M., Lee, H., Arthur, C. D., White, J. M., Kalinke, U., *et al.* (2011). Type I interferon is selectively required by dendritic cells for immune rejection of tumors. J Exp Med *208*, 1989-2003.

Diaz-Valdes, N., Basagoiti, M., Dotor, J., Aranda, F., Monreal, I., Riezu-Boj, J. I., Borras-Cuesta, F., Sarobe, P., and Feijoo, E. (2011). Induction of monocyte chemoattractant protein-1 and interleukin-10 by TGFbeta1 in melanoma enhances tumor infiltration and immunosuppression. Cancer Res *71*, 812-821.

Donia, M., Fagone, P., and Nicoletti, F. (2012a). BRAF inhibition improves tumor recognition by the immune system. Oncoimmuno *1*, 1476-1483

Donia, M., Fagone, P., Nicoletti, F., Andersen, R. S., Hogdall, E., Straten, P. T., Andersen, M. H., and Svane, I. M. (2012b). BRAF inhibition improves tumor recognition by the immune system: Potential implications for combinatorial therapies against melanoma involving adoptive T-cell transfer. Oncoimmunology *1*, 1476-1483.

Dranoff, G., Jaffee, E., Lazenby, A., Golumbek, P., Levitsky, H., Brose, K., Jackson, V., Hamada, H., Pardoll, D., and Mulligan, R. C. (1993). Vaccination with irradiated tumor cells engineered to secrete murine granulocyte-macrophage colony-stimulating factor stimulates potent, specific, and long-lasting anti-tumor immunity. Proc Natl Acad Sci U S A *90*, 3539-3543.

Dudek, A. M., Martin, S., Garg, A. D., and Agostinis, P. (2013). Immature, Semi-Mature, and Fully Mature Dendritic Cells: Toward a DC-Cancer Cells Interface That Augments Anticancer Immunity. Front Immunol *4*.

Dunn, G. P., Bruce, A. T., Ikeda, H., Old, L. J., and Schreiber, R. D. (2002). Cancer immunoediting: from immunosurveillance to tumor escape. Nat Immunol *3*, 991-998.

Dunn, G. P., Koebel, C. M., and Schreiber, R. D. (2006). Interferons, immunity and cancer immunoediting. Nat Rev Immunol *6*, 836-848.

Dunn, G. P., Old, L. J., and Schreiber, R. D. (2004). The three Es of cancer immunoediting. Annu Rev Immunol *22*, 329-360.

Eggermont, A. M. (2010). Advances in systemic treatment of melanoma. Ann Oncol *21 Suppl 7*, vii339-344.

Eisen, T., Ahmad, T., Flaherty, K. T., Gore, M., Kaye, S., Marais, R., Gibbens, I., Hackett, S., James, M., Schuchter, L. M., *et al.* (2006). Sorafenib in advanced melanoma: a Phase II randomised discontinuation trial analysis. Br J Cancer *95*, 581-586.

FDA (2011). Center for Drug Evaluation and ResearchVemurafenib Summary Review In, F.a.D. Administration, ed., pp. 1-17.

Fecher, L. A., Amaravadi, R. K., and Flaherty, K. T. (2008). The MAPK pathway in melanoma. Curr Opin Oncol *20*, 183-189.

Fedorenko, I. V., Wargo, J. A., Flaherty, K. T., Messina, J. L., and Smalley, K. S. (2015). BRAF Inhibition Generates a Host-Tumor Niche that Mediates Therapeutic Escape. J Invest Dermatol, *135(12)*, 3115-3214.

Feng, H., Zeng, Y., Graner, M. W., and Katsanis, E. (2002). Stressed apoptotic tumor cells stimulate dendritic cells and induce specific cytotoxic T cells. Blood *100*, 4108-4115.

Ferrari de Andrade, L., Ngiow, S. F., Stannard, K., Rusakiewicz, S., Kalimutho, M., Khanna, K. K., Tey, S. K., Takeda, K., Zitvogel, L., Martinet, L., and Smyth, M. J. (2014). Natural killer cells are essential for the ability of BRAF inhibitors to control BRAFV600E-mutant metastatic melanoma. Cancer Res *74*, 7298-7308.

Filitis, D. C., Rauh, J., and Mahalingam, M. (2015). The HGF-cMET signaling pathway in conferring stromal-induced BRAF-inhibitor resistance in melanoma. Melanoma Res *25(6)*, 470-478.

Finn, O. J. (2003). Cancer vaccines: between the idea and the reality. Nat Rev Immunol *3*, 630-641.

Fisk, B., Blevins, T. L., Wharton, J. T., and Ioannides, C. G. (1995). Identification of an immunodominant peptide of HER-2/neu protooncogene recognized by ovarian tumor-specific cytotoxic T lymphocyte lines. J Exp Med *181*, 2109-2117.

Fisk, B., and Ioannides, C. G. (1998). Increased sensitivity of adriamycin-selected tumor lines to CTL-mediated lysis results in enhanced drug sensitivity. Cancer Res *58*, 4790-4793.

Flaherty, K. T., and McArthur, G. (2010). BRAF, a target in melanoma: implications for solid tumor drug development. Cancer *116*, 4902-4913.
Flaherty, K. T., Puzanov, I., Kim, K. B., Ribas, A., McArthur, G. A., Sosman, J. A., O'Dwyer, P. J., Lee, R. J., Grippo, J. F., Nolop, K., and Chapman, P. B. (2010). Inhibition of mutated, activated BRAF in metastatic melanoma. N Engl J Med *363*, 809-819.

Fong, T. A., and Mosmann, T. R. (1990). Alloreactive murine CD8+ T cell clones secrete the Th1 pattern of cytokines. J Immunol *144*, 1744-1752.

Fontenot, J. D., Rasmussen, J. P., Williams, L. M., Dooley, J. L., Farr, A. G., and Rudensky, A. Y. (2005). Regulatory T cell lineage specification by the forkhead transcription factor foxp3. Immunity *22*, 329-341.

Francisco, L. M., Salinas, V. H., Brown, K. E., Vanguri, V. K., Freeman, G. J., Kuchroo, V. K., and Sharpe, A. H. (2009). PD-L1 regulates the development, maintenance, and function of induced regulatory T cells. J Exp Med *206*, 3015-3029.

Frederick, D. T., Piris, A., Cogdill, A. P., Cooper, Z. A., Lezcano, C., Ferrone, C. R., Mitra, D., Boni, A., Newton, L. P., Liu, C., *et al.* (2013). BRAF inhibition is associated with enhanced melanoma antigen expression and a more favorable tumor microenvironment in patients with metastatic melanoma. Clin Cancer Res *19*, 1225-1231.

Fries, W., Muja, C., Crisafulli, C., Cuzzocrea, S., and Mazzon, E. (2008). Dynamics of enterocyte tight junctions: effect of experimental colitis and two different anti-TNF strategies. Am J Physiol Gastrointest Liver Physiol *294*, G938-947.

Fuertes, M. B., Kacha, A. K., Kline, J., Woo, S. R., Kranz, D. M., Murphy, K. M., and Gajewski, T. F. (2011). Host type I IFN signals are required for antitumor CD8+ T cell responses through CD8{alpha}+ dendritic cells. J Exp Med *208*, 2005-2016.

Fujii, S., Shimizu, K., Kronenberg, M., and Steinman, R. M. (2002). Prolonged IFN-gamma-producing NKT response induced with alpha-galactosylceramide-loaded DCs. Nat Immunol *3*, 867-874.

Fujii, S., Shimizu, K., Smith, C., Bonifaz, L., and Steinman, R. M. (2003). Activation of natural killer T cells by alpha-galactosylceramide rapidly induces the full maturation of dendritic cells in vivo and thereby acts as an adjuvant for combined CD4 and CD8 T cell immunity to a coadministered protein. J Exp Med *198*, 267-279.

Funck-Brentano, E., Alvarez, J. C., Longvert, C., Abe, E., Beauchet, A., Funck-Brentano, C., and Saiag, P. (2015). Plasma vemurafenib concentrations in advanced BRAFV600mut melanoma patients: impact on tumour response and tolerance. Ann Oncol *26*, 1470-1475.

Gameiro, S. R., Caballero, J. A., Higgins, J. P., Apelian, D., and Hodge, J. W. (2011). Exploitation of differential homeostatic proliferation of T-cell subsets following chemotherapy to enhance the efficacy of vaccine-mediated antitumor responses. Cancer Immunol Immunother *60*, 1227-1242.

Gargett, T., Fraser, C. K., Dotti, G., Yvon, E. S., and Brown, M. P. (2015). BRAF and MEK inhibition variably affect GD2-specific chimeric antigen receptor (CAR) T-cell function in vitro. J Immunother *38*, 12-23.

Genovese, T., Mazzon, E., Crisafulli, C., Di Paola, R., Muia, C., Bramanti, P., and Cuzzocrea, S. (2006). Immunomodulatory effects of etanercept in an experimental model of spinal cord injury. J Pharmacol Exp Ther *316*, 1006-1016.

Gershon, R. K., and Kondo, K. (1970). Cell interactions in the induction of tolerance: the role of thymic lymphocytes. Immunology *18*, 723-737.

Giampietri, A., Bonmassar, A., Puccetti, P., Circolo, A., Goldin, A., and Bonmassar, E. (1981). Drug-mediated increase of tumor immunogenicity in

vivo for a new approach to experimental cancer immunotherapy. Cancer Res *41*, 681-687.

Gibbins, J. D., Ancelet, L. R., Weinkove, R., Compton, B. J., Painter, G. F., Petersen, T. R., and Hermans, I. F. (2014). An autologous leukemia cell vaccine prevents murine acute leukemia relapse after cytarabine treatment. Blood *124*, 2953-2963.

Giblin, A. V., and Thomas, J. M. (2007). Incidence, mortality and survival in cutaneous melanoma. J Plast Reconstr Aesthet Surg *60*, 32-40.

Gibney, G. T., Messina, J. L., Fedorenko, I. V., Sondak, V. K., and Smalley, K. S. (2013). Paradoxical oncogenesis--the long-term effects of BRAF inhibition in melanoma. Nat Rev Clin Oncol *10*, 390-399.

Goel, V. K., Ibrahim, N., Jiang, G., Singhal, M., Fee, S., Flotte, T., Westmoreland, S., Haluska, F. S., Hinds, P. W., and Haluska, F. G. (2009). Melanocytic nevus-like hyperplasia and melanoma in transgenic BRAFV600E mice. Oncogene *28*, 2289-2298.

Gorelik, E., Rosen, B., Copeland, D., Weatherly, B., and Herberman, R. B. (1984). Evaluation of role of natural killer cells in radiation-induced leukemogenesis in mice. J Natl Cancer Inst *72*, 1397-1403.

Gray-Schopfer, V. C., Karasarides, M., Hayward, R., and Marais, R. (2007). Tumor necrosis factor-alpha blocks apoptosis in melanoma cells when BRAF signaling is inhibited. Cancer Res *67*, 122-129.

Greenberg, P. D. (1986). Therapy of murine leukemia with cyclophosphamide and immune Lyt-2+ cells: cytolytic T cells can mediate eradication of disseminated leukemia. J Immunol *136*, 1917-1922.

Groh, V., Wu, J., Yee, C., and Spies, T. (2002). Tumour-derived soluble MIC ligands impair expression of NKG2D and T-cell activation. Nature *419*, 734-738.

Gross, L. (1943). Intradermal immunization of C3H mice against a sarcoma that originated in an animal of the same line. Cancer Res 326-333.

Grusby, M. J., Johnson, R. S., Papaioannou, V. E., and Glimcher, L. H. (1991). Depletion of CD4+ T cells in major histocompatibility complex class II-deficient mice. Science *253*, 1417-1420.

Haabeth, O., Tveita, A. A., and Fauskanger, M. (2014). How do CD4+ T cells detect and eliminate tumor cells that either lack or express MHC class II molecules? Front Immunol *5*.

Halaban, R., Zhang, W., Bacchiocchi, A., Cheng, E., Parisi, F., Ariyan, S., Krauthammer, M., McCusker, J. P., Kluger, Y., and Sznol, M. (2010). PLX4032, a selective BRAF(V600E) kinase inhibitor, activates the ERK pathway and enhances cell migration and proliferation of BRAF melanoma cells. Pigment Cell Melanoma Res *23*, 190-200.

Hamid, O., Robert, C., Daud, A., Hodi, F. S., Hwu, W. J., Kefford, R., Wolchok, J. D., Hersey, P., Joseph, R. W., Weber, J. S., *et al.* (2013). Safety and tumor responses with lambrolizumab (anti-PD-1) in melanoma. N Engl J Med *369*, 134-144.

Hatzivassiliou, G., Song, K., Yen, I., Brandhuber, B. J., Anderson, D. J., Alvarado, R., Ludlam, M. J., Stokoe, D., Gloor, S. L., Vigers, G., *et al.* (2010). RAF inhibitors prime wild-type RAF to activate the MAPK pathway and enhance growth. Nature *464*, 431-435.

Heemskerk, B., Kvistborg, P., and Schumacher, T. N. (2013). The cancer antigenome. EMBO J *32*, 194-203.

Heidorn, S. J., Milagre, C., Whittaker, S., Nourry, A., Niculescu-Duvas, I., Dhomen, N., Hussain, J., Reis-Filho, J. S., Springer, C. J., Pritchard, C., and Marais, R. (2010). Kinase-dead BRAF and oncogenic RAS cooperate to drive tumor progression through CRAF. Cell *140*, 209-221.

Herberman, R. B., Nunn, M. E., Holden, H. T., and Lavrin, D. H. (1975a). Natural cytotoxic reactivity of mouse lymphoid cells against syngeneic and allogeneic tumors. II. Characterization of effector cells. Int J Cancer *16*, 230-239.

Herberman, R. B., Nunn, M. E., and Lavrin, D. H. (1975b). Natural cytotoxic reactivity of mouse lymphoid cells against syngeneic acid allogeneic tumors. I. Distribution of reactivity and specificity. Int J Cancer *16*, 216-229.

Hermans, I. F., Chong, T. W., Palmowski, M. J., Harris, A. L., and Cerundolo, V. (2003a). Synergistic effect of metronomic dosing of cyclophosphamide combined with specific antitumor immunotherapy in a murine melanoma model. Cancer Res *63*, 8408-8413.

Hermans, I. F., Silk, J. D., Gileadi, U., Salio, M., Mathew, B., Ritter, G., Schmidt, R., Harris, A. L., Old, L., and Cerundolo, V. (2003b). NKT Cells Enhance CD4+ and CD8+ T Cell Responses to Soluble Antigen In Vivo through Direct Interaction with Dendritic Cells. J Immunol.

Hirata, E., Girotti, M. R., Viros, A., Hooper, S., Spencer-Dene, B., Matsuda, M., Larkin, J., Marais, R., and Sahai, E. (2015). Intravital imaging reveals how BRAF inhibition generates drug-tolerant microenvironments with high integrin beta1/FAK signaling. Cancer Cell *27*, 574-588.

Ho, P. C., Meeth, K. M., Tsui, Y. C., Srivastava, B., Bosenberg, M. W., and Kaech, S. M. (2014). Immune-based antitumor effects of BRAF inhibitors rely on signaling by CD40L and IFNgamma. Cancer Res *74*, 3205-3217.

Hodi, F. S., O'Day, S. J., McDermott, D. F., Weber, R. W., Sosman, J. A., Haanen, J. B., Gonzalez, R., Robert, C., Schadendorf, D., Hassel, J. C., *et al.* (2010). Improved survival with ipilimumab in patients with metastatic melanoma. N Engl J Med *363*, 711-723.

Hodis, E., Watson, I. R., Kryukov, G. V., Arold, S. T., Imielinski, M., Theurillat, J. P., Nickerson, E., Auclair, D., Li, L., Place, C., *et al.* (2012). A landscape of driver mutations in melanoma. Cell *150*, 251-263.

Hoeflich, K. P., Gray, D. C., Eby, M. T., Tien, J. Y., Wong, L., Bower, J., Gogineni, A., Zha, J., Cole, M. J., Stern, H. M., *et al.* (2006). Oncogenic BRAF is required for tumor growth and maintenance in melanoma models. Cancer Res *66*, 999-1006.

Hogquist, K. A., Jameson, S. C., Heath, W. R., Howard, J. L., Bevan, M. J., and Carbone, F. R. (1994). T cell receptor antagonist peptides induce positive selection. Cell *76*, 17-27.

Hooijkaas, A., Gadiot, J., Morrow, M., Stewart, R., Schumacher, T., and Blank, C. U. (2012a). Selective BRAF inhibition decreases tumor-resident lymphocyte frequencies in a mouse model of human melanoma. Oncoimmunology *1*, 609-617.

Hooijkaas, A. I., Gadiot, J., van der Valk, M., Mooi, W. J., and Blank, C. U. (2012b). Targeting BRAFV600E in an inducible murine model of melanoma. Am J Pathol *181*, 785-794.

Hu-Lieskovan, S., Mok, S., Homet Moreno, B., Tsoi, J., Robert, L., Goedert, L., Pinheiro, E. M., Koya, R. C., Graeber, T. G., Comin-Anduix, B., and Ribas, A. (2015). Improved antitumor activity of immunotherapy with BRAF and MEK inhibitors in BRAF(V600E) melanoma. Sci Transl Med *7*, 279ra241.

Hudson, W. A., Li, Q., Le, C., and Kersey, J. H. (1998). Xenotransplantation of human lymphoid malignancies is optimized in mice with multiple immunologic defects. Leukemia *12*, 2029-2033.

Hung, K., Hayashi, R., Lafond-Walker, A., Lowenstein, C., Pardoll, D., and Levitsky, H. (1998). The central role of CD4(+) T cells in the antitumor immune response. J Exp Med *188*, 2357-2368.

Hunn, M. K., Farrand, K. J., Broadley, K. W., Weinkove, R., Ferguson, P., Miller, R. J., Field, C. S., Petersen, T., McConnell, M. J., and Hermans, I. F. (2012). Vaccination with irradiated tumor cells pulsed with an adjuvant that stimulates NKT cells is an effective treatment for glioma. Clin Cancer Res *18*, 6446-6459.

Ibarrondo, F. J., Yang, O. O., Chodon, T., Avramis, E., Lee, Y., Sazegar, H., Jalil, J., Chmielowski, B., Koya, R. C., Schmid, I., *et al.* (2013). Natural killer T cells in advanced melanoma patients treated with tremelimumab. PLoS One *8*, e76829.

Ilieva, K. M., Correa, I., Josephs, D. H., Karagiannis, P., Egbuniwe, I. U., Cafferkey, M. J., Spicer, J. F., Harries, M., Nestle, F. O., Lacy, K. E., and Karagiannis, S. N. (2014). Effects of BRAF mutations and BRAF inhibition on immune responses to melanoma. Mol Cancer Ther *13*, 2769-2783.

Irving, B. A., Cheung, J., Yang, Y., Moskalenka, M., Kowanetz, M., Maecker, H., and Mellman, I. (2013). MAP kinase inhibitors stimulate T cell and anti-tumor activity in combination with blockade of the PD-L1/PD-1 interaction. Journal for ImmunoTherapy of Cancer *1*, P79.

Ito, M., Hiramatsu, H., Kobayashi, K., Suzue, K., Kawahata, M., Hioki, K., Ueyama, Y., Koyanagi, Y., Sugamura, K., Tsuji, K., *et al.* (2002). NOD/SCID/gamma(c)(null) mouse: an excellent recipient mouse model for engraftment of human cells. Blood *100*, 3175-3182.

Iyoda, T., Shimoyama, S., Liu, K., Omatsu, Y., Akiyama, Y., Maeda, Y., Takahara, K., Steinman, R. M., and Inaba, K. (2002). The CD8+ dendritic cell subset selectively endocytoses dying cells in culture and in vivo. J Exp Med *195*, 1289-1302.

Jaiswal, R. K., Weissinger, E., Kolch, W., and Landreth, G. E. (1996). Nerve growth factor-mediated activation of the mitogen-activated protein (MAP) kinase cascade involves a signaling complex containing B-Raf and HSP90. J Biol Chem *271*, 23626-23629.

Janetzki, S., Palla, D., Rosenhauer, V., Lochs, H., Lewis, J. J., and Srivastava, P. K. (2000). Immunization of cancer patients with autologous cancer-derived heat shock protein gp96 preparations: a pilot study. Int J Cancer *88*, 232-238.

Jilaveanu, L. B., Aziz, S. A., and Kluger, H. M. (2009). Chemotherapy and biologic therapies for melanoma: do they work? Clin Dermatol *27*, 614-625.

Johannessen, C. M., Boehm, J. S., Kim, S. Y., Thomas, S. R., Wardwell, L., Johnson, L. A., Emery, C. M., Stransky, N., Cogdill, A. P., Barretina, J., *et al.* (2010). COT drives resistance to RAF inhibition through MAP kinase pathway reactivation. Nature *468*, 968-972.

Joseph, E. W., Pratilas, C. A., Poulikakos, P. I., Tadi, M., Wang, W., Taylor, B. S., Halilovic, E., Persaud, Y., Xing, F., Viale, A., *et al.* (2010). The RAF inhibitor PLX4032 inhibits ERK signaling and tumor cell proliferation in a V600E BRAF-selective manner. Proc Natl Acad Sci U S A *107*, 14903-14908.

Junttila, M. R., and de Sauvage, F. J. (2013). Influence of tumour micro-environment heterogeneity on therapeutic response. Nature *501*, 346-354.

Kaech, S. M., and Wherry, E. J. (2007). Heterogeneity and cell-fate decisions in effector and memory CD8+ T cell differentiation during viral infection. Immunity *27*, 393-405.

Kaech, S. M., Wherry, E. J., and Ahmed, R. (2002). Effector and memory T-cell differentiation: implications for vaccine development. Nat Rev Immunol *2*, 251-262.

Kagi, D., and Hengartner, H. (1996). Different roles for cytotoxic T cells in the control of infections with cytopathic versus noncytopathic viruses. Curr Opin Immunol *8*, 472-477.

Kagi, D., Ledermann, B., Burki, K., Seiler, P., Odermatt, B., Olsen, K. J., Podack, E. R., Zinkernagel, R. M., and Hengartner, H. (1994). Cytotoxicity

mediated by T cells and natural killer cells is greatly impaired in perforin-deficient mice. Nature *369*, 31-37.

Kagi, D., Ledermann, B., Burki, K., Zinkernagel, R. M., and Hengartner, H. (1996). Molecular mechanisms of lymphocyte-mediated cytotoxicity and their role in immunological protection and pathogenesis in vivo. Annu Rev Immunol *14*, 207-232.

Kaneno, R., Shurin, G. V., Kaneno, F. M., Naiditch, H., Luo, J., and Shurin, M. R. (2011). Chemotherapeutic agents in low noncytotoxic concentrations increase immunogenicity of human colon cancer cells. Cell Oncol (Dordr) *34*, 97-106.

Karre, K., Ljunggren, H. G., Piontek, G., and Kiessling, R. (1986). Selective rejection of H-2-deficient lymphoma variants suggests alternative immune defence strategy. Nature *319*, 675-678.

Kawakami, Y., Eliyahu, S., Delgado, C. H., Robbins, P. F., Rivoltini, L., Topalian, S. L., Miki, T., and Rosenberg, S. A. (1994). Cloning of the gene coding for a shared human melanoma antigen recognized by autologous T cells infiltrating into tumor. Proc Natl Acad Sci U S A *91*, 3515-3519.

Kawano, T., Cui, J., Koezuka, Y., Toura, I., Kaneko, Y., Motoki, K., Ueno, H., Nakagawa, R., Sato, H., Kondo, E.*, et al.* (1997). CD1d-restricted and TCR-mediated activation of valpha14 NKT cells by glycosylceramides. Science *278*, 1626-1629.

Killion, J. J., Radinsky, R., and Fidler, I. J. (1998). Orthotopic models are necessary to predict therapy of transplantable tumors in mice. Cancer Metastasis Rev *17*, 279-284.

Klages, K., Mayer, C. T., Lahl, K., Loddenkemper, C., Teng, M. W., Ngiow, S. F., Smyth, M. J., Hamann, A., Huehn, J., and Sparwasser, T. (2010). Selective depletion of Foxp3+ regulatory T cells improves effective therapeutic vaccination against established melanoma. Cancer Res *70*, 7788-7799.

Knight, D. A., Ngiow, S. F., Li, M., Parmenter, T., Mok, S., Cass, A., Haynes, N. M., Kinross, K., Yagita, H., Koya, R. C., *et al.* (2013). Host immunity contributes to the anti-melanoma activity of BRAF inhibitors. J Clin Invest *123*, 1371-1381.

Koebel, C. M., Vermi, W., Swann, J. B., Zerafa, N., Rodig, S. J., Old, L. J., Smyth, M. J., and Schreiber, R. D. (2007). Adaptive immunity maintains occult cancer in an equilibrium state. Nature *450*, 903-907.

Kolch, W. (2000). Meaningful relationships: the regulation of the Ras/Raf/MEK/ERK pathway by protein interactions. Biochem J *351 Pt 2*, 289-305.

Kontgen, F., Suss, G., Stewart, C., Steinmetz, M., and Bluethmann, H. (1993). Targeted disruption of the MHC class II Aa gene in C57BL/6 mice. Int Immunol *5*, 957-964.

Koya, R. C., Mok, S., Otte, N., Blacketor, K. J., Comin-Anduix, B., Tumeh, P. C., Minasyan, A., Graham, N. A., Graeber, T. G., Chodon, T., and Ribas, A. (2012). BRAF inhibitor vemurafenib improves the antitumor activity of adoptive cell immunotherapy. Cancer Res *72*, 3928-3937.

Kwong, L. N., Boland, G. M., Frederick, D. T., Helms, T. L., Akid, A. T., Miller, J. P., Jiang, S., Cooper, Z. A., Song, X., Seth, S., *et al.* (2015). Co-clinical assessment identifies patterns of BRAF inhibitor resistance in melanoma. J Clin Invest *125*, 1459-1470.

Lake, R. A., and Robinson, B. W. (2005). Immunotherapy and chemotherapy--a practical partnership. Nat Rev Cancer *5*, 397-405.

Lanzavecchia, A., and Sallusto, F. (2000). Dynamics of T lymphocyte responses: intermediates, effectors, and memory cells. Science *290*, 92-97.

Le Blanc, K., Rasmusson, I., Sundberg, B., Götherström, C., Hassan, M., Uzunel, M., and Ringdén, O. (2004). Treatment of severe acute graft-versus-

host disease with third party haploidentical mesenchymal stem cells. *363*, 1439-1441.

Lee, J. H., Choi, J. W., and Kim, Y. S. (2011). Frequencies of BRAF and NRAS mutations are different in histological types and sites of origin of cutaneous melanoma: a meta-analysis. Br J Dermatol *164*, 776-784.

Lee, J. T., Li, L., Brafford, P. A., van den Eijnden, M., Halloran, M. B., Sproesser, K., Haass, N. K., Smalley, K. S., Tsai, J., Bollag, G., and Herlyn, M. (2010). PLX4032, a potent inhibitor of the B-Raf V600E oncogene, selectively inhibits V600E-positive melanomas. Pigment Cell Melanoma Res *23*, 820-827.

Li, X., Hughes, S. C., and Wevrick, R. (2015). Evaluation of melanoma antigen (MAGE) gene expression in human cancers using The Cancer Genome Atlas. Cancer Genet *208*, 25-34.

Lin, J., Goto, Y., Murata, H., Sakaizawa, K., Uchiyama, A., Saida, T., and Takata, M. (2011). Polyclonality of BRAF mutations in primary melanoma and the selection of mutant alleles during progression. Br J Cancer *104*, 464-468.

Lind, E. F., Prockop, S. E., Porritt, H. E., and Petrie, H. T. (2001). Mapping precursor movement through the postnatal thymus reveals specific microenvironments supporting defined stages of early lymphoid development. J Exp Med *194*, 127-134.

Linnemann, C., van Buuren, M. M., Bies, L., Verdegaal, E. M., Schotte, R., Calis, J. J., Behjati, S., Velds, A., Hilkmann, H., Atmioui, D. E., *et al.* (2015). High-throughput epitope discovery reveals frequent recognition of neo-antigens by CD4+ T cells in human melanoma. Nat Med *21*, 81-85.

Lito, P., Pratilas, C. A., Joseph, E. W., Tadi, M., Halilovic, E., Zubrowski, M., Huang, A., Wong, W. L., Callahan, M. K., Merghoub, T., *et al.* (2012). Relief of profound feedback inhibition of mitogenic signaling by RAF inhibitors attenuates their activity in BRAFV600E melanomas. Cancer Cell *22*, 668-682.

Liu, C., Peng, W., Xu, C., Lou, Y., Zhang, M., Wargo, J. A., Chen, J. Q., Li, H. S., Watowich, S. S., Yang, Y., *et al.* (2013). BRAF inhibition increases tumor infiltration by T cells and enhances the antitumor activity of adoptive immunotherapy in mice. Clin Cancer Res *19*, 393-403.

Liu, K., Idoyaga, J., Charalambous, A., Fujii, S., Bonito, A., Mordoh, J., Wainstok, R., Bai, X. F., Liu, Y., and Steinman, R. M. (2005). Innate NKT lymphocytes confer superior adaptive immunity via tumor-capturing dendritic cells. J Exp Med *202*, 1507-1516.

Liu, R., Bal, H. S., Desta, T., Behl, Y., and Graves, D. T. (2006). Tumor necrosis factor-alpha mediates diabetes-enhanced apoptosis of matrix-producing cells and impairs diabetic healing. Am J Pathol *168*, 757-764.

Ljunggren, H. G., and Karre, K. (1985). Host resistance directed selectively against H-2-deficient lymphoma variants. Analysis of the mechanism. J Exp Med *162*, 1745-1759.
Ljunggren, H. G., Van Kaer, L., Ploegh, H. L., and Tonegawa, S. (1994). Altered natural killer cell repertoire in Tap-1 mutant mice. Proc Natl Acad Sci U S A *91*, 6520-6524.

Long, G. V., Menzies, A. M., Nagrial, A. M., Haydu, L. E., Hamilton, A. L., Mann, G. J., Hughes, T. M., Thompson, J. F., Scolyer, R. A., and Kefford, R. F. (2011). Prognostic and clinicopathologic associations of oncogenic BRAF in metastatic melanoma. J Clin Oncol *29*, 1239-1246.

Lundin, K. U., Screpanti, V., Omholt, H., Hofgaard, P. O., Yagita, H., Grandien, A., and Bogen, B. (2004). CD4+ T cells kill Id+ B-lymphoma cells: FasLigand-Fas interaction is dominant in vitro but is redundant in vivo. Cancer Immunology, Immunotherapy *53*, 1135-1145.

Lyons, A. B., and Parish, C. R. (1994). Determination of lymphocyte division by flow cytometry. *171*, 131-137.

Malek, T. R. (2008). The biology of interleukin-2. Annu Rev Immunol *26*, 453-479.

Mandruzzato, S., Callegaro, A., Turcatel, G., Francescato, S., Montesco, M. C., Chiarion-Sileni, V., Mocellin, S., Rossi, C. R., Bicciato, S., Wang, E., *et al.* (2006). A gene expression signature associated with survival in metastatic melanoma. J Transl Med *4(50)*.

Mann, G. J., Pupo, G. M., Campain, A. E., Carter, C. D., Schramm, S. J., Pianova, S., Gerega, S. K., De Silva, C., Lai, K., Wilmott, J. S., *et al.* (2013). BRAF mutation, NRAS mutation, and the absence of an immune-related expressed gene profile predict poor outcome in patients with stage III melanoma. J Invest Dermatol *133*, 509-517.

Mattarollo, S. R., West, A. C., Steegh, K., Duret, H., Paget, C., Martin, B., Matthews, G. M., Shortt, J., Chesi, M., Bergsagel, P. L., *et al.* (2012). NKT cell adjuvant-based tumor vaccine for treatment of myc oncogene-driven mouse B-cell lymphoma. Blood *120*, 3019-3029.

McDermott, D. F., Sosman, J. A., Gonzalez, R., Hodi, F. S., Linette, G. P., Richards, J., Jakub, J. W., Beeram, M., Tarantolo, S., Agarwala, S., *et al.* (2008). Double-blind randomized phase II study of the combination of sorafenib and dacarbazine in patients with advanced melanoma: a report from the 11715 Study Group. J Clin Oncol *26*, 2178-2185.

Mehnert, J. M., and Kluger, H. M. (2012). Driver mutations in melanoma: lessons learned from bench-to-bedside studies. Curr Oncol Rep *14*, 449-457.

Mellman, I., and Steinman, R. M. (2001). Dendritic cells: specialized and regulated antigen processing machines. Cell *106*, 255-258.

Menon, D. R., Wels, C., Bonyadi Rad, E., Joshi, S., Knausz, H., Lade-Keller, J., Brandner, J. M., and Schaider, H. (2013). TGF-beta1 and TNF-alpha differentially regulate Twist1 mediated resistance towards BRAF/MEK inhibition in melanoma. Pigment Cell Melanoma Res *26*, 912-916.

Mercer, K., Chiloeches, A., Huser, M., Kiernan, M., Marais, R., and Pritchard, C. (2002). ERK signalling and oncogene transformation are not impaired in cells lacking A-Raf. Oncogene *21*, 347-355.

Merelli, B., Massi, D., Cattaneo, L., and Mandala, M. (2014). Targeting the PD1/PD-L1 axis in melanoma: biological rationale, clinical challenges and opportunities. Crit Rev Oncol Hematol *89*, 140-165.

Mikula, M., Schreiber, M., Husak, Z., Kucerova, L., Ruth, J., Wieser, R., Zatloukal, K., Beug, H., Wagner, E. F., and Baccarini, M. (2001). Embryonic lethality and fetal liver apoptosis in mice lacking the c-raf-1 gene. EMBO J *20*, 1952-1962.

Moody, D. B., Briken, V., Cheng, T. Y., Roura-Mir, C., Guy, M. R., Geho, D. H., Tykocinski, M. L., Besra, G. S., and Porcelli, S. A. (2002). Lipid length controls antigen entry into endosomal and nonendosomal pathways for CD1b presentation. Nat Immunol *3*, 435-442.

Moore, M. W., Carbone, F. R., and Bevan, M. J. (1988). Introduction of soluble protein into the class I pathway of antigen processing and presentation. Cell *54*, 777-785.

Mosmann, T. R., Cherwinski, H., Bond, M. W., Giedlin, M. A., and Coffman, R. L. (1986). Two types of murine helper T cell clone. I. Definition according to profiles of lymphokine activities and secreted proteins. J Immunol *136*, 2348-2357.

Motohashi, S., and Nakayama, T. (2008). Clinical applications of natural killer T cell-based immunotherapy for cancer. Cancer Sci *99*, 638-645.

Munn, D. H., Sharma, M. D., Hou, D., Baban, B., Lee, J. R., Antonia, S. J., Messina, J. L., Chandler, P., Koni, P. A., and Mellor, A. L. (2004). Expression of indoleamine 2,3-dioxygenase by plasmacytoid dendritic cells in tumor-draining lymph nodes. J Clin Invest *114*, 280-290.

Murphy, K. M. (2011). Janeway's Immunobiology, 8th edn: Garland Science).

Nauta, A. J., and Fibbe, W. E. (2007). Immunomodulatory properties of mesenchymal stromal cells. *110*, 3499-3506.

Nazarian, R., Shi, H., Wang, Q., Kong, X., Koya, R. C., Lee, H., Chen, Z., Lee, M. K., Attar, N., Sazegar, H., *et al.* (2010). Melanomas acquire resistance to B-RAF(V600E) inhibition by RTK or N-RAS upregulation. Nature *468*, 973-977.

Nikolaou, V., and Stratigos, A. J. (2014). Emerging trends in the epidemiology of melanoma. Br J Dermatol *170*, 11-19.

Nishimura, T., Nakui, M., Sato, M., Iwakabe, K., Kitamura, H., Sekimoto, M., Ohta, A., Koda, T., and Nishimura, S. (2000). The critical role of Th1-dominant immunity in tumor immunology. Cancer Chemother Pharmacol *46 Suppl*, S52-61.

O'Shea, J. J., and Paul, W. E. (2010). Mechanisms underlying lineage commitment and plasticity of helper CD4+ T cells. Science *327*, 1098-1102.

Obeid, M., Tesniere, A., Ghiringhelli, F., Fimia, G. M., Apetoh, L., Perfettini, J. L., Castedo, M., Mignot, G., Panaretakis, T., Casares, N., *et al.* (2007). Calreticulin exposure dictates the immunogenicity of cancer cell death. Nat Med *13*, 54-61.

Obenauf, A. C., Zou, Y., Ji, A. L., Vanharanta, S., Shu, W., Shi, H., Kong, X., Bosenberg, M. C., Wiesner, T., Rosen, N., *et al.* (2015). Therapy-induced tumour secretomes promote resistance and tumour progression. Nature *520*, 368-372.

Ostrand-Rosenberg, S., Sinha, P., Beury, D. W., and Clements, V. K. (2012). Cross-talk between myeloid-derived suppressor cells (MDSC), macrophages,

and dendritic cells enhances tumor-induced immune suppression. Semin Cancer Biol *22*, 275-281.

Ott, P. A., and Bhardwaj, N. (2013). Impact of MAPK Pathway Activation in BRAF(V600) Melanoma on T Cell and Dendritic Cell Function. Front Immunol *4*, 346.

Ott, P. A., Henry, T., Baranda, S. J., Frleta, D., Manches, O., Bogunovic, D., and Bhardwaj, N. (2013). Inhibition of both BRAF and MEK in BRAF(V600E) mutant melanoma restores compromised dendritic cell (DC) function while having differential direct effects on DC properties. Cancer Immunol Immunother *62*, 811-822.

Palucka, K., and Banchereau, J. (2012). Cancer immunotherapy via dendritic cells. Nat Rev Cancer *12*, 265-277.

Papin, C., Denouel-Galy, A., Laugier, D., Calothy, G., and Eychene, A. (1998). Modulation of kinase activity and oncogenic properties by alternative splicing reveals a novel regulatory mechanism for B-Raf. J Biol Chem *273*, 24939-24947.

Paraiso, K. H., Xiang, Y., Rebecca, V. W., Abel, E. V., Chen, Y. A., Munko, A. C., Wood, E., Fedorenko, I. V., Sondak, V. K., Anderson, A. R., *et al.* (2011). PTEN loss confers BRAF inhibitor resistance to melanoma cells through the suppression of BIM expression. Cancer Res *71*, 2750-2760.

Parekh, V. V., Wilson, M. T., Olivares-Villagomez, D., Singh, A. K., Wu, L., Wang, C. R., Joyce, S., and Van Kaer, L. (2005). Glycolipid antigen induces long-term natural killer T cell anergy in mice. J Clin Invest *115*, 2572-2583.

Parish, C. R. (2003). Cancer immunotherapy: the past, the present and the future. Immunol Cell Biol *81*, 106-113.

Perez-Diez, A., Joncker, N. T., Choi, K., Chan, W. F., Anderson, C. C., Lantz, O., and Matzinger, P. (2007). CD4 cells can be more efficient at tumor rejection than CD8 cells. Blood *109*, 5346-5354.

Petersen, T. R., Sika-Paotonu, D., Knight, D. A., Simkins, H. M., and Hermans, I. F. (2011). Exploiting the role of endogenous lymphoid-resident dendritic cells in the priming of NKT cells and CD8+ T cells to dendritic cell-based vaccines. PLoS One *6*, e17657.

Peyssonnaux, C., and Eychene, A. (2001). The Raf/MEK/ERK pathway: new concepts of activation. Biol Cell *93*, 53-62.

Pollock, P. M., Harper, U. L., Hansen, K. S., Yudt, L. M., Stark, M., Robbins, C. M., Moses, T. Y., Hostetter, G., Wagner, U., Kakareka, J., *et al.* (2003). High frequency of BRAF mutations in nevi. Nat Genet *33*, 19-20.

Popivanova, B. K., Kitamura, K., Wu, Y., Kondo, T., Kagaya, T., Kaneko, S., Oshima, M., Fujii, C., and Mukaida, N. (2008). Blocking TNF-alpha in mice reduces colorectal carcinogenesis associated with chronic colitis. J Clin Invest *118*, 560-570.

Porcelli, S. A., and Modlin, R. L. (1999). The CD1 system: antigen-presenting molecules for T cell recognition of lipids and glycolipids. Annu Rev Immunol *17*, 297-329.

Postow, M. A., Chesney, J., Pavlick, A. C., Robert, C., Grossmann, K., McDermott, D., Linette, G. P., Meyer, N., Giguere, J. K., Agarwala, S. S., *et al.* (2015). Nivolumab and ipilimumab versus ipilimumab in untreated melanoma. N Engl J Med *372*, 2006-2017.

Poulikakos, P. I., Persaud, Y., Janakiraman, M., Kong, X., Ng, C., Moriceau, G., Shi, H., Atefi, M., Titz, B., Gabay, M. T., *et al.* (2011). RAF inhibitor resistance is mediated by dimerization of aberrantly spliced BRAF(V600E). Nature *480*, 387-390.

Poulikakos, P. I., Zhang, C., Bollag, G., Shokat, K. M., and Rosen, N. (2010). RAF inhibitors transactivate RAF dimers and ERK signalling in cells with wild-type BRAF. Nature *464*, 427-430.

Prehn, R. T., and Main, J. M. (1957). Immunity to methylcholanthrene-induced sarcomas. J Natl Cancer Inst *6*, 769-778.

Prevost-Blondel, A., Zimmermann, C., Stemmer, C., Kulmburg, P., Rosenthal, F. M., and Pircher, H. (1998). Tumor-infiltrating lymphocytes exhibiting high ex vivo cytolytic activity fail to prevent murine melanoma tumor growth in vivo. J Immunol *161*, 2187-2194.

Pritchard, C. A., Samuels, M. L., Bosch, E., and McMahon, M. (1995). Conditionally oncogenic forms of the A-Raf and B-Raf protein kinases display different biological and biochemical properties in NIH 3T3 cells. Mol Cell Biol *15*, 6430-6442.

Qin, Z., and Blankenstein, T. (2000). CD4+ T cell--mediated tumor rejection involves inhibition of angiogenesis that is dependent on IFN gamma receptor expression by nonhematopoietic cells. Immunity *12*, 677-686.

Qiu, C. H., Miyake, Y., Kaise, H., Kitamura, H., Ohara, O., and Tanaka, M. (2009). Novel subset of CD8{alpha}+ dendritic cells localized in the marginal zone is responsible for tolerance to cell-associated antigens. J Immunol *182*, 4127-4136.

Quezada, S. A., Simpson, T. R., Peggs, K. S., Merghoub, T., Vider, J., Fan, X., Blasberg, R., Yagita, H., Muranski, P., Antony, P. A., *et al.* (2010). Tumor-reactive CD4+ T cells develop cytotoxic activity and eradicate large established melanoma after transfer into lymphopenic hosts. J Exp Med *207*, 637-650.

Ramakrishnan, R., Assudani, D., Nagaraj, S., Hunter, T., Cho, H. I., Antonia, S., Altiok, S., Celis, E., and Gabrilovich, D. I. (2010). Chemotherapy enhances

tumor cell susceptibility to CTL-mediated killing during cancer immunotherapy in mice. J Clin Invest *120*, 1111-1124.

Restifo, N. P. (2000). Building better vaccines: how apoptotic cell death can induce inflammation and activate innate and adaptive immunity. Curr Opin Immunol *12*, 597-603.

Restifo, N. P., Dudley, M. E., and Rosenberg, S. A. (2012). Adoptive immunotherapy for cancer: harnessing the T cell response. Nat Rev Immunol *12*, 269-281.

Ribas, A., Hodi, F. S., Callahan, M., Konto, C., and Wolchok, J. (2013). Hepatotoxicity with combination of vemurafenib and ipilimumab. N Engl J Med *368*, 1365-1366.

Riccardi, C., Santoni, A., Barlozzari, T., Puccetti, P., and Herberman, R. B. (1980). In vivo natural reactivity of mice against tumor cells. Int J Cancer *25*, 475-486.

Risso, A., Smilovich, D., Capra, M. C., Baldissarro, I., Yan, G., Bargellesi, A., and Cosulich, M. E. (1991). CD69 in resting and activated T lymphocytes. Its association with a GTP binding protein and biochemical requirements for its expression. J Immunol *146*, 4105-4114.

Rizvi, N. A., Hellmann, M. D., Snyder, A., Kvistborg, P., Makarov, V., Havel, J. J., Lee, W., Yuan, J., Wong, P., Ho, T. S., *et al.* (2015). Cancer immunology. Mutational landscape determines sensitivity to PD-1 blockade in non-small cell lung cancer. Science *348*, 124-128.

Robert, C., Long, G. V., Brady, B., Dutriaux, C., Maio, M., Mortier, L., Hassel, J. C., Rutkowski, P., McNeil, C., Kalinka-Warzocha, E., *et al.* (2015a). Nivolumab in previously untreated melanoma without BRAF mutation. N Engl J Med *372*, 320-330.

Robert, C., Ribas, A., Wolchok, J. D., Hodi, F. S., Hamid, O., Kefford, R., Weber, J. S., Joshua, A. M., Hwu, W. J., Gangadhar, T. C., *et al.* (2014). Anti-programmed-death-receptor-1 treatment with pembrolizumab in ipilimumab-refractory advanced melanoma: a randomised dose-comparison cohort of a phase 1 trial. Lancet *384*, 1109-1117.

Robert, C., Schachter, J., Long, G. V., Arance, A., Grob, J. J., Mortier, L., Daud, A., Carlino, M. S., McNeil, C., Lotem, M., *et al.* (2015b). Pembrolizumab versus Ipilimumab in Advanced Melanoma. N Engl J Med *372*, 2521-2532.

Robert, C., Thomas, L., Bondarenko, I., O'Day, S., Weber, J., Garbe, C., Lebbe, C., Baurain, J. F., Testori, A., Grob, J. J., *et al.* (2011). Ipilimumab plus dacarbazine for previously untreated metastatic melanoma. N Engl J Med *364*, 2517-2526.

Rooney, M. S., Shukla, S. A., Wu, C. J., Getz, G., and Hacohen, N. (2015). Molecular and genetic properties of tumors associated with local immune cytolytic activity. Cell *160*, 48-61.

Rosenberg, S. A., and Dudley, M. E. (2009). Adoptive cell therapy for the treatment of patients with metastatic melanoma. Curr Opin Immunol *21*, 233-240.

Rosenberg, S. A., and Restifo, N. P. (2015). Adoptive cell transfer as personalized immunotherapy for human cancer. Science *348*, 62-68.

Rosenberg, S. A., Sherry, R. M., Morton, K. E., Scharfman, W. J., Yang, J. C., Topalian, S. L., Royal, R. E., Kammula, U., Restifo, N. P., Hughes, M. S., *et al.* (2005). Tumor progression can occur despite the induction of very high levels of self/tumor antigen-specific CD8+ T cells in patients with melanoma. J Immunol *175*, 6169-6176.

Rosenberg, S. A., Yang, J. C., and Restifo, N. P. (2004). Cancer immunotherapy: moving beyond current vaccines. Nat Med *10*, 909-915.

Rosenberg, S. A., Yang, J. C., Schwartzentruber, D. J., Hwu, P., Marincola, F. M., Topalian, S. L., Seipp, C. A., Einhorn, J. H., White, D. E., and Steinberg, S. M. (1999). Prospective randomized trial of the treatment of patients with metastatic melanoma using chemotherapy with cisplatin, dacarbazine, and tamoxifen alone or in combination with interleukin-2 and interferon alfa-2b. J Clin Oncol *17*, 968-975.

Rosenberg, S. A., Yang, J. C., Sherry, R. M., Kammula, U. S., Hughes, M. S., Phan, G. Q., Citrin, D. E., Restifo, N. P., Robbins, P. F., Wunderlich, J. R., *et al.* (2011). Getting Personal with Melanoma. Clin Cancer Res *17*, 4189-4191.

Sakaguchi, S., Sakaguchi, N., Asano, M., Itoh, M., and Toda, M. (1995). Immunologic self-tolerance maintained by activated T cells expressing IL-2 receptor alpha-chains (CD25). Breakdown of a single mechanism of self-tolerance causes various autoimmune diseases. J Immunol *155*, 1151-1164.

Sallusto, F., Lenig, D., Forster, R., Lipp, M., and Lanzavecchia, A. (1999). Two subsets of memory T lymphocytes with distinct homing potentials and effector functions. Nature *401*, 708-712.

Sallusto, F., Schaerli, P., Loetscher, P., Schaniel, C., Lenig, D., Mackay, C. R., Qin, S., and Lanzavecchia, A. (1998). Rapid and coordinated switch in chemokine receptor expression during dendritic cell maturation. Eur J Immunol *28*, 2760-2769.

Sapkota, B., Hill, C. E., and Pollack, B. P. (2013). Vemurafenib enhances MHC induction in BRAF homozygous melanoma cells. Oncoimmunology *2*, e22890.

Scarlett, U. K., Rutkowski, M. R., Rauwerdink, A. M., Fields, J., Escovar-Fadul, X., Baird, J., Cubillos-Ruiz, J. R., Jacobs, A. C., Gonzalez, J. L., Weaver, J., *et al.* (2012). Ovarian cancer progression is controlled by phenotypic changes in dendritic cells. J Exp Med *209*, 495-506.

Schadendorf, D., Fisher, D. E., Garbe, C., Gershenwald, J. E., Grob, J.-J., Halpern, A., Herlyn, M., Marchetti, M. A., McArthur, G., Ribas, A., *et al.* (2015a). Melanoma. Nature Reviews Disease Primers, 15003.

Schadendorf, D., and Hauschild, A. (2014). Melanoma in 2013: Melanoma--the run of success continues. Nat Rev Clin Oncol *11*, 75-76.

Schadendorf, D., Hodi, F. S., Robert, C., Weber, J. S., Margolin, K., Hamid, O., Patt, D., Chen, T. T., Berman, D. M., and Wolchok, J. D. (2015b). Pooled Analysis of Long-Term Survival Data From Phase II and Phase III Trials of Ipilimumab in Unresectable or Metastatic Melanoma. J Clin Oncol *33*, 1889-1894.

Schaerli, P., Willimann, K., Lang, A. B., Lipp, M., Loetscher, P., and Moser, B. (2000). CXC chemokine receptor 5 expression defines follicular homing T cells with B cell helper function. J Exp Med *192*, 1553-1562.

Scheffer, S. R., Nave, H., Korangy, F., Schlote, K., Pabst, R., Jaffee, E. M., Manns, M. P., and Greten, T. F. (2003). Apoptotic, but not necrotic, tumor cell vaccines induce a potent immune response in vivo. Int J Cancer *103*, 205-211.

Schenkel, J. M., and Masopust, D. (2014). Tissue-resident memory T cells. Immunity *41*, 886-897.

Schilling, B., Sondermann, W., Zhao, F., Griewank, K. G., Livingstone, E., Sucker, A., Zelba, H., Weide, B., Trefzer, U., Wilhelm, T., *et al.* (2014). Differential influence of vemurafenib and dabrafenib on patients' lymphocytes despite similar clinical efficacy in melanoma. Ann Oncol *25*, 747-753.

Schilling, B., Sucker, A., Griewank, K., Zhao, F., Weide, B., Gorgens, A., Giebel, B., Schadendorf, D., and Paschen, A. (2013). Vemurafenib reverses immunosuppression by myeloid derived suppressor cells. Int J Cancer *133*, 1653-1663.

Schreiber, R. D., Old, L. J., and Smyth, M. J. (2011). Cancer immunoediting: integrating immunity's roles in cancer suppression and promotion. Science *331*, 1565-1570.

Schultz, L. D., Scweitzer, P. A., Christianson, S. W., Gott, B., Schweitzer, I. B., Tennent, B., McKenna, S., Mobraaten, L., Rajan, T. V., Greiner, D. L., and Leiter, E. H. (1995). Multiple Defects in Innate and Adaptive Immunologic Function in NOD/LtSz-*scid* Mice. The Journal of Immunology *154*, 190-191.

Schumacher, T. N., and Schreiber, R. D. (2015). Neoantigens in cancer immunotherapy. Science *348*, 69-74.

Shao, Y., Le, K., Cheng, H., and Aplin, A. E. (2015). NF-kappaB Regulation of c-FLIP Promotes TNFalpha-Mediated RAF Inhibitor Resistance in Melanoma. J Invest Dermatol *135*, 1839-1848.

Sharma, A., Trivedi, N. R., Zimmerman, M. A., Tuveson, D. A., Smith, C. D., and Robertson, G. P. (2005). Mutant V599EB-Raf regulates growth and vascular development of malignant melanoma tumors. Cancer Res *65*, 2412-2421.

Shi, H., Hugo, W., Kong, X., Hong, A., Koya, R. C., Moriceau, G., Chodon, T., Guo, R., Johnson, D. B., Dahlman, K. B., *et al.* (2014). Acquired resistance and clonal evolution in melanoma during BRAF inhibitor therapy. Cancer Discov *4*, 80-93.

Shimizu, J., Yamazaki, S., and Sakaguchi, S. (1999). Induction of tumor immunity by removing CD25+CD4+ T cells: a common basis between tumor immunity and autoimmunity. J Immunol *163*, 5211-5218.

Shimizu, K., Goto, A., Fukui, M., Taniguchi, M., and Fujii, S. (2007a). Tumor cells loaded with alpha-galactosylceramide induce innate NKT and NK cell-dependent resistance to tumor implantation in mice. J Immunol *178*, 2853-2861.
S

himizu, K., Kurosawa, Y., Taniguchi, M., Steinman, R. M., and Fujii, S. (2007b). Cross-presentation of glycolipid from tumor cells loaded with alpha-galactosylceramide leads to potent and long-lived T cell mediated immunity via dendritic cells. J Exp Med *204*, 2641-2653.

Shin, H., and Iwasaki, A. (2013). Tissue-resident memory T cells. Immunol Rev *255*, 165-181.

Shultz, L. D., Schweitzer, P. A., Christianson, S. W., Gott, B., Schweitzer, I. B., Tennent, B., McKenna, S., Mobraaten, L., Rajan, T. V., Greiner, D. L., and et al. (1995). Multiple defects in innate and adaptive immunologic function in NOD/LtSz-scid mice. J Immunol *154*, 180-191.

Siegel, R., Ma, J., Zou, Z., and Jemal, A. (2014). Cancer statistics, 2014. CA Cancer J Clin *64*, 9-29.

Siegel, R., Naishadham, D., and Jemal, A. (2012). Cancer statistics, 2012. CA Cancer J Clin *62*, 10-29.

Snyder, A., Makarov, V., Merghoub, T., Yuan, J., Zaretsky, J. M., Desrichard, A., Walsh, L. A., Postow, M. A., Wong, P., Ho, T. S., *et al.* (2014). Genetic basis for clinical response to CTLA-4 blockade in melanoma. N Engl J Med *371*, 2189-2199.

Soiffer, R., Lynch, T., Mihm, M., Jung, K., Rhuda, C., Schmollinger, J. C., Hodi, F. S., Liebster, L., Lam, P., Mentzer, S., *et al.* (1998). Vaccination with irradiated autologous melanoma cells engineered to secrete human granulocyte-macrophage colony-stimulating factor generates potent antitumor immunity in patients with metastatic melanoma. Proc Natl Acad Sci U S A *95*, 13141-13146.

Somasundaram, R., Villanueva, J., and Herlyn, M. (2012). Intratumoral heterogeneity as a therapy resistance mechanism: role of melanoma subpopulations. Adv Pharmacol *65*, 335-359.

Sosman, J. A., Kim, K. B., Schuchter, L., Gonzalez, R., Pavlick, A. C., Weber, J. S., McArthur, G. A., Hutson, T. E., Moschos, S. J., Flaherty, K. T., *et al.* (2012). Survival in BRAF V600-mutant advanced melanoma treated with vemurafenib. N Engl J Med *366*, 707-714.

Spaggiari, G. M., Capobianco, A., Abdelrazik, H., Becchetti, F., Mingari, M. C., and Moretta, L. (2008). Mesenchymal stem cells inhibit natural killer-cell proliferation, cytotoxicity, and cytokine production: role of indoleamine 2,3-dioxygenase and prostaglandin E2. *111*, 1327-1333.

Srivastava, N., and McDermott, D. (2014). Update on benefit of immunotherapy and targeted therapy in melanoma: the changing landscape. Cancer Manag Res *6*, 279-289.

Starr, T. K., Jameson, S. C., and Hogquist, K. A. (2003). Positive and negative selection of T cells. Annu Rev Immunol *21*, 139-176.

Steer, H. J., Lake, R. A., Nowak, A. K., and Robinson, B. W. (2010). Harnessing the immune response to treat cancer. Oncogene *29*, 6301-6313.

Steinberg, S. M., Zhang, P., Malik, B. T., Boni, A., Shabaneh, T. B., Byrne, K. T., Mullins, D. W., Brinckerhoff, C. E., Ernstoff, M. S., Bosenberg, M. W., and Turk, M. J. (2014). BRAF inhibition alleviates immune suppression in murine autochthonous melanoma. Cancer Immunol Res *2*, 1044-1050.

Steinman, R. M., Hawiger, D., and Nussenzweig, M. C. (2003). Tolerogenic dendritic cells. Annu Rev Immunol *21*, 685-711.

Steinman, R. M., Turley, S., Mellman, I., and Inaba, K. (2000). The induction of tolerance by dendritic cells that have captured apoptotic cells. J Exp Med *191*, 411-416.

Steitz, J., Bruck, J., Lenz, J., Knop, J., and Tuting, T. (2001). Depletion of CD25(+) CD4(+) T cells and treatment with tyrosinase-related protein 2-

transduced dendritic cells enhance the interferon alpha-induced, CD8(+) T-cell-dependent immune defense of B16 melanoma. Cancer Res *61*, 8643-8646.

Stratton, M. R. (2011). Exploring the genomes of cancer cells: progress and promise. Science *331*, 1553-1558.

Stratton, M. R., Campbell, P. J., and Futreal, P. A. (2009). The cancer genome. Nature *458*, 719-724.

Straussman, R., Morikawa, T., Shee, K., Barzily-Rokni, M., Qian, Z. R., Du, J., Davis, A., Mongare, M. M., Gould, J., Frederick, D. T., *et al.* (2012). Tumour micro-environment elicits innate resistance to RAF inhibitors through HGF secretion. Nature *487*, 500-504.

Sullivan, R. J., and Flaherty, K. (2013). MAP kinase signaling and inhibition in melanoma. Oncogene *32*, 2373-2379.

Sumimoto, H., Imabayashi, F., Iwata, T., and Kawakami, Y. (2006). The BRAF-MAPK signaling pathway is essential for cancer-immune evasion in human melanoma cells. J Exp Med *203*, 1651-1656.

Sun, C., Wang, L., Huang, S., Heynen, G. J., Prahallad, A., Robert, C., Haanen, J., Blank, C., Wesseling, J., Willems, S. M., *et al.* (2014). Reversible and adaptive resistance to BRAF(V600E) inhibition in melanoma. Nature *508*, 118-122.

Szlosarek, P., Charles, K. A., and Balkwill, F. R. (2006). Tumour necrosis factor-alpha as a tumour promoter. Eur J Cancer *42*, 745-750.

Tan, C., Reddy, V., Dannull, J., Ding, E., Nair, S. K., Tyler, D. S., Pruitt, S. K., and Lee, W. T. (2013). Impact of anti-CD25 monoclonal antibody on dendritic cell-tumor fusion vaccine efficacy in a murine melanoma model. J Transl Med *11*, 148.

Terness, P., Bauer, T. M., Rose, L., Dufter, C., Watzlik, A., Simon, H., and Opelz, G. (2002). Inhibition of allogeneic T cell proliferation by indoleamine 2,3-dioxygenase-expressing dendritic cells: mediation of suppression by tryptophan metabolites. J Exp Med *196*, 447-457.

Topalian, S. L., Drake, C. G., and Pardoll, D. M. (2012). Targeting the PD-1/B7-H1(PD-L1) pathway to activate anti-tumor immunity. Curr Opin Immunol *24*, 207-212.

Topalian, S. L., Drake, C. G., and Pardoll, D. M. (2015). Immune checkpoint blockade: a common denominator approach to cancer therapy. Cancer Cell *27*, 450-461.

Topalian, S. L., Sznol, M., McDermott, D. F., Kluger, H. M., Carvajal, R. D., Sharfman, W. H., Brahmer, J. R., Lawrence, D. P., Atkins, M. B., Powderly, J. D., *et al.* (2014). Survival, durable tumor remission, and long-term safety in patients with advanced melanoma receiving nivolumab. J Clin Oncol *32*, 1020-1030.

Tran, E., Turcotte, S., Gros, A., Robbins, P. F., Lu, Y. C., Dudley, M. E., Wunderlich, J. R., Somerville, R. P., Hogan, K., Hinrichs, C. S., *et al.* (2014). Cancer immunotherapy based on mutation-specific CD4+ T cells in a patient with epithelial cancer. Science *344*, 641-645.

Trifari, S., Kaplan, C. D., Tran, E. H., Crellin, N. K., and Spits, H. (2009). Identification of a human helper T cell population that has abundant production of interleukin 22 and is distinct from T(H)-17, T(H)1 and T(H)2 cells. Nat Immunol *10*, 864-871.

Troiani, T., Schettino, C., Martinelli, E., Morgillo, F., Tortora, G., and Ciardiello, F. (2008). The use of xenograft models for the selection of cancer treatments with the EGFR as an example. Critical Reviews in Oncology/Hematology *65*, 200-211.

Trombetta, E. S., and Mellman, I. (2005). Cell biology of antigen processing in vitro and in vivo. Annu Rev Immunol *23*, 975-1028.

Trotter, S. C., Sroa, N., Winkelmann, R. R., Olencki, T., and Bechtel, M. (2013). A Global Review of Melanoma Follow-up Guidelines. J Clin Aesthet Dermatol *6*, 18-26.

Tsai, J., Lee, J. T., Wang, W., Zhang, J., Cho, H., Mamo, S., Bremer, R., Gillette, S., Kong, J., Haass, N. K.*, et al.* (2008). Discovery of a selective inhibitor of oncogenic B-Raf kinase with potent antimelanoma activity. Proc Natl Acad Sci U S A *105*, 3041-3046.

Uyttenhove, C., Pilotte, L., Theate, I., Stroobant, V., Colau, D., Parmentier, N., Boon, T., and Van den Eynde, B. J. (2003). Evidence for a tumoral immune resistance mechanism based on tryptophan degradation by indoleamine 2,3-dioxygenase. Nat Med *9*, 1269-1274.

van der Bruggen, P., Traversari, C., Chomez, P., Lurquin, C., De Plaen, E., Van den Eynde, B., Knuth, A., and Boon, T. (1991). A gene encoding an antigen recognized by cytolytic T lymphocytes on a human melanoma. Science *254*, 1643-1647.

Van Kaer, L., Ashton-Rickardt, P. G., Ploegh, H. L., and Tonegawa, S. (1992). TAP1 mutant mice are deficient in antigen presentation, surface class I molecules, and CD4-8+ T cells. Cell *71*, 1205-1214.

Van Pel, A., and Boon, T. (1982). Protection against a nonimmunogenic mouse leukemia by an immunogenic variant obtained by mutagenesis. Proc Natl Acad Sci U S A *79*, 4718-4722.

Vanneman, M., and Dranoff, G. (2012). Combining immunotherapy and targeted therapies in cancer treatment. Nat Rev Cancer *12*, 237-251.

Veldhoen, M., Hocking, R. J., Atkins, C. J., Locksley, R. M., and Stockinger, B. (2006). TGFbeta in the context of an inflammatory cytokine milieu supports de novo differentiation of IL-17-producing T cells. Immunity *24*, 179-189.

Vella, L. J., Pasam, A., Dimopoulos, N., Andrews, M., Knights, A., Puaux, A. L., Louahed, J., Chen, W., Woods, K., and Cebon, J. S. (2014). MEK inhibition, alone or in combination with BRAF inhibition, affects multiple functions of isolated normal human lymphocytes and dendritic cells. Cancer Immunol Res *2*, 351-360.

Villanueva, J., Vultur, A., Lee, J. T., Somasundaram, R., Fukunaga-Kalabis, M., Cipolla, A. K., Wubbenhorst, B., Xu, X., Gimotty, P. A., Kee, D., *et al.* (2010). Acquired resistance to BRAF inhibitors mediated by a RAF kinase switch in melanoma can be overcome by cotargeting MEK and IGF-1R/PI3K. Cancer Cell *18*, 683-695.

Vivier, E., Ugolini, S., Blaise, D., Chabannon, C., and Brossay, L. (2012). Targeting natural killer cells and natural killer T cells in cancer. Nat Rev Immunol *12*, 239-252.

Wan, P. T., Garnett, M. J., Roe, S. M., Lee, S., Niculescu-Duvaz, D., Good, V. M., Jones, C. M., Marshall, C. J., Springer, C. J., Barford, D., *et al.* (2004). Mechanism of activation of the RAF-ERK signaling pathway by oncogenic mutations of B-RAF. Cell *116*, 855-867.

Wang, X., and Lin, Y. (2008). Tumor necrosis factor and cancer, buddies or foes? Acta Pharmacol Sin *29*, 1275-1288.

Ward, S., Casey, D., Labarthe, M. C., Whelan, M., Dalgleish, A., Pandha, H., and Todryk, S. (2002). Immunotherapeutic potential of whole tumour cells. Cancer Immunol Immunother *51*, 351-357.

Weinkove, R., Brooks, C. R., Carter, J. M., Hermans, I. F., and Ronchese, F. (2013). Functional invariant natural killer T-cell and CD1d axis in chronic

lymphocytic leukemia: implications for immunotherapy. Haematologica *98*, 376-384.

Wilhelm, S. M., Carter, C., Tang, L., Wilkie, D., McNabola, A., Rong, H., Chen, C., Zhang, X., Vincent, P., McHugh, M., *et al.* (2004). BAY 43-9006 exhibits broad spectrum oral antitumor activity and targets the RAF/MEK/ERK pathway and receptor tyrosine kinases involved in tumor progression and angiogenesis. Cancer Res *64*, 7099-7109.

Willrich, M. A., Murray, D. L., and Snyder, M. R. (2015). Tumor necrosis factor inhibitors: clinical utility in autoimmune diseases. Transl Res *165*, 270-282.

Wilmott, J. S., Haydu, L. E., Menzies, A. M., Lum, T., Hyman, J., Thompson, J. F., Hersey, P., Kefford, R. F., Scolyer, R. A., and Long, G. V. (2014). Dynamics of chemokine, cytokine, and growth factor serum levels in BRAF-mutant melanoma patients during BRAF inhibitor treatment. J Immunol *192*, 2505-2513.

Wilmott, J. S., Long, G. V., Howle, J. R., Haydu, L. E., Sharma, R. N., Thompson, J. F., Kefford, R. F., Hersey, P., and Scolyer, R. A. (2012). Selective BRAF inhibitors induce marked T-cell infiltration into human metastatic melanoma. Clin Cancer Res *18*, 1386-1394.

Wojnowski, L., Zimmer, A. M., Beck, T. W., Hahn, H., Bernal, R., Rapp, U. R., and Zimmer, A. (1997). Endothelial apoptosis in Braf-deficient mice. Nat Genet *16*, 293-297.

Xing, F., Persaud, Y., Pratilas, C. A., Taylor, B. S., Janakiraman, M., She, Q. B., Gallardo, H., Liu, C., Merghoub, T., Hefter, B., *et al.* (2012). Concurrent loss of the PTEN and RB1 tumor suppressors attenuates RAF dependence in melanomas harboring (V600E)BRAF. Oncogene *31*, 446-457.

Xing, M. (2013). Molecular pathogenesis and mechanisms of thyroid cancer. Nat Rev Cancer *13*, 184-199.

Yaguchi, T., Sumimoto, H., Kudo-Saito, C., Tsukamoto, N., Ueda, R., Iwata-Kajihara, T., Nishio, H., Kawamura, N., and Kawakami, Y. (2011). The mechanisms of cancer immunoescape and development of overcoming strategies. Int J Hematol *93*, 294-300.

Yancovitz, M., Litterman, A., Yoon, J., Ng, E., Shapiro, R. L., Berman, R. S., Pavlick, A. C., Darvishian, F., Christos, P., Mazumdar, M., *et al.* (2012). Intra- and Inter-Tumor Heterogeneity of BRAFV600EMutations in Primary and Metastatic Melanoma. PLoS ONE *7*, e29336.

Yang, H., Higgins, B., Kolinsky, K., Packman, K., Go, Z., Iyer, R., Kolis, S., Zhao, S., Lee, R., Grippo, J. F., *et al.* (2010). RG7204 (PLX4032), a selective BRAFV600E inhibitor, displays potent antitumor activity in preclinical melanoma models. Cancer Res *70*, 5518-5527.

Ye, Y., Li, Q., Hu, W. L., Tseng, H. Y., Jin, L., Zhang, X. D., Zhang, L. J., and Yang, S. (2013). Loss of PI(4,5)P2 5-Phosphatase A Contributes to Resistance of Human Melanoma Cells to RAF/MEK Inhibitors. Transl Oncol *6*, 470-481.
Yoon, S., and Seger, R. (2006). The extracellular signal-regulated kinase: multiple substrates regulate diverse cellular functions. Growth Factors *24*, 21-44.

Young, R. J., Waldeck, K., Martin, C., Foo, J. H., Cameron, D. P., Kirby, L., Do, H., Mitchell, C., Cullinane, C., Liu, W., *et al.* (2014). Loss of CDKN2A expression is a frequent event in primary invasive melanoma and correlates with sensitivity to the CDK4/6 inhibitor PD0332991 in melanoma cell lines. Pigment Cell Melanoma Res *27*, 590-600.

Zaidi, M. R., and Merlino, G. (2011). The two faces of interferon-gamma in cancer. Clin Cancer Res *17*, 6118-6124.

Zhang, S., Zhang, H., and Zhao, J. (2009). The role of CD4 T cell help for CD8 CTL activation. Biochem Biophys Res Commun *384*, 405-408.

Zhu, J., and Paul, W. E. (2010). Peripheral CD4+ T-cell differentiation regulated by networks of cytokines and transcription factors. Immunol Rev *238*, 247-262.

Zitvogel, L., Apetoh, L., Ghiringhelli, F., and Kroemer, G. (2008). Immunological aspects of cancer chemotherapy. Nat Rev Immunol *8*, 59-73.

Zitvogel, L., Kepp, O., Senovilla, L., Menger, L., Chaput, N., and Kroemer, G. (2010). Immunogenic tumor cell death for optimal anticancer therapy: the calreticulin exposure pathway. Clin Cancer Res *16*, 3100-3104.

Zitvogel, L., Tesniere, A., and Kroemer, G. (2006). Cancer despite immunosurveillance: immunoselection and immunosubversion. Nat Rev Immunol *6*, 715-727.

Appendix A: Representative flow cytometry plots

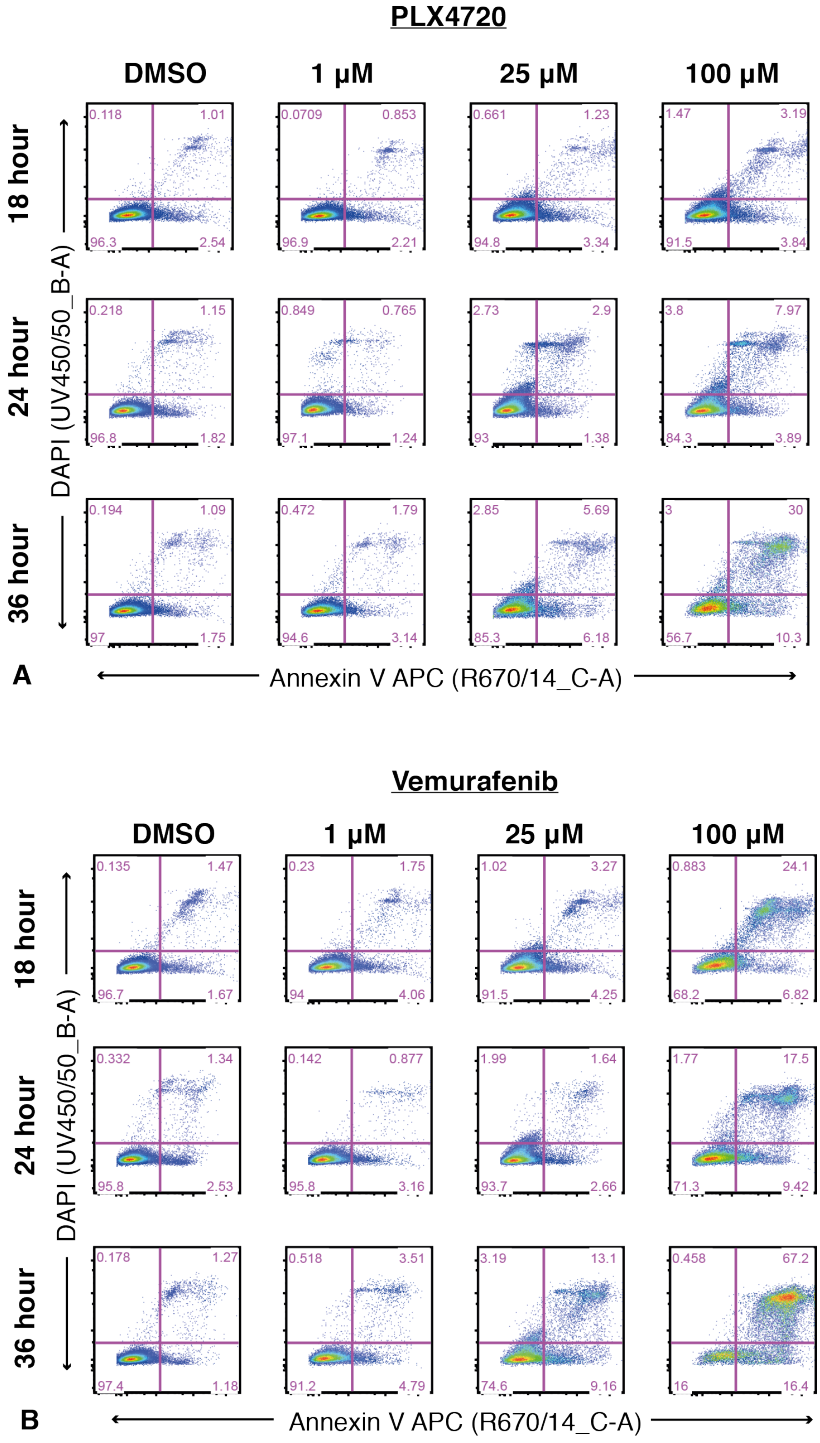

Figure A1: Flow cytometric data showing A375 apoptosis. A375 cells were treated with 1 µM-100 µM PLX4720 (**A)** or Vemurafenib (**B)** for 18-36 hours. Cell viability and phosphatidylserine expression was then analysed by flow cytometry. Representative flow cytometry plots are shown for each treatment condition. $DAPI^-$, AV^- are live cells, $DAPI^-$, AV^+ are early apoptotic cells, and late apoptotic/necrotic cells are $DAPI^+$, AV^+.

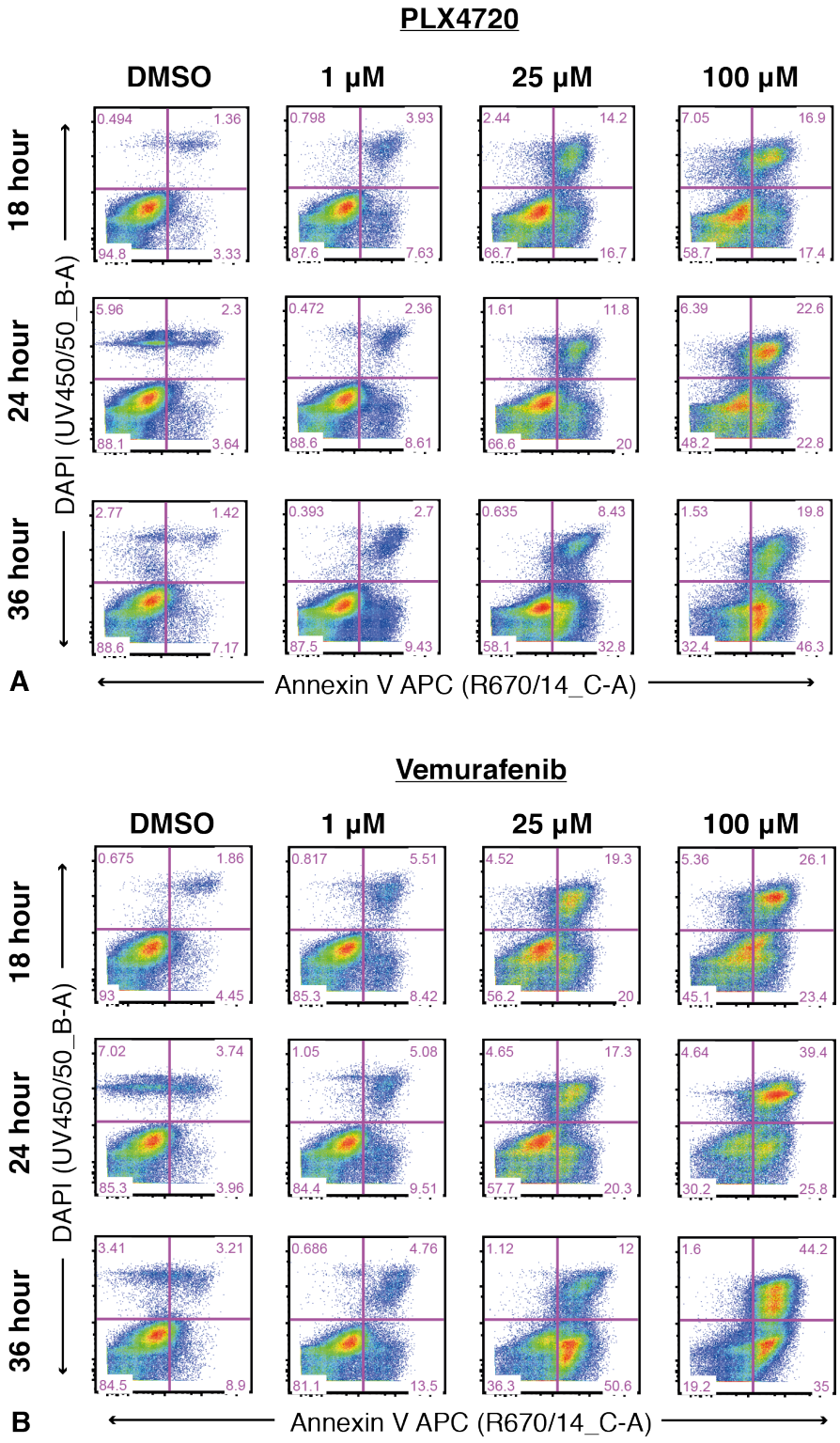

Figure A2: Flow cytometric data showing YUMM1.1 apoptosis. YUMM1.1 cells were treated with 1 μM-100 μM PLX4720 (**A)** or Vemurafenib (**B)** for 18-36 hours. Cell viability and phosphatidylserine expression was then analysed by flow cytometry. Representative flow cytometry plots are shown for each treatment condition. $DAPI^-$, AV^- are live cells, $DAPI^-$, AV^+ are early apoptotic cells, and late apoptotic/necrotic cells are $DAPI^+$, AV^+.

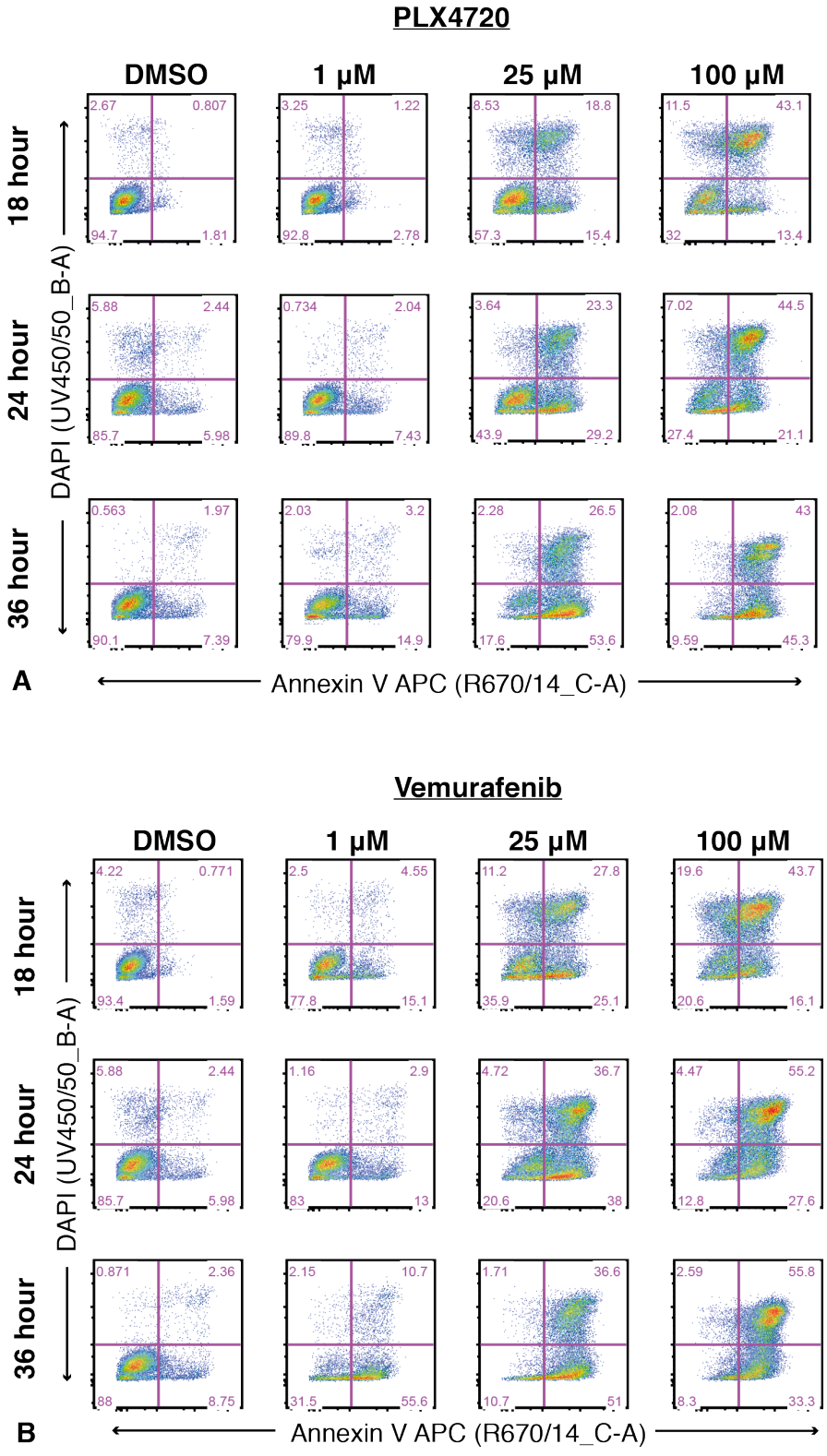

Figure A3: Flow cytometric data showing YUMM1.7 apoptosis. YUMM1.7 cells were treated with 1 μM-100 μM PLX4720 (**A)** or Vemurafenib (**B)** for 18-36 hours. Cell viability and phosphatidylserine expression was then analysed by flow cytometry. Representative flow cytometry plots are shown for each treatment condition. $DAPI^-$, AV^- are live cells, $DAPI^-$, AV^+ are early apoptotic cells, and late apoptotic/necrotic cells are $DAPI^+$, AV^+.

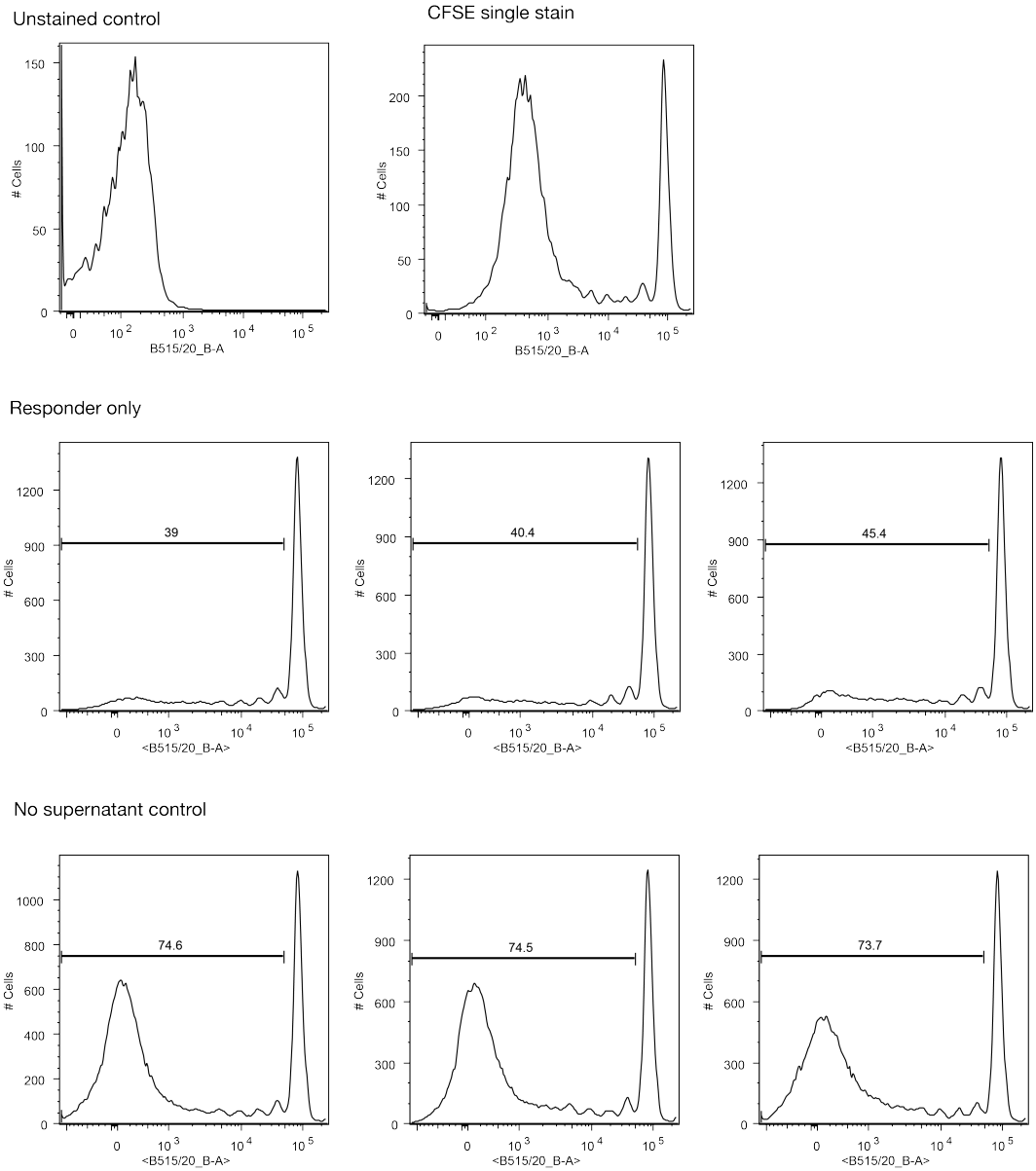

Figure A4: Flow cytometric control data for human MLRs evaluated in Figure 3.11. T cell proliferation was evaluated in a one-way mixed lymphocyte reaction and measured by flow cytometry. Example plots of the unstained and CFSE single stained controls are shown above, as are biological controls in triplicate (responder only to show baseline proliferation and the no supernatant, or untreated, control).

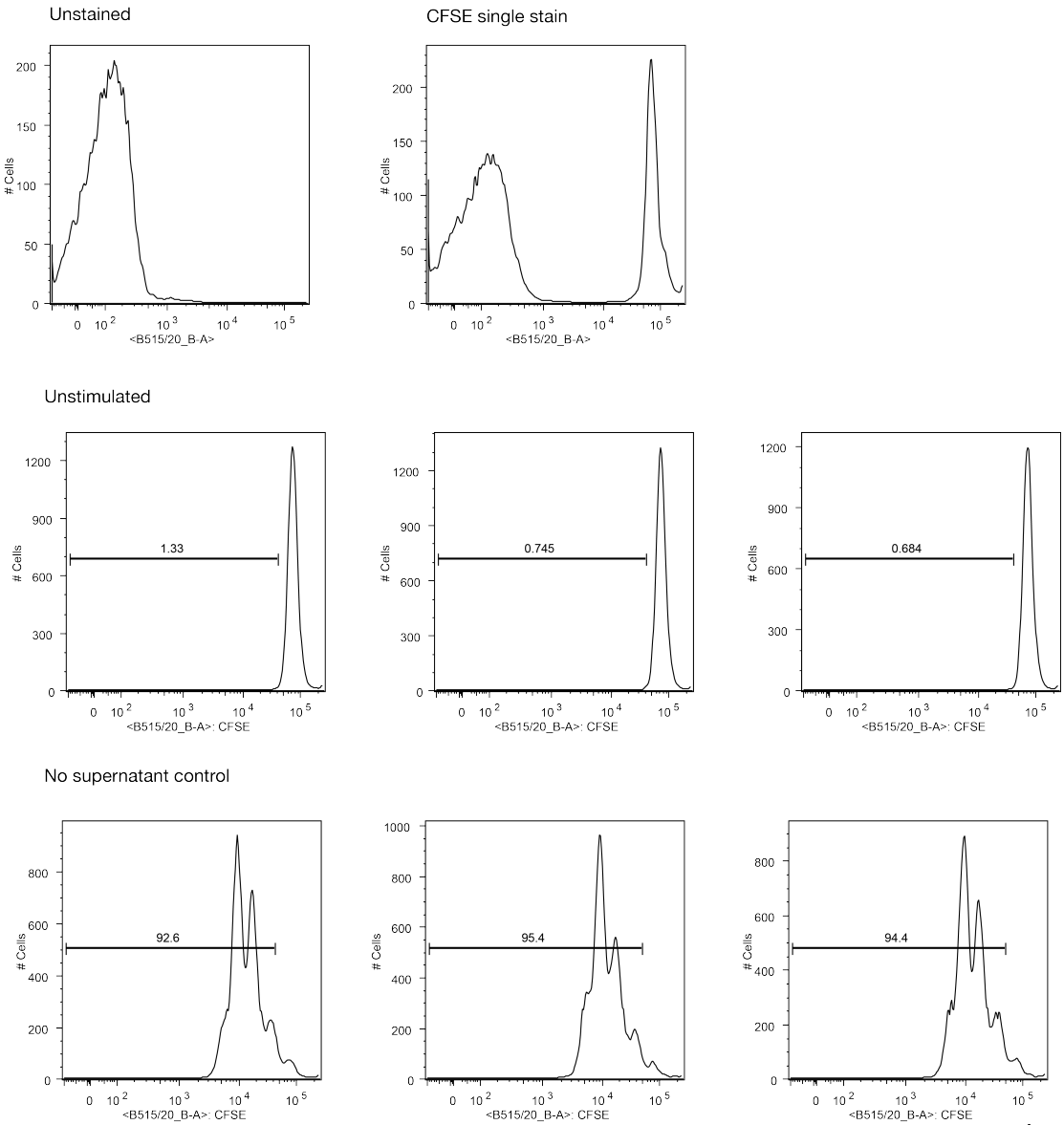

Figure A5: Flow cytometric control data for human anti-CD3/28 stimulation performed in Figure 3.12. T cell proliferation was evaluated following anti-CD3/28 stimulation and measured by flow cytometry. Example plots of the unstained and CFSE single stained controls are shown above, as are biological controls in triplicate (unstimulated to show baseline proliferation and the no supernatant, or untreated, control).

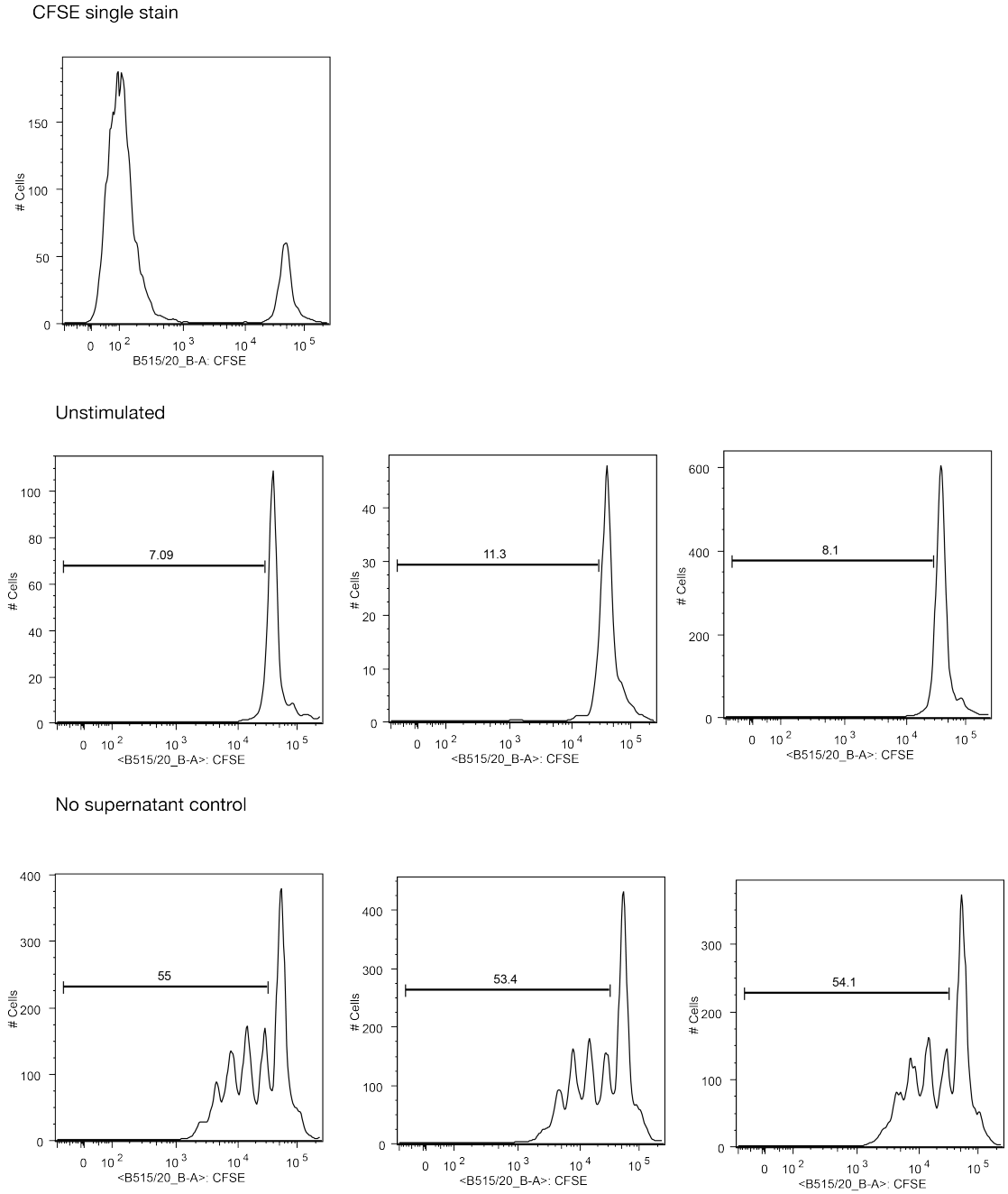

Figure A6: Flow cytometric control data of CFSE staining for murine anti-CD3/28 stimulation performed in Figure 3.13. T cell proliferation was evaluated following anti-CD3/28 stimulation and measured by flow cytometry. Example plots of the CFSE single stained control are shown above, as are biological controls in triplicate (unstimulated to show baseline proliferation and the no supernatant, or untreated, control).

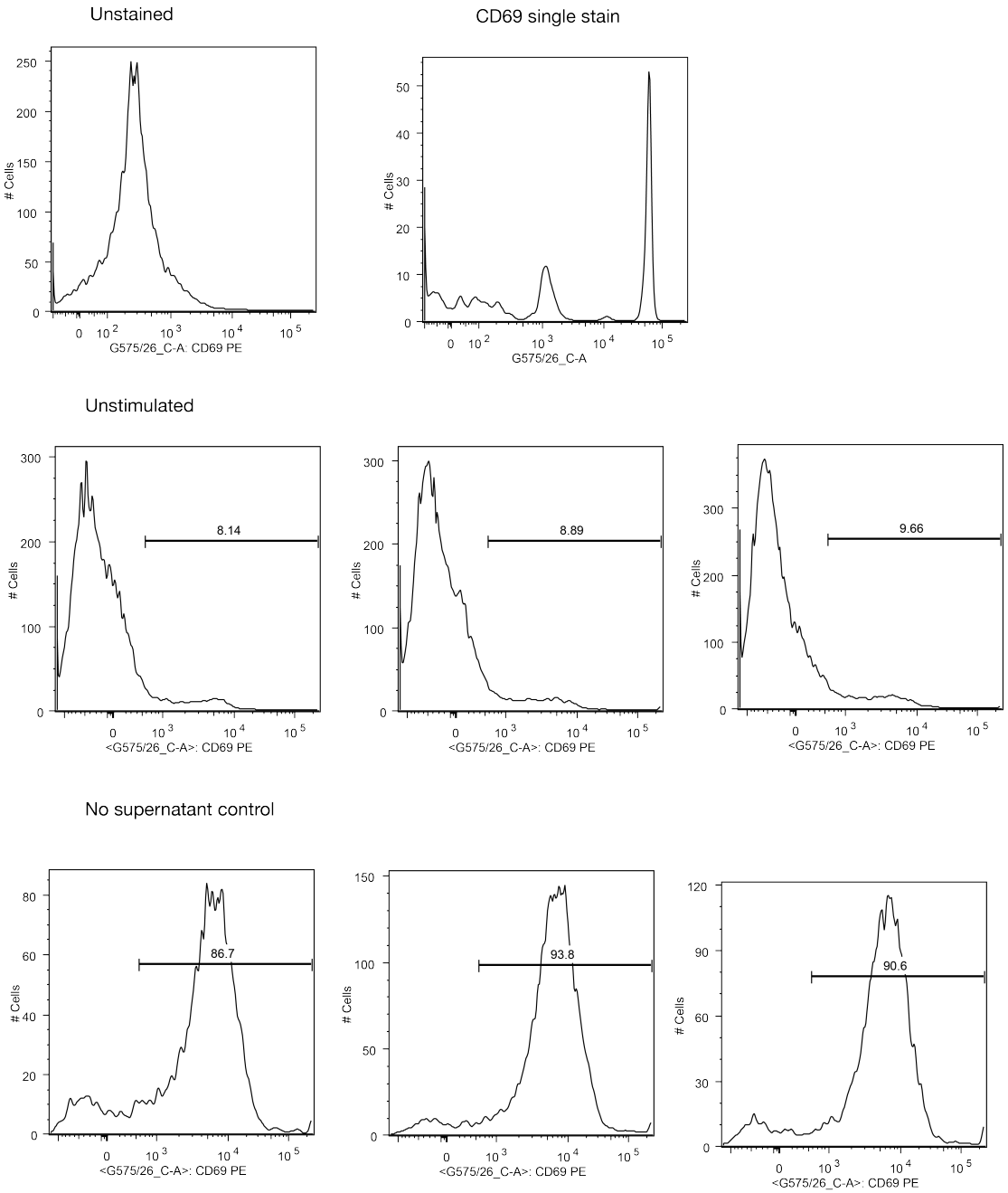

Figure A7: Flow cytometric control data of CD69 staining for murine anti-CD3/28 stimulation performed in Figure 3.13. T cell activation was evaluated following anti-CD3/28 stimulation and measured by flow cytometry. Example plots of the CD69 single stained control are shown above, as are biological controls in triplicate (unstimulated to show baseline proliferation and the no supernatant, or untreated, control).

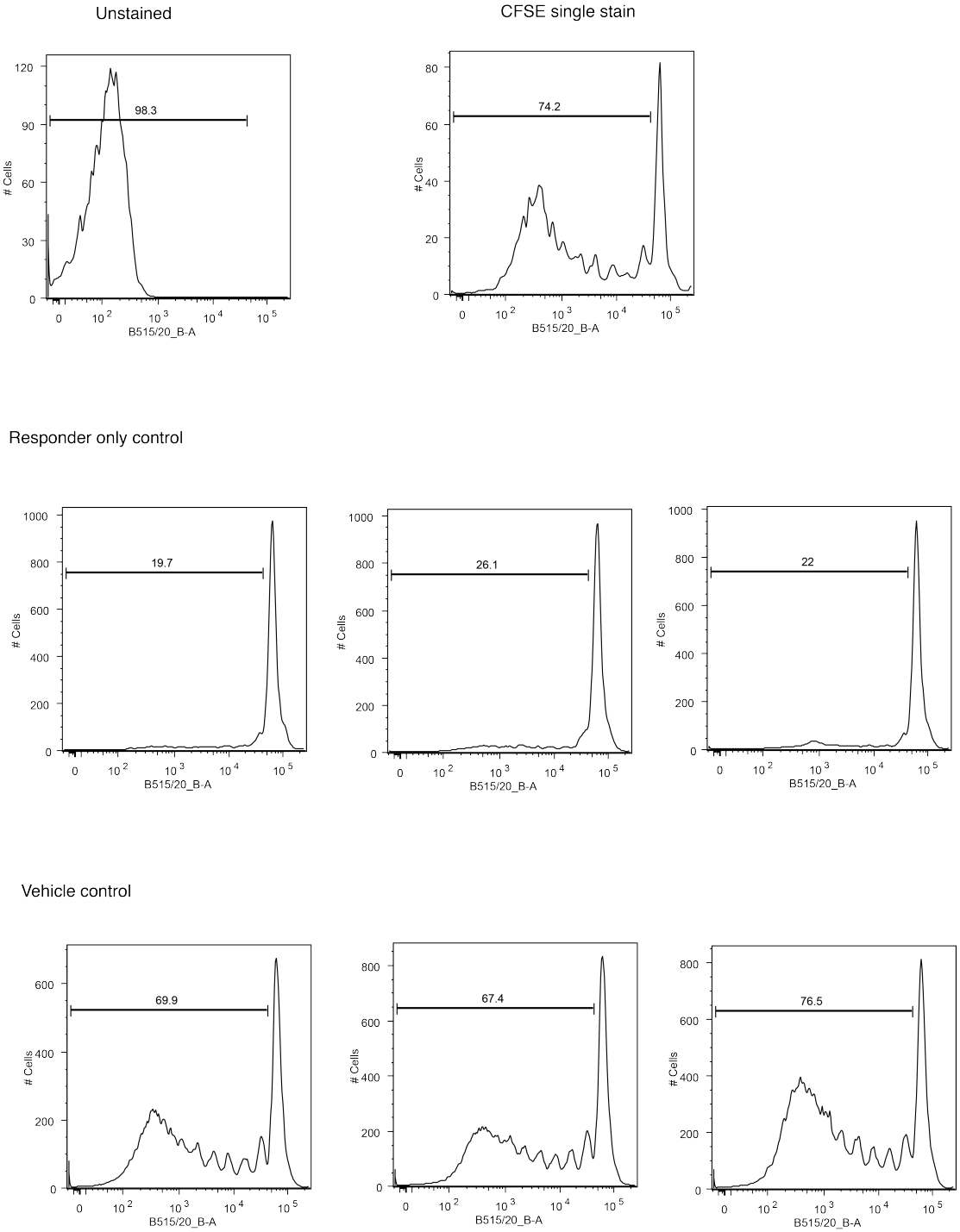

Figure A8: Flow cytometric control data for human MLRs performed in Figure 4.1. T cell proliferation was evaluated following a one-way MLR and measured by flow cytometry. Example plots of the unstained and CFSE single stained controls are shown above, as are biological controls in triplicate (unstimulated to show baseline proliferation and the vehicle control).

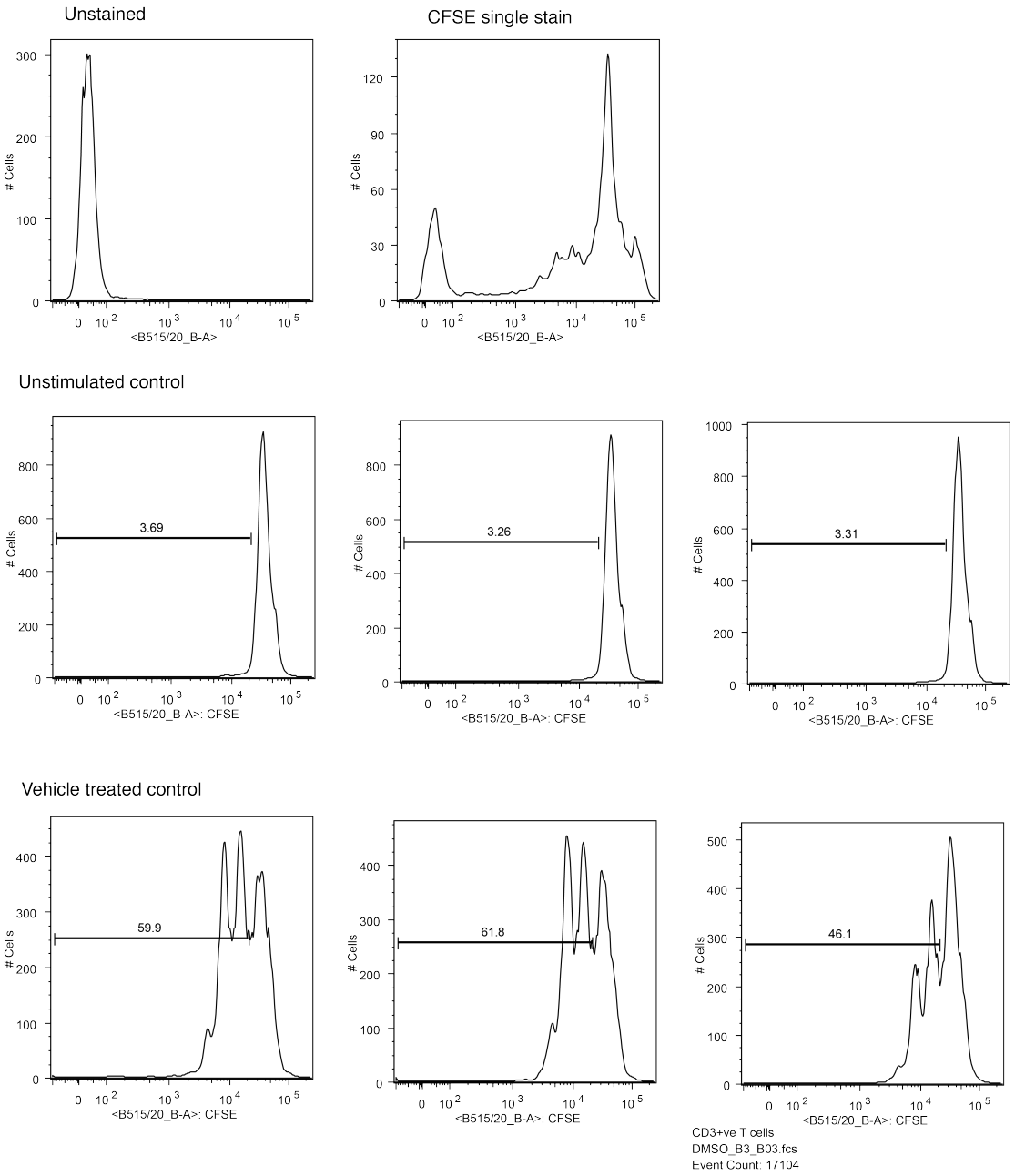

Figure A9: Flow cytometric control data for human anti-CD3/28 stimulation performed in Figure 4.2. Total T cell ($CD3^+$) proliferation was evaluated following anti-CD3/28 stimulation and measured by flow cytometry. Example plots of the unstained and CFSE single stained controls are shown above, as are biological controls in triplicate (unstimulated to show baseline proliferation and the vehicle control).

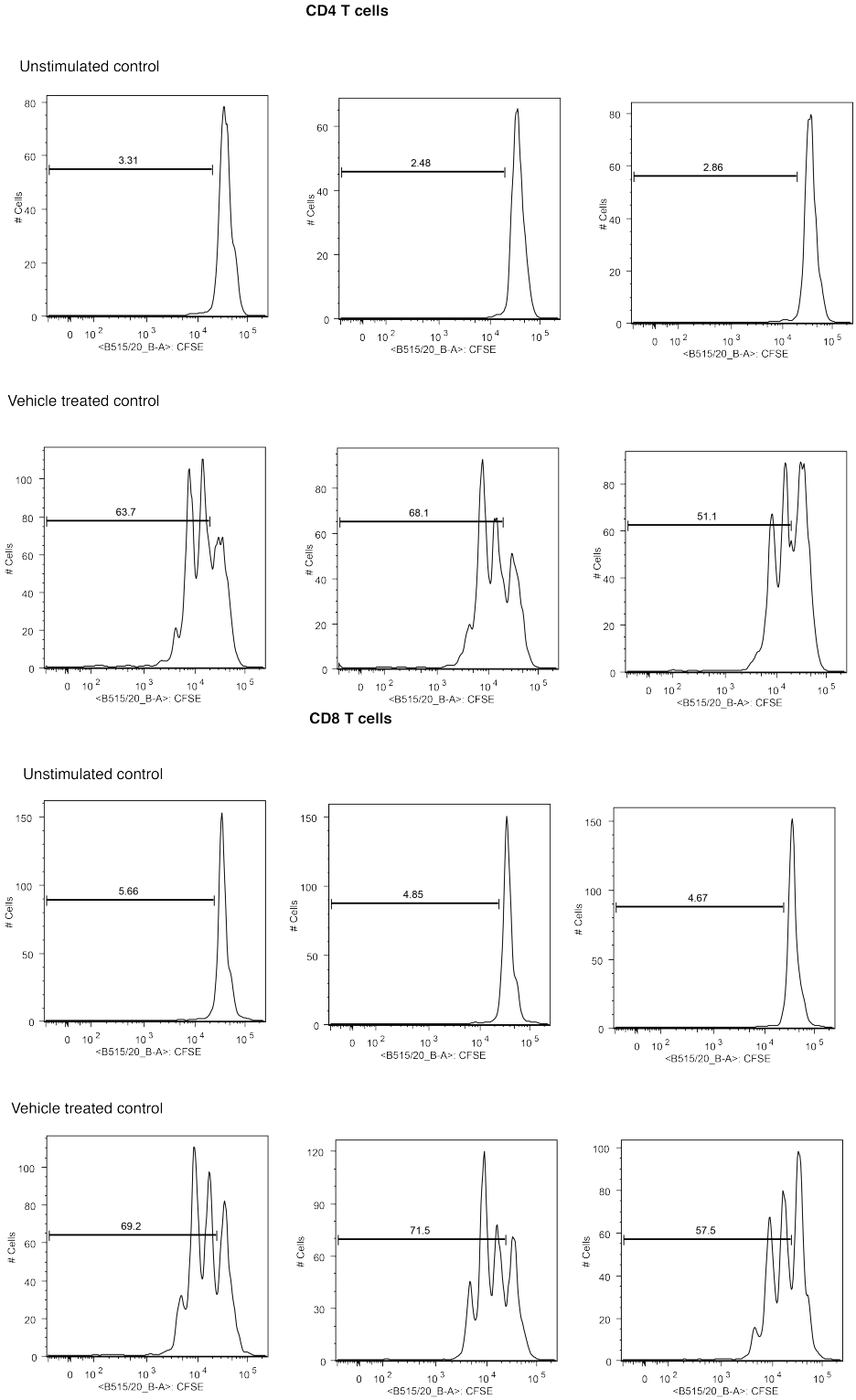

Figure A10: Flow cytometric control data for T cell subsets following human anti-CD3/28 stimulation performed in Figure 4.2. Proliferation of specific T cell subsets ($CD4^+$ or $CD8^+$) was evaluated following anti-CD3/28 stimulation and measured by flow cytometry. Example plots of the biological controls in triplicate are shown above; unstimulated to show baseline proliferation and the vehicle control.

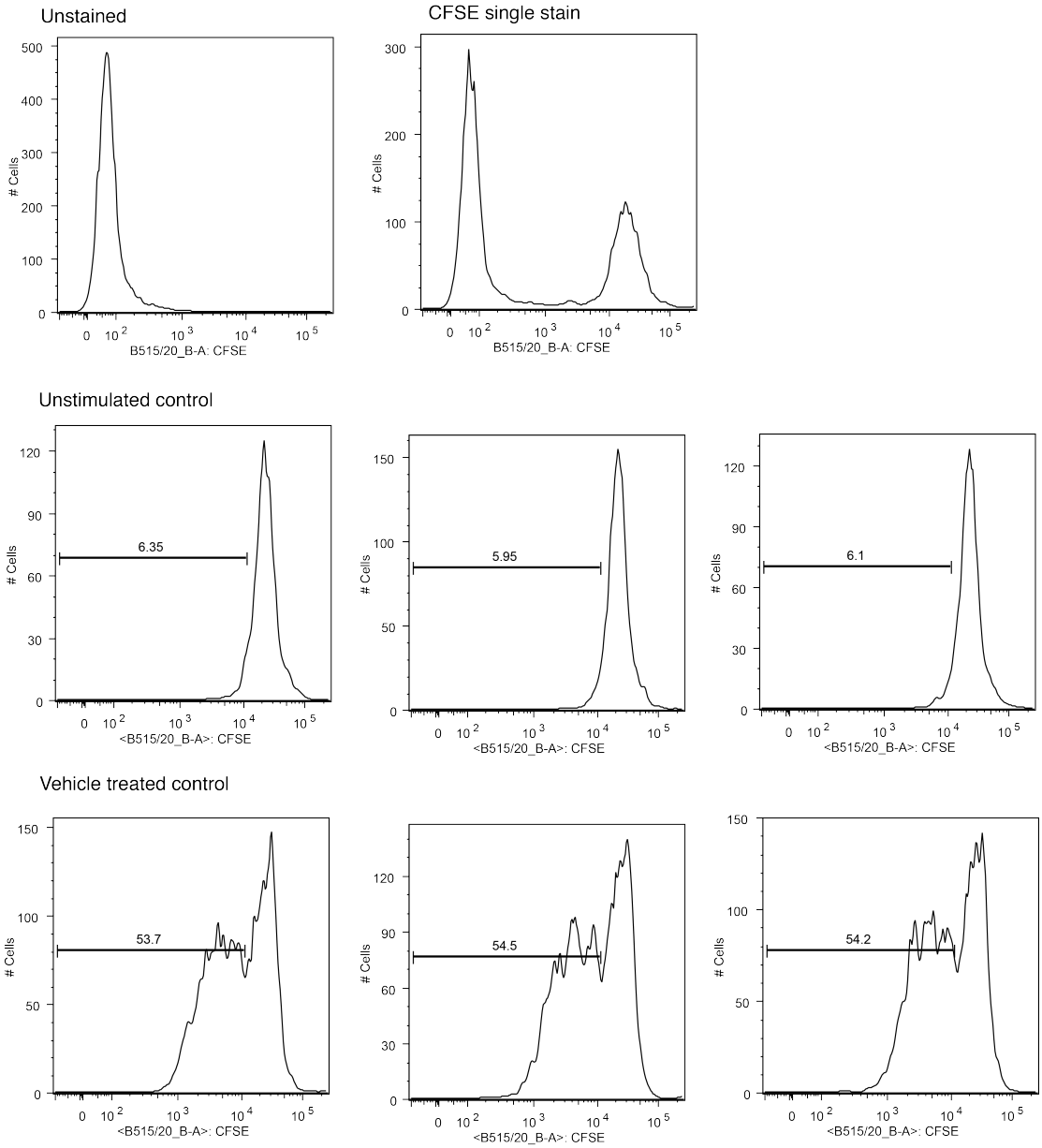

Figure A11; Flow cytometric control data of CFSE staining for murine anti-CD3/28 stimulation performed in Figures 4.4. T cell proliferation was evaluated following anti-CD3/28 stimulation and measured by flow cytometry. Example plots of the unstained and CFSE single stained controls are shown above, as are biological controls in triplicate (unstimulated to show baseline proliferation and the vehicle treated control).

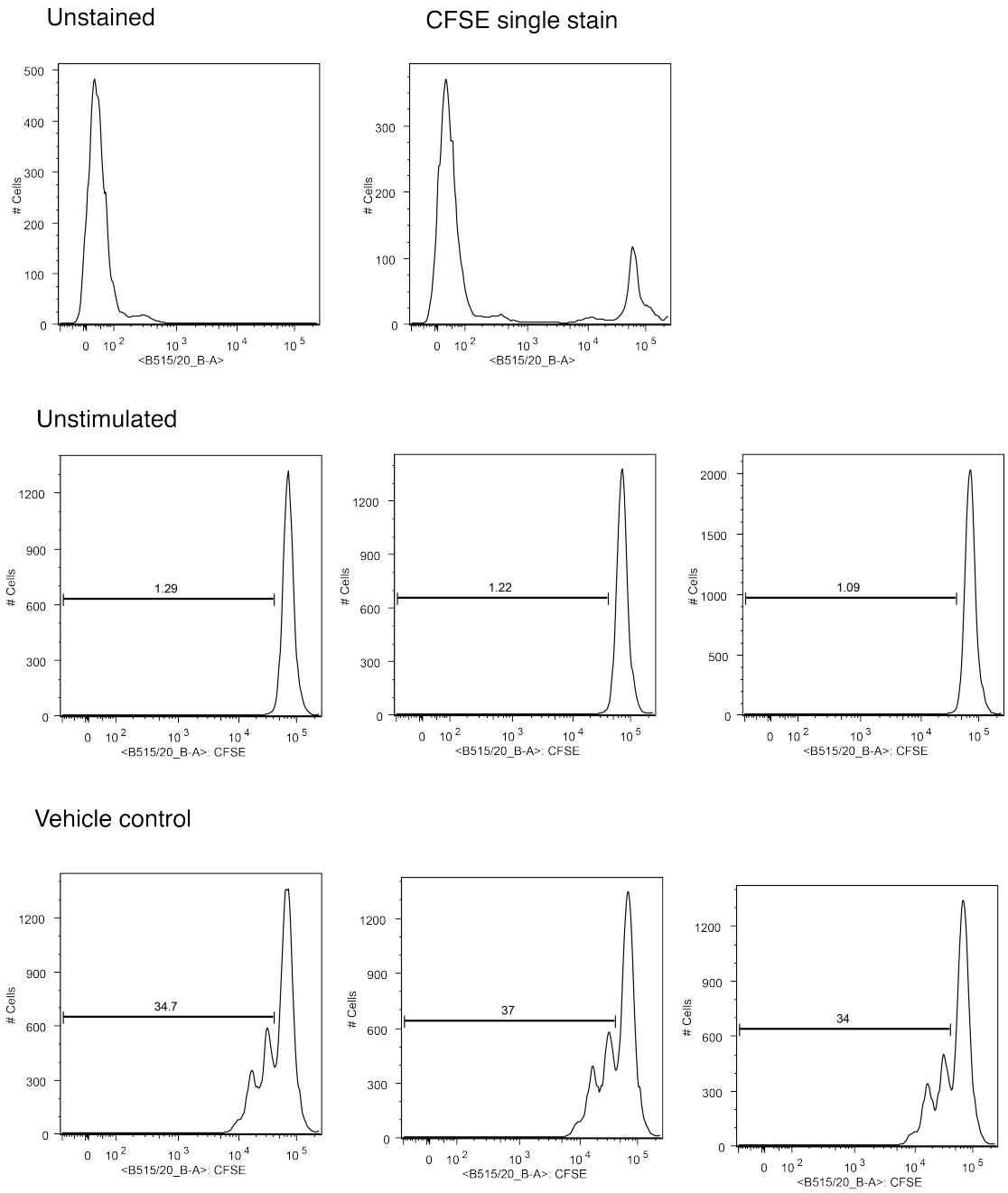

Figure A12: Flow cytometric control data of CFSE staining for human anti-CD3/28 stimulation performed in Figures 4.5 or 4.6. T cell proliferation was evaluated following anti-CD3/28 stimulation and measured by flow cytometry. Example plots of the unstained and CFSE single stained controls are shown above, as are biological controls in triplicate (unstimulated to show baseline proliferation and the vehicle treated control).

Appendix B: Experimental validation

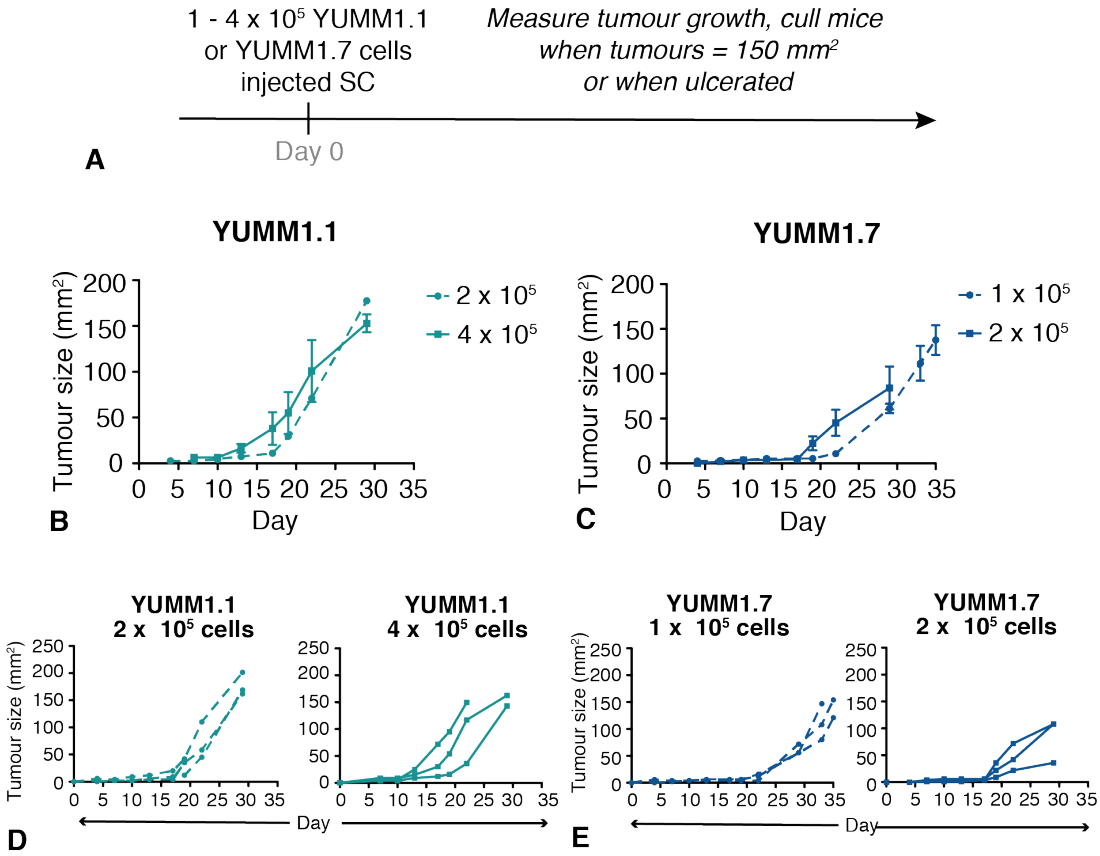

Figure B1: Titration of YUMM1.1 and YUMM1.7 growth *in vivo*. A. C57BL/6 mice were injected subcutaneously in the left flank with 1-4 x 10^5 YUMM1.1 or YUMM1.7 cells, tumour growth was monitored and size recorded. Mice were culled when tumours reached 150 mm^2, or when tumours ulcerated. **B.** Average YUMM1.1 tumour growth is shown. Each symbol represents the mean growth of three mice. Error bars are ± SEM. **C.** Average YUMM1.7 tumour growth is shown. Each symbol represents the mean growth of three mice. Error bars are ± SEM. **D.** Individual YUMM1.1 tumour growth is shown, each symbol represents one mouse. **E.** Individual YUMM1.7 tumour growth is shown, each symbol represents one mouse. This was a preliminary experiment and was only performed once.

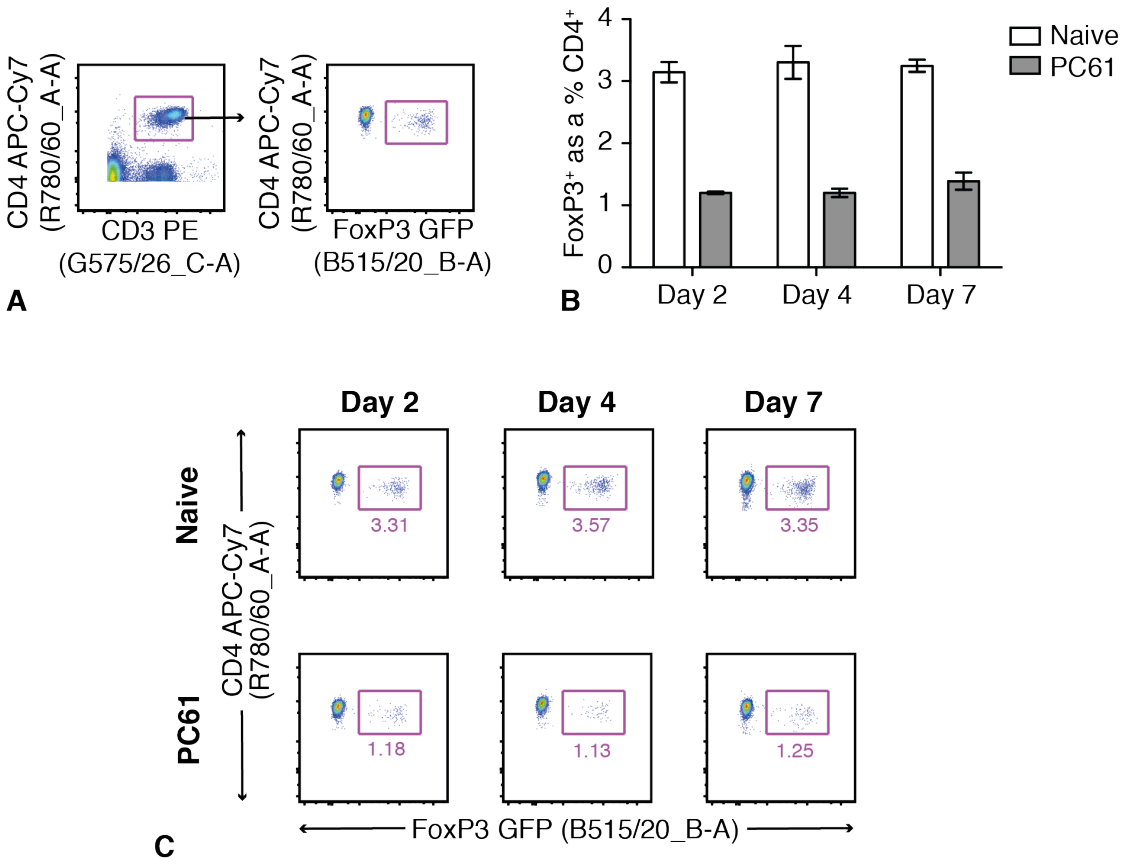

Figure B2: PC61 successfully depletes Tregs within the blood. Naïve FoxP3 GFP mice were injected with 250 µg PC61 or PBS intraperitoneally. Two, four and seven days following PC61 delivery mice were lateral tail vein bleed and peripheral blood was analysed for Treg frequencies by flow cytometry. **A.** Gating strategy used to identify $CD3^+$, $CD4^+$, $FoxP3^+$ Tregs. Samples were pre-gated on single, live cells. **B.** Frequency of Tregs within the $CD4^+$ T cell compartment in peripheral blood with or without PC61 treatment. **C.** Representative flow plots of Treg frequency. Experiment was performed in duplicate, and was repeated twice.

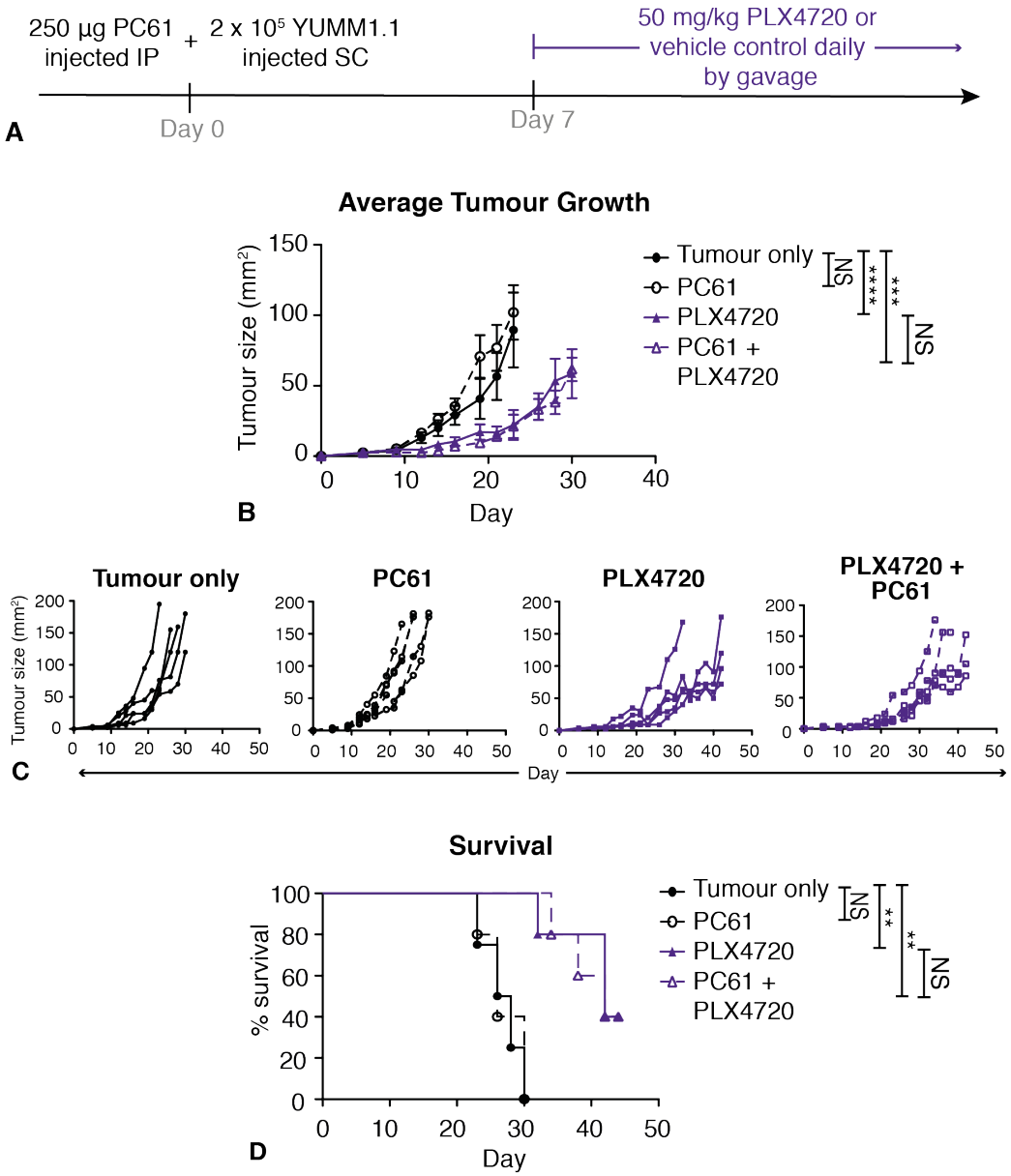

Figure B3: Depletion of Tregs does not affect PLX4720 treatment of YUMM1.1 tumours. A. C57BL/6 mice were injected SC in the left flank with 2 x 10^5 YUMM1.1 cells and given PC61 or PBS IP. Daily drug treatment began 7 days post-tumour challenge with 50 mg/kg PLX4720 given by oral gavage. Control mice received a vehicle solution. Tumour growth was monitored and size recorded. Mice were culled when tumours reached 150 mm^2 or ulcerated. **B.** Average tumour growth is shown, each symbol represents the mean growth of 5 mice. Error bars are ± SEM. NS = non-significant, *** $P < 0.001$, **** $P < 0.0001$, 2-way ANOVA with Bonferroni post-test, statistics shown for Day 23. **C.** Individual tumour growth for each treatment group is shown, each data point represents an individual mouse **D.** Kaplan-Meier plot showing survival for groups of 5 mice. NS = non-significant, ** $P < 0.01$, Mantel-Cox test. Graphs are representative of two independent experiments.

Appendix C: Immunophenotyping of spleens and mdLN following PLX4720 treatment

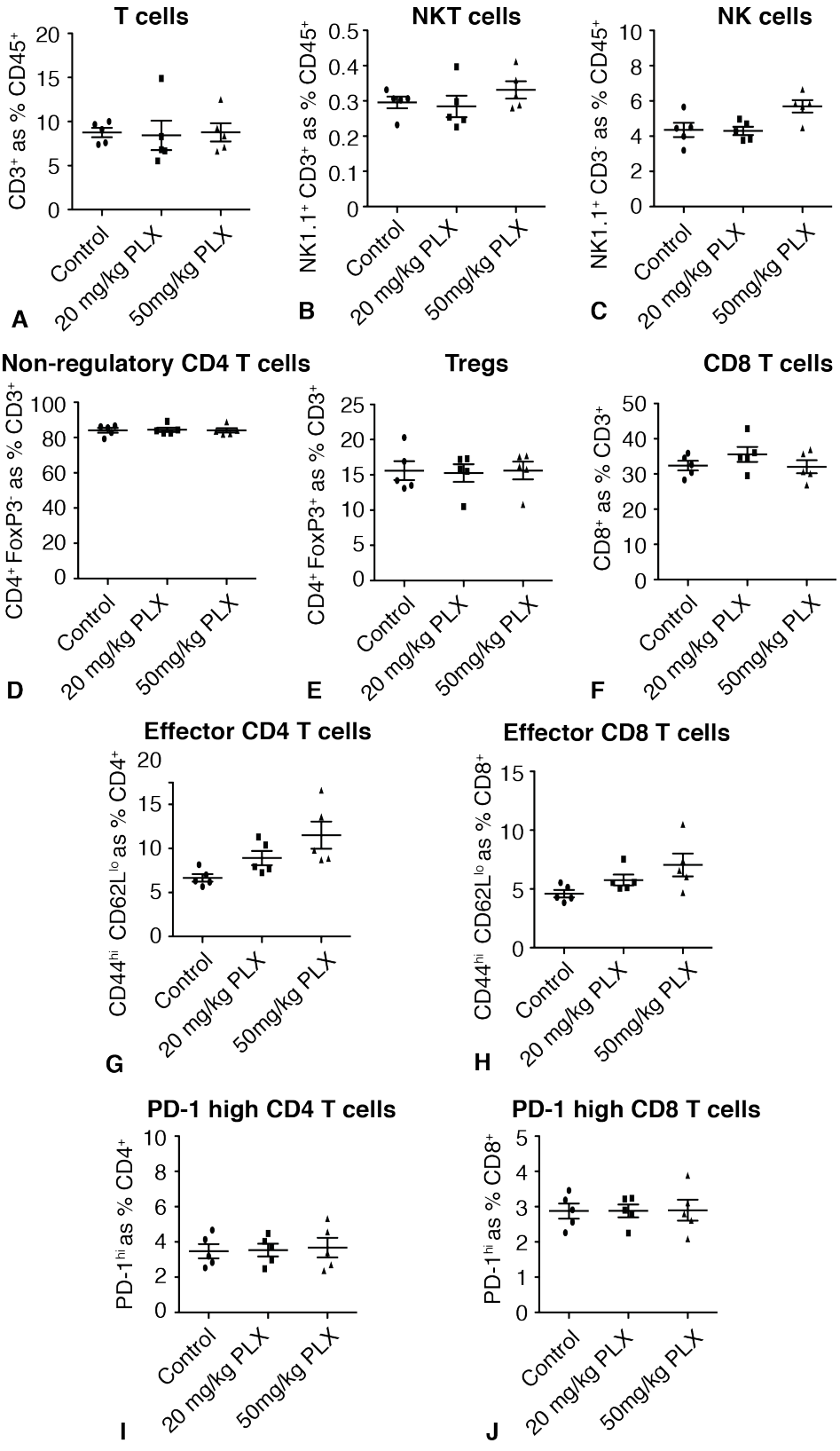

Figure C1: PLX4720 treatment does not alter splenic frequencies of lymphocytes. C57BL/6 mice were treated with PLX4720 as described in Figure 6.1A. One week following initiation of PLX4720 treatment spleens were harvested and immune cell frequencies assessed by flow cytometry. Lymphocyte populations were defined as shown in Figure 5.8B. **A-F.** Frequencies of T cells, NK cells and NKT cells. **G-J.** Frequencies of effector and exhausted $CD4^+$ and $CD8^+$ T cells. Values represent individual mice, with 5 mice used per group. Error bars are ± SEM. Statistical analysis was performed using one-way ANOVA with Bonferroni post-test, no significant differences were identified. Results are representative of two independent experiments.

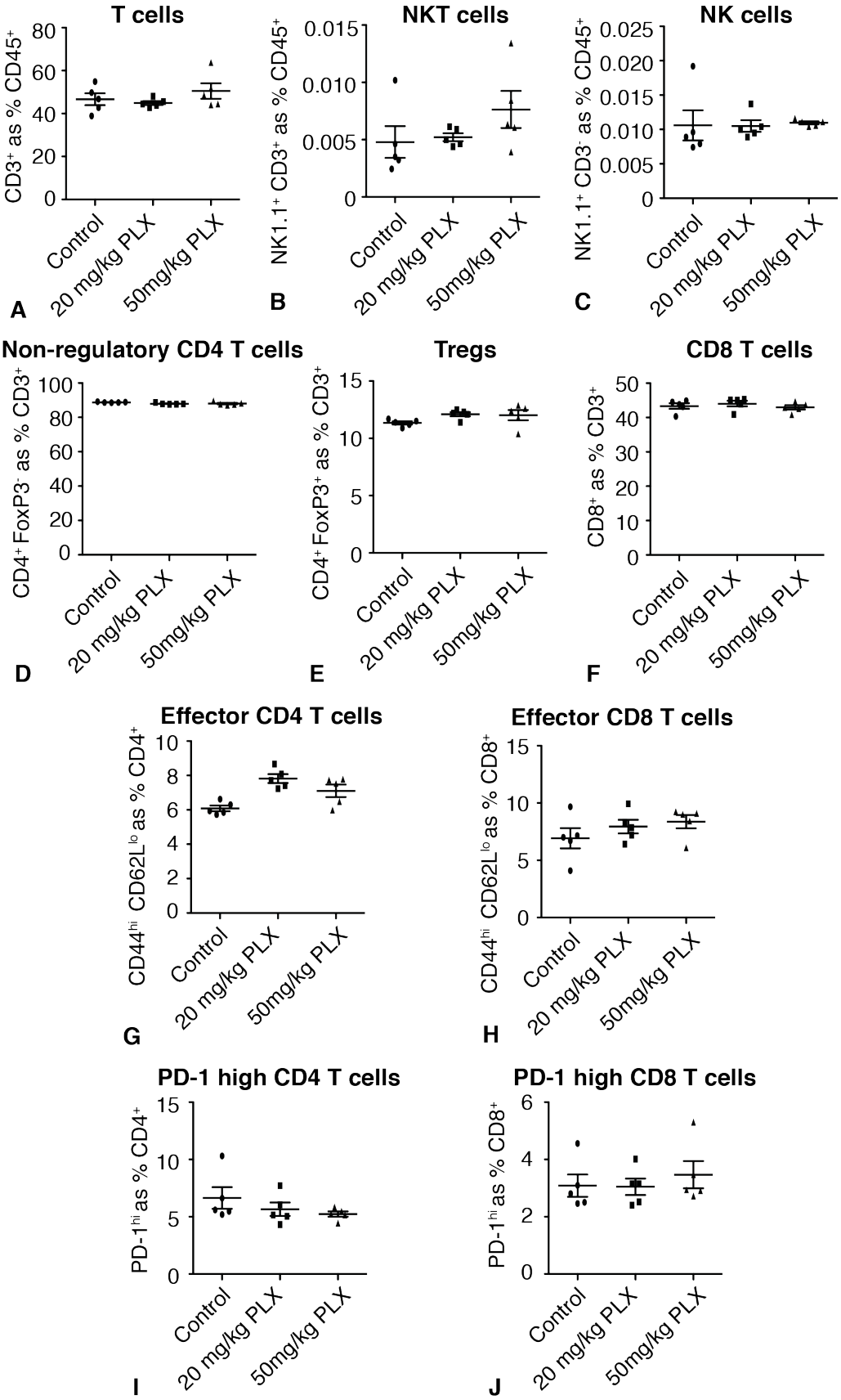
T cells
CD3+ as % CD45+
80
60
40
20
0
Control
20 mg/kg PLX
50mg/kg PLX
A
NKT cells
NK1.1+ CD3+ as % CD45+
0.015
0.010
0.005
0
Control
20 mg/kg PLX
50mg/kg PLX
B
NK cells
NK1.1+ CD3- as % CD45+
0.025
0.020
0.015
0.010
0.005
0
Control
20 mg/kg PLX
50mg/kg PLX
C
Non-regulatory CD4 T cells
CD4+ FoxP3- as % CD3+
100
80
60
40
20
0
Control
20 mg/kg PLX
50mg/kg PLX
D
Tregs
CD4+ FoxP3+ as % CD3+
15
10
5
0
Control
20 mg/kg PLX
50mg/kg PLX
E
CD8 T cells
CD8+ as % CD3+
50
40
30
20
10
0
Control
20 mg/kg PLX
50mg/kg PLX
F
Effector CD4 T cells
CD44hi CD62Llo as % CD4+
10
8
6
4
2
0
Control
20 mg/kg PLX
50mg/kg PLX
G
Effector CD8 T cells
CD44hi CD62Llo as % CD8+
15
10
5
0
Control
20 mg/kg PLX
50mg/kg PLX
H
PD-1 high CD4 T cells
PD-1hi as % CD4+
15
10
5
0
Control
20 mg/kg PLX
50mg/kg PLX
I
PD-1 high CD8 T cells
PD-1hi as % CD8+
6
4
2
0
Control
20 mg/kg PLX
50mg/kg PLX
J

Figure C2: PLX4720 treatment does not alter draining iLN frequencies of lymphocytes. C57BL/6 mice were treated with PLX4720 as described in Figure 6.1A. One week following initiation of PLX4720 treatment draining iLN were harvested and immune cell frequencies assessed by flow cytometry. Lymphocyte populations were defined as shown in Figure 5.8B. **A-F.** Frequencies of T cells, NK cells and NKT cells. **G-J.** Frequencies of effector and exhausted $CD4^+$ and $CD8^+$ T cells. Values represent individual mice, with 5 mice used per group. Error bars are ± SEM. Statistical analysis was performed using one-way ANOVA with Bonferroni post-test, no significant differences were identified. Results are representative of two independent experiments.

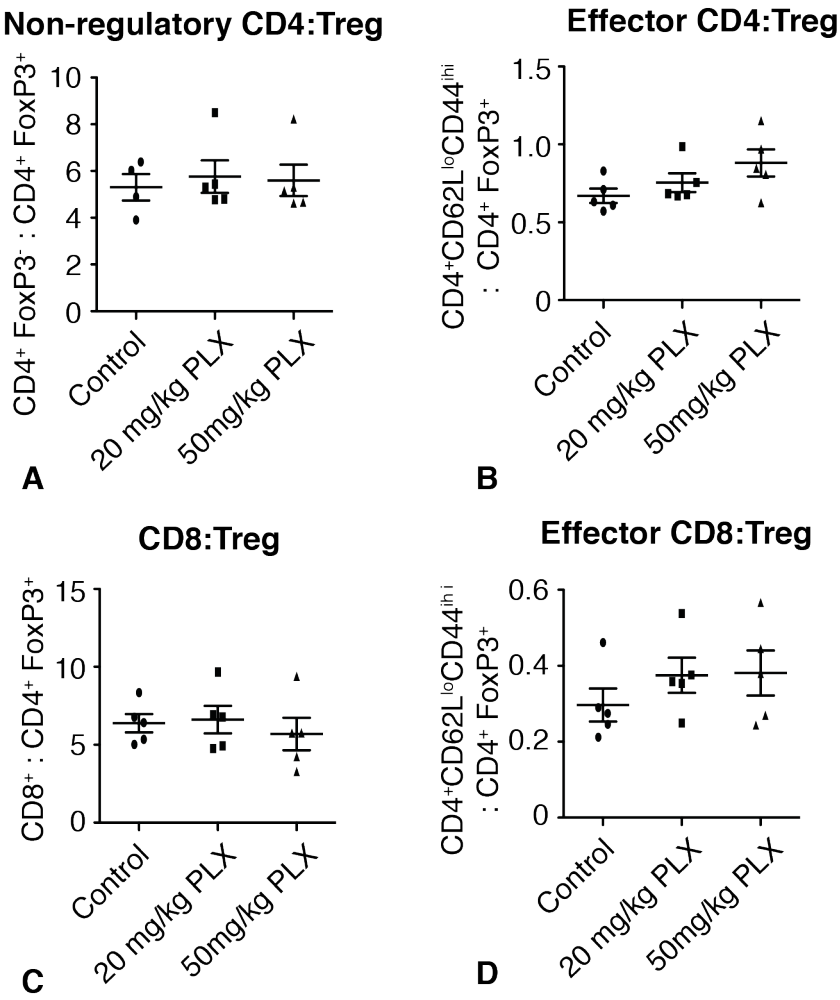

Figure C3: PLX4720 treatment does not alter the splenic ratio of Tregs to non-regulatory CD4 T cells or CD8 T cells, or effector T cells. C57BL/6 mice were treated with PLX4720 as described in Figure 6.1A. One week following initiation of PLX4720 treatment spleens were harvested and immune cell frequencies assessed by flow cytometry, lymphocyte populations were defined as shown in Figure 5.8B. The number of T cells was calculated by multiplying the population percentage by the total number of cells in the preceding gate. Cell numbers within the initial singlet cell gate were determined by multiplying percentages of single cells by total number of live cells as determined by trypan blue exclusion. **A.** Ratio of non-regulatory $CD4^+$ $FoxP3^-$ cells to $CD4^+$ $FoxP3^+$ Tregs. **B.** Ratio of effector $CD4^+$ $FoxP3^-$ cells to Tregs. **C.** Ratio of $CD8^+$ cells to $CD4^+$ $FoxP3^+$ Tregs. **D.** Ratio of effector $CD8^+$ cells to Tregs. Values represent individual mice, with 5 mice used per group. Error bars are ± SEM. Statistical analysis was performed using one-way ANOVA with Bonferroni post-test, no significant differences were identified. Results are representative of two independent experiments.

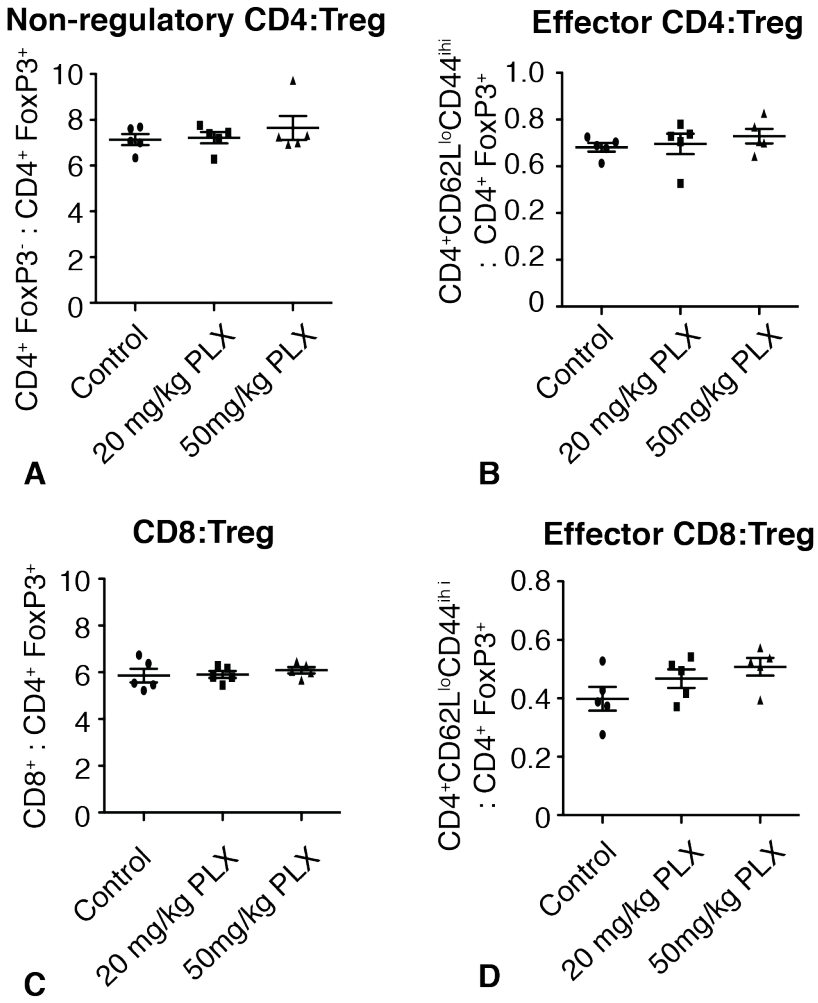

Figure C4: PLX4720 treatment does not alter the ratio of Tregs to non-regulatory CD4 T cells or CD8 T cells, or effector T cells within the draining iLN. C57BL/6 mice were treated with PLX4720 as described in Figure 6.1A. One week following initiation of PLX4720 treatment draining iLN were harvested and immune cell frequencies assessed by flow cytometry, lymphocyte populations were defined as shown in Figure 5.8B. The number of T cells was calculated by multiplying the population percentage by the total number of cells in the preceding gate. Cell numbers within the initial singlet cell gate were determined by multiplying percentages of single cells by total number of live cells as determined by trypan blue exclusion. **A**. Ratio of non-regulatory $CD4^+$ $FoxP3^-$ cells to $CD4^+$ $FoxP3^+$ Tregs. **B.** Ratio of effector $CD4^+$ $FoxP3^-$ cells to Tregs. **C**. Ratio of $CD8^+$ cells to $CD4^+$ $FoxP3^+$ Tregs. **D.** Ratio of effector $CD8^+$ cells to Tregs. Values represent individual mice, with 5 mice used per group. Error bars are ± SEM. Statistical analysis was performed using one-way ANOVA with Bonferroni post-test, no significant differences were identified. Results are representative of two independent experiments.

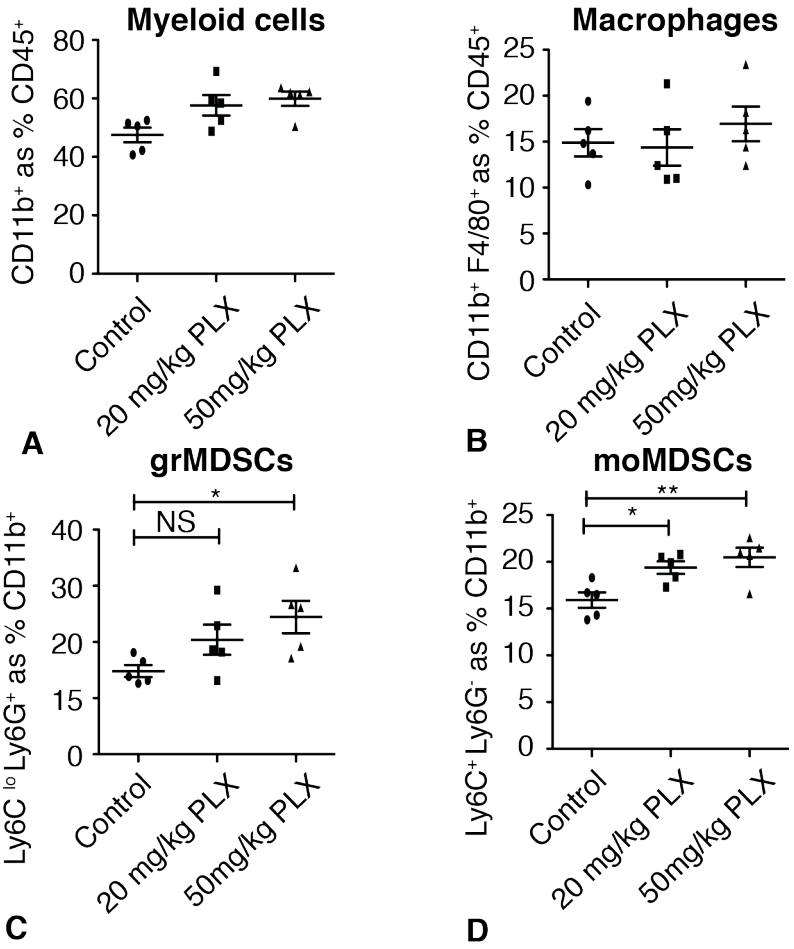

Figure C5: PLX4720 treatment does not significantly alter splenic frequencies of myeloid cells or macrophage, but increases the frequency of MDSCs. C57BL/6 mice were treated with PLX4720 as described in Figure 6.1A. One week following initiation of PLX4720 treatment spleens were harvested and immune cell frequencies assessed by flow cytometry, myeloid populations were defined as shown in Figure 5.8C. **A-D.** Frequencies of CD11b+, macrophage and MDSC populations. Values represent individual mice, with 5 mice used per group. Statistical analysis was performed using one-way ANOVA with Bonferroni post-test, no significant differences were identified. Error bars are ± SEM. Results are representative of two independent experiments.

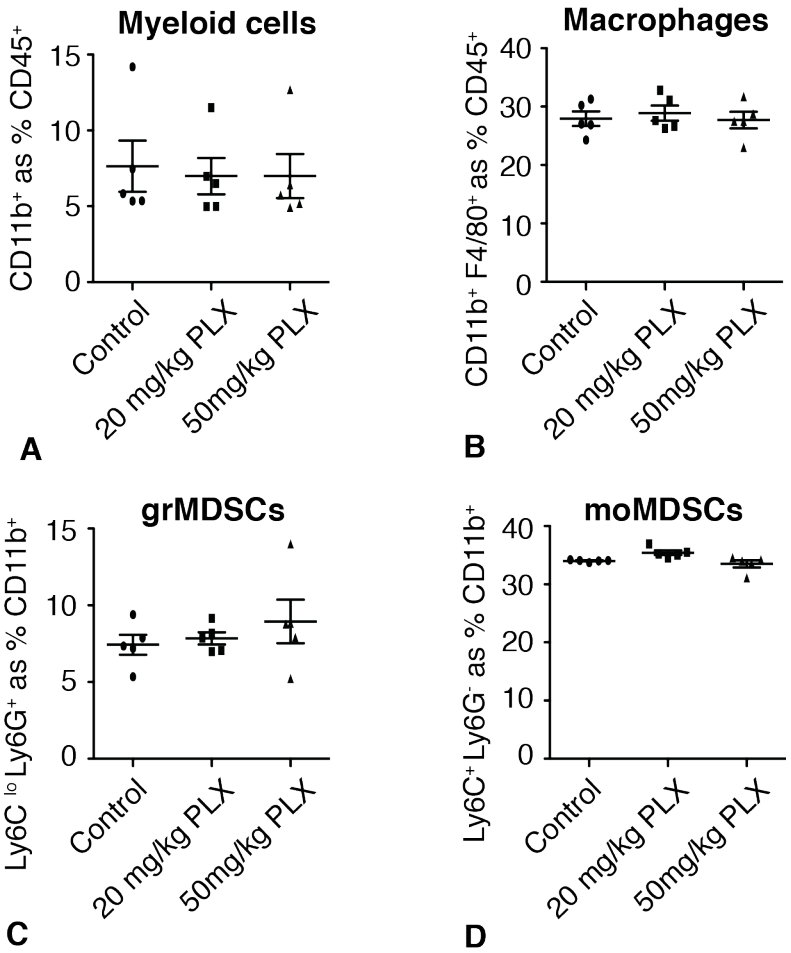

Figure C6: PLX4720 treatment does not significantly alter draining iLN frequencies of myeloid, macrophage or MDSCs. C57BL/6 mice were treated with PLX4720 as described in Figure 6.1A. One week following initiation of PLX4720 treatment draining iLN were harvested and immune cell frequencies assessed by flow cytometry. Myeloid populations were defined as shown in Figure 5.8C. **A-D.** Frequencies of CD11b+, macrophage and MDSC populations. Values represent individual mice, with 5 mice used per group. Statistical analysis was performed using one-way ANOVA with Bonferroni post-test, no significant differences were identified. Error bars are ± SEM. Results are representative of two independent experiments.

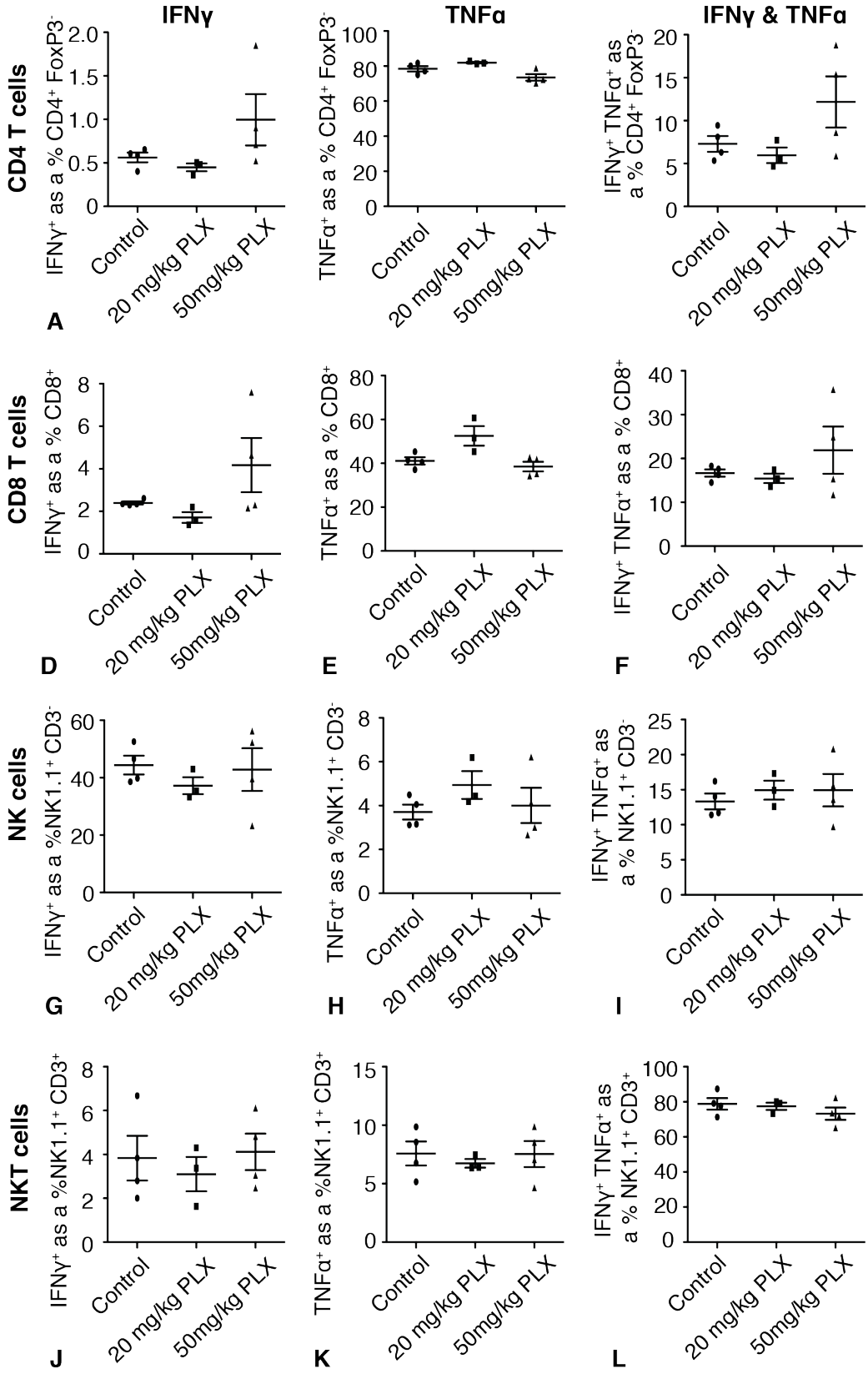
IFNγ
TNFα
IFNγ & TNFα
CD4 T cells
CD8 T cells
NK cells
NKT cells
IFNγ+ as a % CD4+ FoxP3-
TNFα+ as a % CD4+ FoxP3-
IFNγ+ TNFα+ as a % CD4+ FoxP3-
IFNγ+ as a % CD8+
TNFα+ as a % CD8+
IFNγ+ TNFα+ as a % CD8+
IFNγ+ as a %NK1.1+ CD3-
TNFα+ as a %NK1.1+ CD3-
IFNγ+ TNFα+ as a % NK1.1+ CD3-
IFNγ+ as a %NK1.1+ CD3+
TNFα+ as a %NK1.1+ CD3+
IFNγ+ TNFα+ as a % NK1.1+ CD3+
Control
20 mg/kg PLX
50mg/kg PLX
A
D
E
F
G
H
I
J
K
L

Figure C7: PLX4720 treatment does not significantly alter splenic frequencies of lymphocytes producing IFNγ and/or TNFα. C57BL/6 mice were treated with PLX4720 as described in Figure 6.1A. One week following initiation of PLX4720 treatment spleens were harvested and frequencies of IFNγ and TNFα producing lymphocytes were assessed by flow cytometry. Populations were defined as shown in Figure 5.12A. **A-C.** Frequencies of non-regulatory $CD4^+$ T cells producing IFNγ and TNFα. **D-F.** Frequencies of $CD8^+$ T cells producing IFNγ and TNFα. **G-I.** Frequencies of NK cells producing IFNγ and TNFα. **J-L.** Frequencies of NKT cells producing IFNγ and TNFα. Values represent individual mice, with 5 mice used per group. Error bars are ± SEM. Statistical analysis was performed using one-way ANOVA with Bonferroni post-test, no significant differences were identified. Results are representative of two independent experiments.

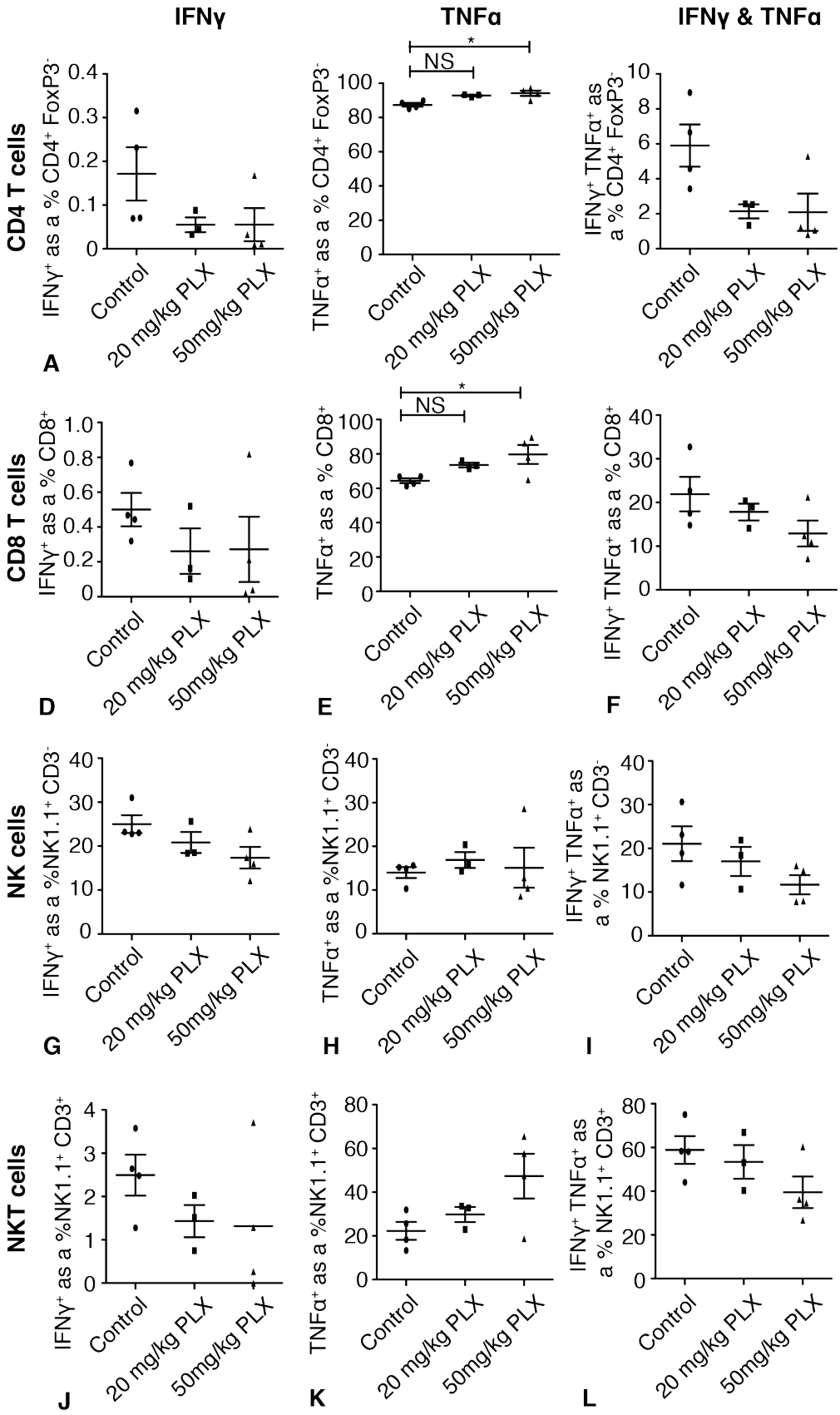
IFNγ
TNFα
IFNγ & TNFα
CD4 T cells
CD8 T cells
NK cells
NKT cells
IFNγ+ as a % CD4+ FoxP3-
TNFα+ as a % CD4+ FoxP3-
IFNγ+ TNFα+ as a % CD4+ FoxP3-
IFNγ+ as a % CD8+
TNFα+ as a % CD8+
IFNγ+ TNFα+ as a % CD8+
IFNγ+ as a %NK1.1+ CD3-
TNFα+ as a %NK1.1+ CD3-
IFNγ+ TNFα+ as a % NK1.1+ CD3-
IFNγ+ as a %NK1.1+ CD3+
TNFα+ as a %NK1.1+ CD3+
IFNγ+ TNFα+ as a % NK1.1+ CD3+
NS
*
Control
20 mg/kg PLX
50mg/kg PLX
A
D
E
F
G
H
I
J
K
L

Figure C8: PLX4720 treatment does not significantly alter draining iLN frequencies of lymphocytes producing IFNγ and/or TNFα. C57BL/6 mice were treated with PLX4720 as described in Figure 6.1A. One week following initiation of PLX4720 treatment draining iLN were harvested and frequencies of IFNγ and TNFα producing lymphocytes were assessed by flow cytometry. Populations were defined as shown in Figure 5.12A. **A-C.** Frequencies of non-regulatory $CD4^+$ T cells producing IFNγ and TNFα. **D-F.** Frequencies of $CD8^+$ T cells producing IFNγ and TNFα. **G-I.** Frequencies of NK cells producing IFNγ and TNFα. **J-L.** Frequencies of NKT cells producing IFNγ and TNFα. Values represent individual mice, with 5 mice used per group. Error bars are ± SEM. Statistical analysis was performed using one-way ANOVA with Bonferroni post-test, no significant differences were identified. Results are representative of two independent experiments.